



HAL
open science

Statistical Properties of the Euclidean Random Assignment Problem

Matteo Pietro d'Achille

► **To cite this version:**

Matteo Pietro d'Achille. Statistical Properties of the Euclidean Random Assignment Problem. Physics [physics]. Université Paris-Saclay, 2020. English. NNT : 2020UPASQ003 . tel-03098672v1

HAL Id: tel-03098672

<https://theses.hal.science/tel-03098672v1>

Submitted on 5 Jan 2021 (v1), last revised 11 Jan 2021 (v2)

HAL is a multi-disciplinary open access archive for the deposit and dissemination of scientific research documents, whether they are published or not. The documents may come from teaching and research institutions in France or abroad, or from public or private research centers.

L'archive ouverte pluridisciplinaire **HAL**, est destinée au dépôt et à la diffusion de documents scientifiques de niveau recherche, publiés ou non, émanant des établissements d'enseignement et de recherche français ou étrangers, des laboratoires publics ou privés.

Statistical Properties of the Euclidean Random Assignment Problem

Thèse de doctorat de l'université Paris-Saclay

École doctorale n° 569 : innovation thérapeutique : du
fondamental à l'appliqué (ITFA)
Spécialité de doctorat: biochimie et biologie structurale
Unité de recherche: Université Paris-Saclay, CEA, CNRS, Institute for
Integrative Biology of the Cell (I2BC), 91198, Gif-sur-Yvette, France.
Réfèrent: Université de Versailles-Saint-Quentin-en-Yvelines

**Thèse présentée et soutenue en visioconférence totale
le 16/10/2020 par**

Matteo Pietro D'ACHILLE

Composition du jury:

Michel LEDOUX Professeur, Université de Toulouse – Paul-Sabatier	Président
Charles BORDENAVE DR CNRS, Aix-Marseille Université	Rapporteur
Massimiliano GUBINELLI Professeur, Université rhénane Frédéric-Guillaume de Bonn	Rapporteur
Guilhem SEMERJIAN MCF, Université PSL, École Normale Supérieure	Examineur
Lenka ZDEBOROVÁ DR CNRS, Université Paris-Saclay, CEA Paris-Saclay	Examinatrice
William JALBY Professeur, Université Paris-Saclay, UVSQ	Directeur
Olivier RIVOIRE CR CNRS, Université PSL, Collège de France	Codirecteur
Andrea SPORTIELLO CR CNRS, Université Sorbonne Paris Nord	Codirecteur
Sergio CARACCILO Professeur, Université de Milan et INFN	Invité

REMERCIEMENTS

Plusieurs personnes ont contribué à la réalisation de cette thèse de doctorat.

Je tiens tout d'abord à remercier William Jalby, Olivier Rivoire et Andrea Sportiello d'avoir accepté d'en être les co-directeurs, de m'avoir fourni des critiques constructives et de m'avoir dirigé vers questions toujours intéressantes avec passion et grande hauteur de vue.

Je remercie Sergio Caracciolo pour ses encouragements et pour notre collaboration de longue date. Nos discussions ont influencé en profondeur ma façon d'aborder les problèmes et, par conséquence, le contenu du présent travail. Gabriele Sicuro est également remercié pour notre collaboration efficace de longue date et de longue portée. Dario Benedetto et Emanuele Caglioti sont remerciés pour plusieurs discussions intéressantes, dont certaines sont contenues dans notre premier travail commun (172).

Carlo Sbordone et le Secrétariat de l'Accademia di Scienze Fisiche e Matematiche à Naples sont remerciés pour leur disponibilité et de m'avoir permis d'accéder au remarque (3).

Charles Bordenave et Massimiliano Gubinelli sont remerciés d'avoir accepté d'être les rapporteurs de cette thèse. Michel Ledoux, Guilhem Semerjian et Lenka Zdeborová sont remerciés de m'avoir fait l'honneur de siéger dans le jury de thèse.

Sophie Lemaire, Clément Nizak, Pierre Pansu et Kay Wiese sont remerciés pour encouragements lors de certaines étapes importantes du voyage doctoral.

Anna Paola Muntoni, Edoardo Sarti et Steven Schulz ont lu attentivement le Chapitre 1 et sont donc remerciés.

Enfin, Christine Bailleul, Nicole Braure, Marie Fontanillas et Isabelle Moudenner-Cohen sont remerciées pour leur assistance administrative compétente.

Je tiens à remercier les institutions qui m'ont soutenu pendant les trois années du voyage doctoral, à Paris comme à l'extérieur. Il s'agit: de l'Université de Versailles–Saint–Quentin–en–Yvelines, qui m'a accordé le contrat doctoral; du Collège de France, pour son environnement de recherche passionnant et pour l'accès à d'excellentes classes de français; de l'Université Sorbonne Paris Nord, qui m'a offert des conditions de travail idéales et m'a honoré du poste de membre associé au Laboratoire d'Informatique; et de l'Université Paris-Saclay, qui m'a accordé un poste de doctorant-enseignant puis de vacataire d'enseignement en Mathématiques à Orsay. Le Centre CEA de Saclay est remercié pour son hospitalité lors de la réalisation d'une partie de ces travaux. Je remercie l'Académie polonaise des sciences et Jacek Miękisz de leur hospitalité et des conditions de travail optimales

à l'occasion d'un séjour de deux semaines en 2018 au Centre Banach de Varsovie.

Finalement je remercie tous ceux qui m'ont soutenu de loin dans ce voyage malgré les difficultés engendrées par la pandémie, en particulier Lucia, Giuseppe, Ornella & Sergio et Roberto. Merci à toi, Sandra, de ta patience, tes sourires et du tiramisu.

RÉSUMÉ SUBSTANTIEL

Cette thèse de doctorat concerne un problème d'optimisation combinatoire aléatoire introduit par Mézard et Parisi comme modèle-jouet de verre de spin en dimension finie (50). Une première motivation pour entreprendre cet effort est que les verres de spin, malgré leur rôle importants ces dernières années, se sont révélées assez difficiles à résoudre (trouver l'énergie de l'état fondamental d'un verre de spin en dimension finie est un problème *NP*-dur) de sorte que, à certains égards, ils restent mystérieuses surtout au-delà de l'approximation de champ moyen, où l'étude rencontre des difficultés même numériques; d'où l'intérêt pour un cadre théorique qui dépasse le champ moyen tout en partageant les caractéristiques de base d'un verre de spin (voir désordre et frustration) tout en restant attachable, tant analytiquement que à l'ordinateur.

Dans ce problème, les lois microscopiques de l'interaction sont données une fois pour toutes et l'aléa est associé aux positions de certains constituants élémentaires » placés dans un espace par ailleurs homogène. Cette hypothèse complique considérablement l'étude des propriétés typiques d'intérêt par rapport au problème d'assignation aléatoire en dimension infinie précédemment étudié par Mézard-Parisi (40), et ensuite rigoureusement par Aldous (88). Maintenant, les constituants élémentaires peuvent modéliser des atomes ou des impuretés. Mathématiquement, ce sont deux familles de n éléments chacune : ils peuvent être représentés comme l'ensemble des sommets $V(\mathcal{K}_{n,n})$ d'un graphe bipartite complet $\mathcal{K}_{n,n}$ (c'est-à-dire, les éléments correspondent aux deux ensembles partis du graphe). Nous appellerons dorénavant ces familles des points les « bleus » et « rouges », et nous leur réserverons deux symboles spéciaux : \mathcal{B} et \mathcal{R} . Enfin, le choix de la loi de probabilité associée aux positions de \mathcal{B} et \mathcal{R} dépend du type de questions que l'on veut poser, et certaines hypothèses seront nécessaires. Par exemple, si \mathcal{B} et \mathcal{R} sont des particules d'encre qui ont été vigoureusement mélangées dans un verre d'eau, l'hypothèse d'une distribution uniforme de \mathcal{B} et \mathcal{R} dans le volume d'eau semble raisonnable pour la plupart des objectifs pratiques ; au contraire, si \mathcal{B} sont des vélos qui doivent être déposés dans des raquettes (\mathcal{R}) dans la ville de Paris, l'hypothèse d'une distribution uniforme pour \mathcal{R} ne semble pas appropriée.

Pour nous situer dans un cadre suffisamment général, nous supposons que $\mathcal{B} = \{b_i\}_{i=1}^n$ et $\mathcal{R} = \{r_j\}_{j=1}^n$ sont des familles de variables aléatoires i.i.d. réparties selon une certaine mesure ν (qui est une donnée du problème). Par exemple, dans un scénario typique, ν est supportée sur (un sous-ensemble de) un espace métrique \mathcal{M} ; ou les points d'une couleur (comme l'étaient les raquettes dans

l'exemple de Paris) sont fixés sur une grille d -dimensionnelle, et les autres sont des variables aléatoires i.i.d. comme ci-dessus (sinon nous n'aurions pas de caractère aléatoire). Dans tous cas, nous appelons la distribution de probabilité associée à la mesure ν l' *ensemble statistique* ou *désordre*, et nous nommons la donnée de \mathcal{B} et \mathcal{R} échantillonnée à partir d'une telle distribution une *instance* ou *réalisation du désordre*. L'interaction entre b_i et r_j (c'est-à-dire le coût de l'assignation de b_i à r_j) a une intensité $c_{ij} := c(b_i, r_j)$ pour une certaine fonction $c : \mathcal{M} \times \mathcal{M} \rightarrow \mathbb{R}$. Les n^2 nombres réels $\{c_{ij}\}_{i,j=1}^n$, qui peuvent être considérés comme positives, peuvent être arrangés dans une matrice de coût d'assignation non symétrique, $n \times n$

$$c = \begin{pmatrix} c(b_1, r_1) & c(b_1, r_2) & \dots \\ \vdots & \ddots & \\ c(b_n, r_1) & & c(b_n, r_n) \end{pmatrix},$$

qui peut être interprétée comme la matrice de contiguïté pondérée du graph $\mathcal{K}_{n,n}$. Un premier énoncé équivalent mais plus succinct en langage physique est que l'hamiltonienne pour ce système ne comprend que des interactions à deux corps inter-couleurs*.

La caractéristique essentielle qui empêche ce cadre de modéliser, par exemple, un plasma à deux composants, est qu'une fois qu'un bleu est couplé à un rouge dans une configuration, il disparaît du système. Une configuration est codée par une permutation $\pi \in \mathcal{S}_n$ et a énergie

$$\mathcal{H}(\pi) = \sum_{i=1}^n c_{i\pi(i)} = \text{Tr} [P_\pi c],$$

où P_π est la matrice de permutation de π (c'est-à-dire, $P_{i,j} = \delta_{j,\pi(i)}$). Plus généralement, la fonction de coût \mathcal{C} peut jouer le rôle d'une énergie, d'une fonction de fitness, ou d'une distance générique. En principe, on peut considérer des fonctions de coût encore plus générales $\mathcal{C} : \mathcal{M} \times \mathcal{M} \rightarrow \mathbb{R}$, mais nous ne discuterons pas ce cas ici. Afin de modéliser les aspects de base d'un système physique critique, et notamment l'invariance de translation, de rotation et d'échelle, nous nous limitons dans ce travail à une fonction de coût $\mathcal{C} : \mathbb{R} \rightarrow \mathbb{R}^+$ qui est le monôme $|x|^p$ dans la

*C'est-à-dire que, en analogie avec l'électrostatique où \mathcal{B} et \mathcal{R} représentent respectivement des charges électrostatiques unitaires positives et négatives, nous négligerons la répulsion de Coulomb.

fonction de distance \mathcal{D}^\dagger , c'est à dire

$$c_{ij}^{(p)} = \mathcal{C}(\mathcal{D}(b_i, r_j)) = \mathcal{D}^p(b_i, r_j), \quad i, j = 1, \dots, n,$$

où nous avons remarqué la dépendance de la matrice c du nombre réel p , appelé l'exposant « énergie-distance ». Dans ce travail, \mathcal{D} est exclusivement la distance euclidienne d -dimensionnelle, mais il est clair que d'autres choix pour la métrique \mathcal{D} sont possibles. Enfin, une assignation optimale π_{opt} satisfait

$$\mathcal{H}_{\text{opt}} := \mathcal{H}(\pi_{\text{opt}}) = \min_{\pi \in \mathcal{S}_n} \mathcal{H}(\pi),$$

où la variable aléatoire \mathcal{H}_{opt} est appelée l'*énergie de l'état fondamental*.

Le choix d'un espace métrique $(\mathcal{M}, \mathcal{D})$, d'un ensemble statistique pour les positions aléatoires de \mathcal{B} et \mathcal{R} , et d'un exposant p identifie un problème d'assignation aléatoire bien défini qui on appelle **problème d'assignation aléatoire euclidien** (ou **ERAP** de l'acronyme de sa traduction anglais, **Euclidean Random Assignment Problem**). Une étude des propriétés statistiques de \mathcal{H}_{opt} en fonction du triple $((\mathcal{M}, \mathcal{D}), (\nu_{\mathcal{R}}, \nu_{\mathcal{B}}), p)$ constitue la principale contribution de ce manuscrit.

Le Chapitre 1 est une promenade à travers divers concepts et idées que nous avons pu identifier comme un contexte plausible pour ce travail de thèse. Compte tenu de la nature introductive du chapitre, nous privilégions un style discursif et donnons la priorité aux motivations plutôt qu'à l'exhaustivité, en fournissant au lecteur intéressé quelques points d'entrée vers les littératures connexes par le biais de critiques et d'articles de référence. L'accent est mis sur les méthodes existantes et les liens pertinents avec d'autres sujets. Ce faisant, nous souhaitons transmettre au moins en partie les idées remarquablement unifiantes qui sous-tendent notre discussion et, nous l'espérons, quelques raisons d'en considérer certaines à la lumière du problème examiné dans cette thèse de doctorat. Suivent des exemples où nous discutons des notions physiques de solution sous-optimales et de passage de niveau dans un cadre algorithmique, et une discussion de certains liens avec d'autres problèmes à l'interface de la physique théorique, des probabilités et de l'informatique théorique. Le Chapitre 1 est clos par un plan du manuscrit et une liste des contributions nouvelles contenues dans cet ouvrage.

Dans le Chapitre 2 nous étudions le cas unidimensionnel pour p et désordre quelconque. Après avoir résumé l'état de l'art, nous présentons certains nouveaux résultats tels que la distribution asymptotique de \mathcal{H}_{opt} dans la cas $\mathcal{M} =$ le cercle unitaire à $p = 2$ pour un désordre uniforme, exprimée en termes de la fonction ϑ_4 de Jacobi (Eq. 2.3.3.15) ; une étude de l'asymptotique de l'espérance mathématique

[†]Nous rappelons qu'une distance \mathcal{D} sur un espace métrique \mathcal{M} est une application binaire symétrique et définie positive $\mathcal{D} : \mathcal{M} \times \mathcal{M} \rightarrow \mathbb{R}^+$ qui satisfait l'inégalité triangulaire. Si cela n'est pas évident d'après le contexte, nous indiquerons un espace métrique avec l'écriture explicite $(\mathcal{M}, \mathcal{D})$.

de \mathcal{H}_{opt} pour différent choix du désordre à $p \geq 1$ (« anomalous scaling »), d’abord avec une méthode inspirée par la régularisation avec cutoff en théorie quantique des champs (§ 2.5, voir aussi l’article (169)), puis avec une approche analytique–combinatoire à n fini (§ 2.6, article correspondant en préparation). Dans § 2.7, dédiée au cas concave $p \in (0, 1)$, nous présentons les « appariements de Dyck », des solutions sous-optimales dont nous avons calculé l’asymptotique de l’énergie moyenne. Sur la base de simulations numériques approfondies, nous conjecturons que les appariements de Dyck partagent la même asymptotique du vrai état fondamental à moins d’une constante multiplicative dépendante de p (Conjecture 2.7.1). Cette section correspond à la publication (173), et nous a permis de compléter la section à $d = 1$ du diagramme de phase du ERAP, qui, remarquablement, présente deux nouveaux points critiques, respectivement à $p = \frac{1}{2}$ et $p = 1$ (Fig. 2.17).

Dans le Chapitre 3, nous considérons le cas bi-dimensionnel à $p = 2$ sur la base de l’approche de théorie de champs proposée par Caracciolo–Lucibello–Parisi–Sicuro (CLPS) (145). En particulier, dans la § 3.1 nous présentons de nouveaux résultats concernant les différences des énergies entre deux variétés Riemanniennes Ω, Ω' et montrons que ces différences peuvent être obtenues à partir du spectre de l’opérateur Laplace–Beltrami de la variété. Nous avons vérifié nos prédictions analytiques à l’aide d’expériences numériques approfondies pour de nombreux choix de variétés (voir les figures 3.3, 3.8). Cette section a donné lieu au travail (172).

Dans § 3.2 nous obtenons des relations linéaires approximatives entre les énergies des problèmes où les configurations des points sont liées par des transformations de symétrie qui préservent le spectre de l’opérateur de Laplace–Beltrami de la variété.

Dans § 3.3, toujours basée sur l’approche CLPS, nous étudions le problème défini sur les 2-torus \mathbb{T}_2 à $p = 2$ dans le cas « Grid–Poisson », c’est à dire, une variante du problème où les points d’une des deux couleurs sont fixés sur une grille déterministe (dans ce cas, la grille carrée bi-dimensionnelle). Dans ce cas, nous développons l’idée que le champ de transport (c’est-à-dire le champ vectoriel associant les bleus aux rouges dans la solution optimale) peut satisfaire, par analogie avec l’électrodynamique, une « décomposition d’Helmholtz » dans une partie longitudinale et une partie transverse. Nous étudions en détails les propriétés statistiques des deux composantes pour le cas d’une distribution uniforme des points et nous montrons que la partie longitudinale et la partie transverse contribuent à un ordre différent dans l’asymptotique du coût moyen optimal.

Le Chapitre 4 concerne une extension du ERAP au cas d’une dimension de Hausdorff $d_H \in (1, 2)$. Dans cette étude, principalement numérique, nous considérons des points bleus et rouges uniformément distribués sur deux ensembles fractals (« fractal de Peano » et « fractal de Cesàro ») qui fournissent une interpolation

différente de l'intervalle $(1, 2)$ dimension de Hausdorff. En particulier, grâce à des simulations numériques approfondies, nous obtenons evidence que, modulo une constante multiplicative, l'exposant leading du cout moyen optimal soit le meme pour les deux fractals dans une grande région du plan (p, d_H) .

Enfin, le Chapitre 5 contient quelques conclusions provisoires et une sélection de perspectives de recherche.

Contents

	PAGE
1 Introduction	1
§1.1 Background	1
§1.2 Random Assignment Problems and extensions	6
§1.3 The Euclidean Random Assignment Problem	9
§1.4 On approximate solutions and level crossing	11
1.4.1 On approximate solutions and greedy heuristics	12
1.4.2 On crossings of ground state energies	15
1.4.3 Possible persistence of transition near $p = 1$ at $d = 2$	16
§1.5 Some related topics	17
§1.6 Plan of the Thesis and list of contributions	20
2 One-dimensional Euclidean Random Assignment Problems	21
§2.1 On convex, concave and \mathcal{C} -repulsive regimes	21
§2.2 Poisson-Poisson, Grid-Poisson ERAPs & the Brownian Bridge	24
§2.3 Lattice and continuum modes of the optimal transport field at $p = 2$	28
2.3.1 Unit interval at fixed n	28
2.3.2 Unit interval in the $n \rightarrow \infty$ limit	32
2.3.3 Distribution of \mathcal{H}_{opt} on the unit circle in the $n \rightarrow \infty$ limit	35
§2.4 Beyond uniform disorder: anomalous vs bulk scaling of $\langle \mathcal{H}_{\text{opt}} \rangle$ at $p \geq 1$	39
§2.5 Anomalous Scaling of the Optimal Cost in the One-Dimensional Random Assignment Problem	40
2.5.1 Notations	40
2.5.2 The problem of regularization	43
2.5.3 Applications	44
2.5.4 Conclusions	57
§2.6 Combinatorial and analytic approach to anomalous scaling: universality classes	58
2.6.1 Notations and setting	58
2.6.2 Families of distributions	61

2.6.3	General technical facts	64
2.6.4	Ensembles in which the average cost is infinite	69
2.6.5	Family of stretched exponentials with endpoint at infinity $\rho_{ie,\alpha}$ and $\rho_{ie,\alpha}^+$	71
2.6.6	Estimation of complete homogeneous functions	78
2.6.7	Non-integer values of s	82
2.6.8	Family with finite endpoint, algebraic zero $\rho_{fa,\beta}$	85
2.6.9	On sub-leading contributions at the critical line $2(p+\beta) =$ $p\beta$	90
2.6.10	Family of distributions with endpoint at infinity and al- gebraic zero $\rho_{ia,\beta}$	94
2.6.11	Family of distributions with internal endpoint, algebraic zero $\rho_{sa,\beta}$	96
2.6.12	$\mathcal{L}_{n,p,\beta}$ ($\mathcal{R}_{n,p,\beta}$) in the bulk region	100
2.6.13	$\mathcal{L}_{n,p,\beta}$ ($\mathcal{R}_{n,p,\beta}$) in the anomalous regime and on the critical line	103
2.6.14	Section provisional conclusions	106
§2.7	The Dyck bound in the concave regime	107
2.7.1	Problem statement and models of random assignment considered	107
2.7.2	Choice of randomness for \mathcal{B} and \mathcal{R}	107
2.7.3	Synthesis of results	110
2.7.4	Basic facts	110
2.7.5	Basic properties of the optimal matching	111
2.7.6	Reduction of the PPP model to the ES model	113
2.7.7	The Dyck matching	115
2.7.8	Numerical results and the average cost of the optimal matching	122
§2.8	Chapter provisional conclusions and research perspectives	125
2.8.1	Convex regime	125

3 Field-theoretic approach to the Euclidean Random Assignment

Problem		131
§3.1	Random Assignment Problems on $2d$ manifolds	132
3.1.1	Regularisation through the integral of the zero-mean reg- ular part of the Green function	135
3.1.2	Zeta regularisation and the Kronecker mass	136
3.1.3	Connection between Robin and Kronecker masses	137
3.1.4	Applications	138
3.1.5	Numerical results	153
3.1.6	Uniform–Poisson transportation and grid effects	154

3.1.7	Section provisional conclusions	156
§3.2	On approximate linear relations among energies	157
3.2.1	General remarks	157
3.2.2	On linear relations in domains with no symmetries	161
3.2.3	Kronecker masses in the case of involutions	163
3.2.4	Section provisional conclusions	170
§3.3	The Lattice Helmholtz decomposition of the transport field on \mathbb{T}_2 at $p = 2$	171
3.3.1	Setup and notations	172
3.3.2	Longitudinal and transverse contributions to the ground state energy \mathcal{H}_{opt}	175
3.3.3	Synthesis of results	176
3.3.4	Statistical properties of $\Delta\phi$ and $\Delta\psi$ in coordinate repre- sentation	176
3.3.5	Two-point correlation functions	178
3.3.6	On $L^2 \langle \widehat{\Delta\phi} ^2 \rangle$ and $L^2 \langle \widehat{\Delta\psi} ^2 \rangle$	180
3.3.7	Section provisional conclusions and perspectives	184
4	Euclidean Random Assignment Problems at non integer Haus- dorff dimensions $d_H \in (1, 2)$	185
§4.1	Introduction	185
§4.2	Setup	186
§4.3	Choice of randomness	187
4.3.1	Peano fractal	187
4.3.2	Cesàro fractal	189
§4.4	Numerical protocol, data analysis, and results	191
§4.5	On the qualitative behavior of $\gamma_{(p,d_H)}^{\text{C(P)}}$ and evidence of universality	193
§4.6	Energy approximate linear relations	194
§4.7	Energy profile at fixed disorder along the $(2, d_H)$ line in the Cesàro fractal	196
§4.8	Conclusions and research perspectives	197
5	General provisional conclusions and research perspectives	198
	Appendices	208
A		209
§A.1	The number of edges of length $2k + 1$ in a Dyck matching at size n (§ 2.7.7)	209

§A.2	Expansion of the generating function $S(z;p)$ via singularity analysis (§ 2.7.7)	213
B		216
§B.1	The first Kronecker limit formula (§ 3.1.2)	216
C		218
§C.1	Calculus on the square lattice (§ 3.3)	218
Bibliography		221

List of Figures

1.1	Example Von Neumann game at $n = 5$	2
1.2	Typical time analysis of Jonker-Volgenant algorithm	4
1.3	Different dynamics of row-column-minima and saddle point configurations	13
1.4	Evidence of energy tradeoff around $p^* = 2$	14
1.5	Evidence for crossing of ground state energies as a function of energy-distance exponent	15
1.6	Evidence of transition around $p^* = 1$ at $d = 2$	16
2.1	Pictorial representation of the solution in one dimension	23
2.2	Example Grid-Poisson and Poisson-Poisson instance at $d = 1$	25
2.3	Sample path from the Brownian Bridge vs rescaled optimal transport field	26
2.4	Cumulative distribution function of \mathcal{H}_{opt} for the Grid-Poisson problem on the unit circle (theory vs experiments)	38
2.5	Comparison with numerical experiments (exponential and Rayleigh distributions)	48
2.6	Comparisons with numerical experiments (Pareto distribution)	50
2.7	Comparison with numerical experiments for the distribution in Eq. (2.5.3.18)	53
2.8	Comparison with numerical experiments (“gapped” distribution, Eq. (2.5.3.34))	56
2.9	Members from $\rho_{\text{fa},\beta}$ family and corresponding R_β functions.	85

2.10	Critical hyperbola separating the region of anomalous and bulk scaling for the class $\rho_{fa,\beta}$	89
2.11	Members from $\rho_{sa,\beta}$ family and corresponding R_β functions.	96
2.12	Critical hyperbola separating the region of anomalous and bulk scaling for the class $\rho_{sa,\beta}$	100
2.13	Example of instance encoding in the PPP model	108
2.14	The Dyck matching π_{Dyck} associated to the Dyck bridge σ in the example of Figure 2.13.	116
2.15	Numerical evidences for the Dyck upper bound conjecture	123
2.16	Fit of scaling coefficients as a function of p	124
2.17	State of the art on bulk scaling exponent depending on p	127
2.18	Supporting Figure to resarch problem 1	129
2.19	Supporting Figure to resarch problem 2	130
3.1	Pictorial representation of an assignment at $n = 3$ on a torus generated by quotient of \mathbb{R}^2 with a periodic lattice, with fundamental parallelogram and the corresponding base vectors.	140
3.2	Contour plot of $\Im(\tau) \eta(\tau) ^4$ in the complex plane τ	141
3.3	Relative differences on expected ground state energies on the rectangle $\mathbb{R}(\rho)$, on the torus $\mathbb{T}(i\rho)$ and on the Boy surface with respect to the case $\rho = 1$ as a function of ρ (theory vs experiments)	142
3.4	The Cylinder.	144
3.5	The Möebius strip.	145
3.6	The Klein bottle.	147
3.7	The Boy surface.	148
3.8	Absolute shift of ground state energies for the cylinder $\mathbb{C}(\rho)$, the Möebius strip $\mathbb{M}(\rho)$ and the Klein bottle $\mathbb{K}(\rho)$ with respect to the case $\rho = 1$ (theory vs experiments)	149
3.9	Typical scatter plot of numerical data ($n = 10^3$, 10^3 points) corresponding to $\delta E^{(1)}$ (Eq. 3.2.1.8) for a domain with an involution (see § 3.2.3).	160
3.10	Comparison of Eq. 3.2.2.5 (dotted black line) and results of numerical experiments, obtained by a linear fit as in Fig. 3.9 (blue dots with error bars). The horizontal black, dashed line denotes the value when the two involved sets have the same cardinality, $\alpha = 1$ ($\tau = 1/2$).	163
3.11	(Left) An instance from Example 2 ($n = 25$). (Right) An instance from Example 3 ($n = 50$).	165
3.12	Pictorial rules of lattice calculus for lattice diagonal derivatives and laplacian	174
3.13	Direct estimation of sub-leading constant	177

3.14	Histograms of rescaled laplacians of ϕ and ψ fields, and symmetrized log probability functions (experiments vs fits)	177
3.15	Experimental evidence for the inequality 3.3.4.1	178
3.16	Expected contributions of Fourier modes to the ground state energy at $n = 2116$, and trigonometric functions sharing the same symmetries	182
3.17	Fits of longitudinal contribution and transverse contribution in $1/n$	183
4.1	Example instances on the Peano fractal at increasing Hausdorff dimensions ($n = 2^{12}$)	188
4.2	Example instances on the Cesàro fractal at increasing Hausdorff dimensions ($n = 2^{12}$)	190
4.3	Empirical evidence for universality	193
4.4	Example approximate energy linear relations at varying d_H (Peano fractal at $p = 2$)	194
4.5	Avg. energy profiles on the Cèsaro fractal at $p = 2$ at varying d_H .	196
4.6	Universality for the problem on Peano and Cesàro fractals at (example at $(d_H, p) = (1.5, 1.33)$)	197
5.1	Example instance of an ERAP on a Brownian loop ($n = 2^{12}, p = 1$)	204

≈ CHAPTER 1 ≈

INTRODUCTION

This chapter starts with a “promenade” through various concepts and ideas which we have been able to identify as a plausible background to this work. We favor a discursive style and give priority to motivations over completeness, providing to the interested reader some entry points to (many) related literatures through reviews and milestone papers. Emphasis is put on existing methods and relevant connections with other topics. In doing so, we wish to convey at least in part the remarkably unifying ideas which underlie our discussion and, hopefully, some reasons to consider any of them in the light of the problem considered in this PhD Thesis, the “Euclidean Random Assignment Problem”. A self-contained definition of this problem is given § 1.3, which can be used as a reference for the remaining part of the manuscript, and it is followed by an example where we discuss the physical notion of level crossing in an algorithmic setting. A discussion of some possibly interesting connections with other problems at the interface of theoretical physics, mathematics and theoretical computer science follows. The chapter ends with the plan of the manuscript and a list of novel contributions contained in this work.

1.1. Background

IN a seminar held at Princeton in 1951 and reported in the second volume of the series “Contributions to the Theory of Games” (14), von Neumann considered the following two-person, non-cooperative zero-sum game (11). There is a square $n \times n$ battlefield (like a $n \times n$ chessboard) and the positions of this battlefield are worth some amount of money which is encoded by a square cost matrix m_{ij} , $i, j = 1, \dots, n$. There are two players: let us call them G and LV. G chooses (or “hides” under) one position of the battlefield with n^2 choices (G’s pure strategies). LV, unaware of G’s choice, guesses either a row or a column (or “seeks” G), with $2n$ choices (LV’s pure strategies). The rule of this game is that if LV finds G at position (i, j) , then G gives m_{ij} to LV; otherwise, G keeps that money for himself. How should G play in order to maximize his return in the long term?

The answer to this question is considerably simplified if G abandons a deterministic approach and thinks in terms of a *probability distribution* over the set of possible choices (also called a mixed strategy in game theory). In this light, what

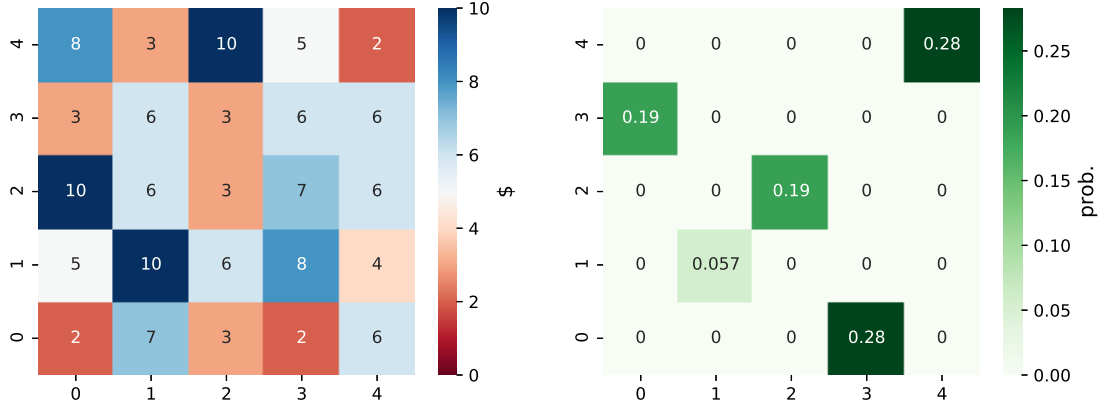


Figure 1.1. – (Left) Example battlefield m for von Neumann’s game at $n = 5$ (annotated prizes are in \$ currency). (Right) G ’s optimal mixed strategy for the battlefield on the left requires G to choose $m_{4,4} = 2\$$ (upper right corner) about 7 times in 25 turns, and $m_{1,1} = 10\$$ slightly more than 1 time out of 20 turns (but never the other 10\$ bills).

von Neumann’s paper shows is that the optimal mixed strategy depends on a small proportion of positions (i.e. n out of the n^2 available positions). These n positions are found by interchanging the columns (or rows) of the matrix $c_{ij} := -1/m_{ij}$ until its trace is minimal. Rows and columns incident to those n positions span the whole battlefield, thus identifying one out of the $n! = n(n-1) \cdots$ ways of placing n rooks (chess pieces) at non-attacking positions onto the $n \times n$ chessboard (an example game at $n = 5$ is given in Fig. 1.1). These special n positions constitute an *assignment* of n row elements to n column elements (and vice-versa), and can thus be specified by a permutation of n objects, which we will generically call $\pi_{\text{opt}}^* \dagger$. The problem of finding a π_{opt} is usually called “the assignment problem[‡]”

*A permutation of a finite set is a bijection on that set. The set of all permutations equipped with composition “ \circ ” is a group called the symmetric group which we denote by \mathcal{S}_n . In the game of von Neumann, if G looks for a rearrangement of rows instead of columns (i.e., if G “rotates” the battlefield by an angle $\frac{\pi}{2}$), he finds the permutation π_{opt}^{-1} , the unique group inverse of π_{opt} satisfying $\pi_{\text{opt}} \circ \pi_{\text{opt}}^{-1} = \pi_{\text{opt}}^{-1} \circ \pi_{\text{opt}} = (1, \dots, n)$ in one line notation.

[†]von Neumann (14) also shows that, rather intuitively, G ’s should think probabilistically and choose the position $\{(k, \pi_{\text{opt}}(k))\}_{k=1}^n$ with probability proportional to $1/m_{k, \pi_{\text{opt}}(k)}$ (the higher the reward, the higher the chance of LV considering a row or column containing that position). von Neumann’s seminal contribution has been extensively discussed later on, possibly due to its many connections with other important problems at the time, such as the Birkhoff-Von Neumann Theorem on doubly stochastic matrices (see e.g. (12)) (to not be confused with the anterior pair of fundamental works (5, 7) by the same authors concerning ergodic theory), or with the problem of allocation of indivisible resources in economics (16).

[‡]An assignment problem is a linear combinatorial optimisation problem in which the function to be minimised (the cost or energy function) is a sum over the entries of a cost matrix. For this reason, it

and the assignment defined by π_{opt} is usually called an “optimal assignment” (since in general there may be more than one π_{opt}).

Fortunately, G can avoid to test every possible permutation, since finding an optimal assignment given the cost matrix requires a number of operations which is a power of n at worse, as it seems to have been known for a long time: other than to von Neumann himself (see (14), end of pag. 5), it has been recently discovered (126) that a procedure for finding the optimal assignment in a matrix of positive integers was known already to Jacobi[§].

One of the best-known methods for solving the assignment problem has been popularised by Kuhn (15), who termed it “the Hungarian method” in honor of a fundamental notion of “duality”[¶] introduced by magyar mathematicians König (4) and Egerváry (6). The Hungarian method solves an assignment problem in worst case $\mathcal{O}(n^3)$ time complexity (17) (incidentally, the same complexity of Gaussian elimination in linear algebra). After the Hungarian method, several algorithms for solving the assignment problem (such as the so-called “primal-dual algorithms”) have been developed (45). Our favorite one is the Jonker-Volgenant algorithm (46), which we have described and tested elsewhere (see (151), Chapter 2); among the other polynomial algorithms for finding a π_{opt} based on different strategies, among the most used algorithms there are the network flow approach (24), the simplex method (22) (see (52) for an historical account), or more recently the auction algorithm (see (71), Chapter 7). The interested reader is referred to (84) for a comprehensive review on the matter.

Large assignment problems served also as computational benchmarks for com-

is sometimes called “Linear Sum Assignment Problem” (see e.g. (80)). Linearity of the cost (or objective) function and convexity of the search space –which is a convex polytope in \mathbb{R}^{n^2} called “Birkhoff polytope” comprising the set of all doubly stochastic matrices– are the fundamental properties that make the assignment problem special among otherwise very similar combinatorial optimisation problems.

[§]In a paper appeared in Crelle’s journal in 1860, communicated posthumously by Weierstrass (140), Jacobi was concerned with the problem of bounding the order of a system of ordinary differential equations. He had already shown the equivalence of this problem to the reduction of certain tables of positive integer numbers representing the order of equation i in variable j , called therein “*schema*” (corresponding to our cost matrix c –recall that the term “matrix” has been introduced only around 1850 by Sylvester, see (135)–), to special tables called “*canones*” (namely, matrices with their maxima in non-attacking rook positions). Within this context, Jacobi discusses a procedure to reduce *canones* to certain *canones simplicissimi* by means of elementary operations, and even gives some application of his procedure to a few 7×7 examples (see (140), pag. 308).

[¶]We are referring here to the bijection between maximum matchings and minimum vertex covers in bipartite graphs, which usually goes under the name of König’s theorem (133). Duality is a sort of leitmotiv in several related problems. We may mention the “Monge-Kantorovich” duality, which arises in the problem of optimal transport of continuum measures. Interestingly, Kantorovich, who played a crucial role in the development of linear-programming (19), is also considered to be one of “the founding fathers of optimal transport” (see (127), pag. 43). Or also the other “duality”, which was implicit in the von Neumann’s game, since LV ’s mixed strategy is “dual” to G ’s in the sense that it is uniquely defined by the latter at the Nash equilibrium of the game.

puting systems already since the early nineties (59). Nowadays, a π_{opt} for a typical dense matrix can be found in less than one second for sizes up to $n \approx 1000$ with common hardware, and roughly less than one minute for n up to 10^4 (Fig. 1.2). Therefore, one may arguably say that the problem of quickly finding a solution has been successfully tied to the technological development for most practical purposes. Notably, this is a consequence of the remarkable mathematical properties of the objective function and search space: the extrema of a *linear* function over a convex set (the set of all convex combinations of the permutations of n objects, also called the Birkhoff polytope) are attained at extremal points (i.e., permutations), modulo possible inessential unicity issues.

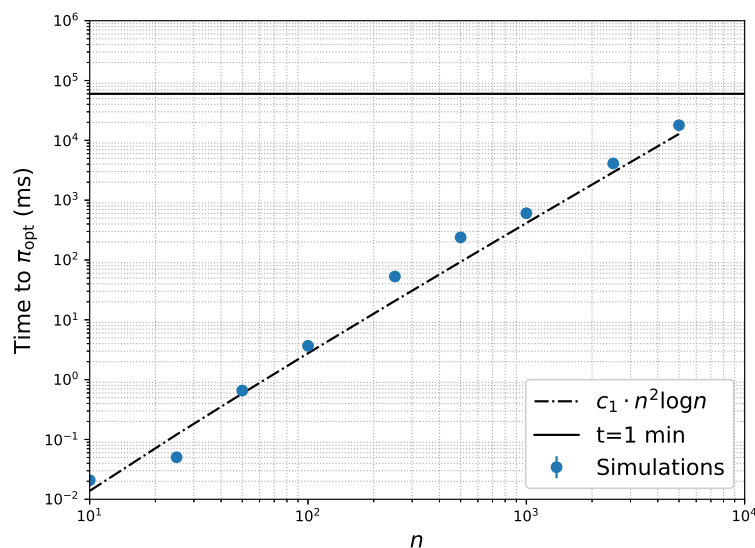


Figure 1.2. – Average time to solution for the assignment problem (*y*-axis) as a function of matrix size (n , *x*-axis). The benchmark has been performed on a 2014 laptop using a 2,5 GHz Intel Core i7 processor, using the Jonker-Volgenant algorithm (46) on $n \times n$ matrices with *i.i.d.* standard normal random entries, in the range $n = 10$ to $n = 5000$ (average over seven independent runs for each n). A least square fit is reported in dash-dotted trait to aid the eye.

A major conceptual breakthrough came in the eighties and involved the removal of a second, completely different layer of deterministic reasoning. Going beyond the specific solution to a combinatorial optimisation problem[‡] at fixed instance, it

[‡]A combinatorial optimisation problem consists in studying the extrema of a real-valued function (sometimes called objective function) defined on a space of finite cardinality (sometimes called search space). See e.g. (38) for an elementary introduction to classical combinatorial optimisation problems with applications to applied problems such as car pooling and the construction of phylogenies.

was realized that, when considering instead random instances of an optimization problem, the typical properties of the solution were accessible with the methods of statistical mechanics in the presence of a quenched randomness (in our case of the assignment problem/von Neumann’s game, this amounts to think at the prizes of matrix m as random variables). The new viewpoint has been pioneered by physicists Mézard and Parisi (40), and Orland (41), who considered some *statistical properties* of minimum weight perfect matchings of the random complete (bipartite) graph (40). The basic idea, which dates back at least to Kirkpatrick et al. (36), is to interpret the problem as a single disordered physical system, and recover the optimal solution as a suitable zero temperature limit of a quenched free energy. Generally, the constraints of the underlining combinatorial problem forbid the existence of microscopic configurations satisfying all the couplings, which is a well-known feature arising in the physics of *disordered* physical systems called *frustration* (31, 44). In particular, the ground state of the system corresponds to the ensemble of globally optimal solutions induced by the distribution of random interactions, and may share the original, fixed instance symmetries only *on average* **. Of course, while this program is appealing, one may argue that 1) there is a certain degree of arbitrariness in considering a “stochastic” version of the assignment problem (instead of other problems), also in consideration that we have not yet motivated such an effort with practical problems where this study may be useful; and 2) the game may not be worth the candle, due to possible specificities of the assignment problem which are not shared by other combinatorial problems. Indeed, what does make the assignment problem so special, among other problems? We shall try to address point 2) in § 1.4 by showing that, before any further developments, stochastic assignment problems are a suitable test-ground for investigating even advanced features of disordered systems, such as level crossing, in an extremely simple way. We believe that this feature, besides its clear pedagogical value, can be useful in the challenge of understanding finite dimensional disordered systems. In order to partially address point 1), in the next section we shall take a small detour to review the development of the simplest, and most studied (mean-field) stochastic version of the assignment problem, and some further remarks on the nature and implications of statistical physics approaches in this area.

**A detailed discussion of the several applications of methods and ideas from the statistical physics of disordered systems to ensembles of combinatorial optimisation problems is beyond the scope of the present work. The interested reader is referred to the classical book (44) for an introduction, and to (90) and (124) for discussions more oriented towards information theory and interdisciplinary applications.

1.2. Random Assignment Problems and extensions

IN the “random assignment problem ^{*}” (40, 41) the cost matrix becomes a random matrix with independent and identically distributed entries. The problem has been studied extensively, so that we can take its historical development as an opportunity to illustrate a nice example of fruitful interaction between physicists, mathematicians and theoretical computer scientists around the broad themes of *universality* and *phase transitions*.

Concerning the first theme, in (40) Mézard and Parisi showed that considerable insight on the problem can be obtained by looking only at the very small edges. More precisely, by means of the replica method, they have shown that the (appropriately rescaled) large n limit of the expected optimal cost (that is, the expected ground state energy in the physical picture) depends on just a real number r , the leading exponent in the small argument expansion of the involved probability density function[†]. In particular, at $r = 0$ (that is, for probability distributions taking a finite value at zero), the limit is given by the non-trivial constant $\zeta(2) = \frac{\pi^2}{6}$ [‡], a remarkable result that was rigorously proven[§] about fifteen years later by Aldous (88).

In the meantime, Parisi uploaded a preprint on the arXiv (77) claiming the much stronger conjecture that the *exact*, finite n expected value of the optimal cost in the random assignment with i.i.d. exponential entries of unit mean equals $\sum_{k=1}^n 1/k^2$ (unpublished). Proofs of the Parisi conjecture, and of its generalisation to the case of rectangular assignment cost matrices termed the Coppersmith-Sorkin

^{*}The random assignment problem has been conceived as a mean-field (or infinite-dimensional) model of “spin glass”. Spin glasses were originally introduced by Edwards and Anderson (25) as theoretical models for understanding experiments showing sharp peaks in the susceptibility of certain magnetic alloys (see e.g. (42) for a review). A well-studied model of mean-field spin glass is due to Sherrington and Kirkpatrick (26, 32). The SK model is often called an “infinite-dimensional” (or also “fully connected”) model because (roughly speaking) the microscopic configurations consist of Ising spins placed on the vertices of the complete graph K_n , and interacting through $\binom{n}{2}$ centered and independent random normal interactions (see (142) for a comprehensive review). The solution of the SK model is due to Parisi (33–35) and has been put on rigorous grounds by Talagrand (113) building on ideas by Guerra (97).

[†]Loosely speaking, the universality of r in $\rho(x) \sim x^r$ as $x \rightarrow 0$ is understood in terms of the leading tail behavior of the Laplace transform of $\rho(x)$

$$\int_0^C dx e^{-tx} x^r \sim t^{-(r+1)}$$

for large t .

[‡]An early investigation of the value of the limit constant in the case of matrix entries uniformly distributed in $[0, 1]$ is due to Donath (23).

[§]Together with the possibly counter-intuitive result, also derived in (40), that the probability for a link of arbitrarily small length to enter an optimal assignment is roughly $1/2$.

conjecture (73), have appeared later on (98, 107), resulting in a number of probabilistic and combinatorial results of independent interest. Random assignment problems and extensions, and more generally statistical properties of Euclidean functionals of discrete sets (58) remain a topic of mathematical interest especially in probability, where more recently some work has been devoted to study recursive distributional equations in connection with the cavity method (105). Existence and unicity of a relevant quantity in the whole range $r \in (0, \infty)$ for this problem, the so-called Parisi order parameter, has been proven only recently (146, 150).

If cross-fertilization between statistical physics and probability around the theme of universality may certainly appear not at all surprising, it is remarkable that methods from statistical physics of disordered systems have been useful also at a research frontier in the direction of theoretical computer science. This frontier, broadly speaking, aims at understanding and quantifying the complexity of combinatorial problems borrowing from physics the notion of *phase transition*.

Following (86), let us recall first that a possible measure of complexity of a problem [¶] involves the largest possible time spent by an algorithm for finding the solution, depending on the size of the problem (worst-case analysis). After devising the algorithm, one derives the leading scaling behavior of the largest time to solution over a given class of instances, depending on the size n . If such leading scaling is a polynomial, the problem belongs to the P class. Besides the assignment problem, other well-known P problems are to find a spanning tree of minimal total weight on a weighted graph (MST) (which is solved in polynomial time with greedy methods such as Prim's algorithm (133)) and to test whether a given number is prime (101). However, there are also problems for which it is not known if a polynomial time algorithm for finding an optimal solution exists but, instead, the optimality of a known solution "given by an oracle" can be certified in polynomial time (NP problems). Lastly, the NP class contains a sub-class of problems, termed NP -complete problems, comprising the hardest NP problems, and the general opinion is that a polynomial time algorithm for solving them does not exist. A prototypical example is to find the shortest closed path among a set of n cities, visiting each city exactly once, also called the Traveling Salesman Problem (TSP). Many efforts have been devoted to this problem since it can be shown that a polynomial algorithm for the TSP could be used to solve any other NP -complete problem in polynomial time. Indeed, establishing if there are NP problems which are not in the P class is a formulation of the well-known $P \stackrel{?}{=} NP$ problem, a major open theoretical problem in computational complexity theory. However, a major

[¶]The classification into complexity classes refers more properly to decision problems. However, any optimization problem can be casted as a decision problem upon application of a threshold (for example, in the von Neumann's game, given a battlefield m , should G expect to gain more than 10 \$ applying its optimal mixed strategy?). In our discussion, when discussing complexity of an optimization problem, we shall always implicitly refer to its decision version.

contribution of the statistical mechanical approach has been to focus on the average properties of the solution, which can be quite different from the worst case one. Indeed, for several random such problems (such as the two dimensional random decision version of TSP (63)), a scalar parameter could be identified, exhibiting a critical value associated to the onset of hard instances, in analogy with the behavior of an order parameter in the physics of phase transitions. Perhaps the most known success in this area is due to Mézard–Parisi–Zecchina, who have shown that, for the random 3sat (a *NP*-hard decision problem), the parameter is the ratio of variables over clauses, and unveiled a SAT-UNSAT transition in the phase diagram following the spin glass interpretation (93). Moreover, the information gained from their analytic approach could be used to build performing algorithms for finding the solution in particular regions.

Coming back to the random assignment, the general belief is that, qualitatively, there should be no such phase transition[‡]. However, an extension of the random assignment problem to the case of k partite graphs has been proposed, termed the Multi-Index Matching Problem (104) (MIMP). In a MIMP (which is *NP*-hard for $k \geq 3$) it has been shown by means of the cavity method that the replica symmetric phase is unstable below a critical temperature, requiring replica symmetry to be broken for consistency (106). The results were extensively supported by numerical experiments but still await to be put on rigorous grounds.

Despite its own interest, in this work we shall not discuss further the infinite dimensional random assignment problem (nor any other mean-field model), nor pursue further the theme of phase transitions and computational complexity which, for the problem that we are going to discuss, is still at its infancy (if not its conception..), and will be addressed only indirectly. For a review on the statistical mechanical approach to phase transitions in optimization problems, the reader may consult (89) and the references therein; for recent results on the random assignment problem with usual methods from statistical physics, see our recent paper (153). Besides an extended review of the problem, it contains an analytical derivation (using the replica method under the replica symmetric ansatz), comforted by numerical experiments, that the aforementioned Mézard–Parisi universality property does not persist at the level of sub-leading asymptotics, with an example in which one can infer whether the support of the distribution is finite from the sign of the finite-size correction.

[‡]This on the account that the solution, which has been obtained under the so-called ansatz of replica symmetry (40), has been confirmed a posteriori by independent rigorous methods. However, direct arguments are still lacking (to the best of our knowledge).

1.3. The Euclidean Random Assignment Problem

INSTEAD, this manuscript concerns a different stochastic assignment problem, which also had early consideration by Mézard and Parisi as a prototypical model of finite-dimensional spin glass (50). At instance with the random assignment problem, which in some cases can be considered as its “mean-field” approximation, the problem is termed *finite-dimensional* since, heuristically, it involves microscopic variables placed in a d -dimensional space, in analogy with finite-dimensional spin glasses. A first motivation to undertake this effort is that spin glasses, despite their breakthrough role in recent years, have shown to be quite hard to solve (to find the ground state energy of a Sherrington-Kirkpatrick model is NP -hard) so that, in certain respects, they remain mysterious especially beyond the mean-field approximation, where they face difficulties even numerically. Thus, the development of a theoretical framework that goes beyond mean-field while sharing all the basic features of a spin glass (namely disorder and frustration) and remains manageable (both to analytical and computational investigations) may be of value.

In this model the microscopic laws of interaction are given once and for all. The quenched randomness, instead that to edges, is now associated to the random positions of some “elementary constituents” (i.e. to vertices of the bipartite graph) placed in an otherwise homogeneous ambient space. This assumption complicates considerably the study of typical properties. The “elementary constituents” model atoms or impurities. Mathematically, they are two families of n elements each: they can be represented as the vertex set $V(\mathcal{K}_{n,n})$ of a complete bipartite graph $\mathcal{K}_{n,n}$ (that is, elements correspond to the two partite sets of the graph). For the sake of brevity, from now on we will refer to such families (or equivalently to their graph theoretical representation) as “blue” and “red” points, and reserve for them two special symbols: \mathcal{B} and \mathcal{R} . Lastly, the choice of randomness for modeling the positions of \mathcal{B} and \mathcal{R} depends on the kind of questions that one may want to ask, and some assumptions will be necessary. For example, if \mathcal{B} and \mathcal{R} are ink particles that have been vigorously mixed in a glass of water, the assumption of \mathcal{B} and \mathcal{R} uniformly distributed in the water volume appears to be reasonable for most practical purposes; on the contrary, if \mathcal{B} are bikes which must be reported to deposit rackets (\mathcal{R}) in the city of Paris, the assumption of uniform distribution for \mathcal{R} does not appear to be appropriate.

To accommodate ourselves in a sufficiently general setting, we shall assume that $\mathcal{B} = \{b_i\}_{i=1}^n$ and $\mathcal{R} = \{r_j\}_{j=1}^n$ are families of i.i.d. random variables distributed according to some measure ν (which is a datum of the problem). For example, in a typical scenario, ν will be supported on (a subset of) a metric space \mathcal{M} ;

or the points of one color (as the rackets in the Paris example were) are fixed on a deterministic d -dimensional grid, and the others are i.i.d. random variables as above (otherwise we would have no randomness). In any case, we will call the probability distribution associated to the measure ν the *statistical ensemble* or *disorder distribution*, and name the datum of \mathcal{B} and \mathcal{R} sampled from such a distribution an *instance* or *realisation of the disorder*. The interaction between b_i and r_j (that is, the cost of assigning b_i to r_j) has an intensity $c_{ij} := c(b_i, r_j)$ for some function $c : \mathcal{M} \times \mathcal{M} \rightarrow \mathbb{R}$. The n^2 real numbers $\{c_{ij}\}_{i,j=1}^n$ (which may be taken to be positive w.l.o.g.) can be arranged into a non-symmetric, $n \times n$ assignment cost matrix

$$c = \begin{pmatrix} c(b_1, r_1) & c(b_1, r_2) & \dots \\ \vdots & \ddots & \\ c(b_n, r_1) & & c(b_n, r_n) \end{pmatrix}, \quad (1.3.0.1)$$

which can be interpreted as the weighted adjacency matrix of the underlining graph $\mathcal{K}_{n,n}$. A first equivalent but more succinct statement in physical language is that the hamiltonian for this system comprises only inter-color, two-body interactions*. The essential feature preventing this framework from modeling e.g. a two-components plasma, is that once a blue is coupled to a red in a configuration, it “disappears” from the system. We shall encode a configuration by a permutation $\pi \in \mathcal{S}_n$ with energy

$$\mathcal{H}(\pi) = \sum_{i=1}^n c_{i\pi(i)} = \text{Tr} [P_\pi c], \quad (1.3.0.2)$$

where P_π is the permutation matrix of π (that is, $P_{i,j} = \delta_{j,\pi(i)}$). More generally, the cost function \mathcal{C} may play the role of an energy, of a fitness function, or of a more general distance[†] in the problem of interest (such as hamming distance, if \mathcal{B} and \mathcal{R} represent strings taken from an alphabet). In order to share basic requirements for a physical system at criticality, and namely translational, rotational and scale invariance, in this work we shall restrict ourselves to a cost function $\mathcal{C} : \mathbb{R} \rightarrow \mathbb{R}^+$ which is a simple monomial $|x|^p$ in the underlining distance function \mathcal{D}^\ddagger , namely

$$c_{ij}^{(p)} = \mathcal{C}(\mathcal{D}(b_i, r_j)) = \mathcal{D}^p(b_i, r_j), \quad i, j = 1, \dots, n, \quad (1.3.0.3)$$

*That is, in an analogy with electrostatics where \mathcal{B} and \mathcal{R} represent respectively positive and negative unit electrostatic charges, we shall neglect Coulomb repulsion.

†In principle, one can consider even more general cost functions $\mathcal{C} : \mathcal{M} \times \mathcal{M} \rightarrow \mathbb{R}$, but we will not discuss this case further here.

‡We recall that a distance \mathcal{D} on a metric space \mathcal{M} is a symmetric and positive definite binary map $\mathcal{D} : \mathcal{M} \times \mathcal{M} \rightarrow \mathbb{R}^+$ which satisfies the triangular inequality. If not obvious from the context, we will indicate a metric space with the explicit writing $(\mathcal{M}, \mathcal{D})$.

where we have stressed the dependence of the matrix c on the real number p , termed the “energy-distance” exponent. In this work, \mathcal{D} will be almost exclusively d -dimensional Euclidean distance, but it is understood that other choices for the metric \mathcal{D} are possible. Finally, an optimal assignment π_{opt} satisfies

$$\mathcal{H}_{\text{opt}} := \mathcal{H}(\pi_{\text{opt}}) = \min_{\pi \in \mathcal{S}_n} \mathcal{H}(\pi), \quad (1.3.0.4)$$

where the random variable \mathcal{H}_{opt} is called the *ground state energy*.

The choice of a metric space $(\mathcal{M}, \mathcal{D})$, of a statistical ensemble for the random positions of \mathcal{B} and \mathcal{R} , and of an exponent p identifies a well-defined stochastic assignment problem which is called the **Euclidean Random Assignment Problem** (or “**ERAP**” for brevity). A study of statistical properties of \mathcal{H}_{opt} depending on the triple $((\mathcal{M}, \mathcal{D}), (\nu_{\mathcal{R}}, \nu_{\mathcal{B}}), p)$ constitutes the main contribution of this manuscript.

1.4. On approximate solutions and level crossing

LET us expand on the statistical mechanical approach to the ERAP and point out some qualitative features of the problem as further motivations to our work. We will consider a two-dimensional system, which in several respects is the most interesting case*, and discuss, at a fixed realization of the disorder as a function of p ,

- ▶ a study of the energy of two canonical excited states, obtained via two simple greedy heuristics;
- ▶ an analysis of the ground state energies and their relative rank as p varies;
- ▶ an investigation of the distribution of the Euclidean lengths of the edges entering in the ground state.

In the first case, it will turn out that the greedy heuristics are not strikingly good, in the sense that the energies of these canonical but otherwise generic states are not good approximations of the ground state, and that moreover their performances appear to exhibit (statistically) a cross-over as a function of p . In the second case, we will show that ground states energies at $p < 1$ ($p > 1$) appear to have a defined order at $p < 1$ ($p > 1$), and that such ordering is reversed at $p > 1$ ($p < 1$) through level crossings in between. Optimal solution at $p > 1$ are typically bad

*For the sake of definiteness, we will consider here a specific statistical ensemble (a “Grid Poisson ERAP on the unit square”, see § 3.3 for definitions), but it should be noted that our analyses, which depend only on the cost matrix, may be of possible interest also beyond the ERAP setting.

candidate solutions at $p < 1$, and viceversa. In the third case, we will show that the distribution of the lengths appears to display a transition from a bell-shaped one at $p > 1$ to a bi-modal one (with an algebraic tail for large values of the Euclidean length) at $p < 1$, a further signature of the persistence of the well-understood transition in the one dimensional problem (see § 2.1 for details). The presence of such interesting cooperative effects can be taken as an indication that the system is poised, in some sense, near a critical point (even at zero temperature).

1.4.1. On approximate solutions and greedy heuristics

Algorithm 1: Row-column minimal configuration	Algorithm 2: Saddle point or row-column minimax configuration
Input : Cost matrix $c^{(p)}$	Input : Cost matrix $c^{(p)}$
Output : Permutation π_{rcm}	Output : Permutation π_{sp}
<pre> 1 Function <u>rcm</u>($c^{(p)}$): 2 $\pi_{\text{rcm}} \leftarrow \text{void}$ 3 $i \leftarrow 0$ 4 while $i < \text{size}(c^{(p)})$ do 5 $(j, k) \leftarrow \arg \min c^{(p)}$ 6 $\pi_{\text{rcm}}(j) \leftarrow k$ 7 $c^{(p)}(j, :) \leftarrow +\infty$ 8 $c^{(p)}(:, k) \leftarrow +\infty$ 9 $i \leftarrow i + 1$ 10 end 11 return π_{rcm} </pre>	<pre> 1 Function <u>sp</u>($c^{(p)}$): 2 $\pi_{\text{sp}} \leftarrow \text{void}$ 3 $i \leftarrow 0$ 4 while $i < \text{size}(c^{(p)})$ do 5 $(j, k) \leftarrow \arg \max_{l \in \text{rows}} \left(\arg \min_{s \in \text{columns}} c^{(p)} \right)$ 6 $\pi_{\text{sp}}(j) \leftarrow k$ 7 delete row j in $c^{(p)}$ 8 delete column k in $c^{(p)}$ 9 $i \leftarrow i + 1$ 10 end 11 return π_{sp} </pre>

For a fixed instance with points \mathcal{B} and \mathcal{R} , besides π_{opt} , consider the following configurations:

- a configuration π_{rcm} (from “row-column-minimal”) obtained in a greedy approach made of successive “annihilation” of nearest neighboring blue and reds (Algorithm 1). In this case, the energy increment at algorithmic time i is strictly monotone increasing in i (Fig. 1.3, blue continuous trait).
- A configuration π_{sp} (from “saddle point”) obtained iteratively matching the farthest blue among the $n - i$ available ($i = 0, \dots, n - 1$) in the set of nearest neighbors of red points, and annihilating that pair (Algorithm 2). Now the energy increment at algorithmic time i is not anymore monotone in i , and

large spikes (reflecting the geometry of the underlining space) appear on top of a roughly constant (if slightly decreasing) baseline (Fig. 1.3, orange dashed trait).

Let us denote with $\mathcal{H}_{\text{label}}^{(p)}$ the energy at a fixed disorder with exponent p for configuration π_{label} , with label $\in \{\text{opt}, \text{rcm}, \text{sp}\}$. Our numerical experiments indicate that there exists a p^* (close to 2), such that, on average, in the limit $n \rightarrow \infty$, $\mathcal{H}_{\text{rcm}}^{(p)} < \mathcal{H}_{\text{sp}}^{(p)}$ if $p < p^*$, and $\mathcal{H}_{\text{rcm}}^{(p)} > \mathcal{H}_{\text{sp}}^{(p)}$ if $p > p^*$ (our findings may even be true in the almost-sure sense, see Fig. 1.4).

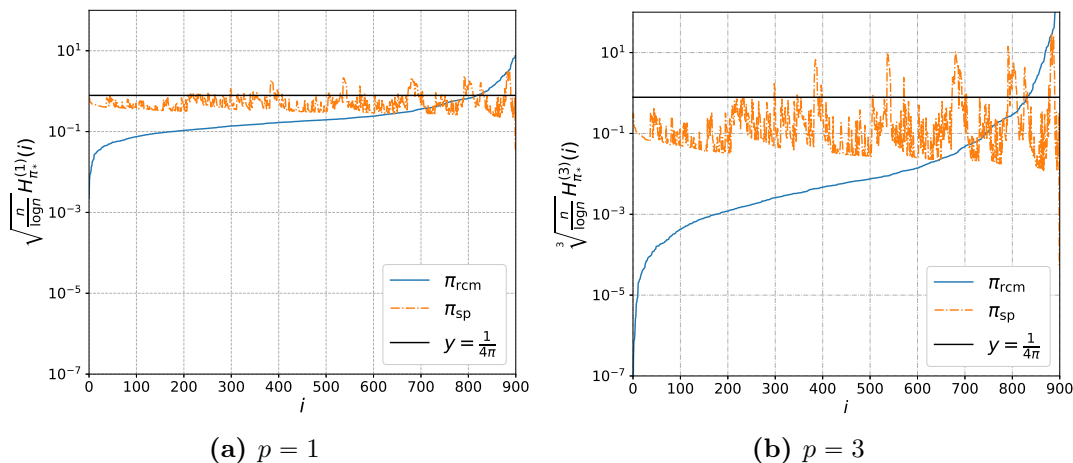


Figure 1.3. – Energy contributions along the execution of algorithms 1 and 2, normalised at the AKT scale, for $p = 1$ (Fig. 1.3a) and $p = 3$ (Fig. 1.3b) at the same disorder (the corresponding total energies are the areas under the curves). The black line is the $n \rightarrow \infty$ limit average contribution of each edge at $p = 2$. Notice the large fluctuations of the π_{sp} trajectories.

Both procedures are faster than the Hungarian algorithm, but their energy difference with the optimal solution trade places with p . In the present case, π_{rcm} is more suitable when the most important aspect of the optimal strategy is not to miss the shortest edges, which is the case when p is small, while π_{sp} is more suitable when the most important aspect of the optimal strategy is not to be forced to use any long edge, which is the case when p is large (notice that the one dimensional ERAP in the $p \rightarrow \infty$ limit, can be understood as a minimax problem, see (144), Eq. 6).

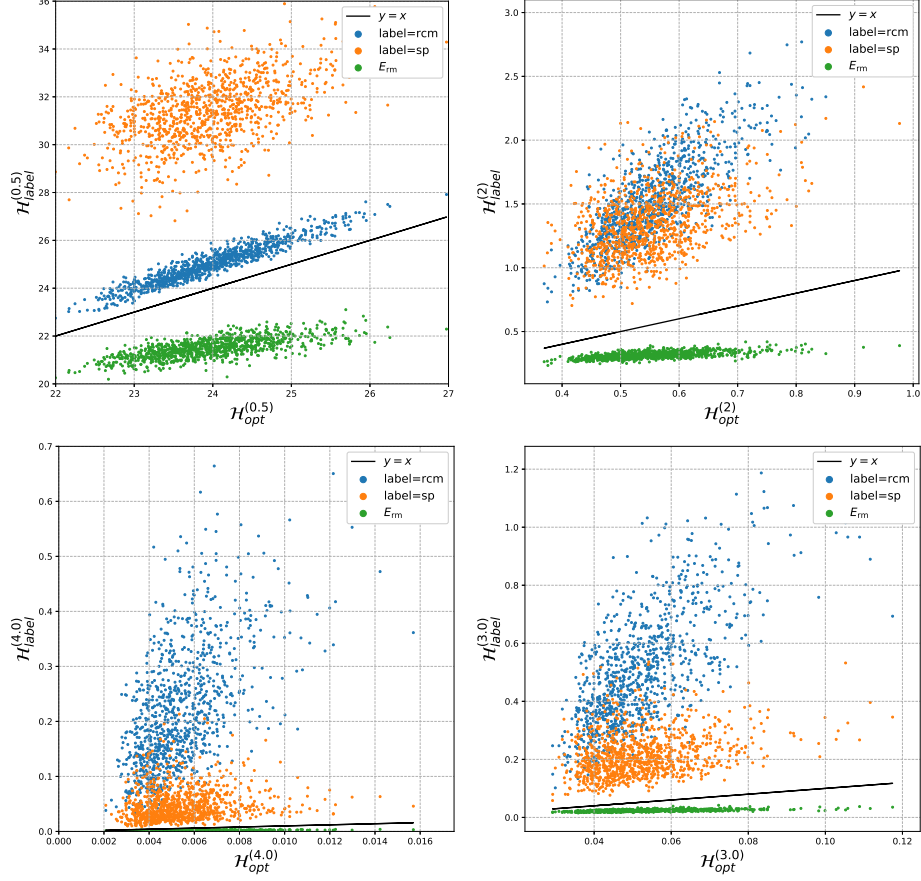


Figure 1.4. – Scatter plots of \mathcal{H}_{opt} (x -axis) vs excited states energies (y -axis, colors) at fixed disorder. The exponent p increases from top-left ($p = .5$) to bottom left ($p = 4$) in clock-wise order, \mathcal{H}_{rcm} corresponds to blue dots, and \mathcal{H}_{sp} to orange dots ($n = 100, 10^3$ realisations). As a function of p , the blue and orange clouds positions relative to the black line (bisector) invert. For comparison, we display also the energy associated to the n row minima E_{rm} (green points), which gives an absolute lower bound –and it is bounded above by the column minima due to our choice of the disorder– but does not generically correspond to a permutation.

1.4.2. On crossings of ground state energies

For a fixed instance of \mathcal{B} and \mathcal{R} , and n large, let $\pi_{\text{opt}}^{(p)}$ be the optimal assignment at exponent p , and let $\mathcal{H}^{(p_1)}(\pi_{\text{opt}}^{(p_2)})$ be the energy for the ground state at $p = p_2$, evaluated at exponent p_1 . By definition, if $p_1 \neq p_2$ then $\mathcal{H}^{(p_1)}(\pi_{\text{opt}}^{(p_2)}) \geq \mathcal{H}^{(p_1)}(\pi_{\text{opt}}^{(p_1)}) = \mathcal{H}_{\text{opt}, p_1}$. One can easily obtain the energy profile $\mathcal{H}^{(p_1)}(\pi_{\text{opt}}^{(p_2)})$ as a function of p_1 , and study these profiles for states that are optimal for at least one value of p_1 (in the considered list). In one dimension, the profiles collapse at $p_1, p_2 > 1$, since $\pi_{\text{opt}}^{(p)}$

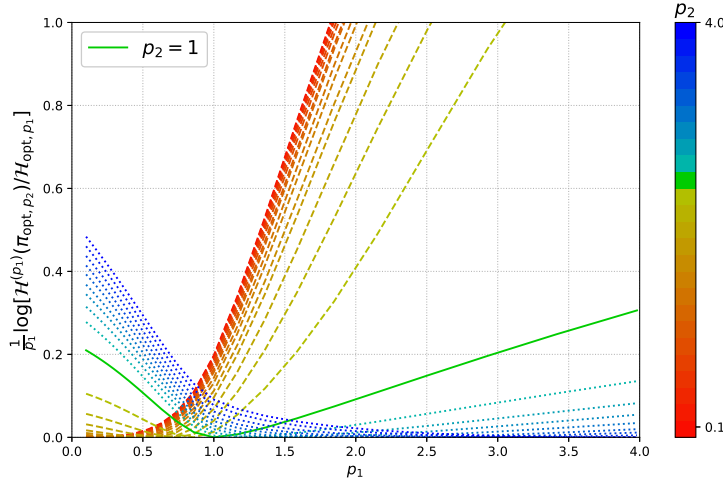


Figure 1.5. – Energy profiles for ground states at $p_2 > 1$ (dotted lines, cold tones) and $p_2 < 1$ (dashed lines, warm tones) depending on p_1 . Energy is measured in units of $\mathcal{H}_{\text{opt}, p_1}$, and we display its logarithm divided by p_1 to better display the small p_1 region for visualization purposes. Protocol: 25 values of p evenly spaced in logarithmic scale between $1/10$ and $10^{3/5} = 3.98107\dots$

is unchanged by monotonicity (see § 2.1 for details). Much less is known also at $d = 1$ for $p < 1$, where it is only known that π_{opt} depends on p (see § 2.7). In two dimensions, we observe that solutions at $p > 1$ are poor approximations of solutions at $p < 1$ (and viceversa). Notably, we observe an ordering $\mathcal{H}^{(p)}(\pi_{\text{opt}}^{(p')}) < \mathcal{H}^{(p)}(\pi_{\text{opt}}^{(p'')})$ if $p' < p''$ at $p \ll 1$, which is completely reversed to $\mathcal{H}^{(p)}(\pi_{\text{opt}}^{(p')}) > \mathcal{H}^{(p)}(\pi_{\text{opt}}^{(p'')})$ if $p' < p''$ at $p \gg 1$, implying a fan of crossings at intermediate values of p (Fig. 1.5).

1.4.3. Possible persistence of transition near $p = 1$ at $d = 2$

Let us fix again a large n (say $n = 10^4$) and, for a fixed disorder instance $(\mathcal{B}, \mathcal{R})$, let us study how the distribution $f_p(|e_n|)$ of the Euclidean length of an edge e_n in the optimal assignment varies with p . We will consider the associated tail function $F_p(x) = \int_x^\infty dy f_p(y)$ that is, the probability that $|e_n|$ is not smaller than x . A uniform lower bound for F_p is obtained from the distribution of nearest neighbors in a Poisson Point Process in two dimensions. The corresponding tail function is

$$t(x) = 1 - \int_0^x dr 2\pi r e^{-\pi r^2} = 1 - (1 - e^{-\pi x^2}) = e^{-\pi x^2}. \quad (1.4.3.1)$$

First, we have observed that the empirical tail function transitions from a region where it is monotone decreasing and concave at $p > 1$ (where the leading, large n scaling of the ground state energy is known, and the histogram is bell-shaped), to a region at $p < 1$ where it becomes non-concave (Fig. 1.6, left). As is well-known,

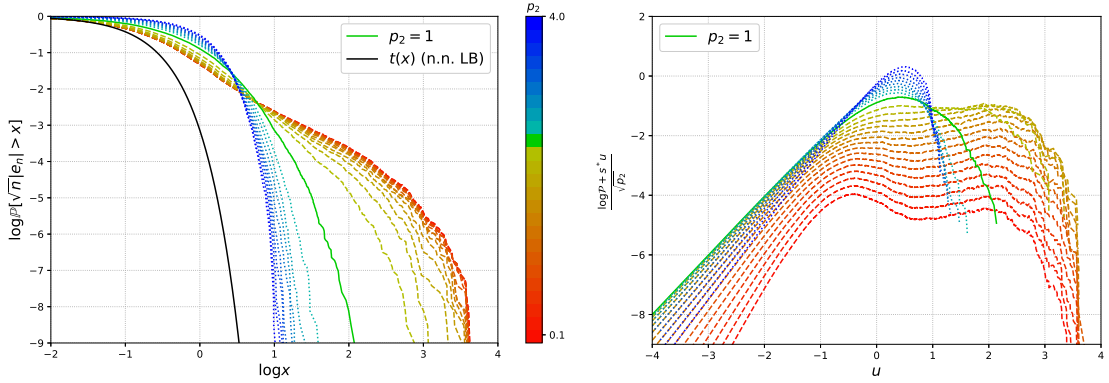


Figure 1.6. – (Left) Empirical tail functions (in log-log scale) for the rescaled edge length $\sqrt{n}|e_n|$ as a function of p_2 at $p_2 > 1$ (dotted lines, cold tones) and $p_2 < 1$ (dashed lines, warm tones). The lower bound of Eq. 1.4.3.1 is represented by a continuous black line. (Right) For $u = \log \sqrt{n}|e_n|$ (x -axis), the Legendre transform of log probability ($s^* = p_2 + 1$), as a function of u (and divided by inessential $\sqrt{p_2}$ for enhanced visualization), transitions from mono-modal curve at $p_2 > 1$ to a bi-modal curve at $p_2 < 1$. Protocol: 25 values of p evenly spaced in logarithmic scale between $1/10$ and $10^{3/5} = 3.98107 \dots$

this corresponds to a double regime in the Mellin transform of ρ :

$$\begin{aligned} [Mf_p](s) &:= \int dx f_p(x) x^{s-1} = (s-1) \int dx F_p(x) x^{s-2} \\ &\stackrel{t=\log x}{=} (s-1) \int dt e^{G(t)+(s-1)t} \end{aligned} \tag{1.4.3.2}$$

where $G(t) = \log F_p(x)|_{t=\log x}$. Indeed, the extremum for the integrand $t^*(s)$, which gives the logarithm of the Euclidean lengths of edges contributing to the moments of ρ , is a smooth function of s if G is concave but discontinuous otherwise. Notice that the Mellin transform $[Mf_p](s)$ is essentially the evaluation of $\mathcal{H}^{(p_1)}(\pi_{\text{opt}}^{(p_2)})$ at $p_1 = s-1$. Hence, the loss of concavity describes here a sort of “moral bi-modality”, in the sense that, in $\mathcal{H}^{(p_1)}(\pi_{\text{opt}}^{(p_2)})$, there is a domination of short or long edges if p_1 is smaller or greater than a certain threshold, that we conjecture to be at around p_2 . The optimal solution balances the contribution of long and short edges, as can be seen in Fig. 1.6 (right).

1.5. Some related topics

IN our previous discussions, several connections with other research topics beyond the original statistical physics motivation were mentioned (explicitly or implicitly). In this section, we wish to emphasize some other connections since, we believe, a methodological transfer of methods and ideas between the involved communities could be of general benefit.

In recent years many efforts have been devoted to a fundamental problem in the Calculus of Variations, which is how to optimally transport continuum measures one into another, or the “Monge–Kantorovich problem” (see (161) for an historical introduction and (114) for a discussion of related problems). It is a simple exercise to show that the ground state energy \mathcal{H}_{opt} in an ERAP (Eq. 1.3.0.2) is proportional to (the p -th power of) the p -Wasserstein (or Kantorovich) distance between the empirical measures associated to \mathcal{B} and \mathcal{R}^* . Another way to state this correspondence is: for measures supported onto a finite collection of points,

*Let $(\mathcal{Y}, \mathcal{D}_{\mathcal{Y}})$ be a Polish metric space, that is, a metric space which is also complete –every Cauchy sequence converges in \mathcal{Y} – and separable – \mathcal{Y} contains a countable dense set– (common Polish metric spaces are: \mathbb{C} , the d -dimensional torus \mathbb{T}^d , unit-cube \mathbb{Q}^d , sphere \mathbb{S}^d . The interested reader may consult (62), Chapter 3). Following Villani (127), the p -Wasserstein distance (to the power p) between two probability measures μ_1, μ_2 on a Polish metric space $(\mathcal{Y}, \mathcal{D}_{\mathcal{Y}})$ is

$$W_p^p(\mu_1, \mu_2) := \inf_{\nu \in \mu_1 \times \mu_2} \int_{\mathcal{Y}} d\nu(x, y) \mathcal{D}_{\mathcal{Y}}^p(x, y), \tag{1.5.0.1}$$

where the infimum is taken among all the product measures $\nu \in \mu_1 \times \mu_2$ with marginals μ_1 and μ_2 . Given an ERAP on $(\mathcal{Y}, \mathcal{D}_{\mathcal{Y}})$, consider the empirical measures for an instance $\mathcal{B} = \{b_i\}_{i=1}^n$ and

transference plans of optimal transport (127) are in bijection with the Birkhoff polytope of doubly stochastic matrices. The correspondence can be traced back at least to Kantorovich’s work (see (127), Chapter 3 and (158) for a recent discussion). This connection will play an important role in Chapter 3. On a parallel line, starting from the seminal work of Beardwood–Halton–Hammersley (18), interest has arisen around almost-sure limits of Euclidean functionals of finite random point sets, including the length functional in the random minimum spanning tree problem, or the aforementioned traveling salesman problem, even in a self-similar setting embedded in two dimensional Euclidean space (54). See (58) for an entry point, and (69, 79) for monographs. See also (136) for a recent account and results on bipartite Euclidean functionals.

A second connection deals with the aforementioned longstanding program of statistical physics approaches to computational complexity theory. It emerges if one insists in thinking that the Hungarian method plays a similar role as Gaussian elimination in linear algebra (49)[†]. The basic observation is that, from the perspective of linear programming, the assignment problem constitutes only a “slight” (but crucial) modification of combinatorial problems in a different complexity class, such as the traveling salesman problem (TSP), which is NP-complete (39), as it falls in the same class of the 3SAT problem (130). The situation shares analogy with a “slight” modification of the 3SAT, called 3-XOR-SAT, which is solvable in polynomial time (for example using Gaussian elimination on $\mathbb{Z}/2\mathbb{Z}$, see also (115)). Hence, the general hope is that the ERAP may serve as a paradigm toy-model simplification for gaining insights on stochastic versions of more difficult NP-complete problems, and a possibly comparative tool to understand what makes them difficult.

A third connection further emerges if one insists on the statistical mechanical description of an ERAP beyond the ground state. In fact, the canonical partition function at inverse temperature β (in units of Boltzmann’s constant) of any ERAP

$\mathcal{R} = \{r_i\}_{i=1}^n$ defined by

$$\rho_{\mathcal{B}}(x) = \frac{1}{n} \sum_{b_i \in \mathcal{B}} \delta(x - b_i), \quad \rho_{\mathcal{R}}(x) = \frac{1}{n} \sum_{r_k \in \mathcal{R}} \delta(x - r_k), \quad (1.5.0.2)$$

where δ is Dirac’s function. Then by straightforward computation

$$nW_p^p(\rho_{\mathcal{B}}, \rho_{\mathcal{R}}) = \mathcal{H}_{\text{opt}} \quad (1.5.0.3)$$

as announced.

[†]Actually, there is more to the analogy since the optimal cost to an assignment problem can be directly seen as a certain determinant of the cost matrix. The price to pay for such an interpretation, which is in the same spirit of the statistical physics approach to optimization problems, is to consider “zero-temperature free energies”, or, more precisely, to formulate the assignment problem on the so-called “tropical semi-ring” (instead of the ring of real numbers) (152). Informally, one replaces $x + y$ by $\min(x, y)$ and xy by $x + y$.

is the permanent of the Hadamard exponential of the $n \times n$ cost matrix $c^{(p)\ddagger}$. Such a correspondence, where both sides are quite generally little understood, allows to ask several questions in both languages. On physical grounds, one would like to access the full quenched free energy $f_q(\beta) = -\frac{1}{\beta}\mathbb{E}[\ln \mathcal{Z}(\beta)]$ (\mathbb{E} denoting expectation with respect to the disorder distribution), or at least some asymptotics for $f_q(\beta)$ for large β . However, the study of excited states in the ERAP (and in other stochastic optimisation problems) turned out to be very difficult, as the spectrum can show non-trivial features (see e.g. § 1.4), so that very little is known about the excited states even for the simplest disorder distributions (see (100) for some work in this direction). On mathematical grounds, the different viewpoint offered by the ERAP may be useful in understanding the statistical properties of permanents of positive random matrices, a topic of interest in probability but considerably less understood than random determinants (see e.g. (53, 66)). Moreover, here one may notice that the permanent constitutes a “slight” (but crucial) modification of the determinant, and functions interpolating between the permanent and the determinant have been studied from different viewpoints during the years (70). In our opinion, the exploration of such themes in the light of computational complexity theory may also be of possible general benefit.

Regarding applications, as we have already mentioned, an ERAP is so elementary in his description that, under appropriate choice of the statistical ensemble for \mathcal{B} and \mathcal{R} , it may conceivably describe several important real-life situations, some of which have been already been hinted at in § 1.5. For another, consider a linear chain, in some configuration within a solvent constituted of monomers which may be “charged” (e.g., they have different electronegativity). The optimal electrostatic pairing of the molecule (say, the optimal pattern of hydrogen bonds) can be reasonably described by an ERAP whose cost or fitness matrix is determined by a function of the Euclidean distance of the candidate positive and negative pairs. In a natural, simplified parametrization, we can imagine that the system is described by two parameters: the fractal effective dimension of the system, d , and the cost exponent, p (that is, the cost for connecting a pair of monomers at distance r scales as r^p). Our focus in this manuscript will mostly be on theoretical aspects, but a discussion of another possibly useful application of our framework is given at the end of Chapter 5.

[‡]That is, defining $[W(\beta)]_{ij} := e^{-\beta c_{ij}^{(p)}}$ for the cost matrix $c^{(p)}$ with exponent p , the partition function of the corresponding ERAP at inverse temperature β is

$$\mathcal{Z}(\beta) = \sum_{\pi \in \mathcal{S}_n} e^{-\beta \sum_{i=1}^n c_{i\pi(i)}^{(p)}} = \sum_{\pi \in \mathcal{S}_n} \prod_{i=1}^n e^{-\beta c_{i\pi(i)}^{(p)}} = \text{perm}[W(\beta)] , \quad (1.5.0.4)$$

where $\text{perm}[W(\beta)]$ is a polynomial of degree n in the $W(\beta)_{ij}$'s with positive coefficients, and the two quantities are equal in distribution.

1.6. Plan of the Thesis and list of contributions

THE manuscript develops as follows: in Chapter 2, focused on the problem in one dimension, we present some new results using mostly analytic and combinatorial methods (plus a conjecture supported by numerical experiments). In Chapter 3, we investigate some aspects of the problem in dimension two, such as the regularization of the asymptotic series of the ground state energy. The study builds on a recently proposed continuum field theoretical approach (145, 148) and involves also the verification of theoretical predictions by numerical experiments. At the end of the Chapter 3, we pose the basis of a finite n , lattice statistical field theory approach for which we report some promising preliminary results. In Chapter 4, we address the question of universality at intermediate dimensions with the introduction of an ERAP at fractal dimension and an extensive numerical investigation of relevant ground state energies scaling exponents. Some specific research problems are reported at the end of each chapter. Novel contributions discussed in this manuscript resulted in the following works (published, submitted or in preparation):

- ▶ 2018: ANOMALOUS SCALING OF THE OPTIMAL ASSIGNMENT IN THE ONE DIMENSIONAL RANDOM ASSIGNMENT PROBLEM,
with Sergio Caracciolo and Gabriele Sicuro, published in the Journal of Statistical Physics (169).
- ▶ 2019: THE DYCK BOUND IN THE CONCAVE 1-DIMENSIONAL RANDOM ASSIGNMENT MODEL,
with Sergio Caracciolo, Vittorio Erba and Andrea Sportiello, published in the Journal of Physics A: Mathematical and Theoretical (173).
- ▶ 2020: RANDOM ASSIGNMENT PROBLEMS ON $2d$ MANIFOLDS,
with Dario Benedetto, Emanuele Caglioti, Sergio Caracciolo, Gabriele Sicuro and Andrea Sportiello, submitted (172).
- ▶ 2020: ANOMALOUS SCALING OF THE OPTIMAL ASSIGNMENT IN THE ONE DIMENSIONAL RANDOM ASSIGNMENT PROBLEM: SOME RIGOROUS RESULTS,
with Andrea Sportiello, in preparation (174).
- ▶ 2020: EUCLIDEAN RANDOM ASSIGNMENT PROBLEMS AT NON-INTEGER HAUSDORFF DIMENSIONS $d_H \in (1, 2)$,
with Andrea Sportiello, in preparation (175).

Some provisional conclusions are given in Chapter 5 followed by a discussion of research perspectives.

ONE-DIMENSIONAL EUCLIDEAN RANDOM ASSIGNMENT PROBLEMS

2.1. On convex, concave and \mathcal{C} -repulsive regimes

AN established fact about one dimensional ERAPs is that there are special values of p separating three qualitatively different regimes^{*}: the convex regime at $p > 1$, the \mathcal{C} -repulsive regime at $p < 0$ and the concave regime at $p \in (0, 1)$ [†]. In each regime, some combinatorial properties of π_{opt} are independent on the choice of disorder, as we shall briefly review.

Lemma 2.1.1 (Convex regime, part I). *Let $\mathcal{M} = \mathbb{R}$ (or a connected subset of \mathbb{R} , such as \mathbb{Q}^1 , or a union of disjoint intervals), equipped with \mathcal{D} the Euclidean distance, and let \mathcal{B} and \mathcal{R} be sorted in natural order. Then, if $p > 1$,*

$$\pi_{\text{opt}} = (1, 2, \dots, n) \tag{2.1.0.1}$$

independently on the disorder distribution.

Proof. See (143), Proposition 2.1, or also (154), Proposition II.3. □

A permutation such as 2.1.0.1 in which the k -th blue is assigned to the k -th red is called *ordered* (see Fig. 2.1a for a pictorial representation). Lemma 2.1.1 (which in fact holds more generally for any convex and strictly increasing cost function) implies, by monotonicity, that π_{opt} remains the same independently on $p > 1$, giving a first example of complexity reduction (from $\mathcal{O}(n^3)$ to $\mathcal{O}(n \log n)$) induced by the knowledge of the mathematical properties of the (admittedly simple) ordered solution. We shall see that following such a guiding principle of algorithmic simplification proved useful also in a less simple case (§ 2.7).

^{*}Names stem from the properties of the cost function $c^{(p)} = \mathcal{D}^p(x, y)$ seen as a real function of $|x - y|$.

[†]The case $p = 0$ is trivial, as every $\pi \in \mathcal{S}_n$ has the same chance to be a π_{opt} independently on the disorder distribution. The qualitative picture in the concave regime $p \in (0, 1)$ is even richer, and only partially understood, and the case $p = 1$ is special. We will discuss them in § 2.7.

Borrowing from physics language, Lemma 2.1.1 describes a case of “open boundary conditions”. Correspondingly, one can consider the case of “periodic boundary conditions”.

Lemma 2.1.2 (Convex regime part II). *Let $\mathcal{M} = \mathbb{S}^1$ be equipped with \mathcal{D} the arc distance, and let \mathcal{B} and \mathcal{R} be sorted in natural order (both clockwise or anti-clockwise). Then, if $p > 1$, there exists an integer k such that*

$$\pi_{\text{opt}}(i) = i + k \pmod{n}, \quad i = 1, \dots, n.$$

Proof. See (154), starting from Corollary II.8. □

Lemma 2.1.2 also gives an improvement with respect to the Hungarian method, as the solution is completely specified by the random variable $\pi_{\text{opt}}(1)$. The search of π_{opt} may thus be restricted to the subgroup of n -cycles \mathcal{C}_n (which contains only n configurations), a configuration in which \mathcal{B} and \mathcal{R} are contained in one “large” permutation cycle (see Fig. 2.1b). Based on these results, it is natural to ask if a π_{opt} must have a prescribed cycle structure also in other regimes. Quite surprisingly, the answer to this question turned out to be affirmative at $p < 0$, in which case the cost function is not upper bounded (being singular at the origin).

Lemma 2.1.3 (\mathcal{C} -repulsive regime). *Let $M = \mathbb{R}$ or \mathbb{S}^1 , and let \mathcal{D} be geodesic distance. For the cost function $c^{(p)} = \mathcal{D}^p$ with $p < 0$, let $c^{(p)}(x, y) = |x - y|^p$. Then there exists k such that*

$$\pi_{\text{opt}}(i) = i + k \pmod{n}, \quad i = 1, \dots, n.$$

Proof. See (154), where there is a characterisation of the cost functions $c(x, y) = f(|x - y|)$ such that the property above holds. It turns out that the defining condition is that

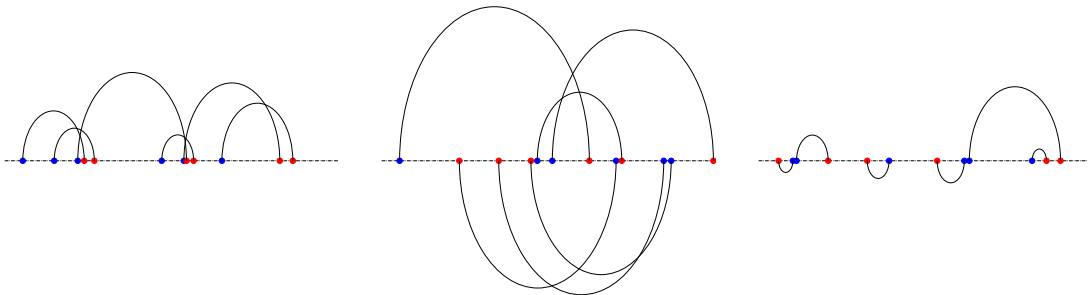
$$f(t_2) - f(t_1) \leq \min [f(t_2 + \eta) - f(t_1 + \eta), f(\hat{\eta} - t_2) - f(\hat{\eta} - t_1)] \quad (2.1.0.2)$$

with $\eta \in [0, 1 - t_2]$, $\hat{\eta} \in [1 - t_2, 1]$, for all $0 < t_1 < t_2 < 1$, and that it is easily verified that the function above satisfies this condition. □

Remark 2.1.1. Condition (2.1.0.2) is equivalent to the convexity requirement for a continuous function f (see (154), Appendix A). Moreover, condition (2.1.0.2) holds for a broader class of cost functions, called \mathcal{C} -functions. A simple example of \mathcal{C} -function is $f_{\alpha_0}(x) := (x - \alpha_0)^2$ on $[0, 1]$ for $\alpha_0 \geq \frac{1}{2}$ (which is convex and strictly increasing on $[0, 1]$ for $\alpha_0 \leq 0$).

The last combinatorial result that we shall review pertains the less studied regime: the concave regime with $p \in (0, 1)$, before which we need the following definition.

Definition 2.1.1 (Non-crossing matching). Let $\mathcal{M} = [0, 1]$ (or \mathbb{S}^1). A matching associated to the permutation π is *non-crossing* if, for all couple of intervals $A = (b_i, r_{\pi(i)})$, $B = (b_j, r_{\pi(j)})$, either $A \cap B = \emptyset$ or $A \subset B$, or $B \subset A$.



(a) Ordered ($p > 1$) (b) Cyclical ($p < 0$) (c) Non-crossing ($0 < p < 1$)

Figure 2.1. – Ordered (a), cyclical (b) and non-crossing (c) permutations.

Use of the term “non-crossing” stems from the fact that if the matching corresponding to π is represented by arcs in the plane joining the involved blue and red points arranged on a line, arcs do not cross (see Fig. 2.1c). By extension, for the sake of brevity from now on we will say that a permutation π is non-crossing to mean that the corresponding matching is non-crossing. In the same way, for the situation in which $A \subset B$ or $B \subset A$ we will say that the corresponding arcs are nested.

Lemma 2.1.4 (Concave case). *Let $M = \mathbb{R}$ (or subset of), \mathcal{D} be geodesic distance and let the cost function be $c^{(p)} = \mathcal{D}^p$ with $p \in (0, 1)$. Then π_{opt} is non-crossing.*

Proof. See (151), Lemma 3 (which is inspired to (82)) for apagogical arguments. \square

An alternative proof of Lemma 2.1.4 is given in § 2.7.5 (Lemma 2.7.2). In the following, §§ 2.3 through 2.6 deal with the convex problem, which is better understood. The concave regime is much less understood, and some aspects of it (such as the approximate optimal solutions known as “Dyck matchings”) are discussed in § 2.7.

2.2. Poisson-Poisson, Grid-Poisson ERAPs & the Brownian Bridge

IN § 2.1 we have reviewed the state of the art on combinatorial properties of the optimal permutation π_{opt} in a one dimensional ERAP. These properties are valid for any disorder distribution due to the particularly simple geometry of the problem.

In this Section we shall add randomness. After recalling three basic definitions, which will turn out to provide a useful compact notation, we recall a useful result about the solution in the continuum limit $n \rightarrow \infty$ for the convex and \mathcal{C} -repulsive regimes.

Definition 2.2.1 (Poisson-Poisson ERAP). An ERAP on a domain \mathcal{M} is of “Poisson-Poisson” kind (abbreviated “PP”) if both $\mathcal{B} = \{b_i\}_{i=1}^n$ and $\mathcal{R} = \{r_i\}_{i=1}^n$ are sets of independent random variables, uniform and i.i.d. on \mathcal{M} .

Definition 2.2.2 (Grid-Poisson ERAP). An ERAP on a domain $\mathcal{M} = [0, 1]$ (resp. $\mathcal{M} = \mathbb{S}_{1/2\pi}^1$) is of “Grid-Poisson” kind (abbreviated “GP”) if $\mathcal{R} = \{r_i\}_{i=1}^n$ is a set of independent random variables, uniformly distributed on \mathcal{M} , while \mathcal{B} is a deterministic grid on the domain $\Lambda_n^{\mathcal{M}}$.

For example, in one dimension, one can consider a GP ERAP with open boundary conditions, where \mathcal{R} are uniform and i.i.d. on $\mathcal{M} = \mathbb{Q}^1$ and

$$\mathcal{B} = \Lambda_n^{\mathbb{Q}^1} = \{b_i \mid b_i = i/(n+1), i = 1, \dots, n\}; \quad (2.2.0.1)$$

or the GP ERAP with periodic boundary conditions, where \mathcal{R} are i.i. uniformly distributed on $\mathcal{M} = \mathbb{S}_{1/2\pi}^1$ whereas

$$\mathcal{B} = \Lambda_n^{\mathbb{S}^1} = \{b_k \mid b_{k+1} - b_k = 1/(n+1), k = 1, \dots, n-1\} \quad (2.2.0.2)$$

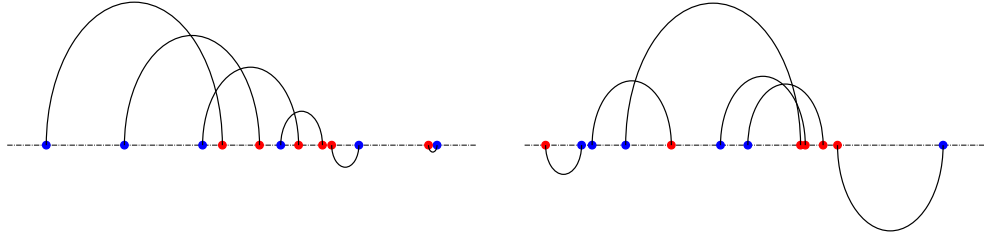
for an arbitrary fixed point b_1 by translation invariance (representations of small instances in a PP and a GP ERAP are given in Fig. 2.2).

Definitions 2.2.1 and 2.2.2 have natural generalizations in $d > 1$, and we shall recall them when needed. Early consideration of the GP ERAP can be found in (143) where the following notion was introduced.

Definition 2.2.3 (Transport field). Consider the Grid-Poisson ERAP on $\mathcal{M} = [0, 1]$ ($\mathcal{M} = \mathbb{S}_{1/2\pi}^1$). For $-$ difference (difference modulo $1/2$), the map $\mu : \Lambda_n^{\mathcal{M}} \rightarrow \mathcal{M}$ defined by

$$\mu(b_i) := r_{\pi_{\text{opt}}(i)} - b_i \quad i = 1, \dots, n \quad (2.2.0.3)$$

is called the *optimal transport field* or *displacement field*.



(a) *Grid Poisson* ($p > 1$).

(b) *Poisson Poisson* ($p > 1$).

Figure 2.2. – Example instances in a *Grid-Poisson ERAP* (Fig. 2.2a) and in a *Poisson-Poisson ERAP* (Fig. 2.2b) at $n = 6$. The optimal assignment π_{opt} is represented pictorially by arcs.

By an abuse of notation we also call the family of “differences” $\{r_{\pi_{\text{opt}}(i)} - b_i\}_{i=1}^n$ in a PP ERAP the optimal transport field. In terms of μ , the ground state energy writes $\mathcal{H}_{\text{opt}} = \sum_i |\mu_i|^p$.

Statistical properties of the optimal transport field for the GP ERAP have also been considered first in (143), and later on in a series of works devoted to both the PP and GP case (144, 154). They have been useful to compute, among other quantities, asymptotic series for the expectation of \mathcal{H}_{opt} in the $n \rightarrow \infty$ limit, and two-point correlation functions, with both open and periodic boundary conditions, in both the convex and \mathcal{C} -repulsive regime (154).

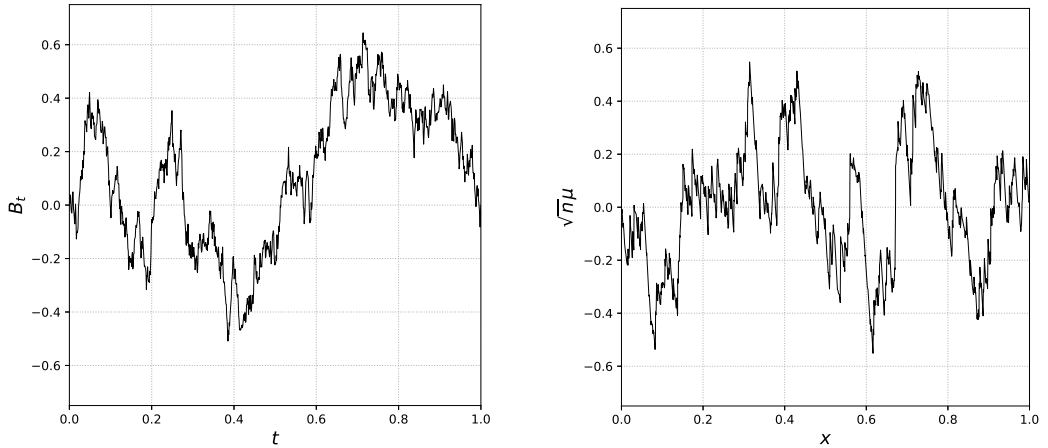
The basic idea builds on a Theorem by Donsker (13), sometimes called “functional central limit theorem” (see also (118)), which we shall briefly review. Given n independent observations $\{x_i\}_{i=1}^n$ sampled from a distribution function $\phi(x)$, if one considers the empirical cdf (i.e. the relative fraction of observations smaller than x)

$$\phi_n(x) := \frac{1}{n} \{\#x_i | x_i < x\} \quad (2.2.0.4)$$

then, as $n \rightarrow \infty$, $\sqrt{n}(\phi_n(x) - \phi(x))$ converges in distribution to a certain continuum gaussian process, called the *Brownian Bridge**. Universality here means that local details are largely irrelevant, as the statement holds *for a vast class of*

*We recall that for W_t the standard Wiener process with $t \in [0, 1]$, the Brownian Bridge can be defined

distribution functions. Due to the combinatorial properties of π_{opt} in the convex and \mathcal{C} -repulsive regimes, Donsker's Theorem thus allows to relate the displacement field μ (rescaled by the Donsker's \sqrt{n} universal term) to a sample path from the Brownian Bridge process in the $n \rightarrow \infty$ limit (or to a linear combination of sample paths in the \mathcal{C} -repulsive regime, see (154), Theorem II.9 and the discussion in § 1 therein). We give an example in Fig. 2.3b for the ordered case. We shall review the relationship between the discrete and continuum transport field in the specially simple case $p = 2$ in § 2.3.



(a) Sample path from the Brownian Bridge with standard methods. (b) Rescaled displacement field for an ERAP at $p > 1$ on the unit interval.

Figure 2.3. – (Fig. 2.3a) Sample path from the standard Brownian Bridge generated with a standard forward method (see e.g. (103)). (Fig. 2.3b) Rescaled optimal transport field for the PP ERAP at $p = 2$. Both plots consist of $n = 100$ linearly interpolated successive points.

As a consequence, in the $n \rightarrow \infty$ limit, relevant quantities for the ERAP (such as $\langle \mathcal{H}_{\text{opt}} \rangle$ or two-point correlation functions for μ) are reduced to gaussian integrals depending on p , and one can even study finite n corrections through the saddle point method (we shall review some calculations in the spirit of this approach

by

$$B_t := W_t - tW_1,$$

so that B_t is centered and gaussian. It follows that

$$\langle B_s B_t \rangle = \langle (W_s - sW_1)(W_t - tW_1) \rangle = \min(s, t) - st, \quad s, t \in [0, 1] \times [0, 1]. \quad (2.2.0.5)$$

The Brownian Bridge is discussed in most textbooks on stochastic processes, see e.g. (137), Example 22.2.1 or (75), pag. 358. The interested reader is referred to (160) for a review of stochastic processes related to Brownian motion.

in § 2.4, see (154) for a detailed account). Theoretical predictions have been confirmed by extensive numerical experiments (143, 144, 154). In conclusion, let us comment on a simple consequence of the remarkable “universality property” underlining our discussion at $p > 1$. If the disorder probability density function has connected support and does not vanish, the ground state energy is made of n contributions which are typically of order $(n^{-1/2})^p$, so that

$$\langle \mathcal{H}_{\text{opt}} \rangle |_{p \geq 1} \sim c_p n^{1-p/2} (1 + o(1)), \quad n \rightarrow \infty, \quad (2.2.0.6)$$

with a constant c_p depending on p and on the choice of distribution (the scaling exponent of sub-leading corrections may depend on the boundary conditions). Notice that the leading order in Eq. 2.2.0.6 is much larger than the scaling of the lower bound E_n^{LB} . The latter is found by assigning points in their Euclidean neighborhoods, so that $E_n^{\text{LB}} \sim n n^{-p/d} |_{d=1} = n^{1-p}$, and is self-averaging by the central limit theorem. As a side remark, it is worth noticing that this “universal property” can be traced back at least to the work of Kolmogorov (see (8), Teorema 1, or (57), § 2 for an english translation), which is often quoted as the basis of a wide-spread goodness-of-fit test in non-parametric statistics, named Kolmogorov-Smirnov statistics (10). We will come back to this point in § 2.5.1. By completely analogous arguments it is simply seen that in the \mathcal{C} -repulsive regime

$$\langle \mathcal{H}_{\text{opt}} \rangle |_{p \leq 0} \sim \frac{1}{2^p} n (1 + o(1)), \quad n \rightarrow \infty, \quad (2.2.0.7)$$

for both \mathbb{S}_1 and \mathbb{Q}_1 , where the factor $\frac{1}{2} = \frac{|\mathcal{M}|}{2}$ is the typical length of an edge in the optimal assignment (see (154) for further details).

If on the contrary the disorder distribution is discontinuous and/or vanishes, the problem is considerably more difficult and the scaling properties of $\langle \mathcal{H}_{\text{opt}} \rangle$ require further efforts to be unveiled, as we will discuss in § 2.6.

2.3. Lattice and continuum modes of the optimal transport field at $p = 2$

IN this Section we shall discuss some statistical properties of both discrete and continuum Fourier modes of the displacement field (Def. 2.2.3) in the special case $p = 2$, where we have already seen that $\lim_{n \rightarrow \infty} \langle \mathcal{H}_{\text{opt}} \rangle$ exists and is finite (Eq. 2.2.0.6). The discussion is elementary in that it combines discrete/continuum Fourier analysis and manipulations of moment generating functions. At fixed n , among other things we shall show that, both in the discrete and continuum case, the problem is “diagonalized” by an appropriate (discrete or continuum) Fourier transform, and the ground state is decomposed into a sum of centered gaussian, uncorrelated modes. We will also show that mode correlations, at finite n , are exactly proportional to the inverse *lattice Laplacian* associated to our choice of grid. For the continuum case, we shall derive exact expressions for the probabilities of contributions from any given mode to \mathcal{H}_{opt} . We will give an expression of the full distribution of \mathcal{H}_{opt} in terms of an elliptic ϑ_4 function in the case of periodic boundary conditions as an application. Besides the intrinsic value of our discussion, which employs old tools but appears to be new in the literature, we shall discuss our calculations in some details also in prevision of the analogous discussion on lattice Fourier modes of the optimal transport field in the more challenging two-dimensional case of Chapter 3.

2.3.1. Unit interval at fixed n

Let us consider $\mathcal{M} = \mathbb{Q}^1$, blue points on the grid $\mathcal{B} = \{b_i\}_{i=1}^n$, $b_i = \frac{i}{n+1}$ with $i = 1, \dots, n$, with the addition of the two endpoints at 0 and 1. For the displacement field defined by

$$\mu_i := r_i - \frac{i}{n+1}, \quad i = 0, \dots, n+1, \quad (2.3.1.1)$$

where reds are $\mathcal{R} = \{r_i\}_{i=1}^n \cup \{0, 1\}$, the ground state energy is just

$$\mathcal{H}_{\text{opt}} = \sum_{i=0}^{n+1} \mu_i^2. \quad (2.3.1.2)$$

Consider the red r_i , which is distributed according to

$$P_i(r_i) := \begin{cases} \delta(r_0) & \text{for } i = 0 \\ i \binom{n}{i} r_i^{i-1} (1 - r_i)^{n-i} & \text{for } 1 \leq i \leq n \\ \delta(r_{n+1} - 1) & \text{for } i = n + 1, \end{cases} \quad (2.3.1.3)$$

where δ is Dirac function. It follows that

$$\langle r_i^k \rangle = \frac{(i+k-1)!n!}{(i-1)!(n+k)!} \quad (2.3.1.4)$$

and therefore the moment generating function is an hypergeometric function

$$\langle e^{-wr_i} \rangle = \sum_{k \geq 0} \frac{(i+k-1)!n!}{(i-1)!(n+k)!} \frac{(-w)^k}{k!} = {}_1F_1(i; n+1; -w). \quad (2.3.1.5)$$

In particular from Eq. 2.3.1.5 we read the balancing condition

$$\langle r_i \rangle = \frac{i}{n+1} \quad (2.3.1.6)$$

and, using for $j \geq i$ the discrete Wiener formula

$$P_{ij}(r_i, r_j) := i(j-i) \binom{n}{i, j-i, n-j} r_i^{i-1} (r_j - r_i)^{j-i-1} (1-r_j)^{n-j}, \quad (2.3.1.7)$$

we get

$$\langle r_i r_j \rangle = \frac{i(j+1)}{(n+1)(n+2)} \quad (2.3.1.8)$$

for $j \geq i$. It follows that the transport field satisfies

$$\begin{aligned} \langle \mu_i \rangle &= 0 \\ \langle \mu_i \mu_j \rangle &= \frac{i(n+1-j)}{(n+1)^2(n+2)}. \end{aligned} \quad (2.3.1.9)$$

As a consequence we recover the exact expression for the expected ground state energy

$$\langle \mathcal{H}_{\text{opt}} \rangle = \sum_{i=1}^n \langle \mu_i^2 \rangle = \frac{n}{6(n+1)} \quad (2.3.1.10)$$

which is half of the well-known Poisson-Poisson value (see e.g. (154), Eq. 54). Let us go now to momentum space. Since μ satisfies Dirichlet boundary conditions, we can perform the expansion

$$\hat{\mu}_s := \sqrt{\frac{2}{n+1}} \sum_{l=1}^n \mu_l \sin\left(\frac{\pi l s}{n+1}\right), \quad s = 1, \dots, n, \quad (2.3.1.11)$$

corresponding to the discrete momenta

$$p_s := \frac{\pi s}{n+1}, \quad s = 1, \dots, n. \quad (2.3.1.12)$$

We immediately get

$$\langle \hat{\mu}_s \rangle = 0, \quad s = 1, \dots, n, \quad (2.3.1.13)$$

and

$$\begin{aligned} \langle \hat{\mu}_s^2 \rangle &= \frac{2}{n+1} \sum_{i,j=1}^n \langle \mu_i \mu_j \rangle \sin\left(\frac{\pi i s}{n+1}\right) \sin\left(\frac{\pi j s}{n+1}\right) \\ &= \frac{2}{n+1} \sum_{i=1}^n \frac{i(n+1-i)}{(n+1)^2(n+2)} \sin^2\left(\frac{\pi i s}{n+1}\right) + \\ &\quad \frac{4}{n+1} \sum_{i=1}^n \sum_{j=i+1}^n \frac{i(n+1-j)}{(n+1)^2(n+2)} \sin\left(\frac{\pi i s}{n+1}\right) \sin\left(\frac{\pi j s}{n+1}\right), \end{aligned} \quad (2.3.1.14)$$

where Eq. 2.3.1.9 has been used. Using the orthogonality relation (δ_{ij} is the Kronecker symbol)

$$\frac{2}{n+1} \sum_{s=1}^n \sin\left(\frac{\pi i s}{n+1}\right) \sin\left(\frac{\pi j s}{n+1}\right) = \delta_{ij}, \quad (2.3.1.15)$$

we can easily verify the Parseval's identity

$$\sum_{s=1}^n \langle \hat{\mu}_s^2 \rangle = \sum_{i=1}^n \langle \mu_i^2 \rangle. \quad (2.3.1.16)$$

Eq. 2.3.1.14 becomes

$$\langle \hat{\mu}_s^2 \rangle = \frac{1}{4(2+3n+n^2) \sin^2\left(\frac{\pi s}{2(n+1)}\right)} = \frac{1}{(n+1)(n+2)} \frac{1}{\hat{p}_s^2}, \quad s = 1, \dots, n, \quad (2.3.1.17)$$

where we have introduced the *lattice Laplacian* \hat{p}^2

$$\hat{p} := 2 \sin \frac{p}{2} \quad (2.3.1.18)$$

which for small p satisfies

$$\hat{p}^2 = p^2 + \mathcal{O}(p^4). \quad (2.3.1.19)$$

Eq. 2.3.1.17 provides *exactly* the contribution to \mathcal{H}_{opt} from the s -th discrete Fourier mode of μ in terms of the inverse lattice Laplacian. Incidentally, notice that

combining Eqs. 2.3.1.10 and 2.3.1.16 gives

$$\sum_{s=1}^n \frac{1}{\hat{p}_s^2} = \frac{n(n+2)}{6}. \quad (2.3.1.20)$$

This fact can be alternatively obtained using the result in (72, B.27) with $L = 2n + 2$

$$\sum_{s=0}^{2n+1} \frac{1}{4 \sin^2\left(\frac{\pi s}{n+1}\right) + \alpha^2} = \frac{2(n+1)}{\alpha\sqrt{4+\alpha^2}} \coth\left[2(n+1) \operatorname{arcsinh}\left(\frac{\alpha}{2}\right)\right] \quad (2.3.1.21)$$

coupled with the identity

$$\sum_{s=0}^{2n+1} \frac{1}{4 \sin^2\left(\frac{\pi s}{n+1}\right) + \alpha^2} = 2 \sum_{s=1}^{n-1} \frac{1}{4 \sin^2\left(\frac{\pi s}{n+1}\right) + \alpha^2} + \frac{1}{4+\alpha^2} + \frac{1}{\alpha^2} \quad (2.3.1.22)$$

in the $\alpha \rightarrow 0$ limit, since

$$\begin{aligned} \sum_{s=1}^n \frac{1}{\hat{p}_s^2} &= \lim_{\alpha \rightarrow 0} \sum_{s=1}^{n-1} \frac{1}{4 \sin^2\left(\frac{\pi s}{n+1}\right) + \alpha^2} = \\ &= \lim_{\alpha \rightarrow 0} \frac{1}{2} \left[\frac{2(n+1)}{\alpha\sqrt{4+\alpha^2}} \coth\left[2(n+1) \operatorname{arcsinh}\left(\frac{\alpha}{2}\right)\right] - \frac{1}{4+\alpha^2} - \frac{1}{\alpha^2} \right] \\ &= \frac{n(n+2)}{6} \end{aligned} \quad (2.3.1.23)$$

as claimed. Lastly, the mode-mode correlation is

$$\langle \hat{\mu}_s \hat{\mu}_t \rangle = \frac{2}{n+1} \sum_{i,j=1}^n \langle \mu_i \mu_j \rangle \sin\left(\frac{\pi i s}{n+1}\right) \sin\left(\frac{\pi j t}{n+1}\right) \quad (2.3.1.24)$$

$$= \frac{2}{n+1} \sum_{i=1}^n \frac{i(n+1-i)}{(n+1)^2(n+2)} \sin\left(\frac{\pi i s}{n+1}\right) \sin\left(\frac{\pi i t}{n+1}\right) + \quad (2.3.1.25)$$

$$\frac{2}{n+1} \sum_{i=1}^n \sum_{j=1}^{i-1} \frac{j(n+1-i)}{(n+1)^2(n+2)} \sin\left(\frac{\pi i s}{n+1}\right) \sin\left(\frac{\pi j t}{n+1}\right) + \quad (2.3.1.26)$$

$$\frac{2}{n+1} \sum_{i=1}^n \sum_{j=i+1}^n \frac{i(n+1-j)}{(n+1)^2(n+2)} \sin\left(\frac{\pi i s}{n+1}\right) \sin\left(\frac{\pi j t}{n+1}\right). \quad (2.3.1.27)$$

By performing the sum over j and using the orthonormality relation we get

$$\langle \hat{\mu}_s \hat{\mu}_t \rangle = \frac{1}{2(n+1)^2(n+2) \sin^2\left(\frac{\pi s}{2(n+1)}\right)} \sum_{i=1}^n \sin\left(\frac{\pi i s}{n+1}\right) \sin\left(\frac{\pi i t}{n+1}\right) \quad (2.3.1.28)$$

$$= \frac{\delta_{st}}{4(n+1)(n+2) \sin^2\left(\frac{\pi s}{2(n+1)}\right)} \quad (2.3.1.29)$$

as claimed. Notice that

$$\lim_{n \rightarrow \infty} \frac{\delta_{st}}{4(n+1)(n+2) \sin^2\left(\frac{\pi s}{2(n+1)}\right)} = \frac{\delta_{st}}{\pi^2 s^2}. \quad (2.3.1.30)$$

Regarding the Poisson Poisson case, recall that in this case for $\mathcal{B} = \{b_i\}_{i=1}^n$ and $\mathcal{R} = \{r_i\}_{i=1}^n$ in increasing order the displacement field is

$$\mu_i := b_i - r_i \quad (2.3.1.31)$$

but now

$$\begin{aligned} \langle r_i \rangle &= \langle b_i \rangle = \frac{i}{n+1} \\ \langle r_i r_j \rangle &= \langle b_i b_j \rangle = \frac{i(j+1)}{(n+1)(n+2)} \end{aligned} \quad (2.3.1.32)$$

for $j \geq i$. It follows that

$$\begin{aligned} \langle \mu_i \rangle &= 0 \\ \langle \mu_i \mu_j \rangle &= 2 \frac{i(n+1-j)}{(n+1)^2(n+2)} \end{aligned} \quad (2.3.1.33)$$

and the whole analysis develops as in the Grid Poisson case, up to a factor 2 (i.e., compare Eqs. 2.3.1.33 and 2.3.1.9).

2.3.2. Unit interval in the $n \rightarrow \infty$ limit

Let us consider the Grid-Poisson case first, and let us take the continuum limit $n \rightarrow +\infty$ as

$$\sqrt{n+1} \mu_i \rightarrow \mu(x_i) \quad (2.3.2.1)$$

with $x_i \in [0, 1]$ so that $\mu(x_i)$ from well-known properties of the Brownian Bridge process for $x_1 \leq x_2$

$$\langle \mu(x_1)\mu(x_2) \rangle = x_1(1 - x_2). \quad (2.3.2.2)$$

We have

$$\hat{\mu}_s := \sqrt{2} \int_0^1 dx \mu(x) \sin(\pi s x) \quad (2.3.2.3)$$

with $s \in \mathbb{N}$, and the orthonormality relations

$$2 \int_0^1 dx \sin(\pi s x) \sin(\pi t x) = \delta_{st}. \quad (2.3.2.4)$$

Then

$$\langle \hat{\mu}_s \hat{\mu}_t \rangle = 2 \int_0^1 dx \int_0^1 dy \langle \mu(x)\mu(y) \rangle \sin(\pi s x) \sin(\pi t y) \quad (2.3.2.5)$$

$$= 2 \int_0^1 dx \int_0^1 dy [\theta(y - x)x(1 - y) + \quad (2.3.2.6)$$

$$\theta(x - y)y(1 - x)] \sin(\pi s x) \sin(\pi t y) \quad (2.3.2.7)$$

$$= \frac{2}{\pi^2 t^2} \int_0^1 dx \sin(\pi s x) \sin(\pi t x) \quad (2.3.2.8)$$

$$= \frac{\delta_{st}}{\pi^2 t^2}, \quad (2.3.2.9)$$

where $\theta(x)$ is Heaviside function (compare to Eq. 2.3.1.30). Now, as the $\mu(x)$ are centered Gaussian variables, also the $\hat{\mu}_s$ are centered Gaussian variables, with variance $(\pi s)^{-2}$. Recalling Parseval's identity $\mathcal{H}_{\text{opt}} = \sum_{s \geq 1} \hat{\mu}_s^2$, we find for the moment generating function

$$\langle e^{-w \mathcal{H}_{\text{opt}}} \rangle = \langle e^{-w \sum_{s=1}^{\infty} \hat{\mu}_s^2} \rangle = \prod_{s=1}^{\infty} \sum_{k_s \geq 0} \frac{(-w)^{k_s}}{k_s!} \langle \hat{\mu}_s^{2k_s} \rangle \quad (2.3.2.10)$$

$$= \prod_{s=1}^{\infty} \sum_{k_s \geq 0} \frac{(-w)^{k_s}}{k_s!} \frac{(2k_s - 1)!!}{(\pi s)^{2k_s}} \quad (2.3.2.11)$$

$$= \prod_{s=1}^{\infty} \frac{1}{\sqrt{1 + \frac{2w}{(\pi s)^2}}} \quad (2.3.2.12)$$

$$= \sqrt{\frac{\sqrt{2w}}{\sinh(\sqrt{2w})}}. \quad (2.3.2.13)$$

In particular, as for a fixed mode

$$\langle e^{-w\hat{\mu}_s^2} \rangle = \frac{1}{\sqrt{1 + \frac{2w}{(\pi s)^2}}}, \quad (2.3.2.14)$$

the probability to get a contribution E_s to \mathcal{H}_{opt} by the s -th mode is given by the inverse Laplace transform

$$\rho_{\mathcal{H}_{\text{opt}}}^{\text{GP}}(E_s)dE_s := \langle \delta(E_s - \hat{\mu}_s^2) \rangle dE_s = \sqrt{\frac{\pi s^2}{2E_s}} e^{-\frac{1}{2}\pi^2 s^2 E_s} dE_s, \quad (2.3.2.15)$$

where $\delta(x)$ is Dirac function. The cdf is thus

$$\Phi_s^{\text{GP}}(z) = \int_0^z dE_s \rho_{\mathcal{H}_{\text{opt}}}^{\text{GP}}(E_s) = \text{erf}\left(\pi s \sqrt{\frac{z}{2}}\right). \quad (2.3.2.16)$$

where $\text{erf}(x)$ denotes the standard error function. For the Poisson-Poisson case, let us set

$$\hat{\mu}_s = \hat{\xi}_s - \hat{\eta}_s, \quad s = 1, \dots, n, \quad (2.3.2.17)$$

which are the contributions from \mathcal{R} and \mathcal{B} once their average values is subtracted. The moment generating function becomes

$$\begin{aligned} \langle e^{-w\mathcal{H}_{\text{opt}}} \rangle &= \langle e^{-w\sum_{s=1}^{\infty}(\hat{\xi}_s - \hat{\eta}_s)^2} \rangle = \prod_{s=1}^{\infty} \sum_{k_s \geq 0} \frac{(-w)^{k_s}}{k_s!} \langle (\hat{\xi}_s - \hat{\eta}_s)^{2k_s} \rangle \\ &= \prod_{s=1}^{\infty} \sum_{k_s \geq 0} \frac{(-w)^{k_s}}{k_s!} \sum_{j_s \geq 0} \binom{2k_s}{2j_s} \langle \hat{\xi}_s^{2k_s - 2j_s} \hat{\eta}_s^{2j_s} \rangle \\ &= \prod_{s=1}^{\infty} \sum_{k_s \geq 0} \frac{(-w)^{k_s}}{k_s! (\pi s)^{2k_s}} \sum_{j_s \geq 0} \binom{2k_s}{2j_s} (2k_s - 2j_s - 1)!! (2j_s - 1)!! \\ &= \prod_{s=1}^{\infty} \sum_{k_s \geq 0} \frac{(-2w)^{k_s}}{k_s!} \frac{(2k_s - 1)!!}{(\pi s)^{2k_s}} \\ &= \prod_{s=1}^{\infty} \frac{1}{\sqrt{1 + \frac{4w}{(\pi s)^2}}} \\ &= \sqrt{\frac{2\sqrt{w}}{\sinh(2\sqrt{w})}}. \end{aligned} \quad (2.3.2.18)$$

In this case the probability to get a contribution E_s from the s -th mode is

$$\rho_{\mathcal{H}_{\text{opt}}}^{\text{PP}}(E_s)dE_s := \langle \delta(E_s - \hat{\mu}_s^2) \rangle dE_s = \sqrt{\frac{\pi s^2}{4E_s}} e^{-\frac{1}{4}\pi^2 s^2 E_s} dE_s \quad (2.3.2.19)$$

whose cdf is

$$\Phi_s^{\text{PP}}(z) = \int_0^z dE_s \rho_{\mathcal{H}_{\text{opt}}}^{\text{PP}}(E_s) = \text{erf}\left(\frac{\pi s \sqrt{z}}{2}\right). \quad (2.3.2.20)$$

A simple relationship between the Poisson-Poisson and Grid-Poisson case

$$\Phi_s^{\text{PP}}(2z) = \Phi_s^{\text{GP}}(z) \quad (2.3.2.21)$$

holds for each s .

2.3.3. Distribution of \mathcal{H}_{opt} on the unit circle in the $n \rightarrow \infty$ limit

Let us consider the problem on $\mathcal{M} = \mathbb{S}^1$ in the continuum limit. In this case the transport field is

$$\mu(t) := B_t - \int_0^1 d\tau B_\tau, \quad (2.3.3.1)$$

where B_t is the Brownian Bridge. As $\langle \mu(t) \rangle$ must be independent from t and with vanishing average on \mathbb{S}^1 , we get

$$\begin{aligned} \langle \mu(t) \rangle &= 0, \\ \langle \mu(t)\mu(t+\tau) \rangle &= \frac{1}{12} - \frac{\tau(1-\tau)}{2}. \end{aligned} \quad (2.3.3.2)$$

Now the Fourier modes are

$$\hat{\mu}_s = \int_0^1 dx \mu(x) e^{2\pi i s x} \quad (2.3.3.3)$$

with $s \in \mathbb{Z} \setminus \{0\}$, complemented with the orthonormality conditions

$$\int_0^1 dx e^{2\pi i (s-t)x} = \delta_{st}. \quad (2.3.3.4)$$

As $\mu(x) \in \mathbb{R}$ we must have

$$\hat{\mu}_s^* = \hat{\mu}_{-s} \quad (2.3.3.5)$$

and we soon get

$$\langle \hat{\mu}_s \rangle = 0. \quad (2.3.3.6)$$

For the correlations, for $s, t \in \mathbb{Z} \setminus \{0\}$

$$\begin{aligned} \langle \hat{\mu}_s^* \hat{\mu}_t \rangle &= \int_0^1 dx \int_0^1 dy \langle \mu(x) \mu(y) \rangle e^{2\pi i(-sx+ty)} \\ &= \int_0^1 dx \int_0^1 dy \langle \mu(x) \mu(x+y) \rangle e^{2\pi i[(t-s)x+ty]} \\ &= \delta_{st} \int_0^1 dy \langle \mu(0) \mu(y) \rangle e^{2\pi i t y} \\ &= -\frac{\delta_{st}}{2} \int_0^1 dy y(1-y) e^{2\pi i t y} \\ &= \frac{\delta_{st}}{4\pi^2 s^2}. \end{aligned} \quad (2.3.3.7)$$

The ground state energy is

$$\langle \mathcal{H}_{\text{opt}} \rangle = \int_0^1 dt \langle \mu^2(t) \rangle = \frac{1}{12}, \quad (2.3.3.8)$$

which coincides with Eq. (2.3.3.2) at $\tau = 0$, a result first derived in (143). The same result may be recovered also through Parseval's identity, since

$$\langle \mathcal{H}_{\text{opt}} \rangle := \sum_{s \neq 0} \langle |\hat{\mu}_s|^2 \rangle = 2 \sum_{s \geq 1} \langle |\hat{\mu}_s|^2 \rangle = \frac{2}{4\pi^2} \sum_{s \geq 1} \frac{1}{s^2} = \frac{2}{4\pi^2} \zeta(2) = \frac{1}{12} \quad (2.3.3.9)$$

as announced. The ground state energy moment generating function is

$$\begin{aligned} \langle e^{-w\mathcal{H}_{\text{opt}}} \rangle &= \left\langle e^{-2w \sum_{s \geq 1} |\hat{\mu}_s|^2} \right\rangle \\ &= \prod_{s=1}^{\infty} \sum_{k_s \geq 0} \frac{(-2w)^{k_s}}{k_s!} \langle |\hat{\mu}_s|^{2k_s} \rangle \\ &= \prod_{s=1}^{\infty} \sum_{k_s \geq 0} \frac{(-2w)^{k_s}}{k_s!} \frac{k_s!}{(2\pi s)^{2k_s}} \\ &= \prod_{s=1}^{\infty} \frac{1}{1 + \frac{w}{2\pi^2 s^2}} \\ &= \frac{\sqrt{\frac{w}{2}}}{\sinh \left[\sqrt{\frac{w}{2}} \right]}. \end{aligned} \quad (2.3.3.10)$$

Using the expansion from (21)

$$\frac{\sqrt{\frac{w}{2}}}{\sinh\left[\sqrt{\frac{w}{2}}\right]} = \sum_{s \geq 1} c_s \frac{1}{1 + \frac{w}{2\pi^2 s^2}} \quad (2.3.3.11)$$

where

$$c_s = \lim_{w \rightarrow -2\pi^2 s^2} \frac{\left(1 + \frac{w}{2\pi^2 s^2}\right) \sqrt{\frac{w}{2}}}{\sinh\left[\sqrt{\frac{w}{2}}\right]} = \lim_{w \rightarrow 1} \frac{(1-w) \pi s \sqrt{w}}{\sin(\pi s \sqrt{w})} = \lim_{\epsilon \rightarrow 0} \frac{\epsilon \pi s}{\sin\left[\pi s \left(1 - \frac{\epsilon}{2}\right)\right]} = 2(-1)^{s-1}, \quad (2.3.3.12)$$

we can inverse Laplace transform Eq. (2.3.3.10) and show that the pdf of the ground state energy can be written as

$$\rho_{\mathcal{H}_{\text{opt}}}(E_s) = \sum_{s \geq 1} (-1)^{s-1} 4\pi^2 s^2 e^{-2\pi^2 s^2 E_s} \quad (2.3.3.13)$$

whose cdf is the elliptic ϑ -function

$$\Phi^{\text{GP}}(x) = \vartheta_4\left(0, e^{-2\pi^2 x}\right). \quad (2.3.3.14)$$

Under the change of variables $\tau(x) = 2\pi i x$, an alternative expression for $\Phi^{\text{GP}}(x)$ is

$$\vartheta_4\left(0, e^{-2\pi^2 x}\right) = \frac{\eta^2\left(\frac{\tau(x)}{2}\right)}{\eta(\tau(x))} \quad (2.3.3.15)$$

where η is the Dedekind function (see also Eq. B.1.0.8 and the discussion therein). By our previous remarks, for the distribution of \mathcal{H}_{opt} in the Poisson-Poisson case we just have

$$\Phi^{\text{PP}}(2x) = \Phi^{\text{GP}}(x). \quad (2.3.3.16)$$

Eq. 2.3.3.15 nicely agrees with results of numerical experiments in both the GP and PP case already at moderately small values of n (Fig. 2.4).

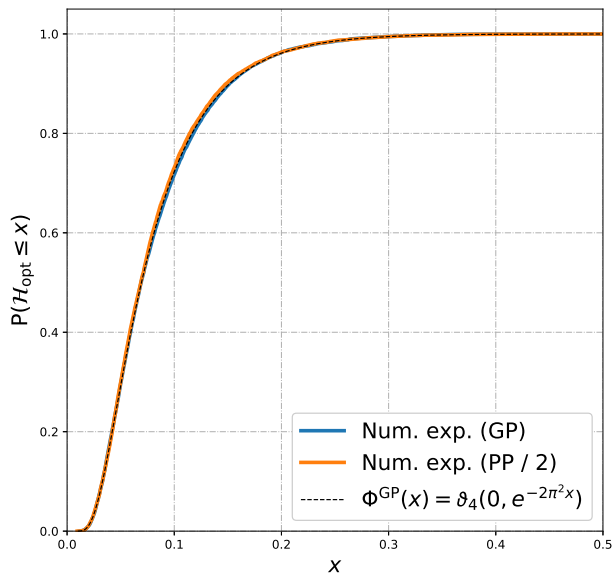


Figure 2.4. – Continuum limit cdf for \mathcal{H}_{opt} for the ERAP with periodic boundary conditions at $p = 2$ (eq. 2.3.3.14 or 2.3.3.15, dashed black line) and results of numerical experiments (blue line for $\mathcal{H}_{\text{opt}}^{\text{GP}}$ and orange line for $2\mathcal{H}_{\text{opt}}^{\text{PP}}$). Simulations were performed at $n = 100$ with 10^4 repetitions.

2.4. Beyond uniform disorder: anomalous vs bulk scaling of $\langle \mathcal{H}_{\text{opt}} \rangle$ at $p \geq 1$

As anticipated in Eq. 2.2.0.6, for general $p \geq 1$ it is well established that $\langle \mathcal{H}_{\text{opt}} \rangle$ is of order $\sim n^{1-p/2}$ as long as the disorder distribution satisfies some mild requirements (namely, its support is compact and the distribution does not vanish). Heuristically, this is because an extensive number of edges all contribute at the same scale (the one fixed by Donsker's Theorem). The optimal transport field converges weakly to the Brownian Bridge process (up to constants in n), a fact that can be exploited to compute several quantities of interest in the continuum limit. What if such requirements on the disorder distribution are removed?

In the following Section we shall discuss a simple method, inspired by cutoff regularisation methods of quantum field theories, to partially address this question and compute the aforementioned constants in some cases. The essence of the method is that leading and/or sub-leading constants for the asymptotics of $\langle \mathcal{H}_{\text{opt}} \rangle$ are computable from a possibly divergent one-dimensional integral, provided the value of a certain cutoff constant is fixed by the results of (extremely simple) numerical experiments (if necessary). This is an analogy with Physics, where so-called coupling constants must be fitted to experimentally measured values in order to have finite results. The method, which is simple but conjectural, has been applied to a number of choices for the disorder distribution, and comparison with results of numerical experiments have served to clarify both its value and limitations. The latter have started to be more properly addressed by the finite n approach of § 2.6.

2.5. Anomalous Scaling of the Optimal Cost in the One-Dimensional Random Assignment Problem

THE content of this Section has been published in (173).

2.5.1. Notations

Let us consider a PDF $\rho(x): \mathbb{R} \rightarrow \mathbb{R}^+$ on the real line, $\int_{-\infty}^{+\infty} dx \rho(x) = 1$ with a support

$$\Omega := \{x \in \mathbb{R} | \rho(x) > 0\} \quad (2.5.1.1)$$

so that $\rho(x) = 0 \forall x \in \mathbb{R} \setminus \Omega$. Let us denote by $\bar{\Omega}$ the closure of Ω , possibly including the points at infinity. The cumulative function $\Phi(x)$ and the complementary cumulative $\bar{\Phi}(x) := 1 - \Phi(x)$ are

$$\Phi(x) := \int_{-\infty}^x \rho(\xi) d\xi =: 1 - \bar{\Phi}(x). \quad (2.5.1.2)$$

Let us suppose now that blue points \mathcal{B} and red points \mathcal{R} are two sets of points generated on the line, independently and with the same PDF ρ . As usual, we will assume \mathcal{B} and \mathcal{R} are labeled in the natural order of the real line, that is in such a way that $b_i < b_{i+1}$ and $r_i < r_{i+1}$ for $i = 1, \dots, n-1$. Consider the transport field

$$\mu_k := r_k - b_k, \quad k = 1, \dots, n \quad (2.5.1.3)$$

which extends the analogous quantity for the Poisson-Poisson case (see § 2.2), at $p \geq 1$,

$$\varepsilon_n := \langle \mathcal{H}_{\text{opt}} \rangle = \sum_{k=1}^n \int |\mu|^p \text{Pr}[\mu_k \in d\mu]. \quad (2.5.1.4)$$

where we have used the notation $z \in dx \Leftrightarrow z \in (x, x + dx)$. As a generalisation of Eq. 2.3.1.3 (which corresponds to the case of uniform distribution for which $\Phi(x) = x$), for a general disorder Φ we just have

$$\text{Pr}[x_k \in dx] = \binom{n}{k} \bar{\Phi}^{n-k}(x) d\Phi^k(x), \quad (2.5.1.5)$$

so that the distribution of μ_k is

$$\text{Pr}[\mu_k \in d\mu] = d\mu \binom{n}{k}^2 \iint \delta(\mu - y + x) \bar{\Phi}^{n-k}(x) \bar{\Phi}^{n-k}(y) d\Phi^k(x) d\Phi^k(y). \quad (2.5.1.6)$$

In order to evaluate ε_n we may just write*

$$\varepsilon_n = \iint_{\Omega \times \Omega} |y - x|^p \sum_{k=1}^n n \binom{n}{k}^2 \bar{\Phi}^{n-k}(x) \bar{\Phi}^{n-k}(y) d\Phi^k(x) d\Phi^k(y) \quad (2.5.1.7a)$$

$$= \iint_{\Omega \times \Omega} |y - x|^p {}_2F_1 \left[1 - n, 1 - n; 1; \frac{\Phi(x)\Phi(y)}{\bar{\Phi}(x)\bar{\Phi}(y)} \right] d\bar{\Phi}^n(x) d\bar{\Phi}^n(y). \quad (2.5.1.7b)$$

Up to now no approximation has been performed. A nontrivial large n limit of Eq. (2.5.1.6) can be obtained setting, for each value of k , $k = (n + 1)s$ and introducing the variables ξ and η such that

$$\Phi(x) = s + \frac{\xi}{\sqrt{n}}, \quad \Phi(y) = s + \frac{\eta}{\sqrt{n}}, \quad (2.5.1.8a)$$

in such a way that s is kept fixed when $n \rightarrow +\infty$. This rescaling has a clear interpretation if we observe that an optimal assignment configuration between \mathcal{B} and \mathcal{R} for $p > 1$ can be mapped, through the cumulative function Φ , to an optimal assignment configuration of the same type between points uniformly distributed on $[0, 1]$, being Φ ordering preserving. We will develop this remark in § 2.6.3.

As shown in Refs. (144, 154) and recalled in § 2.2, the optimal assignment between random points uniformly distributed on the unit interval is asymptotically equivalent to a Brownian Bridge process after a rescaling of the type in Eq. (2.5.1.8a) is performed. This also implies that, as a consequence of Kolmogorov's universality, the (rescaled) transport field itself can be expressed, in the $n \rightarrow +\infty$ limit, in terms of the Brownian bridge process composed with the (inverse) cumulative function Φ^{-1} . Assuming that $\Omega = \bar{\Omega}$ and that $\bar{\Omega}$ is connected — i.e., that $(\rho \circ \Phi^{-1})(s) \neq 0$ for all $s \in [0, 1]$ —, we have

$$\Phi^{-1} \left(s + \frac{\xi}{\sqrt{n}} \right) = \Phi^{-1}(s) + \frac{\xi}{\sqrt{n}\Psi(s)} + o \left(\frac{1}{\sqrt{n}} \right), \quad (2.5.1.8b)$$

*To obtain Eq. (3.1.0.2) we have introduced the Gauss hypergeometric function

$${}_2F_1[a, b; c; z] := \sum_{k=0}^{\infty} \frac{(a)_k (b)_k}{(c)_k} \frac{z^k}{k!}, \quad (x)_k := \prod_{n=0}^{k-1} (x + n),$$

and we have used the fact that

$$\sum_{k=1}^n \binom{n}{k}^2 k^2 z^k = n^2 z \sum_{k=0}^{\infty} \frac{(1-n)_k (1-n)_k}{(1)_k} \frac{z^k}{k!} = n^2 z {}_2F_1[1 - n, 1 - n; 1; z].$$

where we have introduced the function

$$\Psi(s) := (\rho \circ \Phi^{-1})(s). \quad (2.5.1.8c)$$

A similar equation holds for $\Phi^{-1}(s + \eta/\sqrt{n})^\dagger$. This fact suggests that, in order to obtain a non trivial $n \rightarrow +\infty$ limit, μ_k must be rescaled as

$$\mu_k = \frac{\mu(s)}{\sqrt{n}}. \quad (2.5.1.8d)$$

Recall also that

$$\frac{1}{n+1} \leq s \leq 1 - \frac{1}{n+1}, \quad (2.5.1.9)$$

a fact that will have important consequences in the following. At the leading order, we may write the PDF of μ as

$$\begin{aligned} \Pr[\mu(s) \in d\mu] &= d\mu \iint \delta\left(\mu - \frac{\eta - \xi}{\rho(\Phi^{-1}(s))}\right) \frac{\exp\left(-\frac{\xi^2 + \eta^2}{2s(1-s)}\right)}{2\pi s(1-s)} d\xi d\eta \\ &= d\mu \frac{\Psi(s)}{2\sqrt{\pi s(1-s)}} \exp\left\{-\frac{[\Psi(s)]^2}{4s(1-s)}\mu^2\right\}. \end{aligned} \quad (2.5.1.10)$$

If the involved Riemann's sums converge, the sum over k in Eq. (2.5.1.7a) can be replaced with an integral over s

$$\varepsilon_n = \left(\int_0^1 ds \frac{s^{\frac{p}{2}}(1-s)^{\frac{p}{2}}}{[\Psi(s)]^p} \int_{-\infty}^{+\infty} |\mu|^p \frac{e^{-\frac{\mu^2}{4}}}{2\sqrt{\pi}} d\mu \right) n^{1-p/2}(1+o(1)) \quad (2.5.1.11a)$$

$$= \left(\frac{2^p}{\sqrt{\pi}} \Gamma\left(\frac{p+1}{2}\right) \int_0^1 \left[\frac{\sqrt{s(1-s)}}{\Psi(s)} \right]^p ds \right) n^{1-p/2}(1+o(1)) \quad (2.5.1.11b)$$

$$= \left(\frac{2^p}{\sqrt{\pi}} \Gamma\left(\frac{p+1}{2}\right) \int_{\Omega} dx \frac{\Phi^{\frac{p}{2}}(x) \bar{\Phi}^{\frac{p}{2}}(x)}{\rho^{p-1}(x)} \right) n^{1-p/2}(1+o(1)) \quad (2.5.1.11c)$$

which is the leading constant appearing in our argument of Eq. 2.2.0.6, and guarantees the so-called *bulk* scaling $\varepsilon_n = O(n^{1-p/2})$ for large n . This result can be stated in a slightly different way by saying that, if $\rho(x)$ has compact and connected support, then

$$\varepsilon_n = n^{1-p/2} \frac{2^p}{\sqrt{\pi}} \Gamma\left(\frac{p+1}{2}\right) \int_{\Omega} dx \frac{\Phi^{\frac{p}{2}}(x) \bar{\Phi}^{\frac{p}{2}}(x)}{\rho^{p-1}(x)} + o\left(\frac{1}{n^{\frac{p}{2}-1}}\right). \quad (2.5.1.11d)$$

[†]We will develop further these points in § 2.6.3.

On the other hand, we will say that ε_n has an *anomalous* scaling whenever the integral diverges. We will show now how information on the anomalous scaling can be extracted from the very same expression in Eqs. (2.5.1.11d) by means of a regularization recipe.

2.5.2. The problem of regularization

The recipe provided by Eqs. (2.5.1.11) for the calculation of the asymptotic of ε_n might fail due to the presence of divergences that have been neglected assuming $\Omega = \bar{\Omega}$ connected, as may happen for some PDFs. To explore this possibility, we will now relax the condition $\Omega = \bar{\Omega}$, but not the assumption that the closure $\bar{\Omega}$ is connected. The set $\bar{\Omega} \setminus \Omega$ is therefore given at most by isolated points (possibly at infinity). We will consider a disconnected $\bar{\Omega}$ in § 2.5.3.

The divergence of the expression in Eq. (2.5.1.11) suggests that $\lim_n n^{p/2-1} \varepsilon_n = +\infty$, but gives no hints about the scaling of $n^{p/2-1} \varepsilon_n$ in n . In this case, a regularization can be performed which takes into account the discrete nature of the problem, i.e., the finiteness of n . Such a regularization will allow us to extract information on the anomalous scaling of ε_n and, possibly, on the coefficients appearing in the leading or sub-leading asymptotics. Under the hypothesis $\Omega \neq \bar{\Omega}$ with $\bar{\Omega}$ connected, the expression in Eq. (2.5.1.11b) may diverge due to the presence of a point $x_* \in \partial\Omega$ (possibly at infinity) such that $\lim_{x \rightarrow x_*} \rho(x) = 0$. In particular, denoting by $s_* = \lim_{x \rightarrow x_*} \Phi(x) \in [0, 1]$, a non-integrable divergence appears in Eq. (2.5.1.11b) if

$$\Psi(s) = \begin{cases} O(s^{1/2+1/p}) & \text{if } s_* = 0, \\ O(|s - s_*|^{1/p}) & \text{if } 0 < s_* < 1, \\ O((1 - s)^{1/2+1/p}) & \text{if } s_* = 1. \end{cases} \quad (2.5.2.1)$$

Assuming that $\bar{\Omega}$ is connected, $\Omega \neq \bar{\Omega}$ does not automatically imply the presence of an anomalous scaling of ε_n : this is therefore a necessary, but not sufficient, condition.

We avoid the divergence by means of a cut-off. The correct cut-off to be adopted is suggested by the very approximations we have performed to obtain Eqs. (2.5.1.11) from Eq. (3.1.0.2), that is an exact expression.

A first regularization rule is obtained by taking into account Eq. (2.5.1.9) and therefore substituting $\int_0^1 ds \rightarrow \int_{c_0/n}^{1-c_1/n} ds$ in Eq. (2.5.1.11b), where c_0 and c_1 are two positive regularizing constants that are unspecified at this level. The regularization is required to obtain the proper leading scaling of the asymptotic ε_n only if a nonintegrable singularity appears in the integral in Eq. (2.5.1.11b) at $s_* = 0$ and/or $s_* = 1$, and it provides information on the scaling of the $o(1)$ corrections

otherwise.

If a nonintegrable pole $s_* \in (0, 1)$ is present, Eq. (2.5.1.8a) suggests to incorporate a finite-size correction removing an open ball centered at s_* having radius c_*/\sqrt{n} for some positive regularizing constant c_* to be determined. Indeed, in Eq. (2.5.1.8a) we have approximated the quantity $\Phi(x_k)$, image of the position of the k th point through the cumulative Φ , with its average value $s = k(n+1)^{-1}$, introducing an error that scales as $O(1/\sqrt{n})$.

In all cases, it is clear that the coefficients appearing in the scaling of ϵ_n obtained after the regularization will depend on the introduced regularizing constants, that have to be determined by means of a fit procedure. We will give now some examples of the approach described above, comparing the obtained predictions with the results of numerical simulations.

2.5.3. Applications

Absence of singularity: the flat distribution

Let us start from the simplest case $\mathcal{M} = \Omega = [0, 1]$, the Poisson-Poisson case (Def. 2.2.1) discussed in § 2.3.2 at $p = 2$. Here, blue and red points are extracted with uniform distribution $\rho(x) = \theta(x)\theta(1-x)$. The flat PDF case requires no regularization, being $\Psi(s) = 1$ and therefore we will briefly recall the final result only as an application of Eq. (2.5.1.11b) for the sake of completeness and for comparison with other cases studied below. The integral in Eq. (2.5.1.11b) converges for any $p > -2$ and gives

$$\epsilon_n = n^{1-p/2} \frac{\Gamma(p/2 + 1)}{p + 1} + o\left(\frac{1}{n^{p/2-1}}\right). \quad (2.5.3.1)$$

which is the expected ground state energy of our problem at $p > 1$ only. In particular, at $p = 2$, we have $\lim_n \epsilon_n = 1/3$, a result which can be alternatively derived via the $n \rightarrow \infty$ limit of the exact formula, valid $\forall n$, that is

$$\begin{aligned} \epsilon_n &= \sum_{k=1}^n k^2 \binom{n}{k}^2 \iint_0^1 (y-x)^2 (1-x)^{n-k} (1-y)^{n-k} x^{k-1} y^{k-1} dx dy \\ &= \frac{1}{3} \frac{n}{n+1}. \end{aligned} \quad (2.5.3.2)$$

Notice that this exact result is exactly two times the exact result for the Grid-Poisson case obtained by different methods in Eq. 2.3.1.10.

Singularity for $s_* \in \{0, 1\}$

Let us now consider a set of examples in which $\Psi(s_*) = 0$ for a value $s_* \in \{0, 1\}$. We consider both exponentially decaying PDFs (in particular the exponential distribution and the normalized positive part of minus the derivative of a standard gaussian distribution, also called Rayleigh distribution) and power-law decaying PDFs (Pareto laws).

Exponential distribution For the exponential distribution

$$\rho(x) = e^{-x}\theta(x), \quad \Phi(x) = (1 - e^{-x})\theta(x), \quad (2.5.3.3)$$

with $\Omega = [0, +\infty)$, and depending on p a non-integrable singularity may appear in Eq. (2.5.1.11b) for $x \rightarrow +\infty$. For $1 < p < 2$, the integral in Eq. (2.5.1.11b) is convergent and we have

$$n^{p/2-1}\varepsilon_n = \frac{2^p}{\sqrt{\pi}}\Gamma\left(\frac{p+1}{2}\right)\int_0^1\left(\frac{s}{1-s}\right)^{\frac{p}{2}}ds + o(1) = \Gamma(1+p)\Gamma\left(1-\frac{p}{2}\right) + o(1). \quad (2.5.3.4)$$

Formula 2.5.3.4 is fully consistent with numerical results (Fig. 2.5a) and indicates that a divergence appears when $p \rightarrow 2$, due to the rightmost pole of the Γ function on the real axis. Indeed, with reference to Eq. (2.5.2.1), we have that $\Psi(s) = 1-s = O((1-s)^{1/2+1/p})$ if $p \geq 2$. In order to elucidate the nature of this divergence, one can profit of the fact that, as in the case of uniform distribution, ε_n can be computed exactly for the exponential distribution at $p = 2$, directly from Eq. (3.1.0.2) *. It is given by

$$\begin{aligned} \varepsilon_n &= \sum_{k=1}^n k^2 \binom{n}{k}^2 \int_0^1 ds \int_0^1 dt \ln^2 \frac{1-s}{1-t} (st)^{k-1} (1-s)^{n-k} (1-t)^{n-k} \\ &= \sum_{k=1}^n \frac{2}{k} = 2H_n = 2\ln n + 2\gamma_E + \frac{1}{n} - \frac{1}{6n^2} + o\left(\frac{1}{n^2}\right), \end{aligned} \quad (2.5.3.5)$$

where H_n is the n -th harmonic number and γ_E is the Euler's gamma constant. Eq. (2.5.3.5) is compared to numerical experiments in Fig. 2.5b. The appearance of the divergence in our integral expression in Eq. (2.5.1.11b) is therefore due to an actual (logarithmic) divergence of ε_n for $n \rightarrow +\infty$. Following the criterion given

*We will re-obtain this result via a different path in § 2.6.6.

in § 2.5.2, Eq. (2.5.1.11b) for $p \geq 2$ is regularized as

$$\begin{aligned}\varepsilon_n &\approx \frac{2^p}{\sqrt{\pi}} \Gamma\left(\frac{p+1}{2}\right) \int_0^{1-c/n} \left(\frac{s}{1-s}\right)^{\frac{p}{2}} ds \\ &= \frac{2^{p+1}}{(p+2)\sqrt{\pi}} \Gamma\left(\frac{p+1}{2}\right) \left(1 - \frac{c}{n}\right)^{1+p/2} {}_2F_1\left[\frac{p}{2}, \frac{p}{2} + 1; \frac{p}{2} + 2; 1 - \frac{c}{n}\right].\end{aligned}\quad (2.5.3.6)$$

The expression above must be interpreted as a regularization-dependent *asymptotic* formula for the corresponding ε_n . In particular, the large n expansion will provide us the scaling properties of the optimal cost, up to some coefficients depending on the regularization. For example, at $p = 2$ the expression above becomes

$$\varepsilon_n = 2 \ln n - 2 \log c - 2 + o(1), \quad (2.5.3.7)$$

that is perfectly compatible with the exact formula in Eq. (2.5.3.5), whereas the finite-size correction depends on the regularization c . By comparison with Eq. (2.5.3.5) we can infer that

$$c = e^{-\gamma_E - 1} \approx 0.20655. \quad (2.5.3.8)$$

For $p > 2$ we can expand Eq. (2.5.3.6) as

$$n^{p/2-1} \varepsilon_n = \frac{2^{p+1} c^{1-p/2}}{(p-2)\sqrt{\pi}} \Gamma\left(\frac{p+1}{2}\right) n^{\frac{p}{2}-1} + o\left(n^{\frac{p}{2}-1}\right). \quad (2.5.3.9a)$$

In particular, for $2 < p < 4$ we have

$$n^{p/2-1} \varepsilon_n = \frac{2^{p+1} c^{1-p/2}}{(p-2)\sqrt{\pi}} \Gamma\left(\frac{p+1}{2}\right) n^{\frac{p}{2}-1} + \Gamma\left(1 - \frac{p}{2}\right) \Gamma(p+1) + o(1). \quad (2.5.3.9b)$$

In analogy with the discussion of (144), § 3, we obtain therefore the scaling $\varepsilon_n = O(1)$ for the leading term but we cannot give a prediction for the coefficient in front of it, due to its dependence on the regularization constant c . We have, instead, a complete analytic prediction for the first finite-size correction. For $p = 4$, a new logarithmic correction appears. In this case, indeed, our formula in Eq. (2.5.3.6) gives

$$n\varepsilon_n = \frac{12}{c} n - 24 \ln n + O(1). \quad (2.5.3.9c)$$

Once again, the coefficient of the leading term is unaccessible, despite the fact that the correct scaling is recovered, but we obtain a prediction of a logarithmic correction, with its coefficient. We do expect, but it is not obvious *a priori*, that the value of c appearing in Eqs. (2.5.3.9) is the same that we have obtained for

$p = 2$. Performing a fit on our numerical results, presented in Fig. 2.5c, we have obtained $c = 0.203(2)$ for $p = 3$, $0.2084(4)$ for $p = 4$ and $c = 0.2069(5)$ for $p = 5$, that are all within few errors from the value of in Eq. 2.5.3.8 analytically obtained for $p = 2$.

Rayleigh distribution As a further example of regularization in the case of a PDF with exponential tail, we consider now the Rayleigh distribution,

$$\rho(x) = xe^{-\frac{x^2}{2}}\theta(x), \quad \Phi(x) = \left(1 - e^{-\frac{x^2}{2}}\right)\theta(x). \quad (2.5.3.10)$$

In this case $\Omega = (0, +\infty)$ and we have

$$\Psi(s) = (1 - s)\sqrt{-2\ln(1 - s)} \quad (2.5.3.11)$$

which is infinitesimal both in $s = 0$ and in $s = 1$. In particular, $\Psi(s) = \sqrt{2s} + O(s^{3/2})$ for $s \rightarrow 0$ and therefore, according to Eq. (2.5.2.1), there are no integrability issues for $s \rightarrow 0$ for any value of $p > 1$. On the contrary, for $s \rightarrow 1$ $\Psi(s) = O((1 - s)^{1/2+1/p})$ for any $p > 1$. The integral is therefore always divergent and a regularization is needed. We proceed in the usual way, restricting ourselves to the $p = 2$ case,

$$\varepsilon_n \approx \int_0^{1-\frac{\varepsilon}{n}} \frac{s}{s-1} \frac{1}{\ln(1-s)} ds = \gamma_E + \ln \ln \frac{n}{c} + \int_{n/c}^{+\infty} \frac{dz}{z^2 \ln z} = \ln \ln n + \gamma_E + o(1). \quad (2.5.3.12)$$

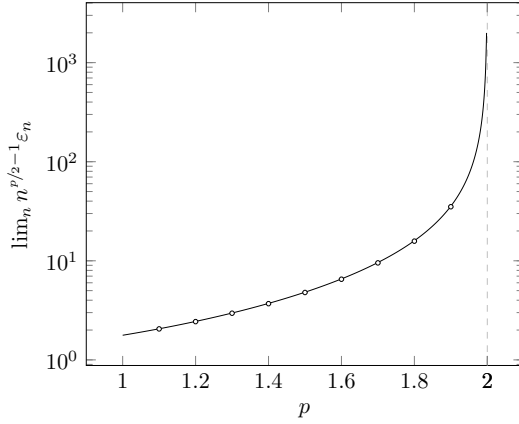
which is in excellent agreement with numerical experiments (Fig. 2.5d).

Pareto distribution Let us now consider a power-law decaying PDF, such as the Pareto distribution,

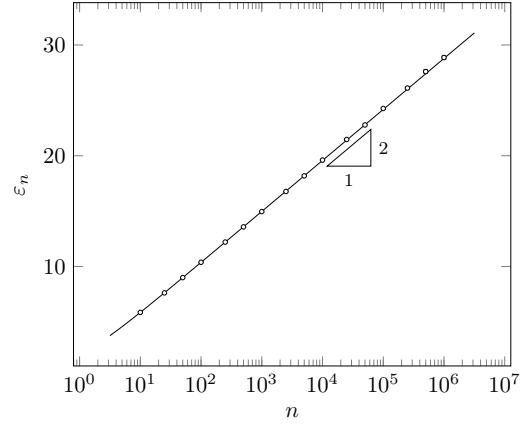
$$\rho_\alpha(x) = \frac{\alpha}{x^{\alpha+1}}\theta(x-1), \quad \Phi_\alpha(x) = \frac{x^\alpha - 1}{x^\alpha}\theta(x-1), \quad \alpha > 0. \quad (2.5.3.13)$$

Here we have $\Omega = [1, +\infty)$. If we consider the case

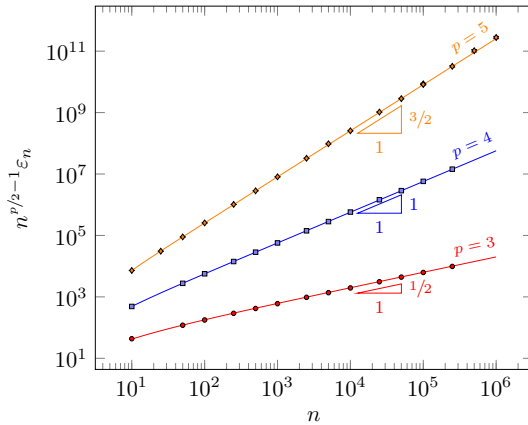
$$p < \frac{2\alpha}{\alpha + 2}, \quad (2.5.3.14)$$



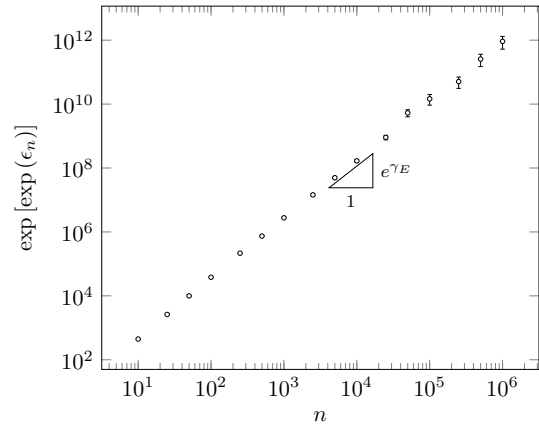
(a) Values of ε_n in the case of exponentially distributed points, obtained for $p \in (1, 2)$ compared with the theoretical prediction in Eq. (2.5.3.4) (smooth line). The asymptotic values of $n^{p/2-1}\varepsilon_n$ for each value of p (points) have been obtained fitting numerical results for n up to $2.5 \cdot 10^5$ points, assuming the scaling $f(n) = \epsilon + \epsilon_1 n^{\frac{p}{2}-1}$.



(b) At $p = 2$ in the case of exponentially distributed points, ε_n shows a logarithmic divergence, in agreement with the prediction in Eq. (2.5.3.7). The smooth line is the prediction in Eq. (2.5.3.5).



(c) Numerical results for ε_n at $p > 2$ in the case of exponentially distributed points. The smooth lines are fits obtained assuming the scaling behavior of Eqs. (2.5.3.9).



(d) Plot for $\exp[\exp(\varepsilon_n)] \sim n e^{\gamma E}$ in the case of Rayleigh distribution and $p = 2$, compared with leading order the theoretical prediction in Eq. (2.5.3.12) (triangle).

Figure 2.5. – Comparison between numerical experiments for ε_n and theoretical predictions in the case of exponential and Rayleigh distributions (error bars are represented but hardly visible).

Eq. (2.5.1.11b) gives a finite result, namely

$$\begin{aligned} \lim_n n^{p/2-1} \varepsilon_n &= \frac{2^p}{\alpha^p \sqrt{\pi}} \Gamma\left(\frac{p+1}{2}\right) \int_0^1 s^{\frac{p}{2}} (1-s)^{\frac{p}{2}-\frac{p}{\alpha}-p} ds \\ &= \frac{2^p}{\alpha^p \sqrt{\pi}} \frac{\Gamma\left(\frac{p}{2}+1\right) \Gamma\left(1-\frac{2+\alpha}{2\alpha}p\right) \Gamma\left(\frac{p+1}{2}\right)}{\Gamma\left(2-\frac{p}{\alpha}\right)}. \end{aligned} \quad (2.5.3.15)$$

This formula has been verified, for a subset of values of p and α , in Fig. 2.6a. When $(2-p)\alpha \leq 2p$ the integral does not converge (in particular, does not converge for any value of α when $p=2$). Indeed, with reference to Eq. (2.5.2.1), $\Psi_\alpha(s) = \alpha(1-s)^{1+\frac{1}{\alpha}}$, and, therefore, a non-integrable singularity appears for $s_* = 1$ when $1 + 1/\alpha \geq 1/2 + 1/p$. We can proceed regularizing the integral for $p \geq \frac{2\alpha}{\alpha+2}$,

$$\begin{aligned} n^{p/2} \varepsilon_n &\approx \frac{2^p}{\alpha^p \sqrt{\pi}} \Gamma\left(\frac{p+1}{2}\right) \int_0^{1-\frac{c}{n}} s^{\frac{p}{2}} (1-s)^{\frac{p}{2}-\frac{p}{\alpha}-p} ds \\ &= \frac{2^{p+1}}{\alpha^p \sqrt{\pi}} \frac{\Gamma\left(\frac{p+1}{2}\right)}{p+2} \left(1-\frac{c}{n}\right)^{\frac{p}{2}+1} {}_2F_1\left[\frac{p}{2}+1, \frac{p\alpha+2}{2\alpha}; \frac{p}{2}+2; 1-\frac{c}{n}\right] \\ &= \begin{cases} \frac{2^{p+1}}{\alpha^{p-1} \sqrt{\pi}} \frac{\Gamma\left(\frac{p+1}{2}\right)}{2p+\alpha p-2\alpha} \left(\frac{n}{c}\right)^{p\frac{\alpha+2}{2\alpha}-1} + o\left(n^{p\frac{\alpha+2}{2\alpha}-1}\right) & \text{for } p > \frac{2\alpha}{\alpha+2}, \\ \frac{p+2}{2} \ln n - \frac{p+2}{2} (H_{p/2} + \ln c) + o(1) & \text{for } p = \frac{2\alpha}{\alpha+2}. \end{cases} \end{aligned} \quad (2.5.3.16)$$

For example, when $p=2$ and $\alpha > 2$ we find

$$\varepsilon_n = \frac{1}{\alpha} \left(\frac{n}{c}\right)^{2/\alpha} - \frac{1}{\alpha-2} + o(1) \quad (2.5.3.17)$$

which is compared to numerical experiments in Fig. 2.6b.

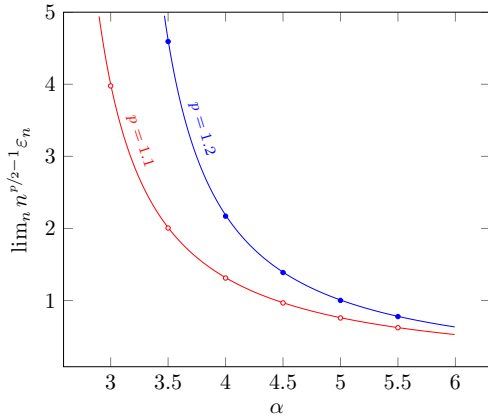
Singularity for $s_* \in (0, 1)$

Let us now consider a PDF such that $\Psi(s_*) = 0$ for $0 < s_* < 1$ and let us derive the scaling properties of the corresponding ε_n in this case. As an example, we consider

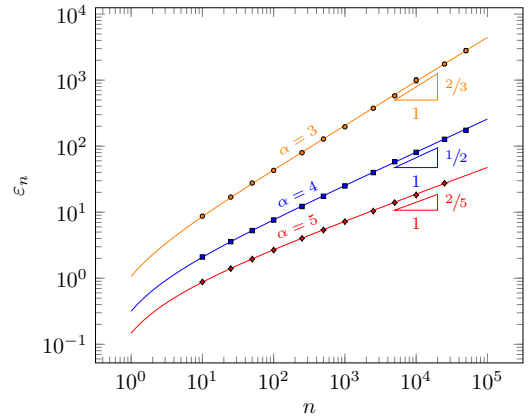
$$\rho_\alpha(x) = \frac{2 \cos^2(\alpha\pi x)}{1 + \text{sinc}(2\pi\alpha)} \theta(x)\theta(1-x), \quad \alpha \in (0, 1], \quad (2.5.3.18a)$$

$$\Phi_\alpha(x) = x \frac{1 + \text{sinc}(2\pi x\alpha)}{1 + \text{sinc}(2\pi\alpha)} \theta(x)\theta(1-x). \quad (2.5.3.18b)$$

(where we have used the common definition $\text{sinc}(x) := \frac{\sin(x)}{x}$). The distribution above recovers the uniform one for $\alpha \rightarrow 0$ and it has a (double) zero for $x = 1/2\alpha \in$



(a) Values of ε_n obtained for $p = 1.1$ and $p = 1.2$ and different values of α , compared with the theoretical prediction in Eq. (2.5.3.15) (smooth lines). The asymptotic value of $n^{p/2-1}\varepsilon_n$ for each value of p has been obtained fitting the numerical results for n up to 10^5 points, assuming the scaling $f(n) = \epsilon + \epsilon_1 n^{p \frac{\alpha+2}{2\alpha} - 1}$.



(b) Numerical results for the ε_n at $p = 2$ and different values of α . The fits are obtained using a fitting function in the form given by Eq. (2.5.3.17); we obtained $c = 0.0668(5)$ for $\alpha = 3$, $c = 0.0939(5)$ for $\alpha = 4$ and $c = 0.1121(6)$ for $\alpha = 5$.

Figure 2.6. – ε_n in the case of Pareto distribution. Error bars are represented but smaller than the markers.

$[1/2, 1]$ if $\alpha \in [1/2, 1]$. The support is therefore $\Omega = [0, 1] \setminus \{1/2\alpha\}$. In particular, for $\alpha \in [1/2, 1]$, we have

$$\Psi_\alpha(s) = \frac{(6\pi\alpha)^{2/3}}{\sqrt[3]{2 + 2\operatorname{sinc}(2\pi\alpha)}} (s - s_*)^{2/3} + o\left((s - s_*)^{2/3}\right),$$

$$\text{with } s_* := \frac{1}{2\alpha} \frac{1}{1 + \operatorname{sinc}(2\pi\alpha)}. \quad (2.5.3.19)$$

Therefore, by the general exposition given above, there are three different regimes for the asymptotic of ε_n depending on α .

For $\alpha \in (0, 1/2)$ the asymptotic of ε_n is finite for any value of $p > 1$. The integral in Eq. (2.5.1.11b) has been evaluated numerically and the prediction has been compared with our numerical results in Fig. 2.7a with excellent agreement.

When $\alpha = 1/2$ the singularity s_* moves to 1. We obtain the regularized integral

$$n^{p/2-1}\varepsilon_n = \frac{2^p}{\sqrt{\pi}} \Gamma\left(\frac{p+1}{2}\right) \int_0^{1-\frac{c_{1/2}}{\sqrt[3]{n}}} dx \frac{\Phi_\alpha^{\frac{p}{2}}(x) \bar{\Phi}_\alpha^{\frac{p}{2}}(x)}{\rho_\alpha^{p-1}(x)} + o(1)$$

$$\propto \begin{cases} n^{\frac{p}{6}-1} & \text{for } p > 6, \\ \ln n & \text{for } p = 6, \\ \text{constant} & \text{for } 1 < p < 6. \end{cases} \quad (2.5.3.20)$$

We verified the scaling above in Fig. 2.7c. In the $p = 6$ case, in particular, we have

$$n^2\varepsilon_n = \frac{160}{27\pi^4} \ln n + O(1). \quad (2.5.3.21)$$

For $\alpha \in (1/2, 1]$, instead, there is a singularity in $s_* \in [1/2, 1)$ and the regularization procedure has to be modified. In this case we have to exclude from the integration domain a ball centered in s_* and radius $O(1/\sqrt{n})$. Observing that

$$\Phi_\alpha^{-1}\left(\frac{1}{2\alpha(1 + \operatorname{sinc}(2\pi\alpha))} \pm \frac{c}{\sqrt{n}}\right) = \frac{1}{2\alpha} \pm \frac{1}{\alpha} \sqrt[3]{\frac{3c(1 + \operatorname{sinc}(2\pi\alpha))}{2\pi^2\sqrt{n}}} + o\left(\frac{1}{\sqrt[6]{n}}\right)$$

$$\equiv \frac{1}{2\alpha} \pm \frac{\hat{c}_\alpha}{\sqrt[6]{n}} + o\left(\frac{1}{\sqrt[6]{n}}\right), \quad (2.5.3.22)$$

and denoting the ‘‘regularized’’ domain by

$$\Omega_\alpha := [0, 1] \setminus \left(\frac{1}{2\alpha} - \frac{\hat{c}_\alpha}{\sqrt[6]{n}}, \frac{1}{2\alpha} + \frac{\hat{c}_\alpha}{\sqrt[6]{n}}\right), \quad (2.5.3.23)$$

we can write the regularized integral as

$$n^{p/2-1}\varepsilon_n = \frac{2^p}{\sqrt{\pi}}\Gamma\left(\frac{p+1}{2}\right) \int_{\Omega_\alpha} dx \frac{\Phi_\alpha^{p/2}(x)\bar{\Phi}_\alpha^{p/2}(x)}{\rho_\alpha^{p-1}(x)} + o(1)$$

$$\propto \begin{cases} n^{\frac{2p-3}{6}} & \text{for } p > 3/2, \\ \ln n & \text{for } p = 3/2, \\ \text{constant} & \text{for } 1 < p < 3/2, \end{cases} \quad (2.5.3.24)$$

where we limited ourselves to the leading asymptotics. The scaling predicted by Eq. (2.5.3.24) has been confirmed by numerical experiments at $p = 2, 3$ (Fig. 2.7b). For $p = 3/2$ in particular, we find

$$n^{3/4-1}\varepsilon_n = \frac{\Gamma(1/4)}{6\alpha(1 + \text{sinc}(2\pi\alpha))} \left(\frac{1 + \text{sinc}(2\pi\alpha) - \frac{1}{2\alpha}}{2\alpha\pi^2} \right)^{3/4} \ln n + O(1). \quad (2.5.3.25)$$

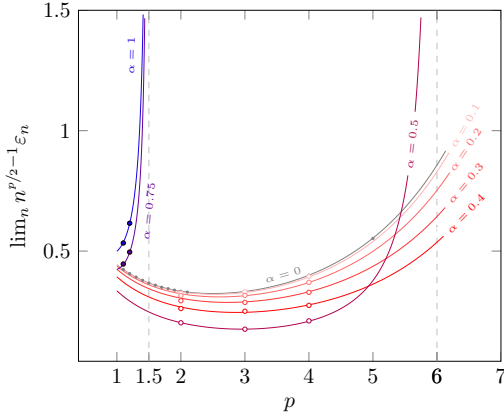
In Fig. 2.7d we show our numerical results for this case, once again in agreement with the prediction. Remark that the different regularization applied in this case implies a completely different scaling of the asymptotic of ε_n with respect to the one obtained for $s_* = 1$.

Assignment on disjoint intervals: an example

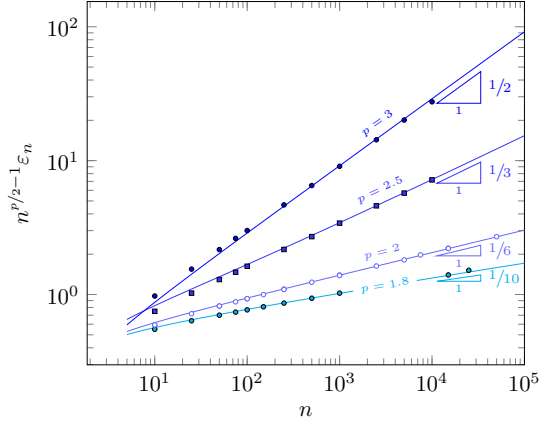
In the examples above, and in the general remarks in § 2.5.2, we have always assumed that the domain Ω is such that $\bar{\Omega}$ is a connected interval, and therefore Φ is an invertible function on $\bar{\Omega}$. This is not the case if the domain Ω has a ‘‘gap’’. In this Section we will study the effects of such a gap on the asymptotic of ε_n . We will limit ourselves to the case $\Omega = A \cup B$ with \bar{A}, \bar{B} connected intervals such that $\bar{A} \cap \bar{B} = \emptyset$. In the following we will assume that $\forall x \in A$ and $\forall y \in B$, $x < y$. To avoid complications due to the presence of singularities in the integrals, we will also assume that $\Omega = \bar{\Omega}$. The lack of invertibility of Φ is due in this case to the fact that $\lim_{x \rightarrow \sup A} \Phi(x) = \lim_{x \rightarrow \inf B} \Phi(x) = \hat{s}$, despite the fact that $a = \sup A \neq \inf B = b$. We expect that our approach proposed in § 2.5 fails in this situation, because the transport field μ_k in Eq. (2.5.1.3) is not infinitesimal in general for $n \rightarrow +\infty$.

In the simple case mentioned here, $\Omega = A \cup B$ with $\bar{A} \cap \bar{B} = \emptyset$, the exact formula in Eq. (3.1.0.2) can be written as

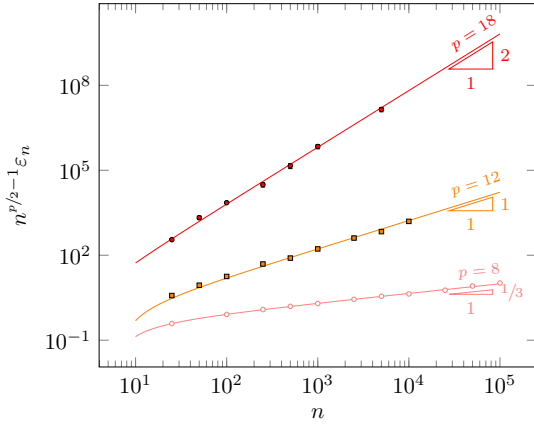
$$\varepsilon_n = \int d\mu |\mu|^p \sum_{k=1}^{\infty} \left[p_k^{(AA)}(\mu) + p_k^{(BB)}(\mu) + p_k^{(AB)}(\mu) + p_k^{(BA)}(\mu) \right]. \quad (2.5.3.26)$$



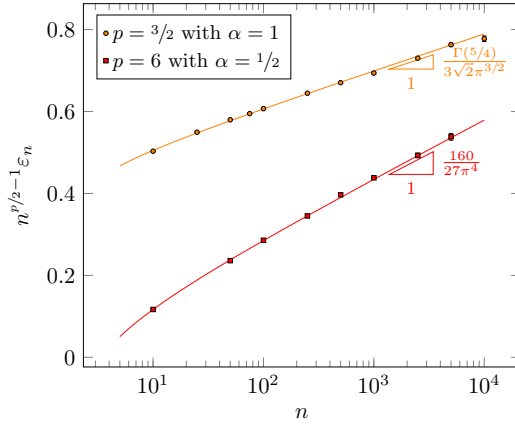
(a) Values of ϵ_n in the case of points distributed with PDF given in Eq. (2.5.3.18), obtained for different values of p and α for which $\lim_n n^{p/2-1}\epsilon_n$ is finite, compared with the theoretical prediction obtained using Eq. (2.5.1.11b) (smooth lines). The limit curve for $\alpha = 0$, given by Eq. (2.5.3.1), is also represented (gray), along with the numerical results for the asymptotic AOC in the uniform distribution case.



(b) Numerical results for ϵ_n in the case of points distributed with PDF given in Eq. (2.5.3.18) with $\alpha = 1$. The smooth lines are fits obtained assuming a scaling of the type $f(n) = n^{p/3-1/2}(\epsilon_1 + \epsilon_2/n) + \epsilon_0$. The obtained scaling are in agreement with the prediction in Eq. (2.5.3.24).



(c) Numerical results for ϵ_n in the case of points distributed with PDF given in Eq. (2.5.3.18) with $\alpha = 1/2$. The represented fits have been obtained assuming a fitting function $f(n) = n^{p/6-1}(\epsilon_1 + \epsilon_2/n) + \epsilon_0$. The obtained scaling laws are in agreement with the prediction in Eq. (2.5.3.20).



(d) Numerical results for ϵ_n in the case of points distributed with PDF given in Eq. (2.5.3.18) in the cases in which a logarithmic divergence appears. The smooth lines are fits obtained assuming a scaling $f(n) = \epsilon \ln n + \epsilon_0 + \epsilon_1/\ln n$, where ϵ has been provided by the predictions in Eq. (2.5.3.25) and Eq. (2.5.3.21).

Figure 2.7. – Comparison between numerical experiments and theoretical predictions for ϵ_n in the case of points distributed with PDF given in Eq. (2.5.3.18). Error bars are represented but hardly visible.

In the expression above, the quantity

$$\begin{aligned} p_k^{(XY)}(\mu) \, d\mu &:= \Pr[\mu_k \in d\mu, x_k \in X, y_k \in Y] \\ &= d\mu \binom{n}{k}^2 \iint_{X \times Y} \delta(\mu - y + x) \bar{\Phi}^{n-k}(x) \bar{\Phi}^{n-k}(y) \, d\bar{\Phi}^k(x) \, d\bar{\Phi}^k(y) \end{aligned} \quad (2.5.3.27)$$

is the joint probability that the k th transport field $\mu_k = y_k - x_k$ takes value in the interval $(\mu, \mu + d\mu)$, $x_k \in X$ and $y_k \in Y$. We expect that, to obtain a nontrivial $n \rightarrow +\infty$ limit from $p_k^{(AA)}$ and $p_k^{(BB)}$, we have to rescale μ_k following Eq. (2.5.1.8), due to the fact that matched points in the same interval can be arbitrarily close in the thermodynamical limit. Indeed, we can repeat the same calculations in § 2.5.1 performing the rescaling in Eqs. (2.5.1.8) and recovering, with the same *caveat*, a limiting distribution exactly in the form given in Eq. (2.5.1.10),

$$\begin{aligned} \frac{1}{n} \sum_{k=1}^n \Pr[\mu_k \in d\mu, x_k \in A, y_k \in A] + \frac{1}{n} \sum_{k=1}^n \Pr[\mu_k \in d\mu, x_k \in B, y_k \in B] \\ = d\mu \int_0^1 ds \frac{\Psi(s)}{2\sqrt{\pi s(1-s)}} \exp \left\{ -\frac{[\Psi(s)]^2}{4s(1-s)} \mu^2 \right\} + o(1). \end{aligned} \quad (2.5.3.28)$$

This formula is exactly the expression we would have obtained if $\bar{\Omega}$ were connected. If convergent, as it will happen under the hypotheses adopted here, this contribution will give a $O(n^{1-p/2})$ term in the expression of ε_n for $n \gg 1$.

On the other hand, the last two contributions in Eq. (2.5.3.26) corresponds to the matching transport between the two components of Ω , i.e., $A \rightarrow B$ or $B \rightarrow A$, and therefore the transport field in this case is of the order of the distance between A and B , namely $\inf B - \sup A$. The asymptotic rescaling given in Eqs. (2.5.1.8), therefore, cannot be applied to this term. However, from the fact that two matched points x_k and y_k have $|\Phi(x_k) - \Phi(y_k)| = O(1/\sqrt{n})$, if $x_k \in A$ and $y_k \in B$ we have

$$\Phi(x_k) = \hat{s} + \frac{\xi_k}{\sqrt{n}}, \quad \Phi(y_k) = \hat{s} + \frac{\eta_k}{\sqrt{n}} \quad (2.5.3.29)$$

with $\xi_k < 0$ and $\eta_k > 0$, and therefore

$$x_k = a + \frac{\xi_k}{\sqrt{n}\rho(a)} + o\left(\frac{1}{\sqrt{n}}\right), \quad y_k = b + \frac{\eta_k}{\sqrt{n}\rho(b)} + o\left(\frac{1}{\sqrt{n}}\right), \quad (2.5.3.30)$$

where $a = \sup A$ and $b = \inf B$ and, under our hypotheses, $\rho(a) \neq 0$ and $\rho(b) \neq 0$. The relations above suggest the rescaling $\mu_k \rightarrow b - a + \hat{\mu}_k/\sqrt{n}$ for $k = ns + 1/2$. A

nontrivial distribution for $\hat{\mu}$ is obtained assuming $s = \hat{s} + \sigma/\sqrt{n}$. Indeed

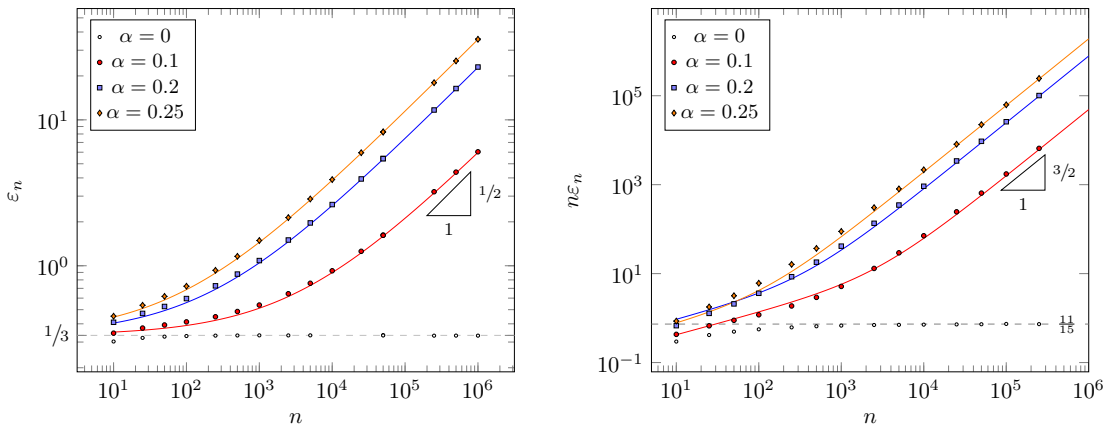
$$\begin{aligned}
& \sum_{k=1}^n \Pr[\mu_k \in d\mu, x_k \in A, y_k \in B] \\
&= d\mu \sum_{k=1}^n \binom{n}{k}^2 \int_0^{\hat{s}} du^k \int_{\hat{s}}^1 dv^k \delta(\mu - \Phi^{-1}(v) + \Phi^{-1}(u)) (1-u)^{n-k} (1-v)^{n-k} \\
&\approx \sqrt{n} d\hat{\mu} \int_{-\infty}^{+\infty} d\sigma \int_{-\infty}^0 d\xi \int_0^{+\infty} d\eta \delta\left(\hat{\mu} - \frac{\eta}{\rho(b)} + \frac{\xi}{\rho(a)}\right) \frac{\exp\left(-\frac{(\xi-\sigma)^2 + (\eta-\sigma)^2}{2\hat{s}(1-\hat{s})}\right)}{2\pi\hat{s}(1-\hat{s})} \\
&= \sqrt{n} d\hat{\mu} \begin{cases} \frac{\rho(a)\rho(b)}{2(\rho(a)-\rho(b))} \left[\operatorname{erf}\left(\frac{\rho(a)\hat{\mu}}{\sqrt{2\hat{s}(1-\hat{s})}}\right) - \operatorname{erf}\left(\frac{\rho(b)\hat{\mu}}{\sqrt{2\hat{s}(1-\hat{s})}}\right) \right] \theta(\hat{\mu}) & \rho(a) \neq \rho(b), \\ \rho^2(a)\hat{\mu} \frac{e^{-\frac{\rho^2(a)\hat{\mu}^2}{4\hat{s}(1-\hat{s})}}}{2\sqrt{\pi\hat{s}(1-\hat{s})}} \theta(\hat{\mu}) & \rho(a) = \rho(b), \end{cases} \\
&:= \sqrt{n} \Pr[\hat{\mu} \in d\hat{\mu}, A \rightarrow B].
\end{aligned} \tag{2.5.3.31}$$

The expression for $\Pr[\hat{\mu} \in d\hat{\mu}, B \rightarrow A]$ can be obtained in a similar manner. Collecting our results, we can write down the contribution to the asymptotic probability for $\hat{\varphi}$ given by the matching between points of different subintervals as

$$\Pr[\hat{\mu}(s) \in d\hat{\mu}, A \leftrightarrow B] = \sqrt{n} d\hat{\mu} \begin{cases} \rho(a)\rho(b) \frac{\operatorname{erf}\left(\frac{\rho(b)|\hat{\mu}|}{\sqrt{2\hat{s}(1-\hat{s})}}\right) - \operatorname{erf}\left(\frac{\rho(a)|\hat{\mu}|}{\sqrt{2\hat{s}(1-\hat{s})}}\right)}{2(\rho(b)-\rho(a))} & \rho(a) \neq \rho(b), \\ \rho^2(a)|\hat{\mu}| \frac{e^{-\frac{\rho^2(a)\hat{\mu}^2}{4\hat{s}(1-\hat{s})}}}{2\sqrt{\pi\hat{s}(1-\hat{s})}} & \rho(a) = \rho(b). \end{cases} \tag{2.5.3.32}$$

Observe that the previous contributions are not normalized in $\hat{\varphi}$. This is due to the fact that they appear as $O(1/\sqrt{n})$ corrections to the distribution $\Pr[\mu(s) \in d\mu]$ that has Eq. (2.5.3.28) as leading term: higher order corrections to $\Pr[\phi_k \in d\phi, x_k \in A, y_k \in A]$ and $\Pr[\phi_k \in d\phi, x_k \in B, y_k \in B]$, that would guarantee for $n \gg 1$ the total integral of the corrections to $\Pr[\varphi(s) \in d\varphi]$ to be zero, have not been computed. This will be irrelevant for our final computation, because the matching field is $O(1/\sqrt{n})$ when matching points in the same interval, but $O(1)$ when matching points in different intervals. The final result is

$$\begin{aligned}
\varepsilon_n &= |b-a|^p \sqrt{n} \int_{-\infty}^{+\infty} \Pr[\hat{\mu}(s) \in d\hat{\mu}, A \leftrightarrow B] + o(\sqrt{n}) \\
&= 2|b-a|^p \sqrt{\frac{\hat{s}(1-\hat{s})}{\pi}} \sqrt{n} + o(\sqrt{n}), \tag{2.5.3.33}
\end{aligned}$$



(a) Numerical results for ε_n in the case of points distributed with PDF given in Eq. (2.5.3.34) with $q = 1/2$ and $p = 2$. The fits are obtained assuming a scaling $f(n) = \alpha^2 \sqrt{n/\pi} + \delta$, where δ is a fitting parameter. The dashed line represents the asymptotic limit for $q = 0$ predicted by Eq. (2.5.1.11).

(b) Numerical results for ε_n in the case of points distributed with PDF given in Eq. (2.5.3.34) with $q = 3/4$ and $p = 4$. The fits are obtained assuming a scaling $f(n) = 1/4 \sqrt{3/\pi} \alpha^4 n^{3/2} + \delta \sqrt{n}$, where δ is a fitting parameter. The dashed line represents the asymptotic limit for $q = 0$ predicted by Eq. (2.5.1.11).

Figure 2.8. – Comparison of numerical experiments and analytical predictions for ε_n in the case of points distributed with the “gapped” PDF given in Eq. (2.5.3.34) (error bars are represented but hardly visible).

irrespectively from the fact that $\rho(a) = \rho(b)$ or not. Remarkably, the coefficient in front of the leading term does not depend on $\rho(x)$ but only on the average fraction of points that are in each of the two subintervals, i.e., on \hat{s} . Moreover, the obtained scaling can be intuitively justified observing that the number of blue points that are expected to fall, e.g., in A are $n\hat{s}$, but the fluctuations to this number scale as \sqrt{n} , and the same reasoning applies to \mathcal{R} . This means that $O(\sqrt{n})$ points in A have necessarily to be matched with points in B , by “crossing the gap”, with a matching cost that is $O(|b - a|^p)$, giving a final $O(\sqrt{n})$ contribution to ε_n .

Uniform distribution with a gap To exemplify the previous remarks, let us consider the following PDF on $\Omega = [0, 1/2 - \alpha/2] \cup [1/2 + \alpha/2, 1]$ with $\alpha \in [0, 1)$ and $q \in (0, 1)$,

$$\rho_{\alpha,q}(x) = \begin{cases} \frac{2q}{1-\alpha} & \text{if } x \in [0, 1/2 - \alpha/2], \\ \frac{2-2q}{1-\alpha} & \text{if } x \in [1/2 + \alpha/2, 1], \\ 0 & \text{otherwise.} \end{cases} \quad (2.5.3.34)$$

A gap of width α is present in $\Omega = \bar{\Omega}$ when $\alpha \neq 0$. With reference to the notation adopted in this Section, in this case we have exactly $\hat{s} = q$ for any value $\alpha \in (0, 1)$ and therefore Eq. (2.5.3.33) applies immediately, giving us

$$\varepsilon_n = 2\alpha^p \sqrt{\frac{q(1-q)}{\pi}} \sqrt{n} + o(\sqrt{n}). \quad (2.5.3.35)$$

This scaling law is compared to numerical experiments in Fig. 2.8a, where we consider $q = 1/2$ and $p = 2$, and in Fig. 2.8b, where we assume $q = 3/4$ and $p = 4$, in both cases with different values of α . The predictions are in excellent agreement with numerical results.

2.5.4. Conclusions

In this Section we have discussed the ERAP with convex weight cost $c(x, y) = \mathcal{D}^p(x, y) = |x - y|^p$ for $p > 1$, assuming the points to be independently and randomly distributed on the line, according to a PDF $\rho(x)$. We have given a general expression for the asymptotic of ε_n (Eq. 2.5.1.11) and we have shown that this general expression is possibly divergent, due to regions of very low density of points, i.e., to the zeros of $\rho(x)$. We have provided a regularization recipe which takes into account the effects of the discreteness of the problem when, denoting by $\Omega = \{x \in \mathbb{R}: \rho(x) > 0\}$, the set $\bar{\Omega} \setminus \Omega$ is made up by isolated points (possibly including the point at infinity). We have then exemplified our approach by applying the regularisation recipe to a set of examples, providing exact scaling of the asymptotic of $\langle \mathcal{H}_{\text{opt}} \rangle$ and, if possible, the coefficients appearing in it. Finally, we have also considered the case in which the set Ω has a gap, i.e., is composed by two disjoint intervals, showing that, in this situation, the effect of fluctuations in the number of points falling in each sub-interval dominates the whole asymptotic of $\langle \mathcal{H}_{\text{opt}} \rangle$, and the asymptotic coefficient is just given by the width of the gap.

2.6. Combinatorial and analytic approach to anomalous scaling: universality classes

THE continuum method discussed in § 2.5 allows to deal with the calculation of asymptotic constants if the involved integrals are convergent, and, when this is not the case, suggested a simple regularisation recipe for understanding the scaling of $\langle \mathcal{H}_{\text{opt}} \rangle$ in some cases.

Although that regularisation recipe could be written in general (such as in the case of a probability density of points vanishing at the frontier of the support), being non-rigorous, it could predict wrong scalings in some cases (such as in the case of probability density functions vanishing in the interior of their support).

Moreover, in the spirit of universality, one may want to know *a priori* what properties of the PDF are relevant for determining deviations from the bulk scaling behavior of $\langle \mathcal{H}_{\text{opt}} \rangle$. The latter task appears to be more difficult to attain through continuum methods, given the broad variety of possible scaling behaviors of $\langle \mathcal{H}_{\text{opt}} \rangle$ which we have found for natural choices of PDF already (power law, logarithmic and even log-log scalings).

A possibility is to take a step back from continuum methods and study the origin of anomalous scalings of $\langle \mathcal{H}_{\text{opt}} \rangle$ “from scratch”, that is, from an analysis of relative contributions of individual edges (or evaluations of transport field) entering the optimal assignment at finite n , and look at their relative magnitudes depending on the choice of PDF. A promising indication in this direction, which has been already foreseen in § 2.3, is that unexpectedly deep analogies (and new facts) have emerged upon studying the problem at finite n and then postponing the $n \rightarrow \infty$ limit as much as possible (see e.g. Eq. 2.3.1.17). These aspects altogether suggest that such a program might not be hopeless, and this is precisely the philosophy and content of the present Section, an extension of which constitutes the manuscript in preparation (174).

2.6.1. Notations and setting

As above, let us consider \mathcal{B} and \mathcal{R} sorted in natural order on $\mathcal{M} = \mathbb{R}$ (or a subset of), that is we have n blue points $x_1 \leq x_2 \leq \dots \leq x_n$ and n red points $y_1 \leq y_2 \leq \dots \leq y_n$. The points of each color are the sorted list of n i.i.d. random variables, sampled according to a probability density $\rho(x)$ (which is the same for red and blue). We call $R(x)$ its cumulant, and $R^{-1}(u)$ the inverse cumulant or quantile function. As a result, we can equivalently consider the extraction of u_i 's and v_j 's, uniform and independent in $[0, 1]$, and $x_i = R^{-1}(u_i)$, $y_i = R^{-1}(v_i)$ *.

*This fact is very much exploited in low-dimensional statistics, where it is sometimes called “inverse transform sampling” or “inversion method” (43).

For π a permutation of size n , the cost function $H_{(x,y)}(\pi)$ is determined by a real parameter $p > 0$, and is

$$H_{(x,y)}^{(p)}(\pi) = \sum_{i=1}^n |x_i - y_{\pi(i)}|^p \quad (2.6.1.1)$$

(the dependence of H from p may be omitted when clear).

We call $\pi_{\text{opt}}^{(p)}$ one optimal matching of the given instance for the exponent p , that is, one matching π that minimises the expression above, π_{id} the (unique) identity matching $\pi_{\text{id}}(i) = i$ (see Lemma 2.1.1), and π_{Dyck} the (unique) Dyck matching[†] (these two notions are independent of p). We call $H_{\text{opt}}^{(p)}(x, y)$, $H_{\text{id}}^{(p)}(x, y)$ and $H_{\text{Dyck}}^{(p)}(x, y)$ the function $H^{(p)}$ evaluated at $\pi = \pi_{\text{opt}}$, π_{id} and π_{Dyck} , respectively. Recall from § 2.5 that $\pi_{\text{opt}} = \pi_{\text{id}}$ if $p > 1$. Here, we will also use the fact that $\pi_{\text{opt}} = \pi_{\text{Dyck}}$ at $p = 1$. Our goal is to evaluate, as precisely as possible (and at least to the leading asymptotics for n large), the quantity $\langle H_{\text{opt}}^{(p)} \rangle_{\rho, n}$, that is averaged over the possible instances of size n sampled according to ρ , determined by the triple $(\rho(x), p, n)$.

As we have already mentioned, the Poisson-Poisson case has already been extensively studied. The case of $\rho(x)$ uniform on the interval $[0, 1]$ has been studied in (154) for the case $p \geq 1$ real, and in the variant in which $p < 0$ (more precisely, in (154) results are established for a whole class of cost functions, called there “ \mathcal{C} -functions”, which include the latter case). Recently (170), exploiting a connection with Selberg integrals, an exact expression in terms of p and n has been obtained for the case of $\rho(x)$ uniform on $[0, 1]$ and $p \geq 1$ real, namely

$$\begin{aligned} \langle H_{\text{opt}} \rangle_n &= n \frac{\Gamma(1 + p/2)}{p + 1} \frac{\Gamma(n + 1)}{\Gamma(n + 1 + p/2)} \\ &= \frac{\Gamma(1 + p/2)}{p + 1} n^{1-p/2} \left(1 - \frac{p(p + 2)}{8n} + \mathcal{O}(n^{-3}) \right). \end{aligned} \quad (2.6.1.2)$$

The case $p \in (0, 1]$ is the most challenging one, and investigations have been started only recently (173) (plus a companion paper in preparation). We report a summary for the asymptotic behavior of $\langle H_{\text{opt}} \rangle$ in Table 2.1.

When ρ is a smooth function valued on a compact connected interval, and $\log \rho$ is bounded on the domain, the asymptotics above does not change, that is, the scaling exponent is *universal* within this class of densities. Furthermore, the edges

[†]For $\sigma \in \{0, 1\}^n$ denoting the interlacing of blue and red points on the real line, we anticipate the construct of its *Dyck matching* π_{Dyck} as follows: first, construct a Dyck bridge by replacing the $+1$ and -1 of σ by up- and down-steps, then, pair, in the unique possible way, up- and down-steps which are at the same height and such that the segment connecting their mid-points doesn’t cross the walk. See § 2.7 for further details.

p	scaling of $\langle H_{\text{opt}} \rangle$
$p \in (0, \frac{1}{2})$	n^{1-p}
$p = \frac{1}{2}$	$n^{\frac{1}{2}} \ln n$
$\frac{1}{2} < p \leq 1$	$n^{\frac{1}{2}}$
$p \geq 1$	$n^{1-\frac{p}{2}}$

Table 2.1.: State of the art regarding the phase diagram of the “bulk” scaling behavior of the expected optimal cost in the one dimensional ERAP (see text for definitions).

give contributions to the cost which are all of the same order (for what concerns the scaling with n), regardless from their position along the segment (and the density in the position). For this reason the corresponding asymptotics is called the *bulk scaling* and is reported in Table 2.1.

However, the situation changes when ρ vanishes, either because it has a zero at a finite value or because it has an unbounded support, and vanishes at infinity. In such cases, depending on the choice of ρ , the large n behavior of $\langle H_{\text{opt}} \rangle$ may be considerably different from the bulk one, due to contributions of few “elongated” edges in the region of low density, which becomes more important than the “bulk” one discussed above. In this regime, we say that $\langle H_{\text{opt}} \rangle$ displays an *anomalous* scaling, and that the “edge” contribution outweighs the “bulk” one.

This situation has been investigated recently in (168) for the optimal transport of continuum measures, and, for the 1-dimensional ERAP, it is discussed in § 2.5 (see also the corresponding paper (169)). The present study is thus to be considered as a natural continuation of the investigations already appeared in (169), with a number of important modifications:

- Among the functions $\rho(x)$ decreasing at infinity faster than algebraically, in (169), only the Gaussian and the exponential cases are considered. Here we study the whole family of stretched-exponential tails, which, as we will see, determine a continuous family of critical exponents;
- The approach of (169) makes use of a non-rigorous and potentially dangerous regularisation scheme of certain diverging integrals, that is avoided here;
- As a further consequence of the “regularised integral” approach of (169), only the asymptotic behaviour could be determined, while the overall multiplicative asymptotic constant remains undetermined. Our approach allows to determine also these constants.

A limitation of our method is that we can only access the exponent values at $p = 1$

and $p \geq 2$ even integer, and we can only conjecture that the results extend to real values of p in suitable intervals, via the analytic continuation which is naturally suggested by the formula.

2.6.2. Families of distributions

As we explain at the end of Section 2.6.3, the possible anomalous behaviour of a general distribution $\rho(x)$ can be “decomposed” on the zeroes of this function, and, for each zero, only the local properties of ρ in a neighbourhood of the zero will determine the leading anomalous behaviour. Because of these facts, once we classify the possible local behaviours of main interest, we would have identified the possible universality classes of anomalous behaviour in our model, and it will suffice to study, for each universality class, a single distribution ρ which has one zero in the class. This analysis is performed here.

Distribution with a gap

First of all, the support of $\rho(x)$ can be connected or not. If it is not connected, we say that there is a *gap*. We start by analysing this simple situation.

Without loss of generality, say that the support of ρ is contained in $] - \infty, 0] \cup [a, +\infty[$, with $a > 0$, and that the integrals of ρ in these two intervals are q and $1 - q$, with $0 < q < 1$. Then, we have N_r^- and N_b^- red and blue points on the left, and $N_r^+ = n - N_r^-$ and $N_b^+ = n - N_b^-$ on the right. On average, both N_r^- and N_b^- are $\simeq qn$. However, these quantities fluctuate, independently, asymptotically in a Gaussian way, with variance $q(1 - q)n$, so that their difference $\delta n := N_r^- - N_b^-$ is Gaussian with variance $2q(1 - q)n$.

While the bulk energy is of the order of $E_{\text{bulk}}(n) \sim n^{1 - \frac{p}{2}}$, we have a trivial lower bound to the contribution to the energy coming from the $\delta n \ll W$ edges that jump across the gap, which has the form $\sqrt{4q(1 - q)/\pi} a^p \sqrt{n}$. Whenever $p > 1$, already this rough lower bound is leading over the bulk behaviour. When $p = 1$, as π_{id} is still optimal, we know that there is an optimal solution with *exactly* δn edges jumping across the gap, so that the energy of an instance is exactly the energy of the same instance in which the points on the right part are translated by $-a$, plus $a \delta n$. So, calling ρ' the translated density, we have that the average energy at $p = 1$ satisfies the relation

$$E_n(\rho) = \left(E_n(\rho') + a \sqrt{\frac{4q(1 - q)}{\pi}} \sqrt{n} \right) (1 + o(1)). \quad (2.6.2.1)$$

In this section we do not address the complicated concave case $p < 1$ (which we leave to a future work), so that the analysis above completely solves the case of a

density with a gap, and from now on we will only consider densities with connected support (more precisely, with a support with connected closure).

Types of zeroes

For a smooth function $\rho(x)$ on a connected support $]a, b[$, with a value x_0 such that $\rho(x_0) = 0$ (or $\lim_{x \rightarrow x_0} \rho(x) = 0$), there are three possibilities:

Finite endpoint: when the zero x_0 is the endpoint a (or b), and it is finite.

Endpoint at infinity: when the zero x_0 is the endpoint a (or b), and it is $a = -\infty$ (or $b = +\infty$).

We will consider the following two possible behaviours (let us write $f(x) \approx g(x)$ when $\ln(f(x)/g(x))/\ln(f(x)g(x)) \rightarrow 0$)

Stretched-exponential: $\rho(x) \approx \exp(-|x - x_0|^{-\alpha})$ for $x \rightarrow x_0$, when x_0 is finite, and $\rho(x) \approx \exp(-x^\alpha)$ for x large, when $x_0 = +\infty$.

Algebraic: $\rho(x) \approx |x - x_0|^{\beta-1}$ for $x \rightarrow x_0$, when x_0 is finite, and $\rho(x) \approx x^{-\beta-1}$ for x large, when $x_0 = +\infty$.

In principle, in the case of an internal zero, we could have different behaviors on the two sides, however, for sake of simplicity, we will not investigate this case.

In light of the universality of the anomalous behaviour discussed above, and of the crucial role of the function $R^{-1}(u)$ in the analytical treatment of the Lemmas in Section 2.6.3, we will choose one representative function for each of the cases described above (and, in particular, whenever the zero x_0 is finite, we will choose $x_0 = 0$), namely:

Endpoint at infinity, stretched exponential: for $\alpha > 0$, we consider the distributions $\rho_{ie,\alpha}(x) = \alpha x^{\alpha-1} \exp(-x^\alpha)$, with support on $[0, \infty[$. In this case $R_{ie,\alpha}(x) = \exp(-x^\alpha)$ and $R_{ie,\alpha}^{-1}(u) = (-\ln u)^{\frac{1}{\alpha}}$.

Finite endpoint, algebraic zero: for $\beta > 0$, we consider the distributions $\rho_{fa,\beta}(x) = \beta x^{\beta-1}$ with support on $[0, 1]$. In this case $R_{fa,\beta}(x) = x^\beta$, and $R_{fa,\beta}^{-1}(u) = u^{\frac{1}{\beta}}$.

Endpoint at infinity, algebraic zero: for $\beta > 0$, we consider the distributions $\rho_{ia,\beta}(x) = \beta x^{-\beta-1}$ with support on $[1, \infty[$. In this case $R_{ia,\beta}(x) = x^{-\beta}$, and $R_{ia,\beta}^{-1}(u) = u^{-\frac{1}{\beta}}$.

Internal, algebraic zero: in this case we just consider the distributions $\rho_{sa,\beta}(x) = \frac{1}{2} \rho_{fa,\beta}(|x|)$ with support on $[-1, 1]$. Thus $R_{sa,\beta}(x) = \frac{1}{2}(\text{sign}(x) |x|^\beta + 1)$, and $R_{sa,\beta}^{-1}(u) = \text{sign}(2u - 1) |2u - 1|^{\frac{1}{\beta}}$.

For each family of distributions we shall establish a “phase diagram” coupling the relevant parameter, α for the exponential cases and β for the algebraic cases, to the energy-distance exponent p . In the stretched exponential case parametrized by α , we will show that the leading scaling is a power of $\log n$ and obtain both the exponent and leading coefficients explicitly. In the algebraic cases parametrized by β , in the phase diagram in the plane (β, p) there is a region where there is no anomalous behavior (that is, the bulk contribution to the energy is larger than the one coming from the summands in the window around the zero), and in this region the energy is just given by the integral which is the continuum limit of Eq. 2.6.4, which has indeed only integrable singularities. Then, the complementary region consists of points where the anomalous contribution is leading. In this case we will also provide an evaluation of the *constant* in front of the leading anomalous term (we will derive the critical line for the internal algebraic zero case and only sketch the computations of aforementioned quantities, leaving the details to appear elsewhere). Then, universality implies that for any distribution we can evaluate the associated constant, by the appropriate decomposition of bulk part of the integral, and of windows around the zeroes. Finally, on the boundary between the two regions, there is a critical line where the type of zero is *marginally-anomalous*. It is often the case that, in this situation, the anomalous behaviour is larger of the bulk one just by a logarithmic factor. In these cases we will try to establish both the leading constant, in front of the logarithmic factor, and the first sub-leading correction.

Families of prob. dens.	leading scaling of $\langle H_{\text{opt}} \rangle$
Stretched exponential (sec. 2.6.5)	$\begin{cases} 2s^2 [\ln(n)]^{2s-1} & p = 2 \\ 2\zeta(p-1)s^p p! [\ln(n)]^{(s-1)p} & p \geq 4 \text{ even} \end{cases}$
Finite endpoint, algebraic zero (sec. 2.6.8)	$\begin{cases} b_{\beta,p} n^{1-p/2} & \text{Bulk regime} \\ a_{\beta,p} n^{-p/\beta} & \text{Anomalous regime} \\ Q(p) n^{2/(2-\beta)} \ln n & \text{Critical line } \beta = 2p/(p-2) \end{cases}$
Internal endpoint, algebraic zero (sec. 2.6.11)	$\begin{cases} 2B_{\beta,p} n^{1-p/2} & \text{Bulk regime} \\ (2A_{\beta,p} + K_{\beta,p}) n^{\frac{1}{2}(1-p/\beta)} & \text{Anomalous regime} \\ R(p) n^{(2-\beta)/(2(1-\beta))} \ln n & \text{Critical line } \beta = p/(p-1) \end{cases}$

Table 2.2.: Summary of results for the families of probability distributions considered in this paper (left column), with corresponding leading asymptotics of $\langle H_{\text{opt}} \rangle$ (right column). Here, ζ denotes Riemann’s zeta function, and the functions $b_{\beta,p}$, $a_{\beta,p}$, $Q(p)$, $B_{\beta,p}$, $A_{\beta,p}$, $K_{\beta,p}$, $R(p)$ are given explicitly in the corresponding sections.

2.6.3. General technical facts

In this section we establish various general lemmas, which apply to the study of all the distributions listed in the previous section, and in fact to any density $\rho(x)$.

Recall that we call $\rho(x)$ the probability density (which is the same for red and blue points), $R(x)$ its cumulant, and $R^{-1}(u)$ the inverse of R .

As we have seen, the probability that the k -th point of one given color is in a given infinitesimal interval, $x_k \in [R^{-1}(u), R^{-1}(u + du)]$, is given by the Beta distribution

$$P_{n,k}(u) du := \frac{n!}{(k-1)!(n-k)!} u^{k-1} (1-u)^{n-k} du. \quad (2.6.3.1)$$

Correspondingly, averages of a function $F(x_k)$ can be performed as

$$\langle F(x_k) \rangle_{\rho,n} = \int_0^1 du P_{n,k}(u) F(R^{-1}(u)). \quad (2.6.3.2)$$

Call (z_1, \dots, z_{2n}) the sorted list of the union on the x_i 's and the y_j 's, that is z_k is k -th point of the $2n$ points, irrespectively on the color. The probability that this point is in a given neighbourhood $z_k \in [R^{-1}(u), R^{-1}(u + du)]$, is given by a similar Beta distribution $P_{2n,k}(u) du$. As a result, averages of a function $F(z_k)$ can be performed as

$$\langle F(z_k) \rangle_{\rho,n} = \int_0^1 du P_{2n,k}(u) F(R^{-1}(u)). \quad (2.6.3.3)$$

More generally, averages of a function of t points, $F(z_{k_1}, z_{k_2}, \dots, z_{k_t})$, for $1 \leq k_1 < k_2 < \dots < k_t \leq 2n$, are described by a multi-dimensional Beta distribution, supported on the t -dimensional simplex $0 = u_0 \leq u_1 \leq \dots \leq u_t \leq u_{t+1} = 1$

$$\begin{aligned} & P_{2n,k_1,\dots,k_t}(u_1, \dots, u_t) du_1 \cdots du_t \\ & := \frac{2n!}{(k_1-1)!(k_2-k_1-1)! \cdots (k_t-k_{t-1}-1)!(2n-k_t)!} \\ & \quad \times u_1^{k_1-1} (u_2-u_1)^{k_2-k_1-1} \cdots (u_t-u_{t-1})^{k_t-k_{t-1}-1} (1-u_t)^{2n-k_t} du_1 \cdots du_t \end{aligned} \quad (2.6.3.4)$$

and we have

$$\langle F(z_{k_1}, \dots, z_{k_t}) \rangle_{\rho,n} = \int_{0 \leq u_1 \leq \dots \leq u_t \leq 1} du_1 \cdots du_t P_{2n,k_1,\dots,k_t}(u_1, \dots, u_t) F(R^{-1}(u_1), \dots, R^{-1}(u_t)). \quad (2.6.3.5)$$

We will use these properties in order to write the summands of our cost function in terms of suitable averages over the Beta distribution. The first Lemma concerns the case of p even.

Lemma 2.6.1 (Case $p \geq 2$ even). Let $R_\rho^{-1}(u)$ be the quantile function corresponding to density ρ . Define

$$M_{n,k,\ell}^{(\rho)} = \langle x_k^\ell \rangle_{\rho,n} = \langle R_\rho^{-1}(u)^\ell \rangle_{P_{n,k}}, \quad \ell \in \mathbb{N}. \quad (2.6.3.6)$$

Then, for $p \geq 2$ even, we have

$$\langle H_{\text{opt}}^{(p)} \rangle_{\rho,n} = \sum_{k=1}^n \sum_{q=0}^p \binom{p}{q} (-1)^{p-q} M_{n,k,q}^{(\rho)} M_{n,k,p-q}^{(\rho)}. \quad (2.6.3.7)$$

Proof. When $p \geq 1$, we know that $H_{\text{opt}} = H_{\text{id}}$ (see Lemma 2.1.1), and thus we can simply calculate $\langle H_{(x,y)}^{(p)}(\pi_{\text{id}}) \rangle_{\rho,n}$, a procedure that involves no optimisation. By definition of π_{id} we just have

$$H_{(x,y)}^{(p)}(\pi_{\text{id}}) = \sum_{k=1}^n |x_k - y_k|^p. \quad (2.6.3.8)$$

By linearity, we can just write

$$\langle H_{(x,y)}^{(p)}(\pi_{\text{id}}) \rangle_{\rho,n} = \sum_{k=1}^n E_{\rho,p,n}(k) \quad (2.6.3.9)$$

$$E_{\rho,p,n}(k) = \int_0^1 \int_0^1 du dv P_{n,k}(u) P_{n,k}(v) |R_\rho^{-1}(u) - R_\rho^{-1}(v)|^p. \quad (2.6.3.10)$$

If p is an even integer we can drop the absolute value and write

$$\begin{aligned} E_{\rho,p,n}(k) &= \sum_{q=0}^p \int_0^1 \int_0^1 du dv P_{n,k}(u) P_{n,k}(v) \binom{p}{q} (-1)^{p-q} R_\rho^{-1}(u)^q R_\rho^{-1}(v)^{p-q} \\ &= \sum_{q=0}^p \binom{p}{q} (-1)^{p-q} \langle R_\rho^{-1}(u)^q \rangle_{P_{n,k}} \langle R_\rho^{-1}(u)^{p-q} \rangle_{P_{n,k}}. \end{aligned} \quad (2.6.3.11)$$

□

The second Lemma concerns the case $p = 1$. In this case we have an annoying absolute value in the expression (2.6.3.10) for $E_{\rho,p,n}(k)$, and we do not know how to perform the calculation along the same line of Lemma 2.6.1. However, we have an alternate strategy that allows us to access our desired quantity. Instead of using the relation $H_{\text{opt}} = H_{\text{id}}$, we profit of the degeneracy at $p = 1$ and use instead $H_{\text{opt}} = H_{\text{Dyck}}$.

Let us consider the ordered list of z_i 's (from the right) of the $2n$ points, and let

us define $p_n(k_1, k_2)$ as the probability that the k_1 -th and k_2 -th steps of a random Dyck bridge are paired in π_{Dyck} (thus, in particular, $p_n(k_1, k_2) \neq 0$ only if $k_2 - k_1$ is odd). Various declinations of the function $p_n(k_1, k_2)$ have been calculated in (173). A version that we need here is as follows. Using the shortcut $h = \frac{k_2 - k_1 - 1}{2}$, and C_h for the Catalan's number, we have

$$p_n(k_1, k_2) = \frac{C_h}{\binom{2n}{n}} \left[\binom{2n - 2h - 2}{n - h - 1} + \frac{1 + (-1)^{k_1 + 1}}{2} \binom{k_1 - 1}{\frac{k_1 - 1}{2}} \binom{2n - k_2}{\frac{2n - k_2}{2}} \right]. \quad (2.6.3.12)$$

A related quantity is $q_n(\ell)$, which is the average number of edges (ij) in π_{Dyck} such that $i \leq \ell < j$, that is

$$q_n(\ell) = \sum_{\substack{i \leq \ell \\ j > \ell}} p_n(i, j), \quad (2.6.3.13)$$

that is, the average of the absolute value of the height of the Dyck bridge in ℓ . We have the following:

Proposition 2.6.2. *If $\frac{\ell}{n} \ll 1$, we have*

$$q_n(\ell) = \left[\sum_{0 \leq k < \frac{\ell}{2}} 2^{-2k} \binom{2k}{k} \right] \left(1 + \mathcal{O}\left(\frac{\ell}{n}\right) \right) \quad (2.6.3.14)$$

while if $\ell, n - \ell \gg 1$ we have

$$q_n(\ell) \simeq \sqrt{\frac{2}{\pi}} \sqrt{\frac{\ell(2n - \ell)}{2n}}. \quad (2.6.3.15)$$

Proof. For the case $\ell, n - \ell \gg 1$, we can apply the Stirling approximation to the expression for the absolute value of the height of the Dyck bridge in ℓ . This gives the Wiener formula for the associated Brownian Bridge, with the appropriate scaling factors. Integrating $|x|$ over the resulting Gaussian distribution gives the claimed result.

For the case $\frac{\ell}{n} \ll 1$, we can apply the Stirling approximation to the binomials $\binom{2n}{n}$, $\binom{2n - 2h - 2}{n - h - 1}$ and $\binom{2n - k_2}{\frac{2n - k_2}{2}}$ in (2.6.3.12), and approximate $\sqrt{n + \mathcal{O}(k_1, k_2)}$ factors by \sqrt{n} . This leads to an analogue of equation (2.6.3.12), valid for generic Dyck walks instead of Dyck bridges (that is, walks not constrained to have height 0 at $2n$). Thus, in this regime the distribution of the height of the Dyck bridge in ℓ is well-approximated by the analogous distribution for the Dyck walk, which is just

the binomial distribution. As a result we have

$$q_n(\ell) \simeq q(\ell) := \sum_{k=0}^{\ell} 2^{-\ell} \binom{\ell}{k} |2k - \ell|. \quad (2.6.3.16)$$

Now, these quantities satisfy a simple recursion: calling $\ell' = \ell - 1$,

$$\begin{aligned} q(\ell) &= 2^{-\ell} \sum_k \left(\binom{\ell-1}{k-1} + \binom{\ell-1}{k} \right) |2k - \ell| \\ &= 2^{-\ell'-1} \sum_{k'} \left(\binom{\ell'}{k'} |2k' - \ell' + 1| + \binom{\ell'}{k'} |2k' - \ell' - 1| \right). \end{aligned} \quad (2.6.3.17)$$

As for $n \in \mathbb{Z}$ we have $|n+1| + |n-1| = 2|n| + 2\delta_{n,0}$, we get

$$q(\ell+1) = \begin{cases} q(\ell) & \ell \text{ is odd;} \\ q(\ell) + 2^{-\ell} \binom{\ell}{\frac{\ell}{2}} & \ell \text{ is even.} \end{cases} \quad (2.6.3.18)$$

□

Lemma 2.6.3 (Case $p = 1$). *For a probability density ρ , let $M_{n,k,q}^{(\rho)}$ be defined as in Lemma 2.6.1. Then at $p = 1$*

$$\langle H_{\text{opt}} \rangle_{\rho,1,n} = \langle H_{\text{Dyck}} \rangle_{\rho,1,n} = \sum_{l=1}^{2n-1} q_n(l) \left(M_{2n,l+1,1}^{(\rho)} - M_{2n,l,1}^{(\rho)} \right). \quad (2.6.3.19)$$

Proof. Since the cost is a linear function of the positions, we have

$$\left\langle H_{\text{Dyck}}^{(p)} \right\rangle_{\rho,n} = \sum_{k_1 < k_2} p_n(k_1, k_2) \langle z_{k_2} - z_{k_1} \rangle_{\rho,n} \quad (2.6.3.20)$$

where z_i 's is the ordered list of the $2n$ points. But $z_{k_2} - z_{k_1}$ is a special case of a function $F(z_{k_1}, z_{k_2})$, and thus is calculated through the case $t = 2$ of the formulas (2.6.3.4) and (2.6.3.5), that is we have, by defining the quantity

$$E_n(k_1, k_2) := \langle z_{k_2} - z_{k_1} \rangle_{\rho,n} = \int_{0 \leq u \leq v \leq 1} du dv P_{2n,k_1,k_2}(u, v) (R_\rho^{-1}(u) - R_\rho^{-1}(v)) \quad (2.6.3.21)$$

that

$$\left\langle H_{\text{Dyck}}^{(1)} \right\rangle_{\rho,n} = \sum_{k_1 < k_2} p_n(k_1, k_2) E_n(k_1, k_2). \quad (2.6.3.22)$$

So we need to evaluate the RHS of equation (2.6.3.21). A useful general fact is that

the expression for this specific function $F(z_{k_1}, z_{k_2})$ separates in the two variables, so that in fact we just have

$$\begin{aligned} E_n(k_1, k_2) &= \int_{0 \leq u \leq 1} du P_{2n, k_1}(u) R_\rho^{-1}(u) - \int_{0 \leq v \leq 1} dv P_{2n, k_2}(v) R_\rho^{-1}(v) \\ &= M_{2n, k_1, 1}^{(\rho)} - M_{2n, k_2, 1}^{(\rho)}. \end{aligned} \quad (2.6.3.23)$$

The claimed expression then follows by telescoping. \square

Now we state a Proposition concerning the bulk behaviour at $p \geq 1$ which has been implicitly used in (169) (see also (154), appendix B). A corollary of this fact is that, if ρ vanishes in more than one point, the anomalous contributions coming from the various zeroes can be treated separately.

Proposition 2.6.4. *Let ρ , R and R^{-1} be as above. For every u such that $\rho(x)$ is continuous and strictly-positive in a neighbourhood of $x = R^{-1}(u)$, the limit $\lim_{\substack{n, k \rightarrow \infty \\ k/n \rightarrow u}} n^{\frac{p}{2}} E_{\rho, p, n}(k)$ exists, is finite, and is given by*

$$\lim_{\substack{n, k \rightarrow \infty \\ k/n \rightarrow u}} n^{\frac{p}{2}} E_{\rho, p, n}(k) = \frac{\Gamma\left(\frac{p+1}{2}\right)}{\sqrt{\pi}} \left(\frac{2\sqrt{u(1-u)}}{\rho(R^{-1}(u))} \right)^p. \quad (2.6.3.24)$$

We only give a sketch of proof of this fact. Let us call $u_k = R(x_k)$ and $v_k = R(y_k)$, and let us inspect the expression (2.6.3.10). By the conditions on ρ , we can use the CLT to infer that the quantities $u_k - u$ and $v_k - u$ are asymptotically independent centered Gaussian random variables with variance $\frac{k(n-k)}{n^3}$ (and the error terms can be easily handled at this point). Similarly, calling $x = R^{-1}(u)$, also $x_k - x$ and $y_k - x$ are asymptotically independent centered Gaussian random variables, now with variance $\frac{1}{\rho(x)^2} \frac{k(n-k)}{n^3}$ (at this point the error terms are more subtle, and involve the Taylor series of the logarithm of ρ around x). As a result, their difference is a centered Gaussian random variable with variance $\frac{2}{\rho(x)^2} \frac{k(n-k)}{n^3}$. As we have

$$\int_{-\infty}^{\infty} dx \frac{|x|^p}{\sqrt{2\pi}\sigma} e^{-\frac{x^2}{2\sigma^2}} = \frac{(\sqrt{2}\sigma)^p}{\sqrt{\pi}} \Gamma\left(\frac{p+1}{2}\right) \quad (2.6.3.25)$$

we deduce that

$$\lim_{\substack{n, k \rightarrow \infty \\ k/n \rightarrow u}} n^{\frac{p}{2}} E_{\rho, p, n}(k) = \lim_{\substack{n, k \rightarrow \infty \\ k/n \rightarrow u}} n^{\frac{p}{2}} \frac{\left(\frac{4}{\rho(x)^2} \frac{k(n-k)}{n^3}\right)^{\frac{p}{2}}}{\sqrt{\pi}} \Gamma\left(\frac{p+1}{2}\right) = \frac{\Gamma\left(\frac{p+1}{2}\right)}{\sqrt{\pi}} \left(\frac{2\sqrt{u(1-u)}}{\rho(R^{-1}(u))} \right)^p, \quad (2.6.3.26)$$

as was to be proven.

Now, suppose to work at n large but finite, and suppose that ρ vanishes in a finite list of points $\{x_1, \dots, x_m\}$ (which may include $\pm\infty$). The images $\{u_1, \dots, u_m\}$ under R are thus a list of values on $[0, 1]$. Fix some “window” value $W \sim n^\gamma$, with $\frac{1}{2} < \gamma < 1$. We can use Proposition 2.6.4 on all k such that $\min_j(|k - nu_j|) > W$, and perform a more careful analysis on the remaining values of k . Such a value of the window is chosen in order to have, asymptotically, two crucial properties. On one side, it is large enough that the proposition above can be applied because, up to exponentially-rare events, the approximation of $\rho(x')$ in a neighbourhood of $x = R^{-1}(k/n)$ by the value at x , and the use of CLT, are legitimate. On the other side, it is small enough that, for n large enough, the set of k 's which need a more careful analysis is split into m intervals, one per zero x_j of the density, so that the zeroes of ρ can be treated separately. Also, the window is small enough that the contribution of each of these intervals of values of k to the total energy depends on the shape of ρ only through the value of u_j , and through the leading local behaviour of $\rho(x)$ in a neighbourhood of $x = x_j$.

Once we classify the possible local behaviours of main interest, we would have identified the possible universality classes of anomalous behaviour in this model. This justifies the restriction of the analysis to the families of distributions described in Section 2.6.2.

2.6.4. Ensembles in which the average cost is infinite

When the support of the distribution ρ is not compact, it may be the case that $\langle H_{\text{opt}} \rangle_n = \infty$ also when $n < \infty$. We want to identify this situation, in order to exclude *a priori* the corresponding region from the study of the phase diagram.

Say that the support is contained within the interval $[0, +\infty[$, and label the points $\{z_1, \dots, z_{2n}\}$ from right to left. Assume, w.l.o.g., that z_1 is blue (the other case is treated identically). Then, there is a probability $q_n(k) = \binom{2n-k-2}{n-1} / \binom{2n-1}{n}$ that the right-most red point is z_{k+2} . As z_1 must be connected to some point of opposite color, and z_{k+2} is the nearest one, we have

$$H_{\text{opt}} \geq (z_1 - z_{k+2})^p \tag{2.6.4.1}$$

that is, using (2.6.3.5),

$$\begin{aligned}
\langle H_{\text{opt}} \rangle_n &\geq \langle (z_1 - z_{k+2})^p \rangle_{\rho, n} = \sum_{k=0}^{n-1} q_n(k) \int_{0 \leq u \leq v \leq 1} dudv P_{2n,1,k+2}(u, v) (R^{-1}(u) - R^{-1}(v))^p \\
&= \sum_{k=0}^{n-1} \frac{\binom{2n-k-2}{n-1}}{\binom{2n-1}{n}} \int_{0 \leq u \leq v \leq 1} dudv \frac{2n! (v-u)^k (1-v)^{2n-k-2}}{k! (2n-k-2)!} (R^{-1}(u) - R^{-1}(v))^p \\
&= 2n^2 \sum_{k=0}^{n-1} \binom{n-1}{k} \int_{0 \leq u \leq v \leq 1} dudv (v-u)^k (1-v)^{2n-k-2} (R^{-1}(u) - R^{-1}(v))^p \\
&= 2n^2 \int_{0 \leq u \leq v \leq 1} dudv ((1-u)(1-v))^{n-1} (R^{-1}(u) - R^{-1}(v))^p.
\end{aligned} \tag{2.6.4.2}$$

This is the general expression for our trivial lower bound to the optimal cost, which we shall check for finiteness.

As $v \geq u$, a slightly simpler bound is given by

$$\langle (z_1 - z_{k+2})^p \rangle_{\rho, n} \geq X_{n,p} := 2n^2 \int_{0 \leq u \leq v \leq 1} dudv (1-v)^{2n-2} (R^{-1}(u) - R^{-1}(v))^p. \tag{2.6.4.3}$$

In general, when the support is on the positive real axis,^{*} we have $R^{-1}(u) > R^{-1}(v)$, and we can perform an expansion, to get, for the quantity in Eq. 2.6.4.3,

$$\frac{X_{n,p}}{2n^2} = \sum_{\ell \geq 0} (-1)^\ell \binom{p}{\ell} \int_{0 \leq u \leq v \leq 1} dudv (1-v)^{2n-2} R^{-1}(u)^{p-\ell} R^{-1}(v)^\ell. \tag{2.6.4.4}$$

In the specific case of our endpoint at infinity, algebraic zero family of distributions $\rho_{\text{ia},\beta}$ (see § 2.6.2) we have

$$\frac{X_{n,p}}{2n^2} = \sum_{\ell \geq 0} (-1)^\ell \binom{p}{\ell} \int_{0 \leq u \leq v \leq 1} dudv (1-v)^{2n-2} u^{-\frac{p-\ell}{\beta}} v^{-\frac{\ell}{\beta}}. \tag{2.6.4.5}$$

When $p/\beta < 1$ we can use the general integral

$$\int_{0 \leq u \leq v \leq 1} dudv (1-v)^{2n-2} u^a v^b = \frac{1}{a+1} \int_0^1 dv (1-v)^{2n-2} v^{a+b+1} = \frac{(2n-2)! \Gamma(a+b+2)}{(a+1) \Gamma(2n+a+b+1)} \tag{2.6.4.6}$$

^{*}When this is not the case, because the support is $[-a, +\infty[$, we can just translate the distribution by a . When the support is the whole real axis, we can still perform the analysis, by “folding” the support, using the fact $H_{\text{opt}}(x_1, \dots, x_n; y_1, \dots, y_n) \geq H_{\text{opt}}(|x_1|, \dots, |x_n|; |y_1|, \dots, |y_n|)$.

which gives

$$\begin{aligned} \frac{X_{n,p}}{2n^2} &= \sum_{\ell \geq 0} (-1)^\ell \binom{p}{\ell} \frac{(2n-2)! \Gamma(2 - \frac{p}{\beta})}{(1 - \frac{p-\ell}{\beta}) \Gamma(2n+1 - \frac{p}{\beta})} \\ &= \frac{(2n-2)! \Gamma(1 - \frac{p}{\beta})}{\Gamma(2n+1 - \frac{p}{\beta})} \frac{\Gamma(1 + \beta - p) \Gamma(1 + p)}{\Gamma(1 + \beta)} \end{aligned} \quad (2.6.4.7)$$

that is, for large n , whenever $p < \beta$,

$$X_{n,p} \simeq n^{\frac{p}{\beta}} \frac{\Gamma(1 - \frac{p}{\beta}) \Gamma(1 + \beta - p) \Gamma(1 + p)}{2^{1 - \frac{p}{\beta}} \Gamma(1 + \beta)} \quad (2.6.4.8)$$

Conversely, when $p \geq \beta$ this expression diverges, as is also evinced from the analytic continuation of the result, which has a factor $\Gamma(1 - \frac{p}{\beta})$ which is singular in the limit $p \nearrow \beta$.

As a result, we evince that, for our family of distributions with endpoint at infinite, algebraic zero, we just have $\langle H_{\text{opt}} \rangle_n = \infty$ whenever $p \geq \beta$. Also, we have a first glance to an ‘‘anomalous behaviour’’: recalling that the bulk energy scales as $n^{1-p/2}$ (see Table 2.1), we see that the leading behaviour in n of $\langle (z_1 - z_{k+2})^p \rangle_{\rho,n}$ takes over the bulk behaviour at least in the region $f(\beta) < p < \beta$, for

$$f(\beta) = \begin{cases} \frac{\beta}{\beta+1} & \beta \leq 1 \\ \frac{\beta}{2} & 1 \leq \beta \leq 2 \\ \frac{\beta}{\beta/2+1} & 2 \leq \beta. \end{cases} \quad (2.6.4.9)$$

2.6.5. Family of stretched exponentials with endpoint at infinity $\rho_{\text{ie},\alpha}$ and $\rho_{\text{ie},\alpha}^+$

Let us consider the 1-parameter family of stretched exponential distributions depending on a parameter $\alpha > 0$

$$\rho_{\text{ie},\alpha}(x) dx = \alpha x^{\alpha-1} \exp(-x^\alpha) \theta(x) dx \quad (2.6.5.1)$$

that is $R_\alpha(x) = \exp(-x^\alpha) \theta(x)$ and hence

$$R_\alpha^{-1}(u) = (-\ln u)^{\frac{1}{\alpha}}. \quad (2.6.5.2)$$

We will use the shortcut $s = 1/\alpha$. We will call

$$E_n^{(s,p)} := \langle H_{\text{opt}} \rangle_{\rho_{\text{ie},\alpha,p,n}} \quad (2.6.5.3)$$

and our goal is to study the function $E_n^{(s,p)}$. A second family of measures also depending on a parameter $\alpha > 0$ is

$$\rho_{\text{ie},\alpha}^+(x) dx = \alpha x^{\alpha-1} \exp(1-x^\alpha) \theta(x-1) dx \quad (2.6.5.4)$$

for which $R_\alpha(x) = \exp(1-x^\alpha) \theta(x-1)$ and hence

$$R_{\alpha^+}^{-1}(u) = (1 - \ln u)^{\frac{1}{\alpha}} = (1 - \ln u)^s. \quad (2.6.5.5)$$

We will correspondingly call

$$E_n^{(s^+,p)} := \langle H_{\text{opt}} \rangle_{\rho_{\text{ie},\alpha^+,p,n}^+} \quad (2.6.5.6)$$

and we also aim to study the function $E_n^{(s^+,p)}$.

As we will see, this second family of distributions will make the calculations more cumbersome. However, it has the advantage that $\rho_{\text{ie},\alpha}^+(x)$, contrarily to $\rho_{\text{ie},\alpha}(x)$ in general, is neither vanishing nor diverging at the left endpoint of the support, so that we know for sure than any anomalous scaling of the cost (w.r.t. the case of uniform distribution) must come from the tail located at $+\infty$, and not from the second singularity in 0 (or from a combination of the two effects). As we will see *a posteriori*, the singularity in zero gives a less relevant anomalous scaling than the singularity at infinity, as $E_n^{(s,p)}$ and $E_n^{(s^+,p)}$ do have the same leading asymptotics.

Exact and asymptotic results at $p > 1$ even

Let us consider the family of distributions (2.6.5.1) first. From Lemma 2.6.1, we just need to compute for $q, k, n \in \mathbb{N}$ the integral

$$M_{n,k;q} := \int_0^1 du P_{n,k}(u) (-\ln u)^q. \quad (2.6.5.7)$$

Of course $M_{k,n;0} = 1$, since the $P_{n,k}$ distributions (eq. (2.6.3.1)) are normalized.

From this point onward, we will assume the basic notions of the theory of Symmetric Functions (see for example (76), chapter one). Let us introduce the *alphabet*

$$A_{k,n} := \left\{ \frac{1}{k}, \frac{1}{k+1}, \dots, \frac{1}{n} \right\} \quad (2.6.5.8)$$

and let us use the symbol $h_k(X)$ for the *complete homogeneous symmetric function* of degree k , in the alphabet X , (and, for future convenience, $e_k(X)$ for the *elementary symmetric functions*), that is, in the case of a finite alphabet of size m

$X = \{x_1, \dots, x_m\}$, the functions

$$h_k(x_1, \dots, x_m) = \sum_{1 \leq j_1 \leq \dots \leq j_k \leq m} x_{j_1} x_{j_2} \cdots x_{j_k}, \quad (2.6.5.9)$$

$$e_k(x_1, \dots, x_m) = \sum_{1 \leq j_1 < \dots < j_k \leq m} x_{j_1} x_{j_2} \cdots x_{j_k}. \quad (2.6.5.10)$$

We also set the useful convention $h_0(X) = e_0(X) = 1$. We have

Lemma 2.6.5.

$$M_{n,k;q} = q! h_q(A_{k,n}). \quad (2.6.5.11)$$

In order to establish Lemma 2.6.5 we will need a useful (simple) technical Lemma:

Lemma 2.6.6. *Let $p \in \mathbb{N}$. Let $A(q) = a_p q^p + a_{p-1} q^{p-1} + \dots + a_0$ be a polynomial of degree at most p . Then we have*

$$\sum_{q=0}^p \binom{p}{q} (-1)^{p-q} A(q) = p! a_p. \quad (2.6.5.12)$$

Proof of Lemma 2.6.6. Rewrite $A(q)$ as

$$A(q) = \sum_{k=0}^p b_k q(q-1) \cdots (q-k+1). \quad (2.6.5.13)$$

In particular, $b_p = a_p$. In this basis we have

$$\begin{aligned} \sum_{q=0}^p \binom{p}{q} (-1)^{p-q} A(q) &= \sum_{k=0}^p b_k \sum_{q=0}^p \binom{p}{q} (-1)^{p-q} q(q-1) \cdots (q-k+1) \\ &= \sum_{k=0}^p b_k \sum_{q=k}^p \frac{p!}{q!(p-q)!} (-1)^{p-q} q(q-1) \cdots (q-k+1) \\ &= \sum_{k=0}^p \frac{b_k p!}{(p-k)!} \sum_{r=0}^{p-k} \frac{(p-k)!}{r!(p-k-r)!} (-1)^{(p-k)-r} = \sum_{k=0}^p \frac{b_k p!}{(p-k)!} \delta_{p,k} = p! b_p \end{aligned} \quad (2.6.5.14)$$

This completes the proof. \square

Proof of Lemma 2.6.5. Using the fact $-\ln t = \lim_{u \rightarrow 0} \frac{t^{-u} - 1}{u}$, we can write $M_{n,k;p} = \lim_{u \rightarrow 0} M_{n,k;p}(u)$, where the expression

$$M_{n,k;p}(u) := \int_0^1 dt t^{k-1} (1-t)^{n-k} \left(\frac{t^{-u} - 1}{u} \right)^p \frac{\Gamma(n+1)}{\Gamma(k)\Gamma(n-k+1)} \quad (2.6.5.15)$$

is well-defined for $u < p^{-1}$, and in particular in a neighborhood of $u = 0$. Expanding the binomial $(t^{-u} - 1)^p$, we recognise that each term in the sum can be evaluated in terms of a Beta integral, and we just get

$$\begin{aligned}
M_{n,k;p}(u) &= u^{-p} \langle (t^{-u} - 1)^p \rangle_{P_{n,k}} \\
&= u^{-p} \sum_{q=0}^p \binom{p}{q} (-1)^{p-q} \langle t^{-qu} \rangle_{P_{n,k}} \\
&= u^{-p} \sum_{q=0}^p \binom{p}{q} (-1)^{p-q} \frac{\Gamma(n+1)\Gamma(k-qu)}{\Gamma(k)\Gamma(n+1-qu)} \\
&= u^{-p} \sum_{q=0}^p \binom{p}{q} (-1)^{p-q} \prod_{h=k}^n \left(1 - \frac{qu}{h}\right)^{-1} \\
&= u^{-p} \sum_{q=0}^p \binom{p}{q} (-1)^{p-q} \sum_{\ell \geq 0} q^\ell u^\ell h_\ell(A_{k,n}).
\end{aligned} \tag{2.6.5.16}$$

At this point, Lemma 2.6.6 allows to compute the limit $u \rightarrow 0$ straightforwardly:

$$\begin{aligned}
M_{n,k;p} &= \lim_{u \rightarrow 0} u^{-p} \sum_{q=0}^p \binom{p}{q} (-1)^{p-q} \sum_{\ell \geq 0} q^\ell u^\ell h_\ell(A_{k,n}) \\
&= \lim_{u \rightarrow 0} u^{-p} (p! u^p h_p(A_{k,n}) + \mathcal{O}(u^{p+1})) = p! h_p(A_{k,n}).
\end{aligned} \tag{2.6.5.17}$$

□

Since $M_{n,k,l}^{(\text{ie},s)} = M_{n,k;sl}$, Lemma 2.6.5 implies

$$\begin{aligned}
E_{(s,p),n}(k) &= \sum_{q=0}^p \binom{p}{q} (-1)^{p-q} M_{n,k;sq} M_{n,k;s(p-q)} \\
&= \sum_{q=0}^p (-1)^q \binom{p}{q} (sq)!(s(p-q))! h_{sq}(A_{k,n}) h_{s(p-q)}(A_{k,n}).
\end{aligned} \tag{2.6.5.18}$$

As of our second family of distributions (2.6.5.4), $M_{n,k,q}^{(\text{ie},\alpha^+)} := \langle (1 - \ln u)^{sq} \rangle_{P_{n,k}}$ can still be written in terms of the $M_{n,k,h}$'s, namely

$$M_{n,k,q}^{(\text{ie},\alpha^+)} = \sum_{r=0}^{sq} \binom{sq}{r} M_{n,k;r} \tag{2.6.5.19}$$

so that by Lemma 2.6.1 we have

$$\begin{aligned}
E_{(s^+,p),n}(k) &= \sum_{\substack{0 \leq q \leq p \\ 0 \leq r \leq sq \\ 0 \leq r' \leq s(p-q)}} \binom{p}{q} \binom{sq}{r} \binom{s(p-q)}{r'} (-1)^{p-q} M_{n,k,r} M_{n,k,r'} \\
&= \sum_{\substack{0 \leq q \leq p \\ 0 \leq r \leq sq \\ 0 \leq r' \leq s(p-q)}} \binom{p}{q} \binom{sq}{r} \binom{s(p-q)}{r'} (-1)^{p-q} r! r'! h_r(A_{k,n}) h_{r'}(A_{k,n})
\end{aligned} \tag{2.6.5.20}$$

where in the last step Lemma 2.6.5 has again been used.

In the case $s = 1$, corresponding to an exponential decay at $+\infty$, an important simplification occurs and we have an exact result. Call $H(t, X) = \sum_{\ell \geq 0} h_\ell(X) t^\ell = \prod_{x \in X} (1 - tx)^{-1}$ and $E(t, X) = \sum_{\ell \geq 0} e_\ell(X) t^\ell = \prod_{x \in X} (1 + tx)$. Then

$$\begin{aligned}
E_{(1,p),n}(k) &= p! \sum_{q=0}^p (-1)^q h_q(A_{k,n}) h_{p-q}(A_{k,n}) \\
&= p! [t^p] H(t, A_{k,n}) H(-t, A_{k,n}).
\end{aligned} \tag{2.6.5.21}$$

For $X = \{x_1, x_2, \dots\}$, call X^2 the alphabet $X^2 = \{x_1^2, x_2^2, \dots\}$. We obviously have $H(t, X)H(-t, X) = H(t^2, X^2)$, and we recognise

$$E_{(1,p),n}(k) = p! [t^p] H(t^2, A_{k,n}^2) = p! h_{p/2}(A_{k,n}^2) \tag{2.6.5.22}$$

(recall that we assumed that p is even). Also, $E_{(1^+,p),n}(k) = E_{(1,p),n}(k)$, as in fact $\rho_{ie,\alpha}^+(x) = \rho_{ie,\alpha}(x-1)$ at $\alpha = 1$, and of course the cost function is invariant under a global translation of the $2n$ points.

For general s we only have an asymptotic result. Call as customary $p_k(X)$ the power-sum functions $p_k(X) = \sum_{x \in X} x^k$. Define $P(t, X) = \sum_{k \geq 1} k^{-1} p_k(X) t^k$ *. Then we have $H(t, X) = \exp(P(t, X))$ and $E(t, X) = \exp(-P(-t, X))$. The first of these two formulas provides polynomial expressions in the p_j 's for the h_i 's. If all the elements of the alphabet X are real-positive, the generalised-mean inequalities imply that $(p_j(X))^{1/j}$ form a decreasing monotonic sequence.

In a situation in which $p_1 \gg \sqrt{p_2}$, we can study a perturbative expansion of the expressions for $E_{(s,p),n}(k)$ and $E_{(s^+,p),n}(k)$ w.r.t. this parameter. Call $P_+(t, X) =$

*Note that, contrarily to $H(t, X)$, and its companion $E(t, X)$ for elementary symmetric functions, in which there exists a single natural definition, in literature there exist different choices of definition for a generating function $P(t, X)$, and we have chosen the one that is more convenient in our context, so our formulas involving P may differ from the ones the reader is accustomed to.

$P(t, X) - tp_1(X)$. Then we have

$$h_k(X) = [t^k]H(t, X) = [t^k] \exp(P(t, X)) = \sum_{\ell=0}^k \frac{1}{(k-\ell)!} p_1(X)^{k-\ell} [t^\ell] \exp(P_+(t, X)). \quad (2.6.5.23)$$

Let us start the analysis with the case of the family in eq. (2.6.5.1). Substituting eq. (2.6.5.23) in (2.6.5.18), gives

$$E_{(s,p),n}(k) = \sum_{q=0}^p (-1)^q \binom{p}{q} (sq)!(s(p-q))! \sum_{\ell, \ell'} \frac{p_1(A_{k,n})^{sp-\ell-\ell'}}{(sq-\ell)!(s(p-q)-\ell')!} \quad (2.6.5.24)$$

$$\times ([t^\ell] \exp(P_+(t, A_{k,n}))) ([t^{\ell'}] \exp(P_+(t, A_{k,n}))).$$

The smaller ℓ and ℓ' are, the larger is the power of p_1 , which, under our assumption, is the leading factor. However, the associated factor $\frac{(sq)!(s(p-q))!}{(sq-\ell)!(s(p-q)-\ell')!}$ is a polynomial in q of degree $\ell + \ell'$, so that by Lemma 2.6.6 we know that all the contributions with $\ell + \ell' < p$ vanish exactly. The leading contribution thus comes from the terms with $\ell + \ell' = p$, which give

$$E_{(s,p),n}(k) \simeq \sum_{q=0}^p (-1)^q \binom{p}{q} (sq)!(s(p-q))! \sum_{\ell} \frac{p_1(A_{k,n})^{(s-1)p}}{(sq-\ell)!(s(p-q)-(p-\ell))!}$$

$$\times ([t^\ell] \exp(P_+(t, A_{k,n}))) ([t^{p-\ell}] \exp(P_+(t, A_{k,n})))$$

$$= p! s^p p_1(A_{k,n})^{(s-1)p}$$

$$\times \sum_{\ell=0}^p (-1)^{-\ell} ([t^\ell] \exp(P_+(t, A_{k,n}))) ([t^{p-\ell}] \exp(P_+(t, A_{k,n})))$$

$$= p! s^p p_1(A_{k,n})^{(s-1)p} [t^p] (\exp(P_+(t, A_{k,n})) \exp(P_+(-t, A_{k,n}))) \quad (2.6.5.25)$$

Now observe that

$$\exp(P_+(t, X)) \exp(P_+(-t, X)) = \exp(P_+(t, X) + P_+(-t, X))$$

$$= \exp(P(t, X) + P(-t, X)) = H(t^2, X^2) \quad (2.6.5.26)$$

so that, in conclusion,

$$E_{(s,p),n}(k) \simeq p! s^p p_1(A_{k,n})^{(s-1)p} h_{p/2}(A_{k,n}^2). \quad (2.6.5.27)$$

Note that this approximated formula for generic s matches the exact formula at $s = 1$, equation (2.6.5.22).

The validity of the approximation above relies on the fact that $p_1(A_{k,n}) \sim \ln(n) - \ln(k) + \mathcal{O}(1)$ whenever $n \gg k$, while $p_h(A_{k,n}) \sim \frac{1}{h-1}(k^{1-h} - n^{1-h})$ if $n \gg k \gg 1$, so that, in any case, whenever $n \gg k$ we have that $p_1/\sqrt{p_2}$ is at least of order $\ln(n)$. Within the same precision of approximation, we can thus replace $p_1(A_{k,n})$ with $\ln(n)$ in (2.6.5.27), and get

$$E_{(s,p),n}(k) = p! s^p \ln(n)^{(s-1)p} h_{p/2}(A_{k,n}^2) (1 + \mathcal{O}((1 + \ln k)/\ln n)). \quad (2.6.5.28)$$

This implies the possibly surprising fact that the ratio of the average weights of the k_1 -th and k_2 -th edges of the matching, whenever $n \gg k_1, k_2$, depends only on p , and not on $\alpha = 1/s$.

Now we perform the analysis with the more complicated expression (2.6.5.20). We have

$$\begin{aligned} E_{(s^+,p),n}(k) &= \sum_{\substack{0 \leq q \leq p \\ 0 \leq r \leq sq \\ 0 \leq r' \leq s(p-q)}} \binom{p}{q} \binom{sq}{r} \binom{s(p-q)}{r'} (-1)^{p-q} r! r'! h_r(A_{k,n}) h_{r'}(A_{k,n}) \\ &= \sum_{\substack{0 \leq q \leq p \\ 0 \leq r \leq sq \\ 0 \leq r' \leq s(p-q) \\ 0 \leq \ell \leq r \\ 0 \leq \ell' \leq r'}} \binom{p}{q} \binom{sq}{r} \binom{s(p-q)}{r'} (-1)^{-q} r! r'! \\ &\quad \times \frac{p_1(A_{k,n})^{r+r'-\ell-\ell'}}{(r-\ell)!(r'-\ell')!} ([t^\ell] \exp(P_+(t, A_{k,n}))) ([t^{\ell'}] \exp(P_+(t, A_{k,n}))). \end{aligned} \quad (2.6.5.29)$$

Consider the sum over r . Isolating only the relevant factors gives

$$\begin{aligned} \sum_{0 \leq r \leq sq} \binom{sq}{r} r! \frac{p_1(A_{k,n})^{r-\ell}}{(r-\ell)!} &= \frac{(sq)!}{(sq-\ell)!} \sum_{\ell \leq r \leq sq} \binom{sq-\ell}{r-\ell} p_1(A_{k,n})^{r-\ell} \\ &= \frac{(sq)!}{(sq-\ell)!} (p_1(A_{k,n}) + 1)^{sq-\ell} \end{aligned} \quad (2.6.5.30)$$

This gives that $E_{(s^+,p),n}(k)$ has exactly the same expression (2.6.5.24) for $E_{(s,p),n}(k)$, with $p_1(A_{k,n})$ replaced by $p_1(A_{k,n}) + 1$. As a result, we can obtain directly the analogue of (2.6.5.27)

$$E_{(s^+,p),n}(k) \simeq p! s^p (p_1(A_{k,n}) + 1)^{(s-1)p} h_{p/2}(A_{k,n}^2). \quad (2.6.5.31)$$

Note again that this approximated formula for generic s matches the exact formula (2.6.5.22) for $s = 1$.

As in the previous case, within the same precision of approximation, we may replace $p_1(A_{k,n}) + 1$ with $\ln(n)$ and get

$$\begin{aligned} E_{(s^+,p),n}(k) &= p! s^p \ln(n)^{(s-1)p} h_{p/2}(A_{k,n}^2) (1 + \mathcal{O}((1 + \ln k)/\ln n)) \\ &= E_{(s,p),n}(k) (1 + \mathcal{O}((1 + \ln k)/\ln n)) \end{aligned} \quad (2.6.5.32)$$

as announced.

2.6.6. Estimation of complete homogeneous functions

Equations (2.6.5.28) and (2.6.5.32) provide explicit expressions for $E_{(s,p),n}(k)$ and $E_{(s^+,p),n}(k)$, and thus for the desired quantity $E_n^{(s,p)} = \sum_{k=1}^n E_{(s,p),n}(k)$ (and its s^+ analogue). Nonetheless, we are left with the task of estimating the relevant quantity

$$F_{n,q} := \sum_{k=1}^n h_q(A_{k,n}^2). \quad (2.6.6.1)$$

We do this in the present section. Each monomial entering the sum has the form

$$\frac{1}{i_1^2 i_2^2 \cdots i_q^2} \quad (2.6.6.2)$$

for some q -tuple $1 \leq i_1 \leq i_2 \leq \cdots \leq i_q \leq n$. Such a monomial enters exactly i_1 times in the sum. Thus we can write

$$F_{n,q} = \sum_{1 \leq i_1 \leq i_2 \leq \cdots \leq i_q \leq n} \frac{1}{i_1^2 i_2^2 \cdots i_q^2} = \sum_{k=1}^n \frac{1}{k} h_{q-1}(A_{k,n}^2). \quad (2.6.6.3)$$

When $q = 1$ this simply gives

$$F_{n,1} = H_n \quad (2.6.6.4)$$

where H_n is the n -th Harmonic number, and in particular, from the well-known perturbative expansion for H_n ,

$$F_{n,1} = \ln(n) + \gamma + \frac{1}{2n} + \mathcal{O}(1/n^2). \quad (2.6.6.5)$$

When $q \geq 2$, as for a real-positive alphabet we have $\frac{1}{q!} h_1(X)^q \leq h_q(X) \leq h_1(X)^q$, we have in particular that $h_{q-1}(A_{k,N}^2) \sim k^{-(q-1)}$ for $n \gg k$, and the whole sum is convergent in the limit $n \rightarrow \infty$.

In this limit, we can identify the exact result (2.6.6.3) with a special case of the so-called ‘‘symmetric sums’’, or ‘‘multiple ζ^* values’’ (56) which are modifications of multiple ζ values that generalise classical special values of the Riemann’s ζ

function (61). Multiple ζ values are not new in physics, as they naturally arise, for example, in the calculation of scattering amplitudes in perturbative quantum field theory (67).

We have, for $q \geq 2$,

$$F_{+\infty,q} = \zeta^*(2^{q-1}, 1). \quad (2.6.6.6)$$

It is a well-known fact that $\zeta^*(2, 1) = \zeta(2, 1) + \zeta(3)$ (by simple inspection), and that $\zeta(2, 1) = \zeta(3)$ (by a famous identity of Euler, see e.g. (74) for a derivation). This gives

$$F_{+\infty,2} = 2\zeta(3). \quad (2.6.6.7)$$

More generally we have $\zeta^*(2^{q-1}, 1) = 2\zeta(2q - 1)$ (this result can be found as (3a) in (119), or also as (1.8) in (132) or in (111), example (b) with $m = 1$), so that for generic $q \geq 2$ we have the result

$$F_{+\infty,q} = 2\zeta(2q - 1). \quad (2.6.6.8)$$

Combining (2.6.6.8) with (2.6.5.28) and (2.6.5.32) finally gives, for s and $p/2$ positive integers,

$$E_n^{(s,p)} \simeq E_n^{(s^+,p)} \simeq \begin{cases} 2s^2 \ln(n)^{2s-1} & p = 2 \\ 2\zeta(p-1) s^p p! \ln(n)^{(s-1)p} & p \geq 4 \end{cases}. \quad (2.6.6.9)$$

Notice that at $s = 1$ eq. (2.6.6.9) is the leading order asymptotics of the known, exact result for the exponential distribution (see (169), eq. 23), namely

$$E_n^{(1,2)} = \sum_{k=1}^n \frac{1}{k}. \quad (2.6.6.10)$$

Hence, for a generic distribution composed both of a bulk part with a stretched exponential tail, an anomalous scaling of the optimal cost is always observed at $p \geq 2$.

Case of s integer and $p = 1$

Using our general Theorem 2.6.3, for the first family of distributions we just have

$$\begin{aligned} E_{n,s}(k_1, k_2) &= \langle (-\ln u)^s \rangle_{P_{2n,k_1}} - \langle (-\ln u)^s \rangle_{P_{2n,k_2}} \\ &= M_{2n,k_1,s} - M_{2n,k_2,s} \end{aligned} \quad (2.6.6.11)$$

In the case of the second family we have

$$\begin{aligned} E_{n,s^+}(k_1, k_2) &= \langle (1 - \ln u)^s \rangle_{P_{2n, k_1}} - \langle (1 - \ln u)^s \rangle_{P_{2n, k_2}} \\ &= \sum_{r=0}^s \binom{s}{r} (M_{2n, k_1, r} - M_{2n, k_2, r}). \end{aligned} \quad (2.6.6.12)$$

Yet again the $s = 1$ (that is, of exponential tail) case is specially simple*, and we just obtain the exact formula

$$E_{n,1}(k_1, k_2) = E_{n,1^+}(k_1, k_2) = h_1(A_{k_1, 2n}) - h_1(A_{k_2, 2n}) = \sum_{\ell=k_1}^{k_2-1} \frac{1}{\ell}. \quad (2.6.6.15)$$

In the general stretched exponential case $s \neq 1$, for the first family of distributions, we have

$$\frac{1}{s!} E_{n,s}(k_1, k_2) = h_s(A_{k_1, 2n}) - h_s(A_{k_2, 2n}) = \sum_{\ell=k_1}^{k_2-1} \frac{1}{\ell} h_{s-1}(A_{\ell, 2n}). \quad (2.6.6.16)$$

For the second family we have the analogous

$$\frac{1}{s!} E_{n,s^+}(k_1, k_2) = \sum_{\ell=k_1}^{k_2-1} \frac{1}{\ell} \sum_{r=1}^s \binom{s}{r} h_{r-1}(A_{\ell, 2n}). \quad (2.6.6.17)$$

*Notice that the same expression in Eq. (2.6.6.15) is obtained if we consider another distribution with simple exponential tail, such as a logistic pdf $\rho(x)dx = \frac{e^{-x}}{(1+e^{-x})^2} dx$. Indeed, in this case $R^{(-1)}(u) = \log \frac{1-u}{u}$ and we have

$$M_{n,k,1}^{\text{logistic}} = \langle R^{(-1)}(u) \rangle_{P_{n,k}} = \psi^{(0)}(n-k+1) - \psi^{(0)}(k) = \sum_{l=k}^{n-k+1} \frac{1}{l}, \quad (2.6.6.13)$$

where $\psi^{(m)}(z) := \frac{\partial^{m+1}}{\partial u^{m+1}} \ln(\Gamma(z))$ is the PolyGamma function of order m . Therefore

$$E_{n,1}^{\text{logistic}}(k_1, k_2) = M_{2n, k_1, 1}^{\text{logistic}} - M_{2n, k_2, 1}^{\text{logistic}} = \sum_{l=k_1}^{k_2-1} \frac{1}{l} \quad (2.6.6.14)$$

as announced.

As a result we have

$$\begin{aligned}
E_n^{(s,1)} &= s! \sum_{\ell=1}^{2n-1} \frac{q_n(\ell)}{\ell} h_{s-1}(A_{\ell,2n}), \\
E_n^{(s^+,1)} &= s! \sum_{\ell=1}^{2n-1} \frac{q_n(\ell)}{\ell} \sum_{r=1}^s \binom{s}{r} h_{r-1}(A_{\ell,2n}).
\end{aligned} \tag{2.6.6.18}$$

Now, under our assumptions

$$h_s(A_{\ell,2n}) \simeq \frac{1}{s!} p_1(A_{\ell,2n})^s = \frac{1}{s!} (\ln(2n) - \ln \ell + \gamma_E + \mathcal{O}(1/\ell))^s, \tag{2.6.6.19}$$

so that, upon introducing $x = \ell/(2n)$, $l \ll n$, Theorem 2.6.3 implies

$$\begin{aligned}
E_n^{(s,1)} &\simeq s! \sum_{\ell=1}^{2n-1} \sqrt{\frac{2}{\pi}} \sqrt{\frac{\ell(2n-\ell)}{2n}} \frac{1}{\ell} \frac{1}{(s-1)!} (\ln(2n) - \ln \ell)^{s-1} \\
&\simeq 2sn \int_0^1 dx \sqrt{\frac{2}{\pi}} \frac{1}{\sqrt{2n}} \sqrt{\frac{1-x}{x}} (-\ln x)^{s-1} \\
&= s\sqrt{\pi n} \frac{2}{\pi} \int_0^1 dx \sqrt{\frac{1-x}{x}} (-\ln x)^{s-1}
\end{aligned} \tag{2.6.6.20}$$

(and the same expression for $E_n^{(s^+,1)}$). Note how now the leading contribution comes from the bulk, and the terms $\ell = \Theta(1)$ are sub-leading, so that there is no anomalous exponent, as \sqrt{n} coincides is the bulk (Dyck) behavior at $p = 1$ (see table 2.1). In this regime eq. (2.6.6.20) recovers also the asymptotic constants depending on s , eq. (15b) in (169). The first few values are

$$\sqrt{\pi}, 2\sqrt{\pi}(1 + \ln 4), \frac{\pi^3 + 3\pi(2 + 2 \ln 4) + (\ln 4)^2}{\sqrt{\pi}}, \dots, \quad s = 1, 2, 3, \dots \tag{2.6.6.21}$$

Incidentally the integrals $\frac{2}{\pi} \int_0^1 dx \sqrt{\frac{1-x}{x}} (-\ln x)^s$ just make by means of our standard trick (used e.g. in eq.(2.6.5.16)) the combinations

$$\lim_{u \rightarrow 0} u^{-s} \sum_{q=0}^s \binom{s}{q} (-1)^{s-q} \frac{\Gamma(\frac{1}{2} - qu)\Gamma(2)}{\Gamma(\frac{1}{2})\Gamma(2 - qu)}, \tag{2.6.6.22}$$

which are indeed polynomial combinations of Riemann $\zeta(s)$'s and $\ln 4$. They are given by

$$\begin{aligned} Y_s &:= \frac{2}{\pi} \int_0^1 dx \sqrt{\frac{1-x}{x}} (-\ln x)^s = \frac{\partial^s}{\partial u^s} \frac{\Gamma(\frac{1}{2}-u)\Gamma(2)}{\Gamma(\frac{1}{2})\Gamma(2-u)} \Big|_{u=0} \\ &= \frac{\partial^s}{\partial u^s} \frac{1}{1-u} \frac{\Gamma(\frac{1}{2}-u)}{\Gamma(\frac{1}{2})\Gamma(1-u)} \Big|_{u=0} = \frac{\partial^s}{\partial u^s} \frac{4^u}{1-u} \frac{\Gamma(1-2u)}{\Gamma(1-u)^2} \Big|_{u=0} \end{aligned} \quad (2.6.6.23)$$

where the duplication formula for the Gamma function has been used. Indeed, the Y_s are obtained from the fundamental quantities

$$X_s := \frac{\partial^s}{\partial u^s} \ln \frac{\Gamma(\frac{1}{2}-u)}{\Gamma(2-u)} \Big|_{u=0}, \quad (2.6.6.24)$$

which satisfy

$$X_s = \begin{cases} \psi^{(0)}(2) - \psi^{(0)}(1/2) = 1 + \ln 4 & s = 1 \\ (s-1)!(1 + (2^{s-1} - 1)2\zeta(s)) & s \geq 2, \end{cases} \quad (2.6.6.25)$$

($\psi^{(m)}(z)$ are the PolyGamma functions of order m) simply via

$$\sum_{k \geq 0} \frac{t^k}{k!} Y_k = \exp \left(\sum_{k \geq 1} \frac{t^k}{k!} X_k \right). \quad (2.6.6.26)$$

2.6.7. Non-integer values of s

When $s = 1/\alpha$ is not an integer, the functions $R_\alpha^{-1}(t)$ and $R_{\alpha^+}^{-1}(t)$ are not polynomials of $(-\ln t)$, and we cannot use directly our formula for the moments in Lemma 2.6.5. Nonetheless, we can access some information on $M_{n,k,s}$ when s is not an integer, through a strategy that we now illustrate.

For $s \in \mathbb{R}^+ \setminus \mathbb{N}$, let $s = S - \sigma$, with $S \in \mathbb{N}$ and $\sigma \in (0, 1)$. Then we will use the representation

$$(-\ln t)^s = (-\ln t)^S (-\ln t)^{-\sigma} = \lim_{u \rightarrow 0} \left(\frac{t^{-u} - 1}{u} \right)^S \int_0^\infty dx \frac{x^{\sigma-1}}{\Gamma(\sigma)} \exp(x \ln t). \quad (2.6.7.1)$$

As a result we have

$$\begin{aligned}
M_{n,k;s} &= \lim_{u \rightarrow 0} \int_0^\infty dx \frac{x^{\sigma-1}}{\Gamma(\sigma)} \int_0^1 dt t^{k-1} (1-t)^{n-k} \left(\frac{t^{-u} - 1}{u} \right)^S t^x \frac{\Gamma(n+1)}{\Gamma(k)\Gamma(n-k+1)} \\
&= \lim_{u \rightarrow 0} u^{-S} \int_0^\infty dx \frac{x^{\sigma-1}}{\Gamma(\sigma)} \sum_{q=0}^S \binom{S}{q} (-1)^{S-q} \\
&\quad \times \int_0^1 dt t^{k-1} (1-t)^{n-k} t^{x-qu} \frac{\Gamma(n+1)}{\Gamma(k)\Gamma(n-k+1)} \\
&= \lim_{u \rightarrow 0} u^{-S} \int_0^\infty dx \frac{x^{\sigma-1}}{\Gamma(\sigma)} \sum_{q=0}^S \binom{S}{q} (-1)^{S-q} \\
&\quad \times \frac{\Gamma(k+x-qu)\Gamma(n-k+1)}{\Gamma(n+1+x-qu)} \frac{\Gamma(n+1)}{\Gamma(k)\Gamma(n-k+1)} \\
&= \int_0^\infty dx \frac{x^{\sigma-1}}{\Gamma(\sigma)} \frac{\Gamma(k+x)\Gamma(n+1)}{\Gamma(k)\Gamma(n+1+x)} \\
&\quad \times \lim_{u \rightarrow 0} u^{-S} \sum_{q=0}^S \binom{S}{q} (-1)^{S-q} \frac{\Gamma(k+x-qu)\Gamma(n+1+x)}{\Gamma(k+x)\Gamma(n+1+x-qu)} \\
&= \int_0^\infty dx \frac{x^{\sigma-1}}{\Gamma(\sigma)} \frac{\Gamma(k+x)\Gamma(n+1)}{\Gamma(k)\Gamma(n+1+x)} S! h_S(A_{k+x,n+x})
\end{aligned} \tag{2.6.7.2}$$

where, consistently with our previous notation, $A_{k+x,n+x}$ is the alphabet where the inverse of the symbols are shifted by x , $\{(k+x)^{-1}, (k+x+1)^{-1}, \dots, (n+x)^{-1}\}$. Note that

$$\frac{\Gamma(k+x)\Gamma(n+1)}{\Gamma(k)\Gamma(n+1+x)} = \prod_{\ell=k}^n \left(1 - \frac{x}{\ell} \right) \tag{2.6.7.3}$$

which is both equal to $E(-x, A_{k+x,n+x}) = \exp(-P(x, A_{k+x,n+x}))$ and to $H(-x, A_{k,n}) = \exp(P(-x, A_{k,n}))$. Thus we can give the two representations

$$\begin{aligned}
M_{n,k;s} &= S! \int_0^\infty dx \frac{x^{\sigma-1}}{\Gamma(\sigma)} e^{-P(x, A_{k+x,n+x})} [t^S] e^{P(t, A_{k+x,n+x})} \\
&= S! \int_0^\infty dx \frac{x^{\sigma-1}}{\Gamma(\sigma)} e^{P(-x, A_{k,n})} [t^S] e^{P(t, A_{k+x,n+x})}
\end{aligned} \tag{2.6.7.4}$$

The second representation is specially convenient when $s < 1$, that is $S = 1$. In

this case we just have

$$M_{n,k;1-\sigma} = \int_0^\infty dx \frac{x^{\sigma-1}}{\Gamma(\sigma)} e^{P(-x, A_{k,n})} p_1(A_{k+x, n+x}) \quad (2.6.7.5)$$

and we can write

$$p_1(A_{k+x, n+x}) = p_1(A_{k,n}) - xp_2(A_{k,n}) + x^2 p_3(A_{k,n}) - x^3 p_4(A_{k,n}) + \dots \quad (2.6.7.6)$$

Let us just write p_j for $p_j(A_{k,n})$. Then we have

$$M_{n,k;1-\sigma} = \int_0^\infty dx \frac{x^{\sigma-1}}{\Gamma(\sigma)} p_1 e^{-xp_1} \exp\left(\frac{x^2 p_2}{2} - \frac{x^3 p_3}{3} + \dots\right) \left(1 - \frac{xp_2}{p_1} + \frac{x^2 p_3}{p_1} - \dots\right). \quad (2.6.7.7)$$

Again, p_1 is a ‘‘large’’ parameter (of order $\ln n$ whenever $n \gg k$, and of order 1 when $n \sim k$, but in this case $p_j \sim k^{-j+1} \ll 1$ for $j \geq 2$), so that we can treat perturbatively the two rightmost factors in Eq. (2.6.7.7), and get

$$M_{n,k;1-\sigma} = p_1^{1-\sigma} \left(1 + \sum_{\ell \geq 2} \binom{1-\sigma}{\ell} \ell! p_1^{-\ell} \sum_{\substack{(m_2, m_3, \dots) \\ \sum_j j m_j = \ell}} \prod_{j \geq 2} \frac{p_j^{m_j}}{j^{m_j} m_j!}\right) \quad (2.6.7.8)$$

where we recall that $p_j = p_j(A_{k,n})$, and we have the following the result.

Lemma 2.6.7. *Call $s^a = s(s-1)(s-2)\dots(s-a+1)$. For $m = (m_2, m_3, \dots)$, call $|m| := \sum_j j m_j$. Then for all $s > 0$ we have*

$$M_{n,k;s} = p_1^s \sum_{(m_2, m_3, \dots)} s^{|m|} p_1^{-|m|} \prod_{j \geq 2} \frac{p_j^{m_j}}{j^{m_j} m_j!}. \quad (2.6.7.9)$$

Remark 2.6.1. If $s \in \mathbb{N}$ $M_{n,k;s}$ is a special evaluation of the complete Bell polynomial $B_s(x_1, \dots, x_s)$ (see e.g. (96)) at $x_i = (i-1)! p_i$ or, equivalently, it is proportional to the cycle index of the symmetric group \mathcal{S}_s acting on the formal variables p_1, \dots, p_s . That is

$$M_{n,k;s} = B_s(p_1, 2p_2, \dots, (s-1)!p_s) = s! h_s(A_{k,n}), \quad (2.6.7.10)$$

which coincides with our result (Eq. (2.6.5.17)) if s is an integer. Our approach allows to study e.g. the gaussian case $s = 1/2$ also considered in the case of continuum measures (168). The details of this calculation, where rather delicate cancellations at the level of Eq. 2.6.5.25 happen, will be the subject of a future investigation.

2.6.8. Family with finite endpoint, algebraic zero $\rho_{\text{fa},\beta}$

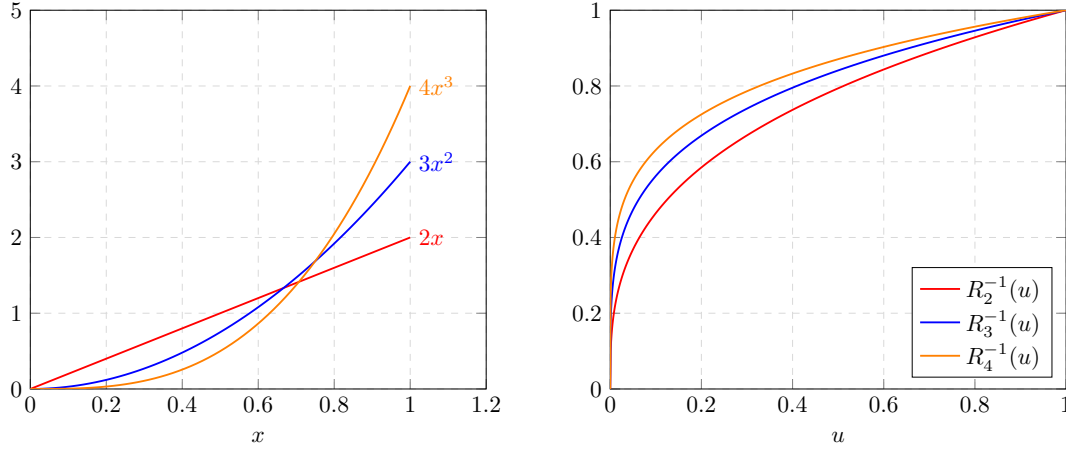


Figure 2.9. – Members from the family in eq. 2.6.8.1 at $\beta = 2, 3, 4$ (left), and corresponding R_β^{-1} functions (right).

Recall the family of probability distributions

$$\rho_{\text{fa},\beta}(x) = \beta x^{\beta-1} \quad (x \in [0, 1]) \quad (2.6.8.1)$$

indexed by a real $\beta > 0$, for which $R_{\text{fa},\beta}^{-1}(u) = u^{\frac{1}{\beta}}$. For them

$$M_{k,n;q}^{(\text{fa}),\beta} = \left\langle (u^{\frac{1}{\beta}})^q \right\rangle_{P_{n,k}} = \frac{\Gamma(n')\Gamma(k + \frac{q}{\beta})}{\Gamma(k)\Gamma(n' + \frac{q}{\beta})}. \quad (2.6.8.2)$$

where we have used $n' = n+1$ for notational convenience. In light of the application of Theorem 2.6.1 we profit of the following fact.

Lemma 2.6.8. *The function*

$$\psi_n(\beta) := \ln \left[\frac{n^\beta \Gamma(n)}{\Gamma(n + \beta)} \right] \quad (2.6.8.3)$$

has the series expansion

$$\begin{aligned} \psi_n(\beta) &= \frac{\beta - \beta^2}{2n} + \frac{\beta - 3\beta^2 + 2\beta^3}{12n^2} + \frac{-\beta + 2\beta^3 - \beta^4}{12n^3} + \dots \\ &= \sum_{k,l} c_{k,l} n^{-k} \beta^{l+1} \end{aligned} \quad (2.6.8.4)$$

where

$$c_{k,\ell} = (-1)^k B_{k-\ell} \frac{\Gamma(k)}{\Gamma(\ell)\Gamma(k-\ell+1)}, \quad k \geq 1, \quad 0 \leq \ell \leq k, \quad (2.6.8.5)$$

and B_s is the s -th Bernoulli number.*

Now, at leading order in $\frac{1}{n}$, the coefficient of β^p in

$$e^{\psi_n(\beta)} = \exp \left(-\frac{\beta^2}{2n} \sum_{\substack{k \geq 1 \\ 0 \leq l \leq k}} (-2c_{k,l}) \left(\frac{\beta}{n}\right)^{2k-l-1} \left(\frac{\beta^2}{n}\right)^{-(k-l)} \right) \quad (2.6.8.7)$$

concentrates around the term with $k = l = 1$ (that is, at the minimum of $2k - l - 1$ within the range $k \geq 1, 0 \leq l \leq k$), and we can work with just the first term in eq. (2.6.8.4). We thus get

$$M_{k,n;q}^{(\text{fa}),\beta} \sim \begin{cases} \frac{\Gamma(k+\frac{q}{\beta})}{\Gamma(k)} n^{-q/\beta} & k \text{ small} \\ \exp\left(-\frac{1}{2n} \left(\frac{q^2}{\beta}\right) (1-x^{-1})\right) x^{q/\beta} & x = \frac{k}{n'} = \Theta(1) \end{cases} \quad (2.6.8.8)$$

which by Theorem 2.6.1 gives

$$E_{(\beta,p),n}(k) = \sum_{q=0}^p \binom{p}{q} (-1)^{p-q} M_{k,n;q}^{(\text{fa}),\beta} M_{k,n;p-q}^{(\text{fa}),\beta} \\ \sim \begin{cases} n^{-p/\beta} \sum_{q=0}^p \binom{p}{q} (-1)^{p-q} \frac{\Gamma(k+\frac{q}{\beta})\Gamma(k+\frac{p-q}{\beta})}{\Gamma^2(k)} & k \text{ small} \\ x^{p/\beta} \sum_{q=0}^p \binom{p}{q} (-1)^{p-q} \exp\left(-\frac{1-x^{-1}}{2n\beta^2} (q^2 + (p-q)^2) + \mathcal{O}\left(\frac{1}{n^2}\right)\right) & x = \frac{k}{n'} = \Theta(1). \end{cases} \quad (2.6.8.9)$$

Let us consider first the contributions coming from edges that are “far” from the region of low density of points, $k = xn'$ (i.e. the bulk regime). By Lemma 2.6.6,

*A further series expansion, satisfied by the difference of contiguous expressions (2.6.8.3), to be combined with the fact that $\psi_1(\beta) = -\ln\Gamma(\beta)$, is that, for $n \geq 2$,

$$\psi_n(\beta) - \psi_{n-1}(\beta) = (1-\beta) \log\left(\frac{n-1}{n}\right) - \log\left(1 + \frac{\beta-1}{n}\right) = \frac{1-\beta}{n^2} \sum_{m=0}^{\infty} \frac{(1-\beta)^{m+1} - 1}{(m+2)n^m}. \quad (2.6.8.6)$$

we just have

$$E_{(\beta,p),n}(k) \sim x^{p/\beta} \left(\frac{-1+x^{-1}}{n\beta^2} \right)^{p/2} \frac{1}{\Gamma(p/2+1)}, \quad k = xn'. \quad (2.6.8.10)$$

Therefore, given a cutoff $\Lambda = \mathcal{O}(\sqrt{n})$, the Riemann's sums $\sum_{k=\Lambda}^n$ may be transformed into integrals without affecting the leading asymptotics, giving

$$E_{(\beta,p),n} \sim n^{1-p/2} \int_{\Lambda/n}^1 dx x^{\frac{p}{\beta}-\frac{p}{2}} P(x), \quad (2.6.8.11)$$

where $P(x)$ is a polynomial in x . The integral in (2.6.8.11) does not diverge as long as $\frac{p}{\beta} - \frac{p}{2} > -1$, and in this case we may just take the limit $\Lambda \rightarrow 0$ and make the substitution $\int_{\Lambda/n}^1 \rightarrow \int_0^1$ (we “remove” the ultraviolet cutoff Λ , in physics language), to get the following result.

Lemma 2.6.9 (Bulk regime). *For the family $\rho_{\text{fa},\beta}$ with a finite endpoint, algebraic zero of order $\beta - 1$ (2.6.8.1), if*

$$2\beta + 2p - p\beta > 0 \quad (2.6.8.12)$$

then

$$E_{(\beta,p),n} = n^{1-p/2} b_{\beta,p} (1 + o(1)), \quad (2.6.8.13)$$

where

$$\begin{aligned} b_{\beta,p} &= \frac{p!}{(p/2)!\beta^p} \int_0^1 dx x^{p/\beta} (-1+x^{-1})^{p/2} \\ &= \frac{p!}{(p/2)!\beta^p} \frac{\Gamma(\frac{p}{2}+1) \Gamma\left(1 - \frac{p(\beta-2)}{2\beta}\right)}{\Gamma\left(2 + \frac{p}{\beta}\right)}. \end{aligned} \quad (2.6.8.14)$$

Remark 2.6.2. In the $\beta \rightarrow 1^+$ limit, the distribution $\rho_{\text{fa},1}$ recovers the uniform distribution supported on $[0, 1]$, and we just get

$$\begin{aligned} \lim_{\beta \rightarrow 1^+} b_{\beta,p} &= \frac{p!}{(p/2)!} \frac{\Gamma(\frac{p}{2}+1) \Gamma(1+p/2)}{\Gamma(2+p)} \\ &= \frac{\Gamma(1+p/2)}{p+1}, \end{aligned} \quad (2.6.8.15)$$

which coincides with the known leading asymptotic constant, Eq. (2.6.1.2).

Let us consider now the anomalous contributions coming from edges in the region

of the zero, that is, Eq. (2.6.8.9) at small k . We have

$$E_{(\beta,p),n}(k) \sim n^{-p/\beta} \sum_{k=1}^{\Lambda} \frac{1}{\Gamma^2(k)} \sum_{q=0}^p \binom{p}{q} (-1)^q \Gamma\left(k + \frac{q}{\beta}\right) \Gamma\left(k + \frac{p-q}{\beta}\right), \quad (2.6.8.16)$$

which, at first sight, may seem to grow as $k^{p/\beta}$. However, one easily sees that the cancellations due to the $\binom{p}{q}(-1)^q$ combination lower the growth in k down to the one of the bulk contribution, that is, $E_{(\beta,p),n}(k) \sim n^{-p/\beta} k^{\frac{p}{\beta} - \frac{p}{2}}$. Recalling the hypergeometric identity

$$\sum_{k=1}^{\infty} \frac{\Gamma(k+a)\Gamma(k+b)}{\Gamma^2(k)} = \Gamma(-1-a-b) \frac{\Gamma(a+1)}{\Gamma(-a)} \frac{\Gamma(b+1)}{\Gamma(-b)}, \quad (2.6.8.17)$$

when the sum in Eq. 2.6.8.16 does not diverge, we can just take $\Lambda \rightarrow \infty$ limit (i.e. we remove the infrared cutoff) [†] and get the following result.

Lemma 2.6.10 (Strict anomaly). *For the family with a finite endpoint, algebraic zero of order $\beta - 1$ $\rho_{\text{fa},\beta}$ (Eq. 2.6.8.1), if*

$$2\beta + 2p - p\beta < 0 \quad (2.6.8.19)$$

then

$$E_{(\beta,p),n} \sim a_{\beta,p} n^{-p/\beta} \quad (2.6.8.20)$$

where

$$a_{\beta,p} = \Gamma(-1 - p/\beta) \sum_{q=0}^p \binom{p}{q} (-1)^q \frac{\Gamma(1 + \frac{q}{\beta})\Gamma(1 + \frac{p-q}{\beta})}{\Gamma(-\frac{q}{\beta})\Gamma(-\frac{p-q}{\beta})}. \quad (2.6.8.21)$$

Lastly, let us consider the limiting case

$$2\beta + 2p - p\beta = 0, \quad (2.6.8.22)$$

which defines a critical hyperbola (Fig. 2.10).

In this case the anomalous and bulk contributions are of the same order (that is, $E_{(n,p)} \sim E_{(n,p)}^{\text{bulk}} + E_{(n,p)}^{\text{tail}}$ at leading order in n), and we need to keep a finite cutoff

[†]Inserting the Γ function definitions in eq. 2.6.8.16, and then summing over q and k leads to

$$E_{(\beta,p),n} \sim n^{-p/\beta} \int_0^\infty \frac{dt_1}{t_1} \frac{dt_2}{t_2} e^{-(t_1+t_2)} (t_1^{\frac{1}{\beta}} - t_2^{\frac{1}{\beta}})^p \left(I_0(2\sqrt{t_1 t_2}) - 1 - \frac{(t_1 t_2)^{\Lambda+1}}{\Gamma^2(\Lambda+2)} \sum_{s=0}^{\infty} \frac{(t_1 t_2)^s}{((\Lambda+2)_s)^2} \right), \quad (2.6.8.18)$$

where $I_0(x)$ is the modified Bessel function of the first kind of order 0, so that the last term is negligible in the $\Lambda \rightarrow \infty$ limit.

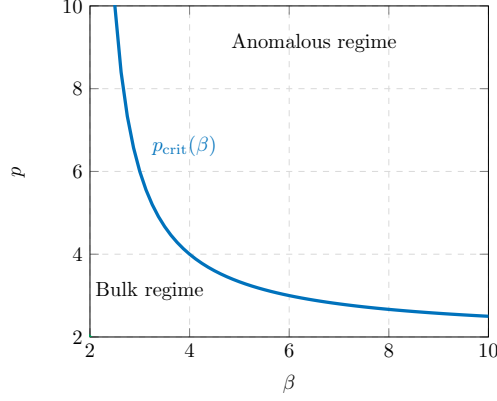


Figure 2.10. – Critical line separating the region of anomalous scaling ($p > p_{\text{crit}}(\beta)$) from the region of bulk scaling ($p < p_{\text{crit}}(\beta)$) for a density with a zero of order $\beta - 1$ at one border of the support.

$1 \ll \Lambda \ll n$ throughout the calculation.

The bulk part is given by

$$E_{(n,p)}^{\text{bulk}} \sim \int_{\Lambda/n}^1 dx \frac{1 + xR(x)}{x} \sim \int_{\Lambda/n}^1 dx \frac{1}{x} + \int_0^1 dx R(x) \quad (2.6.8.23)$$

where $R(x)$ is a polynomial in x (as it was in (2.6.8.11)). In order to study the relevant asymptotics, recall the useful integral representation for the k -th Harmonic number H_k

$$\begin{aligned} \int_0^1 \frac{dx}{x} ((1-x)^k - 1) &= -H_k \\ &= -\sum_{j=1}^k \frac{1}{j}, \quad k \in \mathbb{N}, \end{aligned} \quad (2.6.8.24)$$

and introduce the function

$$Q(p) := \frac{p!}{(p/2)! \beta^p} \Big|_{\beta=\beta_c(p)=\frac{2p}{p-2}} = \frac{p!}{(p/2)!} \left(\frac{p-2}{2p} \right)^p. \quad (2.6.8.25)$$

Eq. (2.6.8.23) then becomes

$$E_{(n,p)}^{\text{bulk}} \sim n^{1-p/2} \int_{\Lambda/n}^1 dx \frac{Q(p)}{x} (1-x)^{p/2} = n^{1-p/2} Q(p) [(\ln n - \ln \Lambda) + \left(1 + \frac{1}{2} + \dots + \frac{2}{p}\right)]. \quad (2.6.8.26)$$

Now we have to deal with the small k part contributing to $E_{(n,p)}^{\text{tail}}$.

2.6.9. On sub-leading contributions at the critical line

$$2(p + \beta) = p\beta$$

Recall that for a series of general term a_k s.t. $a_k \sim \frac{c}{k}$ for large k , we have

$$\begin{aligned} \sum_{k=1}^{\Lambda} a_k &= \sum_{k=1}^{\Lambda} \left(a_k - \frac{c}{k}\right) + cH_{\Lambda} \\ &= \sum_{k=1}^{\infty} \left(a_k - \frac{c}{k}\right) + cH_{\Lambda} + \mathcal{O}\left(\frac{1}{\Lambda}\right) \\ &= c(\ln \Lambda + \gamma_E) + \lim_{x \rightarrow 1^-} \left(c \frac{\ln(1-x)}{x} + \sum_{k=1}^{\infty} a_k x^{k-1}\right) + \mathcal{O}\left(\frac{1}{\Lambda}\right). \end{aligned} \quad (2.6.9.1)$$

Recall also that

$$\sum_{k \geq 1} \frac{\Gamma(k+a)\Gamma(k+b)}{\Gamma^2(k)} x^{k-1} = \Gamma(a+1)\Gamma(b+1) {}_2F_1(a+1, b+1; 1; x) \quad (2.6.9.2)$$

where ${}_2F_1(m, n; q; x)$ is Gauss hypergeometric function. We thus have

$$E_{(n,p)}^{\text{tail}, \beta} \sim \sigma_p n^{1-\frac{p}{2}} \quad (2.6.9.3)$$

with

$$\begin{aligned} \sigma_p &:= \left[Q(p)(\ln \Lambda + \gamma_E) + \lim_{x \rightarrow 1^-} \left(\sum_{q=0}^p \binom{p}{q} (-1)^q \Gamma\left(1 + \frac{q}{\beta}\right) \Gamma\left(1 + \frac{p-q}{\beta}\right) \cdot \right. \right. \\ &\quad \left. \left. \cdot {}_2F_1\left(1 + \frac{q}{\beta}, 1 + \frac{p-q}{\beta}; 1; x\right) + Q(p) \frac{\ln(1-x)}{x} \right) \right] \end{aligned} \quad (2.6.9.4)$$

(the last term being $\frac{\ln(1-z)}{z} = {}_2F_1(1, 1; 2; z)$), and by simple comparison with eq. (2.6.8.26) we have the following crucial remark.

Remark 2.6.3. At leading order in n , the bulk (resp. tail) part of the energy carries a $+Q(p) \log \Lambda$ (resp., $-Q(p) \log \Lambda$) contribution, so that the quantity $E_{(n,p)}^{\text{tail}} + E_{(n,p)}^{\text{bulk}}$ is independent on Λ .

We wish now to evaluate the relevant limit

$$\begin{aligned} \tilde{\sigma}_p &:= \sigma_p - Q(p) (\log \Lambda + \gamma_E) \\ &= \lim_{x \rightarrow 1^-} \left(\sum_{q=0}^p \binom{p}{q} (-1)^q \Gamma\left(1 + \frac{q}{\beta}\right) \Gamma\left(1 + \frac{p-q}{\beta}\right) {}_2F_1\left(1 + \frac{q}{\beta}, 1 + \frac{p-q}{\beta}; 1; x\right) \right. \\ &\quad \left. + Q(p) \frac{\ln(1-x)}{x} \right) \end{aligned} \tag{2.6.9.5}$$

on the critical line $\beta_c = \frac{2p}{p-2}$. In order to do so, we need to manipulate ${}_2F_1(a, b; c; x)$ when $a + b - c \in \mathbb{N}$, and this can be done with the aid of formulas 15.8.12 and 15.8.10 of <https://dlmf.nist.gov/15.8>. For $a = 1 + \frac{q}{\beta}$, $b = 1 + \frac{p-q}{\beta}$ and $c = 1$, since at the critical line

$$\begin{aligned} c - b - a &= 1 - \left(1 + \frac{p-2}{2p}q\right) - \left(1 + (p-q)\frac{p-2}{2p}\right) \\ &= -\frac{p}{2}, \end{aligned} \tag{2.6.9.6}$$

using the identity 15.8.12 we get

$${}_2F_1\left(1 + \frac{q}{\beta_c}, 1 + \frac{p-q}{\beta_c}; 1; x\right) = (1-x)^{-p/2} {}_2F_1\left(-\frac{p-q}{\beta_c}, -\frac{q}{\beta_c}; 1; x\right). \tag{2.6.9.7}$$

Using the other identity 15.8.10, with

$$\begin{aligned} a &= 1 - \frac{p}{2} + \frac{q}{\beta_c} = -\frac{p-q}{\beta_c}, \\ b &= -\frac{q}{\beta_c}, \\ c &= a + b + \frac{p}{2}, \end{aligned} \tag{2.6.9.8}$$

so that $\Gamma\left(a + \frac{p}{2}\right) = \Gamma\left(1 + \frac{q}{\beta}\right)$ and $\Gamma\left(b + \frac{p}{2}\right) = \Gamma\left(\frac{p}{2} - \frac{q}{\beta}\right)$, and Eq. 2.6.9.7, we

easily get

$$\begin{aligned}
\tilde{\sigma}_p = \lim_{x \rightarrow 1^-} & \left\{ Q(p) \frac{\log(1-x)}{x} + (1-x)^{-p/2} \sum_{q=0}^p \binom{p}{q} (-1)^q \Gamma\left(1 + \frac{q}{\beta_c}\right) \Gamma\left(1 + \frac{p-q}{\beta_c}\right) \right. \\
& \cdot \left[\frac{1}{\Gamma\left(1 + \frac{q}{\beta_c}\right) \Gamma\left(\frac{p}{2} - \frac{q}{\beta_c}\right)} \sum_{k=0}^{\frac{p}{2}-1} \frac{(1 - \frac{p}{2} + \frac{q}{\beta_c})_k (-\frac{q}{\beta_c})_k (\frac{p}{2} - k - 1)}{k!} (x-1)^k + \right. \\
& - \frac{(x-1)^{\frac{p}{2}}}{\Gamma\left(1 - \frac{p}{2} + \frac{q}{\beta_c}\right) \Gamma\left(-\frac{q}{\beta_c}\right)} \sum_{k \geq 0} \frac{(1 + \frac{q}{\beta_c})_k (\frac{p}{2} - \frac{q}{\beta_c})_k}{k! (k + \frac{p}{2})!} (1-x)^k \\
& \left. \left. \cdot \left(\log(1-x) - \psi(k+1) - \psi\left(k + \frac{p}{2} + 1\right) + \psi\left(k + 1 + \frac{q}{\beta_c}\right) + \psi\left(\frac{p}{2} - \frac{q}{\beta_c} + k\right) \right) \right] \right\}. \tag{2.6.9.9}
\end{aligned}$$

where $(a)_k$ is Pochhammer symbol and ψ is the Digamma function. Eq. 2.6.9.9 can be considerably simplified by the following remarks. First of all, we can discard the whole first summand in square parentheses, which is a polynomial of degree strictly $< p$ in q and thus lie in the kernel of $\sum_{q=0}^p \binom{p}{q} (-1)^q$. Secondly, we can discard all terms with $k \geq 1$ in the second summand in square parentheses, as they vanish in the $x \rightarrow 1^-$ limit. Hence, by straightforward algebra, we are just left with

$$\begin{aligned}
\tilde{\sigma}_p = \lim_{x \rightarrow 1^-} & \left[Q(p) \frac{\log(1-x)}{x} + \frac{(-1)^{1+\frac{p}{2}}}{(p/2)!} \sum_{q=0}^p \binom{p}{q} (-1)^q \frac{\Gamma\left(1 + \frac{q}{\beta_c}\right) \Gamma\left(1 + \frac{p-q}{\beta_c}\right)}{\Gamma\left(-\frac{q}{\beta_c}\right) \Gamma\left(-\frac{p-q}{\beta_c}\right)} \right. \\
& \left. \cdot \left(\log(1-x) - \psi(1) - \psi\left(1 + \frac{p}{2}\right) + \psi\left(1 + \frac{q}{\beta_c}\right) + \psi\left(\frac{p}{2} - \frac{q}{\beta_c}\right) \right) \right]. \tag{2.6.9.10}
\end{aligned}$$

Now, the symmetry of Eq. 2.6.9.10 suggests to consider the function

$$\gamma(z) := \frac{\Gamma(z+1)}{\Gamma(-z)} = \frac{\Gamma^2(z+1)}{\pi} \sin(\pi z) \tag{2.6.9.11}$$

in terms of which we have the remarkable simplification

$$\begin{aligned}
\frac{(-1)^{\frac{p}{2}+1}}{(p/2)!} \sum_{q=0}^p \binom{p}{q} (-1)^q \frac{\gamma(\frac{q}{\beta})}{\gamma(\frac{q}{\beta} - \frac{p}{2})} &= \frac{(-1)^{\frac{p}{2}+1}}{(p/2)!} \sum_{q=0}^p \binom{p}{q} (-1)^q \left[\left(\frac{q}{\beta_c} \right)^{\frac{p}{2}} \right]^2 \underbrace{\frac{\sin(\pi \frac{q}{\beta_c})}{\sin\left(\pi \left(\frac{q}{\beta_c} - \frac{p}{2} \right)\right)}}_{=(-1)^{p/2} \text{ at } p \text{ even}} \\
&= -\frac{1}{(p/2)!} \sum_{q=0}^p \binom{p}{q} (-1)^q \left[\left(\frac{q}{\beta_c} \right)^{\frac{p}{2}} \right]^2 = -\frac{p!}{(p/2)! \beta_c^p} \\
&= -Q(p),
\end{aligned} \tag{2.6.9.12}$$

where we have used, recalling the falling factorial notation $s^a = s(s-1)(s-2)\cdots(s-a+1)$, that

$$\prod_{l=0}^{\frac{p}{2}-1} \left(\frac{q}{\beta_c} - l \right) = \left(\frac{q}{\beta_c} \right)^{\frac{p}{2}} \tag{2.6.9.13}$$

so that $\left(\frac{q}{\beta} \right)^{\frac{p}{2}}$ is the ordinary generating function for the Stirling numbers of the first kind

$$\left(\frac{q}{\beta_c} \right)^{\frac{p}{2}} = \sum_{k=0}^{\frac{p}{2}} s\left(\frac{p}{2}, k\right) \left(\frac{q}{\beta_c} \right)^k. \tag{2.6.9.14}$$

Hence, since $\lim_{x \rightarrow 1^-} Q(p) \left(\frac{\log(1-x)}{x} - \log(1-x) \right) = 0$, we can perform the $x \rightarrow 1^-$ limit, noting that all contributions independent on q just give a $-Q(p)$ factor, and get the following

Lemma 2.6.11 (Tail contribution at the critical line). *For the family $\rho_{\text{fa},\beta}$, the tail contribution at the critical line has no logarithmic correction. It is given by*

$$E_{(n,p)}^{\text{tail},\beta_c} \sim n^{1-\frac{p}{2}} \left[Q(p) \left(H_{\frac{p}{2}} - 2\gamma_E \right) + v_p \right] \tag{2.6.9.15}$$

where H_k is the k -th harmonic number, γ_E the Euler-Mascheroni constant, and the

$$v_p := -\frac{1}{(p/2)!} \sum_{q=0}^p \binom{p}{q} (-1)^q \left[\left(\frac{q}{\beta_c} \right)^{\frac{p}{2}} \right]^2 \left(\psi \left(1 + \frac{q}{\beta_c} \right) + \psi \left(\frac{p}{2} - \frac{q}{\beta_c} \right) \right) \tag{2.6.9.16}$$

for ψ the Digamma function.

Lemma 2.6.11 combined with Eq. 2.6.8.26 imply that for this family of distribu-

tions, at the critical line

$$E_{(\beta_c, p), n} = n^{1-\frac{p}{2}} \ln n Q(p) \left(1 + \mathcal{O}\left(\frac{1}{\log n}\right) \right) \quad (2.6.9.17)$$

which is always (even if only logarithmically) leading over the Selberg contribution $\sim n^{1-\frac{p}{2}}$. We shall call the emergence of a logarithmic correction to scaling along the critical line a *marginal anomaly*. We remark the particularly small range of the constants at the critical line, $Q([2, 4]) = [0, \frac{3}{64}]$.

2.6.10. Family of distributions with endpoint at infinity and algebraic zero $\rho_{\text{ia}, \beta}$

Let us recall our family of probability densities depending on a parameter $\beta > 0$

$$\rho_{\text{ia}, \beta}(x) dx = \frac{\beta}{x^{\beta+1}} \theta(x-1) dx \quad (2.6.10.1)$$

for which, counting from the right, $R_{\text{ia}, \beta}^{-1}(u) = \left(\frac{1}{u}\right)^{\frac{1}{\beta}}$. We have a *duality relation* with the family with finite endpoint, algebraic zero $\rho_{\text{fa}, \beta}$ (see Section 2.6.8), under the transformation $\beta \rightarrow -\beta$. We thus immediately get

$$M_{k, n; q}^{(\text{ia}), \beta} = \frac{\Gamma(n+1)\Gamma(k-\frac{q}{\beta})}{\Gamma(k)\Gamma(n+1-\frac{q}{\beta})} = M_{k, n; q}^{(\text{fa}), -\beta} = M_{k, n; -q}^{(\text{fa}), \beta}. \quad (2.6.10.2)$$

(compare with eq. (2.6.8.2)).

We get immediately

$$\begin{aligned} E_{(\beta, p), n}(k) &= \sum_{q=0}^p \binom{p}{q} (-1)^q M_{k, n; q}^{(\text{ia}), \beta} M_{k, n; p-q}^{(\text{ia}), \beta} = \sum_{q=0}^p \binom{p}{q} (-1)^q M_{k, n; -q}^{(\text{fa}), \beta} M_{k, n; -p+q}^{(\text{fa}), \beta} \\ &\sim \begin{cases} n^{p/\beta} \sum_{q=0}^p \binom{p}{q} (-1)^q \frac{\Gamma(k-\frac{q}{\beta})\Gamma(k+\frac{p+q}{\beta})}{\Gamma^2(k)} & k \text{ small} \\ x^{-p/\beta} \sum_{q=0}^p \binom{p}{q} (-1)^q \exp\left(-\frac{1-x^{-1}}{2n\beta^2} (q^2 + (p-q)^2) + \mathcal{O}\left(\frac{1}{n^2}\right)\right) & x = \frac{k}{n'} = \Theta(1). \end{cases} \end{aligned} \quad (2.6.10.3)$$

Still by duality, the critical line is given by

$$2(p-\beta) = -p\beta \quad (2.6.10.4)$$

(or also $p_c(\beta) = \frac{2\beta}{\beta+2}$), and in this case the bulk regime is at $p < p_c(\beta)$, and the strictly anomalous one at $p > p_c(\beta)$. Therefore, the asymptotic coefficient is just

given by Eq. 2.6.8.14 under $\beta \rightarrow -\beta$, that is

$$b_{\beta,p}^{\text{ia}} := b_{-\beta,p}^{\text{fa}} = \frac{\Gamma(p+1)}{\beta^p} \frac{\Gamma(1 - \frac{\beta+2}{2\beta}p)}{\Gamma(2 - \frac{p}{\beta})}, \quad (2.6.10.5)$$

which recovers (169), Eq. 29 upon renaming $\beta = \alpha$ and the use of Legendre formula for the Γ function.

2.6.11. Family of distributions with internal endpoint, algebraic zero $\rho_{\text{sa},\beta}$

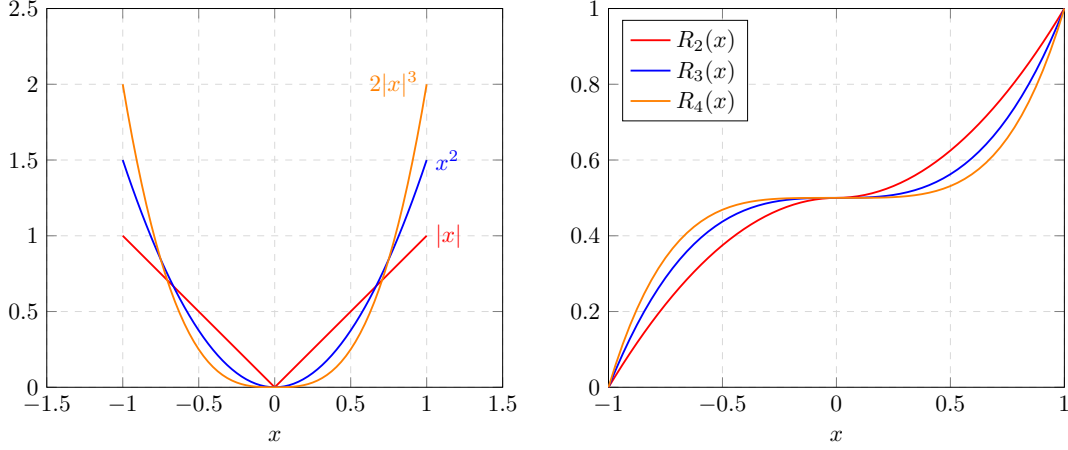


Figure 2.11. – Members from the family in Eq. 2.6.11.1 at $\beta = 2, 3, 4$ (left), and corresponding R_β functions (right).

In this section we consider the situation in which ρ vanishes due to a zero at a finite value inside the support. We exemplify this case with a 1-parameter family of polynomial measures with a zero of order $\beta - 1$ in the interior of the support $\Omega = (-1, 1)$, namely

$$\rho_\beta(x)dx = \frac{\beta}{2}|x|^{\beta-1}\theta(x+1)\theta(1-x)dx, \quad (2.6.11.1)$$

so that $R_\beta(x) = \frac{1}{2}(1 + \text{sgn}(x)|x|^\beta)$ (examples are given in Fig. 2.11). In this case $\langle (R_\beta^{-1}(u))^q \rangle_{P_{n,k}}$ does not lend itself to simple direct manipulations*, and we follow a different strategy. First of all, let us split the interval in half $\Omega = (-1, 0) \cup (0, 1) := \Omega_L \cup \Omega_R$. Let us also assume that we have n_1 reds and $n_1 + dn$ blues on

*We have the equivalent representations

$$\begin{aligned} M_{n,k,m;q}^{\text{double}} &:= \left\langle (2u-1)^{\frac{q}{2m+1}} \right\rangle_{P_{n,k}} \\ &= \sum_{s=0}^{\frac{q}{2m+1}} \binom{\frac{q}{2m+1}}{s} (-1)^{\frac{q}{2m+1}-s} 2^s \frac{\Gamma(k+s)}{\Gamma(k)} \frac{\Gamma(n+1)}{\Gamma(n+1+s)} \\ &= (-1)^{\frac{q}{2m+1}} {}_2F_1 \left(k, -\frac{q}{2m+1}; n+1; 2 \right) \\ &= 2 \frac{\Gamma(n+1)}{\Gamma(k)\Gamma(n-k+1)} \int_0^{\pi/2} d\theta (\cos(2\theta))^{q/(2m+1)} \cos^{2k-1}(\theta) \sin^{2(n-k)+1}(\theta). \end{aligned} \quad (2.6.11.2)$$

the left of the zero; and $n_2 + dn$ reds and n_2 blues on the right, with $n_1 + n_2 + dn = n$ (we may assume that $dn \geq 0$, otherwise the argument is identical upon exchanging reds and blues). As usual, we wish to evaluate \mathcal{H}_{id} , so that, on Ω_L , we wish to assign the n_1 red points to the left-most n_1 blue points, in order, and on Ω_R , we wish to assign the n_2 blue points with the rightmost n_2 red points; lastly, we want to assign dn blue points in Ω_L to the dn leftmost red points on Ω_R . With this decomposition, it is advantageous to enumerate points starting from the zero (around which the largest contributions are expected a priori) allowing to extend finite sums to series. Hence, we shall enumerate points from left to right on Ω_R and from right to left on Ω_L .

Let $B_n(m) = \frac{1}{4^n} \binom{2n}{m}$, and let n'_r (resp., n'_b) be the number of red (resp., blue) points to the left of the zero. Let us introduce

$$\begin{cases} n' &= \min(n'_r, n'_b) \\ n'' &= n - \max(n'_r, n'_b) \\ n''' &= n - n' - n'' = \max(n'_r, n'_b) - \min(n'_r, n'_b). \end{cases} \quad (2.6.11.3)$$

The total energy is given by

$$\begin{aligned} E_{n,p}^\beta &= \sum_{n'_r, n'_b \geq 0} B_n(n'_b) B_n(n'_r) \cdot \left[\sum_{k'=1}^{n'} \mathbb{E} (|R_{n'}^{-1}(u_{k'}) - R_{n'+n''}^{-1}(u_{k'+n''})|^p) + \right. \\ &+ \sum_{k''=1}^{n''} \mathbb{E} (|R_{n''}^{-1}(u_{k''}) - R_{n''+n'''}^{-1}(u_{k''+n'''})|^p) \\ &+ \left. \sum_{k'''=1}^{n'''} \mathbb{E} (|R_{n'+n'''}^{-1}(u_{k'''}) + R_{n'''+n'''}^{-1}(u_{n'''+1-k'''})|^p) \right] \\ &= \sum_{n'_r, n'_b \geq 0} B_n(n'_b) B_n(n'_r) \left[\sum_{k'=1}^{n'} L_{k',p,\beta} + \sum_{k''=1}^{n''} R_{k'',p,\beta} + \sum_{k'''=1}^{n'''} C_{k''',p,\beta} \right] \end{aligned} \quad (2.6.11.4)$$

Hence in eq. (2.6.11.4) the \mathcal{L} (\mathcal{R}) contributions come from edges falling entirely within Ω_L (resp. Ω_R); and the \mathcal{C} contributions (notice the plus sign in their definitions) come from edges “on top” of the zero, that is, edges matching points in Ω_L to points in Ω_R . It can be easily calculated that

$$\langle R_{n'}^{-1}(u_{k'})^q \rangle = \frac{\Gamma(k' + \frac{q}{\beta})}{\Gamma(k')} \frac{\Gamma(n' + 1)}{\Gamma(n' + 1 + \frac{q}{\beta})}. \quad (2.6.11.5)$$

Expanding the binomials in eq. 2.6.11.4 at $p > 1$ and even, the three contributions

are constituted of simple ratios of Γ functions, respectively (note that there is no minus sign $(-1)^q$ in the third expression)

$$\begin{aligned}
L_{k',p,\beta} &= \sum_{q=0}^p \binom{p}{q} (-1)^q \frac{\Gamma\left(k' + \frac{q}{\beta}\right)}{\Gamma(k')} \frac{\Gamma(n' + 1)}{\Gamma\left(n' + 1 + \frac{q}{\beta}\right)} \frac{\Gamma\left(k' + n''' + \frac{p-q}{\beta}\right)}{\Gamma(k' + n''')} \frac{\Gamma(n' + n''' + 1)}{\Gamma\left(n' + n''' + 1 + \frac{p-q}{\beta}\right)}, \\
R_{k'',p,\beta} &= \sum_{q=0}^p \binom{p}{q} (-1)^q \frac{\Gamma\left(k'' + \frac{q}{\beta}\right)}{\Gamma(k'')} \frac{\Gamma(n'' + 1)}{\Gamma\left(n'' + 1 + \frac{q}{\beta}\right)} \frac{\Gamma\left(k'' + n''' + \frac{p-q}{\beta}\right)}{\Gamma(k'' + n''')} \frac{\Gamma(n'' + n''' + 1)}{\Gamma\left(n'' + n''' + 1 + \frac{p-q}{\beta}\right)}, \\
C_{k''',p,\beta} &= \sum_{q=0}^p \binom{p}{q} \frac{\Gamma\left(k''' + \frac{q}{\beta}\right)}{\Gamma(k''')} \frac{\Gamma(n' + n''' + 1)}{\Gamma\left(n' + n''' + 1 + \frac{q}{\beta}\right)} \frac{\Gamma\left(n''' + 1 - k''' + \frac{p-q}{\beta}\right)}{\Gamma\left(n''' + 1 - k'''\right)} \frac{\Gamma(n'' + n''' + 1)}{\Gamma\left(n'' + n''' + 1 + \frac{p-q}{\beta}\right)},
\end{aligned} \tag{2.6.11.6}$$

so that, calling

$$\mathcal{L}_{n,p,\beta} = \sum_{k'=1}^{n'} L_{k',p,\beta}, \quad \mathcal{R}_{n,p,\beta} = \sum_{k''=1}^{n''} R_{k'',p,\beta}, \quad \mathcal{C}_{n,p,\beta} = \sum_{k'''=1}^{n'''} C_{k''',p,\beta}, \tag{2.6.11.7}$$

the energy is given by $E_{n,p}^\beta = \mathcal{L}_{n,p,\beta} + \mathcal{C}_{n,p,\beta} + \mathcal{R}_{n,p,\beta}$. The first remark is that $n' - \frac{n}{2} = \mathcal{O}(\sqrt{n})$ (almost surely) so that, at $\frac{q}{\beta} = \mathcal{O}(1)$, we get

$$\frac{\Gamma(n' + 1)}{\Gamma\left(n' + 1 + \frac{q}{\beta}\right)} = \frac{\Gamma\left(n' - \frac{n}{2} + \frac{n}{2} + 1\right)}{\Gamma\left(n' - \frac{n}{2} + \frac{n}{2} + 1 + \frac{q}{\beta}\right)} = \left(\frac{n}{2}\right)^{-\frac{q}{\beta}} \left(1 + \mathcal{O}\left(\frac{1}{\sqrt{n}}\right)\right) \tag{2.6.11.8}$$

(and an analogous expression mutatis mutandi for ratios of Γ functions involving n'' and n''' , and terms in which $q \leftrightarrow p - q$). Let us focus first on the central contribution C . Since $\frac{1}{\Gamma(k''')\Gamma(n''' + 1 - k''')} = \frac{1}{(n''' - 1)!} \binom{n''' - 1}{k''' - 1}$, we just get

$$\begin{aligned}
C_{k''',p,\beta} &\sim \left(\frac{n}{2}\right)^{-\frac{p}{\beta}} \sum_{q=0}^p \binom{p}{q} \frac{\Gamma\left(k''' + \frac{q}{\beta}\right)}{\Gamma(k''')} \frac{\Gamma\left(n''' + 1 - k''' + \frac{p-q}{\beta}\right)}{\Gamma(n''' + 1 - k''')} \\
&\sim \left(\frac{n}{2}\right)^{-\frac{p}{\beta}} \int_0^\infty dt \int_0^\infty du \left(t^{\frac{1}{\beta}} + u^{\frac{1}{\beta}}\right)^p \frac{t^{k''' - 1} u^{n''' - k'''}}{(n''' - 1)!} \binom{n''' - 1}{k''' - 1} e^{-(t+u)}.
\end{aligned} \tag{2.6.11.9}$$

Hence

$$\begin{aligned}
\mathcal{C}_{n,p,\beta} &\sim \left(\frac{n}{2}\right)^{-\frac{p}{\beta}} \int_0^\infty dt \int_0^\infty du \left(t^{\frac{1}{\beta}} + u^{\frac{1}{\beta}}\right)^p \frac{(t+u)^{n'''-1}}{(n'''-1)!} e^{-(t+u)} \\
&\sim \int_0^1 dx \left(x^{\frac{1}{\beta}} + (1-x)^{\frac{1}{\beta}}\right)^p \left(\frac{n}{2}\right)^{-\frac{p}{\beta}} \int_0^\infty dV \frac{V^{n''' + \frac{p}{\beta}}}{(n'''-1)!} e^{-V} \\
&\sim K_{\beta,p} \left(\frac{n}{2}\right)^{-\frac{p}{\beta}} \frac{\Gamma\left(n''' + 1 + \frac{p}{\beta}\right)}{\Gamma(n''')},
\end{aligned} \tag{2.6.11.10}$$

where the change of variables $t = Vx$ and $u = V(1-x)$ (such that $dudt = VdVdx$) has been suggested by the homogeneity properties of the integrand, and the limit constants are just

$$K_{\beta,p} = \sum_{q=0}^p \binom{p}{q} \frac{\Gamma\left(1 + \frac{q}{\beta}\right) \Gamma\left(1 + \frac{p-q}{\beta}\right)}{\Gamma\left(2 + \frac{p}{\beta}\right)} \tag{2.6.11.11}$$

(notice the absence of the $(-1)^q$ term). Since also $n''' = \mathcal{O}(\sqrt{n})$ (almost surely), so that

$$\frac{\Gamma\left(n''' + 1 + \frac{p}{\beta}\right)}{\Gamma(n''')} = n^{\frac{1}{2}\left(1 + \frac{p}{\beta}\right)} \left(1 + \mathcal{O}\left(\frac{1}{\sqrt{n}}\right)\right), \tag{2.6.11.12}$$

we just have

$$\mathcal{C}_{n,p,\beta} = n^{-\frac{p}{\beta}} n^{\frac{1}{2}\left(1 + \frac{p}{\beta}\right)} K_{\beta,p} (1 + o(1)) = n^{\frac{1}{2}\left(1 - \frac{p}{\beta}\right)} K_{\beta,p} (1 + o(1)). \tag{2.6.11.13}$$

Thus, a contribution from edges jumping above the region of low density of points scales as the bulk one, $n^{1 - \frac{p}{\beta}}$, if it were that the contributions of the \mathcal{L} and \mathcal{R} parts have no stronger scaling,

$$p + \beta = p\beta. \tag{2.6.11.14}$$

Eq. (2.6.11.14) defines a critical hyperbola $p_c(\beta) = \frac{\beta}{\beta-1}$ (or equivalently $\beta_c(p) = \frac{p}{p-1}$) separating the anomalous from the bulk regime (Fig. 2.12). Incidentally, except for a factor 2 at lhs, it corresponds to the critical line for the family of densities with a single zero, eq. (2.6.8.22).

Let us now evaluate the ‘‘single-sided’’ contributions to the energy $\mathcal{L}_{n,p,\beta}$ ($\mathcal{R}_{n,p,\beta}$ can be evaluated analogously). We shall address the evaluation in two ways:

1. an approach inspired by § 2.5 and valid for the bulk regime $\beta < \beta_c$, in which we treat k' in $L_{k',p,\beta}$ as a variable of order n . The explicit expression of

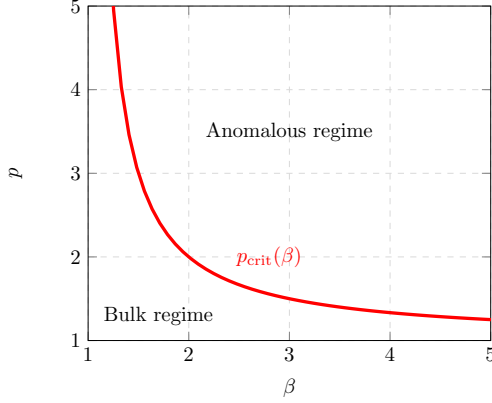


Figure 2.12. – Critical hyperbola separating the region of anomalous scaling ($p > p_{\text{crit}}(\beta)$) from the region of bulk scaling ($p < p_{\text{crit}}(\beta)$) for the family of probability densities (2.6.11.1). Notice the $p \leftrightarrow \beta$ symmetry (with corresponding self-dual point at $(\beta_c, p_c) = (2, 2)$), and that there can be no anomalous correction to the Dyck scaling ($p = 1$), which is always bulk.

$L_{k',p,\beta}$ in terms of inverse cumulative functions is evaluated with the saddle point approximation of the involved beta distribution (which is valid when k is order n), and is divergent at the critical hyperbola;

2. an approach tailored for the anomalous regime $\beta > \beta_c$ in which we assume that the dominant k' are the small ones.

These two computations are done in § 2.6.12 and § 2.6.13.

2.6.12. $\mathcal{L}_{n,p,\beta}$ ($\mathcal{R}_{n,p,\beta}$) in the bulk region

The explicit expression for the contribution of the k -th edge on the left is

$$\begin{aligned}
 L_{k,p,\beta} &= \int_0^{\frac{1}{2}} \int_0^{\frac{1}{2}} dudv P_{n,k}(u)P_{n,k}(v) \left((1-2u)^{\frac{1}{\beta}} - (1-2v)^{\frac{1}{\beta}} \right)^p \\
 &= \mathcal{N}_{n,k} \int_0^{\frac{1}{2}} \int_0^{\frac{1}{2}} dudv e^{n(\phi(u)+\phi(v))} \left[(1-2u)^{\frac{1}{\beta}} - (1-2v)^{\frac{1}{\beta}} \right]^p \quad (2.6.12.1) \\
 &\simeq \int \int dudv G(u_{\text{sp}}, \sigma_{\text{sp}}^2/n) G(v_{\text{sp}}, \sigma_{\text{sp}}^2/n) \left[(1-2u)^{\frac{1}{\beta}} - (1-2v)^{\frac{1}{\beta}} \right]^p
 \end{aligned}$$

where the integration is restricted to $[0, \frac{1}{2}] \times [0, \frac{1}{2}]$ since the endpoints of the edge are both to the left of the zero, in the second line the normalization constant is

$\mathcal{N}_{n,k} = \binom{n-1}{k}^2$, and in the third line $G(m, \sigma^2)$ is a gaussian of mean m and variance σ^2 . It is obtained from the quadratic expansion around the extremum of

$$\phi(t) := \frac{k-1}{n} \log(t) + \frac{n-k}{n} \log(1-t) \quad (2.6.12.2)$$

so that $\frac{d}{dt}\phi(t)|_{t=t_{\text{sp}}} = 0$ and $\frac{1}{\sigma_{\text{sp}}^2} = \frac{d^2}{dt^2}\phi(t)|_{t=t_{\text{sp}}}$. Let us put $u = u_{\text{sp}} + \delta u$ and $v = v_{\text{sp}} + \delta v$, and let us expand $\left((1-2u)^{\frac{1}{\beta}} - (1-2v)^{\frac{1}{\beta}}\right)^p$ around the saddle point. We have

$$\left((1-2u)^{\frac{1}{\beta}} - (1-2v)^{\frac{1}{\beta}}\right)^p = (1-2u_{\text{sp}})^{\frac{p}{\beta}} \left[\left(1 + \frac{2}{1-2u_{\text{sp}}}\delta u\right)^{\frac{1}{\beta}} - \left(1 + \frac{2}{1-2u_{\text{sp}}}\delta v\right)^{\frac{1}{\beta}} \right]^p \quad (2.6.12.3)$$

since $u_{\text{sp}} = v_{\text{sp}}$. Calling $c = \frac{2}{1-2u_{\text{sp}}}$, we can now perform the integrations and get

$$\begin{aligned} \int du G(u_{\text{sp}}, \sigma_{\text{sp}}^2/n) (1+c\delta u)^{\frac{q}{\beta}} &= \sum_a \frac{c^a}{a!} \left(\frac{q}{\beta}\right)_a \langle \delta u^a \rangle = \sum_{a \text{ even}} \frac{c^a}{a!} \left(\frac{q}{\beta}\right)_a \left(\frac{\sigma_{\text{sp}}^2}{n}\right)^{\frac{a}{2}} (a-1)!! \\ \int dv G(v_{\text{sp}}, \sigma_{\text{sp}}^2/n) (1+c\delta v)^{\frac{p-q}{\beta}} &= \sum_b \frac{c^b}{b!} \left(\frac{p-q}{\beta}\right)_b \langle \delta v^b \rangle = \sum_{b \text{ even}} \frac{c^b}{b!} \left(\frac{p-q}{\beta}\right)_b \left(\frac{\sigma_{\text{sp}}^2}{n}\right)^{\frac{b}{2}} (b-1)!! \end{aligned} \quad (2.6.12.4)$$

where $(y)_k = y(y+1)\cdots(y+k-1)$. We are thus left with

$$\begin{aligned} L_{k,p,\beta} &\simeq (1-2u_{\text{sp}})^{\frac{p}{\beta}} \iint dudv G(u_{\text{sp}}, \sigma_{\text{sp}}^2/n) G(v_{\text{sp}}, \sigma_{\text{sp}}^2/n) \sum_q \binom{p}{q} (-1)^{p-q} (1+c\delta u)^{\frac{q}{\beta}} (1+c\delta v)^{\frac{p-q}{\beta}} \\ &= (1-2u_{\text{sp}})^{\frac{p}{\beta}} \sum_q \binom{p}{q} (-1)^{p-q} \sum_{a,b \text{ even}} \frac{c^{a+b}}{a!b!} \left(\frac{q}{\beta}\right)_a \left(\frac{p-q}{\beta}\right)_b \left(\frac{\sigma_{\text{sp}}^2}{n}\right)^{\frac{a+b}{2}} (a-1)!!(b-1)!! \\ &= (1-2u_{\text{sp}})^{p(\frac{1}{\beta}-1)} 2^p \frac{p!}{\beta^p} \left(\frac{\sigma_{\text{sp}}}{\sqrt{n}}\right)^p \sum_{\substack{a+b=p \\ a,b \text{ even}}} \frac{(a-1)!!(b-1)!!}{a!b!} \end{aligned} \quad (2.6.12.5)$$

where from the second to the third line we have used Lemma 2.6.6 (which has forced $a + b = p$). But

$$\begin{aligned}
\sum_{\substack{a+b=p \\ a,b \text{ even}}} \frac{(a-1)!!(b-1)!!}{a!b!} &= 2^{-\frac{p}{2}} \sum_{\substack{a+b=p \\ a,b \text{ even}}} \frac{1}{\left(\frac{a}{2}\right)!} \frac{1}{\left(\frac{b}{2}\right)!} = 2^{-\frac{p}{2}} \sum_{\substack{a+b=p \\ a,b \text{ even}}} \frac{1}{\left(\frac{a}{2}\right)!} \frac{1}{\left(\frac{b}{2}\right)!} \frac{\left(\frac{p}{2}\right)!}{\left(\frac{p}{2}\right)!} \\
&= \frac{2^{-\frac{p}{2}}}{\left(\frac{p}{2}\right)!} \sum_{\substack{a+b=p \\ a,b \text{ even}}} \frac{\left(\frac{p}{2}\right)!}{\left(\frac{a}{2}\right)! \left(\frac{b}{2}\right)!} \\
&= \frac{1}{\left(\frac{p}{2}\right)!}.
\end{aligned} \tag{2.6.12.6}$$

Now we can evaluate $\mathcal{L}_{n,p,\beta}$ in the regime $x = \frac{k}{n}$ (for $x \in [0, 1/2]$). The saddle point equation becomes

$$u_{\text{sp}} = \frac{k}{n} \equiv x, \quad \sigma_{\text{sp}}^2 = x(1-x) \tag{2.6.12.7}$$

so that

$$\mathcal{L}_{n,p,\beta} \simeq n^{1-\frac{p}{2}} \frac{2^p}{\beta^p} \frac{p!}{\left(\frac{p}{2}\right)!} \int_0^{\frac{1}{2}} dx (1-2x)^{p\left(\frac{1}{\beta}-1\right)} [x(1-x)]^{\frac{p}{2}}. \tag{2.6.12.8}$$

Lastly, since

$$\begin{aligned}
\int_0^{\frac{1}{2}} dx (1-2x)^a [x(1-x)]^b &\stackrel{t=1-2x}{=} \int_0^1 dt t^a (1-t^2)^b \\
&\stackrel{s=t^2}{=} \int_0^1 ds s^{\frac{a+1}{2}-1} (1-s)^{b+1-1} \\
&= 2^{-2b} \frac{\Gamma\left(\frac{a+1}{2}\right) \Gamma(b+1)}{\Gamma\left(\frac{a+1}{2} + b + 1\right)}
\end{aligned} \tag{2.6.12.9}$$

we just get that, in the bulk regime $p\left(\frac{1}{\beta} - 1\right) < 1$ (see Fig. 2.12),

$$\mathcal{L}_{n,p,\beta} = n^{1-\frac{p}{2}} B_{\beta,p} (1 + o(1)) \tag{2.6.12.10}$$

with

$$B_{\beta,p} = \frac{1}{\beta^p} \frac{\Gamma(p+1) \Gamma\left(\frac{p}{2\beta} - \frac{p}{2} + \frac{1}{2}\right)}{\Gamma\left(\frac{p}{2\beta} + \frac{3}{2}\right)}, \tag{2.6.12.11}$$

and $\mathcal{R}_{n,p,\beta} = \mathcal{L}_{n,p,\beta}$ by symmetry.

Remark 2.6.4. Let us call the total energy of the single-sided contributions (i.e. the sum of left and right contributions)

$$E_{p,\beta}^{\text{sa},\mathcal{L}+\mathcal{R}}(n) = \mathcal{L}_{n,p,\beta} + \mathcal{R}_{n,p,\beta}. \quad (2.6.12.12)$$

In the $\beta \rightarrow 1^+$ limit, the distribution $\rho_{\text{sa},1}$ recovers the uniform distribution supported on the interval $\Omega = [-1, 1]$ and there is no central term, so that the total energy is asymptotically

$$E_{p,1}^{\text{sa},\mathcal{L}+\mathcal{R}}(n) = n^{1-\frac{p}{2}} 2 \frac{\sqrt{\pi} \Gamma(p+1)}{\Gamma\left(\frac{p}{2} + \frac{3}{2}\right)} (1 + o(1)). \quad (2.6.12.13)$$

On the other hand, the asymptotic series for the energy where points are uniformly distributed on $[0, 1]$ is (see Eq. (2.6.1.2))

$$s_{p,n} = n^{1-p/2} \frac{\Gamma(1+p/2)}{p+1} (1 + o(1)), \quad (2.6.12.14)$$

so that their ratio is

$$\frac{E_{p,1}^{\text{sa},\mathcal{L}+\mathcal{R}}(n)}{s_{p,n}} = \left(\frac{|\Omega|}{|[0, 1]|} \right)^p (1 + o(1)) = 2^p (1 + o(1)) \quad (2.6.12.15)$$

as expected.

2.6.13. $\mathcal{L}_{n,p,\beta}$ ($\mathcal{R}_{n,p,\beta}$) in the anomalous regime and on the critical line

Recall from Eq. 2.6.11.6 that

$$L_{k',p,\beta} = \sum_{q=0}^p \binom{p}{q} (-)^q \frac{\Gamma\left(k' + \frac{q}{\beta}\right)}{\Gamma(k')} \frac{\Gamma\left(k' + n''' + \frac{p-q}{\beta}\right)}{\Gamma(k' + n''')} \left(\frac{n}{2}\right)^{-\frac{p}{\beta}} \quad (2.6.13.1)$$

so that, for $\Lambda_1 \ll \sqrt{n}$, we have

$$\begin{aligned} \sum_{k'=1,\dots,\Lambda_1} L_{k',p,\beta} &\lesssim \sum_{k'} \sum_{q=0}^p \binom{p}{q} (k')^{\frac{q}{\beta}} (k' + n''')^{\frac{p-q}{\beta}} \left(\frac{n}{2}\right)^{-\frac{p}{\beta}} \\ &\approx \Lambda_1 (\sqrt{n})^{\frac{p}{\beta}} \left(\frac{n}{2}\right)^{-\frac{p}{\beta}} = c \Lambda_1 n^{-\frac{p}{2\beta}} = o\left(n^{\frac{1}{2}-\frac{p}{2\beta}}\right) \\ &= o(\mathcal{C}_{n,p,\beta}) \end{aligned} \quad (2.6.13.2)$$

which is always sub-leading with respect to the central contribution $\mathcal{C}_{n,p,\beta}$. Hence, the contribution from the first Λ_1 edges may be discarded without affecting the leading scaling and for $k' \gg \sqrt{n}$ the continuous approximation of the sum with an integral up to the appropriate upper cutoff Λ_2 can be done. Calling $k' = \zeta n'$ and $n' = \xi \sqrt{n}$, so that $k' = \zeta \xi \sqrt{n}$, we have that $\max(\zeta \xi \sqrt{n}) = \frac{n}{2}$, so that $\Lambda_n(\xi) = \frac{\sqrt{n}}{2\xi}$ (observe that a.s. $\xi = \Theta(1)$). We thus get

$$\begin{aligned} \mathcal{L}_{n,p,\beta} &= \sum_{k'=\mathcal{O}(\sqrt{n})}^{n'} L_{k',p,\beta} \sim \sqrt{n} \int_0^{\sqrt{n}/2} d\zeta L_{\zeta \xi \sqrt{n},p,\beta} \\ &= \sqrt{n} \int_0^{\sqrt{n}/2} d\zeta \sum_{q=0}^p \binom{p}{q} (-1)^q (\zeta \sqrt{n})^{\frac{p-q}{\beta}} ((\zeta + \xi) \sqrt{n})^{\frac{q}{\beta}} \left(\frac{n}{2}\right)^{-\frac{p}{\beta}} \\ &= n^{\frac{1}{2}(1-\frac{p}{\beta})} 2^{\frac{p}{\beta}} \left\langle \int_0^{\sqrt{n}/2} d\zeta \sum_{q=0}^p \binom{p}{q} (-1)^q \zeta^{\frac{p-q}{\beta}} (\zeta + \xi)^{\frac{q}{\beta}} \right\rangle_{\xi} \end{aligned} \quad (2.6.13.3)$$

where $\langle \dots \rangle_{\xi}$ denotes average with respect to the distribution of ξ . But $\xi \sqrt{n} \stackrel{d}{=} m_1 + m_2$ with m_1, m_2 indep. and distrib. with p_{binomial} , where

$$p_{\text{binomial}}(m) = \frac{1}{\sqrt{2\pi n^{\frac{1}{4}}}} e^{-\frac{m^2}{2n^{\frac{1}{4}}}} dm, \quad (2.6.13.4)$$

i.e. $p(\xi)d\xi = \frac{2}{\sqrt{\pi}} e^{-\xi^2} \theta(\xi) d\xi$, so that, in particular $\langle \xi^\alpha \rangle = \frac{\Gamma(\frac{\alpha+1}{2})}{\sqrt{\pi}}$. Setting $\eta = \xi \zeta$, we get

$$\mathcal{L}_{n,p,\beta} = n^{\frac{1}{2}(1-\frac{p}{\beta})} 2^{\frac{p}{\beta}} \left\langle \xi^{\frac{p}{\beta}} \int_0^{\Lambda_n(\xi)} d\eta \sum_{q=0}^p \binom{p}{q} (-1)^q \eta^{\frac{p-q}{\beta}} (\eta + 1)^{\frac{q}{\beta}} \right\rangle_{\xi}. \quad (2.6.13.5)$$

Since a.s. $\Lambda_n(\xi) \gg 1$, we may split the integration as

$$\begin{aligned} \int_0^{\Lambda_n(\xi)} d\eta \eta^a (\eta + 1)^b &= \int_0^1 d\eta \eta^a \sum_{\ell \geq 0} \binom{b}{\ell} \eta^\ell + \int_1^{\Lambda_n(\xi)} d\eta \eta^{a+b} \sum_{\ell \geq 0} \binom{b}{\ell} \eta^{-\ell} \\ &= \sum_{\ell \geq 0} \binom{b}{\ell} \left[\frac{1}{a + \ell + 1} + \rho(\ell - a - b - 1, \Lambda(\xi)) \right] \end{aligned} \quad (2.6.13.6)$$

where

$$\rho(x, y) = \begin{cases} \frac{1}{x} + \mathcal{O}\left(\frac{1}{\sqrt{n}}\right) & x \neq 0 \\ \ln y + \mathcal{O}(1) & x = 0. \end{cases} \quad (2.6.13.7)$$

We thus get

$$\mathcal{L}_{n,p,\beta} = n^{\frac{1}{2}(1-\frac{p}{\beta})} 2^{\frac{p}{\beta}} \left\langle \sum_{q=0}^p \binom{p}{q} (-1)^q \sum_{\ell \geq p} \binom{q/\beta}{\ell} \left[\frac{1}{\frac{p-q}{\beta} + \ell + 1} + \rho \left(\frac{p}{\beta} + \ell - 1, \Lambda(\xi) \right) \right] \xi^{\frac{p}{\beta}} \right\rangle_{\xi} \quad (2.6.13.8)$$

where the second sum has been restricted to $\ell \geq p$ as the discarded terms would be zeroed in light of Lemma 2.6.6. In the anomalous region above the critical hyperbola $\beta + p = \beta p$, $\frac{p}{\beta} + \ell - 1 > 0$ for all $\beta > p$. If we are on the critical hyperbola, then the only dangerous term is $\ell = p$. In the first case (see the function ρ) we have no further dependence on ξ and

$$\left\langle \xi^{\frac{p}{\beta}} \right\rangle_{\xi} = \frac{\Gamma\left(\frac{1+\frac{p}{\beta}}{2}\right)}{\sqrt{\pi}} \quad (2.6.13.9)$$

is factored out. In the second case there is one single ‘‘dangerous’’ term from the upper extremum of integration

$$\left\langle \ln \left(\frac{\sqrt{n}}{2\xi} \right) \xi^{\frac{p}{\beta}} \right\rangle_{\xi} = \left(\frac{1}{2} \ln n - \ln 2 \right) \frac{\Gamma\left(\frac{1+\frac{p}{\beta}}{2}\right)}{\sqrt{\pi}} - \frac{1}{2} \frac{\Gamma\left(\frac{1+\frac{p}{\beta}}{2}\right)}{\sqrt{\pi}} \psi \left(\frac{1+\frac{p}{\beta}}{2} \right) \quad (2.6.13.10)$$

where ψ is the Digamma function. In conclusion

$$\mathcal{L}_{n,p,\beta} \sim n^{\frac{1}{2}(1-\frac{p}{\beta})} 2^{\frac{p}{\beta}} \frac{\Gamma\left(\frac{1+\frac{p}{\beta}}{2}\right)}{\sqrt{\pi}} \cdot \begin{cases} \sum_{q=0}^p \binom{p}{q} (-1)^q \sum_{\ell \geq p} \binom{q/\beta}{\ell} \left[\frac{1}{\frac{p-q}{\beta} + \ell + 1} + \frac{1}{\frac{p}{\beta} + \ell - 1} \right] & p + \beta < p\beta \\ \sum_{q=0}^p \binom{p}{q} (-1)^q \left[\binom{q/\beta}{p} \left(\frac{1}{\frac{p-q}{\beta} + p + 1} + \frac{1}{2} \ln n + \right. \right. & p + \beta = p\beta \\ \left. \left. - \frac{1}{2} \psi \left(\frac{1+\frac{p}{\beta}}{2} \right) - \ln 2 \right) + \sum_{\ell \geq p} \binom{q/\beta}{\ell} \left(\frac{1}{\frac{p-q}{\beta} + \ell + 1} + \frac{1}{\frac{p}{\beta} + \ell - 1} \right) \right] & \end{cases} \quad (2.6.13.11)$$

In particular, we have a logarithmic correction to scaling on the critical hyperbola $\beta = p/(p-1)$:

Lemma 2.6.12 (Marginal anomaly for the family ρ_{sa}). *At the critical line $p + \beta =$*

$p\beta$ where $C_{n,p,\frac{p}{p-1}} = o(\mathcal{L}_{n,p,\frac{p}{p-1}})$, we have

$$E_{n,p}^{\frac{p}{p-1}} = \mathcal{L}_{n,p,\frac{p}{p-1}} + \mathcal{R}_{n,p,\frac{p}{p-1}} + \dots = n^{1-p/2} R(p) \ln n \left(1 + \mathcal{O}\left(\frac{1}{\ln n}\right) \right) \quad (2.6.13.12)$$

with

$$R(p) = \frac{2^{p-1}}{\sqrt{\pi}} p! \left(\frac{p}{2} - 1\right)! \left(\frac{p-1}{p}\right)^p. \quad (2.6.13.13)$$

Instead in the anomalous region $p > \beta/(\beta-1)$ $\mathcal{L}_{n,p,\beta}$, $\mathcal{R}_{n,p,\beta}$ and $C_{n,p,\beta}$ are of the same order and we get

$$E_{n,p}^\beta = n^{\frac{1}{2}(1-\frac{p}{\beta})} (2A_{\beta,p} + K_{\beta,p}) (1 + o(1)), \quad p + \beta < p\beta, \quad (2.6.13.14)$$

where

$$A_{\beta,p} = 2^{\frac{p}{\beta}} \frac{\Gamma\left(\frac{1+\frac{p}{\beta}}{2}\right)}{\sqrt{\pi}} \sum_{q=0}^p \binom{p}{q} (-1)^q \sum_{\ell \geq p} \binom{q/\beta}{\ell} \left[\frac{1}{\frac{p-q}{\beta} + \ell + 1} + \frac{1}{\frac{p}{\beta} + \ell - 1} \right] \quad (2.6.13.15)$$

and $K_{p,\beta}$ is given in Eq. 2.6.11.11.

2.6.14. Section provisional conclusions

In this Section we have studied possible anomalous scaling behaviors of the optimal cost in the convex regime $p \geq 1$. We have derived phase diagrams which involve p and the relevant exponent characterizing the kind of zero of the probability distribution of points at a finite or infinite endpoint. For stretched exponential distributions parametrized by α , the leading scaling is $\sim a_1(\alpha, p) (\ln n)^{a_2(\alpha, p)}$, and we have explicitly determined both a_1 and a_2 . During the derivation, several connections to topics (and recent results) in number theory have emerged, such as with multiple zeta values (§ 2.6.6). For the algebraic cases parametrized by β , an even simpler pattern has emerged: in the (p, β) plane hyperbolae separate a bulk from an anomalous region. The hyperbolae are $2(p + \beta) = p\beta$ for the case of a finite endpoint, and $p + \beta = p\beta$ for the case of an internal endpoint (finite and infinite endpoints being related by $\beta \rightarrow -\beta$). In the bulk regimes the leading scaling is the Donsker's Theorem one (i.e. $\sim n^{1-p/2}$), and the leading coefficients have been determined explicitly; in the anomalous regimes the leading scalings have also been determined explicitly being respectively $\sim n^{-p/\beta}$ and $\sim n^{1/2(1-p/\beta)}$. The corresponding leading constants have been also obtained. In both cases, at the critical lines a logarithmic correction to scaling was found (“marginally anomalous scaling”), and the leading and first-sub-leading coefficients were also obtained.

2.7. The Dyck bound in the concave regime

THE content of this Section has been published in (173).

2.7.1. Problem statement and models of random assignment considered

Contrary to the convex regime $p > 1$, where in $d = 1$ the optimal matching is completely determined, and the \mathcal{C} -repulsive case $p < 0$, where in $d = 1$ it is known that the optimal matching has certain cyclic properties and can thus be readily found in a subset of the symmetric group, the non-crossing property is not sufficient to fully characterize the optimal assignment; the regime $0 < p < 1$ is thus much more challenging to study.

The relevance of non-crossing matching configurations among elementary units aligned on a line has emerged both in physics and in biology. In the latter case, this is due to the fact that they appear in the study of the secondary structure of single stranded DNA and RNA chains in solution (85). These chains tend to fold in a planar configuration, in which complementary nucleotides are matched, and planar configurations are exactly described by non-crossing matchings between nucleotides. The secondary structure of a RNA strand is therefore a problem of optimal matching on the line, with the restriction on the optimal configuration to be planar (95, 110, 141). The statistical physics of the folding process is highly non-trivial and it has been investigated by many different techniques (91, 99), also in presence of disorder and in search for glassy phases (64, 87, 91, 92, 141). Therefore, as a further motivation for the present work, understanding the statistical properties of the solution to ERAP with a concave cost function could yield results and techniques to better understand these models of RNA secondary structure.

2.7.2. Choice of randomness for \mathcal{B} and \mathcal{R}

Let us fix Ω to be a segment, that is we consider the problem with open boundary conditions (the alternate possible choice of considering Ω as a circle is not considered here).

Notice that in the literature Ω is typically taken to be deterministically the unit segment $[0, 1]$, while in this §we will find easier to work with a segment $[0, L]$, where L may be a stochastic variable, whose distribution depends on n . We will work in the framework of constant density, that is $\mathbb{E}(L) \sim n$, so that, for comparison with the existing literature, our results should be corrected by multiplying by a factor of the order n^{-p} .

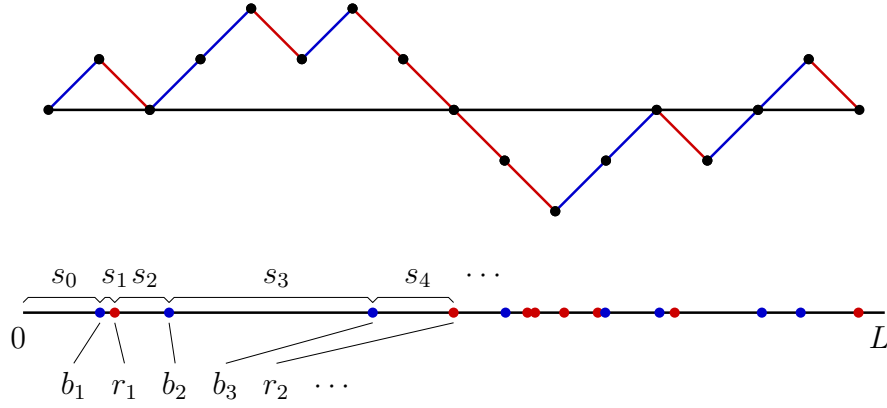


Figure 2.13. – Example of instance $J = (\mathcal{B}, \mathcal{R}) = [\vec{s}, \sigma]$, in the PPP model. Bottom: the configuration of points. Top: the Dyck bridge associated to σ . Here $n = 8$, and $\sigma = \{+, -, +, +, -, +, -, -, -, +, +, -, +, +, -\}$.

We can encode an instance $J = (\mathcal{B}, \mathcal{R})$ by the ordered lists $\mathcal{B} = (b_1, b_2, \dots, b_n)$, $b_i \leq b_{i+1}$, and $\mathcal{R} = (r_1, r_2, \dots, r_n)$, $r_i \leq r_{i+1}$. A useful alternate encoding of the instance is $J = [\vec{s}, \sigma]$, where $s = (s_0, s_1, \dots, s_{2n})$, $s_i \in \mathbb{R}^+$, encodes the distances between consecutive points (and between the first/last point with the respective endpoint of the segment Ω) and the vector $\sigma = (\sigma_1, \sigma_2, \dots, \sigma_{2n}) \in \{-1, +1\}^{2n}$, with $\sum_i \sigma_i = 0$, encodes the sequence of colours of the points (see Fig. 2.13, where the identification blue = +1 and red = -1 is adopted). In other words, the partial sums of \vec{s} , i.e. $(s_0, s_0 + s_1, s_0 + s_1 + s_2, \dots, s_0 + \dots + s_{2n-1})$, constitute the ordered list of $\mathcal{B} \cup \mathcal{R}$, and σ describes how the elements of \mathcal{B} and \mathcal{R} do interlace. In this notation, the domain of the instance $\Omega = [0, L]$ is determined by $L = \sum_{i=0}^{2n} s_i$. Remark that the cardinality of the space of possible vectors σ is just the central binomial,

$$B_n := \binom{2n}{n}. \quad (2.7.2.1)$$

For simplicity, we consider here only the non-degenerate case, in which almost surely all the s_i 's are strictly positive, that is, the values in $\mathcal{B} \cup \mathcal{R}$ are all distinct.

In this Section, and more crucially in subsequent work, we shall consider two families of measures. In all these measures, we have a factorisation $\mu([\vec{s}, \sigma]) = \mu_1(\vec{s})\mu_2(\sigma)$, and the measure on σ is just the uniform measure.

Independent spacing models (ISM). The measure $\mu(\vec{s})$ is factorised, and the s_i 's are i.i.d. with some distribution $\rho(s)$ with support on \mathbb{R}^+ (and, for simplicity, say with all moments finite, $\int ds s^k \rho(s) < \infty$ for all k). Without loss of generality, we will assume that the average of $\rho(s)$ is 1, i.e. the average of L is $2n + 1$. In particular, we will consider:

Uniform spacings (US): the s_i 's are deterministic, identically equal to 1, and thus $L = 2n + 1$ for all instances;

Exponential spacings (ES): the s_i 's are i.i.d. with an exponential distribu-

tion $\rho(s) = g_1(s) = \exp(-s)$, and thus L concentrates on $2n + 1$, but has a variance of order n .

Exchangeable process model (EPM). This is a generalisation of the ISM above, but now the s_i 's are not necessarily i.i.d., they are instead *exchangeable variables*, that is, for all $0 \leq i < 2n$,

$$\mu(s_0, \dots, s_i, s_{i+1}, \dots, s_{2n}) = \mu(s_0, \dots, s_{i+1}, s_i, \dots, s_{2n}). \quad (2.7.2.2)$$

In particular, within this class of models we could have that μ is supported on the hyper-tetrahedron \mathbb{T}_{2n} described by $s_i \geq 0$, and $L = \sum_i s_i = 2n + 1$. In this paper, we will consider:

Poisson Point Process (PPP): the s_i 's are the spacings among the sorted list of $0, 2n + 1$, and $2n$ uniform random points in the interval $[0, 2n + 1]$.

Each of these three models has its own motivations. The PPP case is, in a sense, the most natural one for what concerns applications and the comparison with the models in arbitrary dimension d . Implicitly, it is the one described in the introduction. The ES case is useful due to a strong relation with the PPP case (see Remark 2.7.1 and Lemma 2.7.5 later on in Section 2.7.6). In a sense, it is the ‘‘Poissonisation’’ of the PPP case (where in this case it is the quantity L that has been ‘‘Poissonised’’, that is, it is taken stochastic with its most natural underlying measure, instead of deterministic). The US case will prove out, in future work, to be the most tractable case for what concerns lower bounds to the optimal cost.

As all of the measures above are factorized in σ and \vec{s} , and the measure over σ is uniform, it is useful to define two shortcuts for two recurrent notions of average.

Definition 2.7.1. For any quantity $A(J) = A(\sigma, \vec{s})$, we denote by \overline{A} the average of A over σ

$$\overline{A} := \mathbb{E}_\sigma(A) = \frac{1}{B_n} \sum_\sigma A(\sigma, \vec{s}); \quad (2.7.2.3)$$

This average is independent from the choice of model among the classes above. We denote by

$$\langle A \rangle := \mathbb{E}_{\mu(\vec{s})}(A) \quad (2.7.2.4)$$

the average of A over \vec{s} , with its appropriate measure dependence on the choice of model. Finally, we denote by $\mathbb{E}_n(A)$ the result of both averages, in which we stress the dependence from the size parameter n in the measure, that is

$$\mathbb{E}_n(A) := \mathbb{E}_{\sigma, \mu(\vec{s})}(A) = \overline{\langle A \rangle} = \langle \overline{A} \rangle. \quad (2.7.2.5)$$

For a given instance, parametrised as $J = (\mathcal{B}, \mathcal{R})$, or as $J = [\vec{s}, \sigma]$, (and in which

the cost function also has an implicit dependence from the exponent p), we will call as usual π_{opt} one optimal configuration, so that $H_{\text{opt}}(J) = H_J(\pi_{\text{opt}})$.

2.7.3. Synthesis of results

In this Section we will introduce the notion of *Dyck matching* π_{Dyck} of an instance J and we will compute its average cost $H_{\text{Dyck}} := \mathbb{E}_n(H_J(\pi_{\text{Dyck}}))$ for the measures ES and PPP (with a brief discussion on the US case).

In particular we prove the following theorem:

Theorem 2.7.1. *For the three measures ES, US and PPP, let $\mathbb{E}_n(H_{\text{Dyck}})$ denote the average cost of the Dyck matchings. Then*

$$\mathbb{E}_n(H_{\text{Dyck}}) \simeq \begin{cases} n & 0 \leq p < \frac{1}{2} \\ n \ln n & p = \frac{1}{2} \\ n^{\frac{1}{2}+p} & \frac{1}{2} < p \leq 1 \end{cases} \quad (2.7.3.1)$$

where $a(n) \simeq b(n)$ if $\frac{a(n)}{b(n)}$ tends to a finite, non-zero constant when $n \rightarrow \infty$.

This Theorem follows directly from the combination of our suitable Lemmas, namely Proposition 2.7.6 and Corollary 2.7.6 appearing later on. In fact, our results are more precise than what is stated in the Theorem above (we describe the first two orders in a series expansion for large n , including formulas for the associated multiplicative constants), details are given in the forementioned propositions.

The average cost of Dyck matchings provides an upper bound on the average cost of the optimal solution; numerical simulations for the PPP measure, described in Section 2.7.8, suggest the following conjecture, that we leave for future investigations:

Conjecture 1. *For the three measures ES, US and PPP, and all $0 < p < 1$,*

$$\lim_{n \rightarrow \infty} \frac{\mathbb{E}_n(H_{\text{opt}})}{\mathbb{E}_n(H_{\text{Dyck}})} = k_p, \quad (2.7.3.2)$$

with $0 < k_p < 1$.

2.7.4. Basic facts

Before starting our main proof, let us introduce some more notations, and recall some basic properties of the optimal solution for convenience.

2.7.5. Basic properties of the optimal matching

A *Dyck path of semi-length n* is a lattice path from $(0, 0)$ to $(2n, 0)$ consisting of n ‘up’ steps (i.e. steps of the form $(1, 1)$) and n ‘down’ steps (i.e., steps $(1, -1)$), which never goes below the x -axis. There are C_n Dyck path of semi-length n , where

$$C_n = \binom{2n}{n} - \binom{2n}{n+1} = \frac{1}{n+1} \binom{2n}{n} \quad (2.7.5.1)$$

are the *Catalan numbers*. Therefore the generating function for the Dyck paths is

$$C(z) := \sum_{k \geq 0} C_k z^k = \frac{1 - \sqrt{1 - 4z}}{2z} = \frac{2}{1 + \sqrt{1 - 4z}} \quad (2.7.5.2)$$

The historical name ‘Dyck path’ is somewhat misleading, as it leaves us with no natural name for the most obvious notion, that is, the walks of length n with steps in $\{(1, 1), (1, -1)\}$. With analogy with the theory of Brownian motion (which relates to lattice walks via the Donsker’s theorem) ([160](#)), we will define four types of paths, namely walks, meanders, bridges and excursions, according to the following table:

	$y(2n) = 0$	$y(x) \geq 0 \forall x$
walk	no	no
meander	no	yes
bridge	yes	no
excursion	yes	yes

(of course, by “no” we mean “not necessarily”). Thus, in fact, the “paths” are the most constrained family of walks, that is the excursions.

In general a Dyck path (i.e., a Dyck excursion) can touch the x -axis several times. We shall call an *irreducible Dyck excursion* a Dyck path which touches the x -axis only at the two endpoints. It is trivially seen that the generating function for the irreducible Dyck excursions is simply $zC(z)$. As we said above a *Dyck bridge* is a walk made with the same kind of steps of Dyck paths, but without the restriction of remaining in the upper half-plane, and which returns to the x -axis. The generating function for the Dyck bridges is

$$B(z) := \frac{1}{1 - 2zC(z)} = \frac{1}{\sqrt{1 - 4z}} = \sum_{k \geq 0} B_k z^k \quad (2.7.5.3)$$

with B_k the central binomials ([2.7.2.1](#)), and k is the semi-length of the bridge (just like excursions, all Dyck bridges must have even length). The factor 2 in the functional form of $B(z)$ in terms of $C(z)$ enters because a bridge is a concatenation of irreducible excursions, each of which can be in the upper- or the lower-half-plane.

Now, it is clear that each configuration σ corresponds uniquely to a Dyck bridge of semi-length n , with $\sigma_i = +1$ or -1 if the i -th step of the walk is an up or down step, respectively.

In a Dyck walk we shall call $(k_{\text{blue}}(i), h_{\text{blue}}(i))$ the two coordinates of the mid-point of the i -th ascending step of the walk (minus $(\frac{1}{2}, \frac{1}{2})$, in order to have integer coordinates and enlighten the notation), and call $(k_{\text{red}}(i), h_{\text{red}}(i))$ the coordinates of the mid-point of the i -th descending step (again, minus $(\frac{1}{2}, \frac{1}{2})$). For $e = (i, j)$ an edge of a matching π , call $\|e\| = k_{\text{blue}}(i) - k_{\text{red}}(j)$ the horizontal distance on the walk, and $|e| = |b_i - r_j|$ the Euclidean distance on the domain segment.

For a given Dyck bridge σ , we say that $\pi \in \mathcal{S}_n$ is *non-crossing* if, for every pair of distinct edges $e_1 = (i_1, j_1)$ and $e_2 = (i_2, j_2)$ in π , we do not have the pattern $k_{\text{blue}}(i_1) < k_{\text{blue}}(i_2) < k_{\text{red}}(j_1) < k_{\text{red}}(j_2)$, or the analogous patterns with $k_{\text{blue}}(i_1) \leftrightarrow k_{\text{red}}(j_1)$, or $k_{\text{blue}}(i_2) \leftrightarrow k_{\text{red}}(j_2)$, or $(\cdot)_1 \leftrightarrow (\cdot)_2$ (recall Lemma 2.1.4, see also bottom part of Figure 2.14). Note that the notion of π being non-crossing only uses the vector σ .

For a given Dyck bridge σ , we say that $\pi \in \mathcal{S}_n$ is *sliced* if, for every edge $e = (i, j) \in \pi$, we have $h_{\text{blue}}(i) = h_{\text{red}}(j)$.

Two easy Lemmas have a crucial role in our analysis.

Lemma 2.7.2. *All the optimal matchings are non-crossing.*

Proof. (This is Lemma 2.1.4. However, the proof appears to be new and for this reason we report it here.) The proof is by absurd. Suppose that π is a crossing optimal matching. If we have a pattern as $k_{\text{B}}(i_1) < k_{\text{red}}(j_2) < k_{\text{red}}(j_1) < k_{\text{B}}(i_2)$, then the matching π' with edges $e'_1 = (i_1, j_2)$ and $e'_2 = (i_2, j_1)$ has $H_J(\pi') < H_J(\pi)$, because $|e'_1| < |e_1|$ and $|e'_2| < |e_2|$.

If we have a pattern as $k_{\text{B}}(i_1) < k_{\text{B}}(i_2) < k_{\text{red}}(j_1) < k_{\text{red}}(j_2)$, then again the matching π' with edges $e'_1 = (i_1, j_2)$ and $e'_2 = (i_2, j_1)$ has $H_J(\pi') < H_J(\pi)$, although this holds for a more subtle reason. Calling $a = x_2 - x_1$, $b = y_1 - x_2$ and $c = y_2 - y_1$, we have $|e_1| = a + b$, $|e_2| = b + c$, $|e'_1| = a + b + c$ and $|e'_2| = b$. It is the case that, for $a, b, c > 0$ and $0 < p < 1$,

$$(a + b)^p + (b + c)^p > (a + b + c)^p + b^p. \quad (2.7.5.4)$$

A proof of this inequality goes as follows. Call $F(a, b, c) = (a + b)^p + (b + c)^p - (a + b + c)^p - b^p$. We have $F(a, b, 0) = 0$, and

$$\frac{1}{p} \frac{\partial}{\partial c} F(a, b, c) = \frac{1}{(b + c)^{1-p}} - \frac{1}{(a + b + c)^{1-p}} > 0. \quad (2.7.5.5)$$

All the other possible crossing patterns are in the first or the second of the forms discussed above, up to trivial symmetries. \square

The second Lemma states that a necessary condition for an optimal matching to be optimal is to be sliced.

Lemma 2.7.3. *All the optimal matchings are sliced.*

Proof. The proof is by absurd. Suppose that π is a non-sliced optimal matching. If we have $(i, j) \in \pi$ with $h_{\text{blue}}(i) \neq h_{\text{red}}(j)$, say $h_{\text{blue}}(i) - h_{\text{red}}(j) = \delta h \neq 0$, we have that the point x_i is matched to y_j , and that, between x_i and y_j , there are n_{blue} and n_{red} blue and red points, respectively, with $n_{\text{blue}} - n_{\text{red}} = -\delta h \neq 0$. So there must be at least $|\delta h|$ points inside the interval (x_i, y_j) which are matched to points outside this interval, and thus, together with (i, j) , constitute pairs of crossing edges. So, by Lemma 2.7.2, π cannot be optimal. \square

The slicing of optimal assignments was studied in (134).

2.7.6. Reduction of the PPP model to the ES model

Theorem 2.7.1 (and, hopefully, Conjecture 1), in principle, shall be proven for three different models, Uniform Spacings (US), Exponential Spacings (ES) and the Poisson Point Process (PPP). However, as we anticipated, the PPP case is a minor variant of ES. In this Section we give a precise account of this fact.

The starting point is a relation between the two measures:

Remark 2.7.1. We can sample a pair $[\vec{s}', \sigma]$ with the measure μ_n^{ES} by sampling a pair $[\vec{s}, \sigma]$ with the measure μ_n^{PPP} , a value $L \in \mathbb{R}^+$ with the measure $g_{2n+1}(L) = \frac{L^{2n}}{(2n)!} \exp(-L) dL$, and then defining $s'_i = s_i \frac{L}{2n+1}$.

Indeed, the measure on \vec{s} in the PPP can be seen as the measure over independent exponential variables conditioned to the value of the sum; thus, the procedure leads at sight to a measure over \vec{s}' which is unbiased within vectors \vec{s}' with the same value of $L = \sum_i s'_i$. Then, from the independence of the spacings in the ES model we easily conclude that the distribution of L must be exactly $g_1^{*(2n+1)}(L)$, i.e. the convolution of $2n + 1$ exponential distributions.

More precisely, for k an integer, define the Gamma measure

$$g_k(x) := \frac{x^{k-1}}{\Gamma(k)} e^{-x} = g_1^{*k}(x). \quad (2.7.6.1)$$

We use the same notation for its analytic continuation to k real positive.

We introduce (the analytic continuation of) the rising factorial (following a notation due to Knuth (55)):

$$n^{\bar{p}} := \frac{\Gamma(n+p)}{\Gamma(n)} = \int dx g_n(x) x^p. \quad (2.7.6.2)$$

This choice of notation is motivated by the fact that $n^{\bar{1}} = n^1 = n$, and that, for $n \gg p^2$, $n^{\bar{p}} = n^p(1 + \mathcal{O}(p^2/n))$. More precisely we have:

Lemma 2.7.4. *For $0 \leq p \leq 1$ and $n > 1$*

$$(n + p - 1)^p \leq n^{\bar{p}} \leq n^p. \quad (2.7.6.3)$$

Proof. It is well known that the Gamma function is logarithmically convex (147). In particular, for any $0 \leq p \leq 1$,

$$\ln \Gamma(n + p) \leq (1 - p) \ln \Gamma(n) + p \ln \Gamma(n + 1) = \ln \Gamma(n) + p \ln n, \quad (2.7.6.4)$$

that is

$$n^{\bar{p}} = \exp(\ln \Gamma(n + p) - \ln \Gamma(n)) \leq \exp(p \ln n) = n^p. \quad (2.7.6.5)$$

Analogously, we have

$$\ln \Gamma(n) \leq (1 - p) \ln \Gamma(n + p) + p \ln \Gamma(n + p - 1) = \ln \Gamma(n + p) - p \ln(n + p - 1), \quad (2.7.6.6)$$

that is

$$n^{\bar{p}} = \exp(\ln \Gamma(n + p) - \ln \Gamma(n)) \geq \exp(p \ln(n + p - 1)) = (n + p - 1)^p. \quad (2.7.6.7)$$

□

See (139) for a recent review of inequalities involving $n^{\bar{p}}$. Summing up, Remark 2.7.1 and Lemma 2.7.4 allow to prove that:

Lemma 2.7.5. *The following inequalities hold:*

$$\left(\frac{2n}{2n + 1} \right)^{p(1-p)} \mathbb{E}(H_{\text{opt}}^{\text{ES}}) \leq \mathbb{E}(H_{\text{opt}}^{\text{PPP}}) \leq \mathbb{E}(H_{\text{opt}}^{\text{ES}}). \quad (2.7.6.8)$$

Also the corresponding inequalities with H_{opt} replaced by H_{Dyck} do hold, as well as for any other quantity $H(\pi^(J))$, whenever π^* is some matching determined by the instance, and invariant under scaling of the instance, that is $\pi^*[\vec{s}, \sigma] = \pi^*[\lambda \vec{s}, \sigma]$.*

Proof. For compactness of notation, we do the proof only for the H_{opt} case, but the generalisation is straightforward. Of course, $H_{[\lambda \vec{s}, \sigma]}(\pi) = \lambda^p H_{[\vec{s}, \sigma]}(\pi)$ for all instances $[\vec{s}, \sigma]$, all configurations π , and all scaling factors $\lambda > 0$ (so as $\pi^*[\vec{s}, \sigma] = \pi^*[\lambda \vec{s}, \sigma]$, it follows that $H_{[\lambda \vec{s}, \sigma]}(\pi^*[\lambda \vec{s}, \sigma]) = \lambda^p H_{[\vec{s}, \sigma]}(\pi^*[\vec{s}, \sigma])$). In particular, $H_{\text{opt}}([\lambda \vec{s}, \sigma]) = \lambda^p H_{\text{opt}}([\vec{s}, \sigma])$. In light of Remark 2.7.1, we can describe the average over $\mu_{\text{ES}}[\vec{s}, \sigma]$ in terms of an average over $\mu_{\text{PPP}}[\vec{s}, \sigma]$, and over

$g_{2n+1}(L)$. More precisely

$$\begin{aligned}
\mathbb{E}(H_{\text{opt}}^{\text{ES}}) &= \int d\mu_{\text{ES}}[\vec{s}', \sigma] H_{\text{opt}}([\vec{s}', \sigma]) \\
&= \int d\mu_{\text{PPP}}[\vec{s}, \sigma] \int dL g_{2n+1}(L) \left(\frac{L}{2n+1}\right)^p H_{\text{opt}}([\vec{s}, \sigma]) \\
&= \mathbb{E}(H_{\text{opt}}^{\text{PPP}}) \int dL g_{2n+1}(L) \left(\frac{L}{2n+1}\right)^p \\
&= \mathbb{E}(H_{\text{opt}}^{\text{PPP}}) \frac{(2n+1)^{\bar{p}}}{(2n+1)^p}.
\end{aligned} \tag{2.7.6.9}$$

The upper bound follows directly from Lemma 2.7.4. The lower bound follows as:

$$\frac{(2n+1)^{\bar{p}}}{(2n+1)^p} \geq \left(1 - \frac{1-p}{2n+1}\right)^p \geq \left(1 - \frac{1}{2n+1}\right)^{p(1-p)} \tag{2.7.6.10}$$

where first one uses Lemma 2.7.4, then the inequality $(1 - q\epsilon)^p \geq (1 - \epsilon)^{pq}$ (valid for $\epsilon, p, q \in [0, 1]$), with $\epsilon = \frac{1}{2n+1}$ and $q = 1 - p$. \square

In light of this Lemma, it is sufficient to consider Theorem 2.7.1 (and Conjecture 1) only for the US and ES models.

The precise statement of our conclusions is the following:

Corollary.

$$\mathbb{E}_n^{\text{PPP}}(H_{\text{Dyck}}) = \mathbb{E}_n^{\text{ES}}(H_{\text{Dyck}}) (1 + \mathcal{O}(n^{-1})). \tag{2.7.6.11}$$

The relevance of this statement lies in the fact that, in the forthcoming equation (2.7.7.1), we provide an expansion for $\mathbb{E}_n^{\text{ES}}(H_{\text{Dyck}})$ in which corrections of relative order $1/n$ appear as the third term in the expansion (and we provide explicit results only for the first two terms). As a result, the very same conclusions that we have for the ES model do apply verbatim to the PPP model.

2.7.7. The Dyck matching

For every instance $[\vec{s}, \sigma]$, there is a special matching, that we call π_{Dyck} , which is sliced and non-crossing for σ . This is the matching obtained by the canonical pairing of up- and down-steps within every excursion of the Dyck bridge (see Figure 2.14 for an example). In analogy with our notation $H_{\text{opt}}(J) = H_J(\pi_{\text{opt}})$, let us introduce the shortcut $H_{\text{Dyck}}(J) = H_J(\pi_{\text{Dyck}})$.

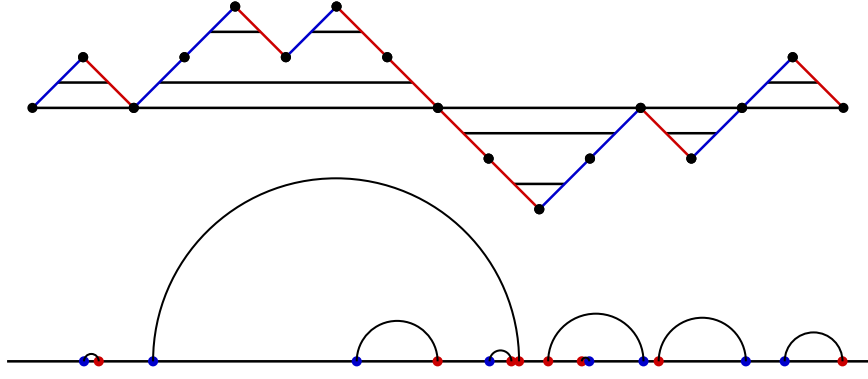


Figure 2.14. – The Dyck matching π_{Dyck} associated to the Dyck bridge σ in the example of Figure 2.13.

Remark 2.7.2. The Dyck matching π_{Dyck} is determined by the order of the colours of the points, σ . In particular it does not depend on the actual spacings between them, \vec{s} , and it does not depend on the cost exponent p .

Remark 2.7.2 is a crucial fact that makes possible the evaluation of the statistical properties of π_{Dyck} , with a moderate effort. In particular, it will lead to the main result:

Proposition 2.7.6. For all independent spacing models

$$\mathbb{E}_n(H_{\text{Dyck}}) \sim \begin{cases} \frac{A_p}{2}n + \frac{2^p\Gamma(p-\frac{1}{2})}{4\Gamma(p+1)}n^{\frac{1}{2}+p} + \mathcal{O}(1) & p < \frac{1}{2} \\ \frac{1}{\sqrt{2\pi}}n \log n + \left(\frac{A_*}{2} + A'_*\right)n + \mathcal{O}(\log n) & p = \frac{1}{2} \\ \frac{2^p\Gamma(p-\frac{1}{2})}{4\Gamma(p+1)}n^{\frac{1}{2}+p} + \frac{A_p}{2}n + \mathcal{O}(n^{-\frac{1}{2}+p}) & p > \frac{1}{2} \end{cases}. \quad (2.7.7.1)$$

where A_p and A_* are model-dependent quantities, which are not larger than

$$A_p^{\max} := \frac{2^{p+1}}{(1-2p)\Gamma(1-p)}, \quad A_*^{\max} = \sqrt{\frac{2}{\pi}}(\log 2 + \gamma_E). \quad (2.7.7.2)$$

and

$$A'_* = \frac{\gamma_E + 2 \log 2 - 2}{\sqrt{2\pi}}. \quad (2.7.7.3)$$

In particular, for the ES model

$$A_p^{\text{ES}} = \frac{\Gamma(\frac{1}{2}-p)\Gamma(p+1)}{2^{p-1}\sqrt{\pi}\Gamma(2-p)}, \quad A_*^{\text{ES}} = \sqrt{\frac{2}{\pi}}(5 \log 2 + \gamma_E - 4). \quad (2.7.7.4)$$

The remaining of this Section is devoted to the proof of this Proposition. First, we factorize the average over the instance $J = [\vec{s}, \sigma]$ in two independent averages,

the average over σ and the one over \vec{s} (see Definition 2.7.1):

$$\begin{aligned}\mathbb{E}_n(H_{\text{Dyck}}) &= \mathbb{E} \left(\sum_{i=1}^n J_{i, \pi_{\text{Dyck}}(i)} \right) = \overline{\sum_{i=1}^n \langle J_{i, \pi_{\text{Dyck}}(i)} \rangle} \\ &= B_n^{-1} \sum_{\sigma} \sum_{i=1}^n \langle |k_{\text{B}}(i) - k_{\text{red}}(\pi_{\text{Dyck}}^{\sigma}(i))|^p \rangle ,\end{aligned}\tag{2.7.7.5}$$

where in the last line we emphasize that π_{Dyck} depends only on σ , as stated in Remark 2.7.2, and we adopted again the shortcut $B_n = \binom{2n}{n}$ for the total number of configurations σ .

Due to the fact that the spacings s_i are independent, the quantity appearing above, $\langle |k_{\text{B}}(i) - k_{\text{red}}(\pi_{\text{Dyck}}^{\sigma}(i))|^p \rangle$, only depends on the length $\|e\| = 2k + 1$ of the corresponding link $e = (i, \pi_{\text{Dyck}}(i))$, via the formula

$$S_k^{(p)} := \langle |k_{\text{B}}(i) - k_{\text{red}}(\pi_{\text{Dyck}}^{\sigma}(i))|^p \rangle = \left\langle \left(\sum_{j=0}^{2k} s_j \right)^p \right\rangle ,\tag{2.7.7.6}$$

where the s_j 's are i.i.d. variables sampled with the distribution $\rho(s)$ (that is, in the ES model, i.i.d. exponential random variables).

Then, as a general paradigm for observables of the form $\overline{\sum_{e \in \pi} \langle F(|e|) \rangle}$, we rewrite the sum over all possible σ and over all links e of a given matching $\pi = \pi_{\text{Dyck}}(\sigma)$ as a sum over the forementioned parameter k , with a suitable combinatorial factor $v_{n,k}$:

$$\overline{\sum_{e \in \pi} \langle F(|e|) \rangle} = B_n^{-1} \sum_{k=0}^{n-1} v_{n,k} \left\langle F \left(\sum_{j=0}^{2k} s_j \right) \right\rangle\tag{2.7.7.7}$$

$$v_{n,k} = \sum_{\sigma} \sum_{e \in \pi_{\text{Dyck}}(\sigma)} \delta_{\|e\|, 2k+1} .\tag{2.7.7.8}$$

(note that $\sum_k v_{n,k} = nB_n = 2 \binom{2n-1}{n}$). In particular, in our case,

$$\mathbb{E}_n(H_{\text{Dyck}}) = B_n^{-1} \sum_{k=0}^{n-1} v_{n,k} S_k^{(p)} .\tag{2.7.7.9}$$

So we face two separate problems: (1) determining the combinatorial coefficients $v_{n,k}$, which are “universal” (i.e., the same for all independent-spacing models, for all cost exponents p and for all observables F as above); (2) determining the quantities $S_k^{(p)}$, that is, the average over the Euclidean length $|e|$ of the link (which depends from the function $f(s)$ that defines the independent-spacing model, and from the

exponent p).

For what concerns $S_k^{(p)}$, this can be computed exactly both in the US and ES cases: in the US case $S_k^{(p)} = (2k+1)^p$, as in fact $|e| = 2k+1 = \|e\|$ deterministically, while in the ES case $S_k^{(p)} = \Gamma(2k+1+p)/\Gamma(2k+1)$. More generally, for any model with independent spacings we would have that $S_k^{(p)} = \int dx x^p f^{*2k+1}(x)$ that is, the sum of $2k+1$ i.i.d. random variables is distributed as the $(2k+1)$ -fold convolution of the single-variable probability distribution. For the ES case this is exactly the Gamma distribution $g_{2k+1}(s)$. Up to this point, we could have also evaluated the analogous quantity for the PPP model, although with a bigger effort (but, from Section 2.7.6, we know that this is not necessary).

For what concerns $v_{n,k}$, in Appendix A.1 we prove that

$$v_{n,k} = C_k \left[4^{n-k-1} + \frac{n-k}{2} B_{n-k} \right] =: C_k V_{n-k-1}. \quad (2.7.7.10)$$

In particular, the simple expression for V_{n-k-1} gives in a straightforward way

$$V(z) := \sum_{j=0}^{\infty} V_j z^j = (1-4z)^{-1} + (1-4z)^{-\frac{3}{2}}. \quad (2.7.7.11)$$

We pause to study the distribution of the lengths $\|e\|$ of links in π_{Dyck} , that is, the normalised distribution (in k), with parameter n , given by the expression $v_{n,k}/(nB_n)$. It is known that planar secondary structures have a universal behaviour for the tail of such a distribution, with exponent $-\frac{3}{2}$. Indeed, by performing a large n expansion at fixed k , and then studying the large k behaviour, one has

$$\begin{aligned} \frac{v_{n,k}}{nB_n} &= \frac{C_k}{nB_n} \left[4^{n-k-1} + \frac{n-k}{2} B_{n-k} \right] \\ &\stackrel{n \rightarrow \infty}{\approx} 2 C_k 4^{-k} \stackrel{k \rightarrow \infty}{\approx} \sqrt{\frac{2}{\pi}} k^{-\frac{3}{2}}, \end{aligned} \quad (2.7.7.12)$$

reproducing the known behaviour.

Equation (2.7.7.9), with the help of (2.7.7.10) and (2.7.7.11), can be used to relate the generating functions

$$E(z; p) := \sum_{n=0}^{\infty} B_n \mathbb{E}_n(H_{\text{Dyck}}) z^n \quad (2.7.7.13)$$

$$S(z; p) := \sum_{k=0}^{\infty} C_k S_k^{(p)} z^k. \quad (2.7.7.14)$$

Lemma 2.7.7.

$$E(z; p) = z V(z) S(z; p) \quad (2.7.7.15)$$

Proof.

$$\begin{aligned} E(z; p) &:= \sum_{n=0}^{\infty} B_n \mathbb{E}_n(H_{\text{Dyck}}) z^n \\ &= \sum_{n=0}^{\infty} \sum_{k=0}^{n-1} C_k V_{n-k-1} S_k^{(p)} z^n \\ &= \left(\sum_{k=0}^{\infty} C_k S_k^{(p)} z^k \right) \left(\sum_{n=k+1}^{\infty} V_{n-k-1} z^{n-k} \right) \\ &= z V(z) S(z; p). \end{aligned} \quad (2.7.7.16)$$

□

The behaviour at large k of $S_k^{(p)}$ is determined by the theory of large deviations. Said heuristically, the sum of the $2k + 1$ i.i.d. variables s_i concentrates on $2k + 1$, with tails which are sufficiently tamed that the average of x^p is equal to $(2k + 1)^p(1 + \mathcal{O}(k^{-1}))$. That is, $S_k^{(p)} \sim (2k + 1)^p \sim 2^p k^p$, and we have

$$C_k S_k^{(p)} \sim \frac{2^p}{\sqrt{\pi}} 4^k k^{p-\frac{3}{2}}. \quad (2.7.7.17)$$

We recall a fundamental fact in the theory of generating functions: the singularities of a generating function determine the asymptotic behaviour of its coefficients. In particular, the modulus of the dominant singularity (that nearest to the origin) determines the exponential behaviour, and the nature of the singularity determines the subexponential behaviour (see (123), Ch. 6 for a comprehensive treatment of singularity analysis, and Appendix A.2 for a short summary of results). This tells us that we just need an expression for $E(z; p)$ around its dominant singularity to extract asymptotic information on the total cost, i.e. we just need to evaluate $S(z; p)$ locally around the dominant singularity of $E(z; p)$.

First of all, one needs to locate the dominant singularity of $S(z; p)$ and compare it with the $z = \frac{1}{4}$ singularity of $V(z)$. From Equation 2.7.7.17, we find an exponential behaviour $\sim 4^n$ of the coefficient of $S(z; p)$, trivially due to the entropy of Dyck walks of length $2n$, thus, the singularity must be in $z = \frac{1}{4}$. Notice that this agrees with the dominant singularity of $V(z)$ (which also is, essentially, a generating function of Dyck walks up to algebraic corrections), so that both generating functions will combine to give the final average-cost asymptotics.

At the dominant singularity, the power-law behaviour of the coefficients is given

by a generating function of the kind

$$S(z; p) = A_p + B_p(1 - 4z)^{g_p} + o((1 - 4z)^{g_p}), \quad (2.7.7.18)$$

where A_p encodes the regular terms at the singularity, and $o((1 - 4z)^{g_p})$ accounts for all other singular terms leading to non trivial subleading corrections (among them one finds power, logarithms... in the variable $1 - 4z$).

In fact, in such a simple situation as in our case, we expect a more precise behaviour, $S(z; p) = A_p(1 + \mathcal{O}(1 - 4z)) + B_p(1 - 4z)^{g_p}(1 + \mathcal{O}(1 - 4z))$, where we have two series of corrections, in integer powers, associated to the regular and singular parts of the expansion around the singularity (up to the special treatment of the degenerate case $g_p \in \mathbb{Z}$).

Notice that B_p and g_p can be found by computing the asymptotic behaviour of the coefficients of Equation 2.7.7.18

$$S_k^{(p)} \sim \frac{B_p}{\Gamma(-g_p)} 4^k k^{-g_p-1} = \frac{2^p}{\sqrt{\pi}} 4^k k^{p-\frac{3}{2}}, \quad (2.7.7.19)$$

giving, by comparison with Equation 2.7.7.17,

$$g_p = \frac{1}{2} - p \quad B_p = \frac{2^p \Gamma(p - \frac{1}{2})}{\sqrt{\pi}}. \quad (2.7.7.20)$$

Nothing can be said on the coefficient A_p without performing the exact resummation of the generating function at the singularity (possibly, after having subtracted a suitable diverging part).

This analysis results in an asymptotic expression for $E(z; p)$:

$$E(z; p) \sim \frac{1}{4} \left[A_p (1 - 4z)^{-\frac{3}{2}} + \frac{2^p \Gamma(p - \frac{1}{2})}{\sqrt{\pi}} (1 - 4z)^{-(1+p)} \right] \quad (2.7.7.21)$$

for $p \neq \frac{1}{2}$, and

$$\begin{aligned} E(z; p = \frac{1}{2}) &= \frac{1}{4} (1 - 4z)^{-\frac{3}{2}} \left[A_{\frac{1}{2}+\epsilon} + \frac{1}{\epsilon} \sqrt{\frac{2}{\pi}} + \sqrt{\frac{2}{\pi}} \log\left(\frac{1}{1-4z}\right) + o(\epsilon) \right] \\ &= \frac{1}{4} (1 - 4z)^{-\frac{3}{2}} \left[A^* + \sqrt{\frac{2}{\pi}} \log\left(\frac{1}{1-4z}\right) \right] \end{aligned} \quad (2.7.7.22)$$

for $p = \frac{1}{2}$, where $\epsilon = p - \frac{1}{2}$. The hypothesis of $S(z; p)$ being non-singular in p

implies that A_p must cancel the $\frac{1}{\epsilon}$ singularity, leaving a regular part

$$A_* = \lim_{\epsilon \rightarrow 0} \left[A_{\frac{1}{2}+\epsilon} + \frac{1}{\epsilon} \sqrt{\frac{2}{\pi}} \right]. \quad (2.7.7.23)$$

This set of results has remarkable consequences, as it unveils a certain universality feature for $E(z; p)$. In fact, for all models in our large classes, the nature of the dominant singularity of $E(z; p)$ is the same, giving a universal asymptotic scaling in n for the average cost of Dyck matchings. Moreover, in the $p \geq \frac{1}{2}$ regime, also the coefficient of the dominant singularity is universal.

We can now expand the generating function using standard techniques (Appendix A.2, (123)) and the fact that $B_n \sim \frac{4^n}{\sqrt{\pi n}}$, obtaining

$$\mathbb{E}_n \sim \begin{cases} \frac{A_p}{2} n + o(n) & p < \frac{1}{2} \\ \frac{1}{\sqrt{2\pi}} n \log n + o(n \log n) & p = \frac{1}{2} \\ \frac{2^p \Gamma(p-\frac{1}{2})}{4\Gamma(p+1)} n^{\frac{1}{2}+p} + o(n^{\frac{1}{2}+p}) & p > \frac{1}{2} \end{cases}. \quad (2.7.7.24)$$

and in fact, more precisely,

$$\mathbb{E}_n \sim \begin{cases} \frac{A_p}{2} n + \frac{2^p \Gamma(p-\frac{1}{2})}{4\Gamma(p+1)} n^{\frac{1}{2}+p} + \mathcal{O}(1) & p < \frac{1}{2} \\ \frac{1}{\sqrt{2\pi}} n \log n + \left(\frac{A_*}{2} + A'_* \right) n + \mathcal{O}(\log n) & p = \frac{1}{2} \\ \frac{2^p \Gamma(p-\frac{1}{2})}{4\Gamma(p+1)} n^{\frac{1}{2}+p} + \frac{A_p}{2} n + \mathcal{O}(n^{-\frac{1}{2}+p}) & p > \frac{1}{2} \end{cases}. \quad (2.7.7.25)$$

where the terms of the expansion are just the same for the $p < \frac{1}{2}$ and $p > \frac{1}{2}$ cases, but have been arranged differently, in the order of dominant behaviour. The quantity A_* has been defined in (2.7.7.23), for the behaviour of $S(z; \frac{1}{2})$, while the quantity

$$A'_* = \frac{\gamma_E + 2 \log 2 - 2}{\sqrt{2\pi}} \quad (2.7.7.26)$$

is a further (universal) correction coming from taking into account how $S(z; \frac{1}{2})$ enters in $E(z; \frac{1}{2})$, via $V(z)$ (and γ_E is the Euler–Mascheroni constant).

The formulas above gives the precise asymptotics, up to relative corrections of the order n^{-1} . As a corollary, we have this very same behaviour in the PPP model, as, from Lemma 2.7.5 and Corollary 2.7.6, we know that also the relative corrections between ES and PPP models are of the order n^{-1} .

For higher-order corrections, one would need to take into account more subleading terms in Equation 2.7.7.18.

For the ES case the resummation of $E(z; p)$ can be performed analytically by

writing the Catalan number in terms of Gamma functions, namely

$$C_k = \frac{4^k \Gamma(k + \frac{1}{2})}{\sqrt{\pi} \Gamma(k + 2)}. \quad (2.7.7.27)$$

giving

$$S(z; p) = \Gamma(p + 1) F\left(\frac{p+1}{2}, \frac{p+2}{2} \mid 4z\right) \quad (2.7.7.28)$$

where F is the ${}_2F_1$ hypergeometric function (a reminder is in Appendix A.2, equation (A.2.0.5)). This allows for an explicit computation of the two non-universal quantities in our expansion:

$$A_p^{\text{ES}} = \frac{\Gamma(\frac{1}{2} - p) \Gamma(p + 1)}{2^{p-1} \sqrt{\pi} \Gamma(2 - p)} \quad A_*^{\text{ES}} = \sqrt{\frac{2}{\pi}} (5 \log 2 + \gamma_E - 4). \quad (2.7.7.29)$$

note how the A_* and A'_* terms involve combinations of quantities of the same algebraic nature. See Appendix A.2 for the details of the derivation.

Similar but more complex resummations seem possible in the independent spacing case, when the function $f(x)$ is a Gamma distribution, $f(x) = ag_a(ax)$ for $a \in \mathbb{N}/2$, and $S(z; p)$ is obtained in terms of generalised hypergeometric functions ${}_{k+1}F_k$. However no exact resummation seems possible for the US case (which would require a limit $a \rightarrow \infty$ in this procedure).

2.7.8. Numerical results and the average cost of the optimal matching

Our main results concern the leading behaviour of the average cost of the Dyck matching, which, of course, provides an upper bound to the average cost of the optimal matching. The explicit investigation of small-size instances suggests that the optimal matching is often quite similar to the Dyck matching, in the sense that the symmetric difference between π_{opt} and π_{Dyck} typically consists of “few” cycles, which are “compact”, in some sense. Thus, a natural question arises: could it be that the large- n average properties of optimal matchings and Dyck matchings are the same? If not, in which respect do they differ? In order to try to answer this question, we have performed numerical simulations by generating random instances with measure μ_n^{PPP} , and we have computed the average cost associated to the optimal and to the Dyck matching.

Figure 2.15 gives a comparison between the two average costs by plotting their ratio as a function of n for various values of p . The corresponding fits seem to

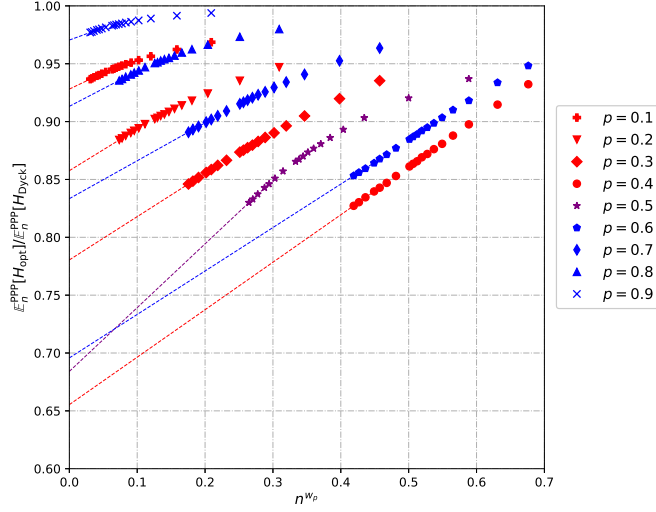


Figure 2.15. – Ratio of the average cost of optimal matchings over that of Dyck matchings as a function of n^{w_p} , where $w_p = -|p - \frac{1}{2}|$. For $p = \frac{1}{2}$, the ratio is plotted against $1/\log_{10} n$. Dashed lines are linear extrapolations for $n^{w_p} \rightarrow 0$. The number of simulated instances at each value of (p, n) is 10000, whenever $n \leq 4000$, and 5000, whenever $n = 5000$ or 6000.

exclude the possibility that the limit for large n of the ratio of average costs go to zero algebraically in n (and also makes it reasonable that there are no logarithmic factors, although this is less evident), that is, these data support the content of Conjecture 1.

In order to further test this hypothesis, we fitted the optimal average cost to the same scaling behaviour found for the Dyck matching average cost, i.e.

$$\begin{cases} a_p n + b_p n^{\frac{1}{2}+p} & p \neq \frac{1}{2} \\ c n (\log n + d) & p = \frac{1}{2} \end{cases} \quad (2.7.8.1)$$

fixing the scaling exponents and aiming to compute the scaling coefficients. Notice that the term $a_p n$ is leading for $0 < p < \frac{1}{2}$, while $b_p n^{\frac{1}{2}+p}$ is leading for $\frac{1}{2} < p < 1$. Figure 2.16 summarizes the fitted parameters.

For the Dyck matching, the fitted parameter for the leading scaling coefficient agrees perfectly with the computed coefficient, as expected. The coefficient of the subleading term seems to agree with the computed coefficient in a less precise way, probably due to stronger higher-order corrections. For the optimal matching, the fitted coefficients behave qualitatively as the coefficients that we have computed for the Dyck case, but the agreement is visibly not quantitative. The fit seems to

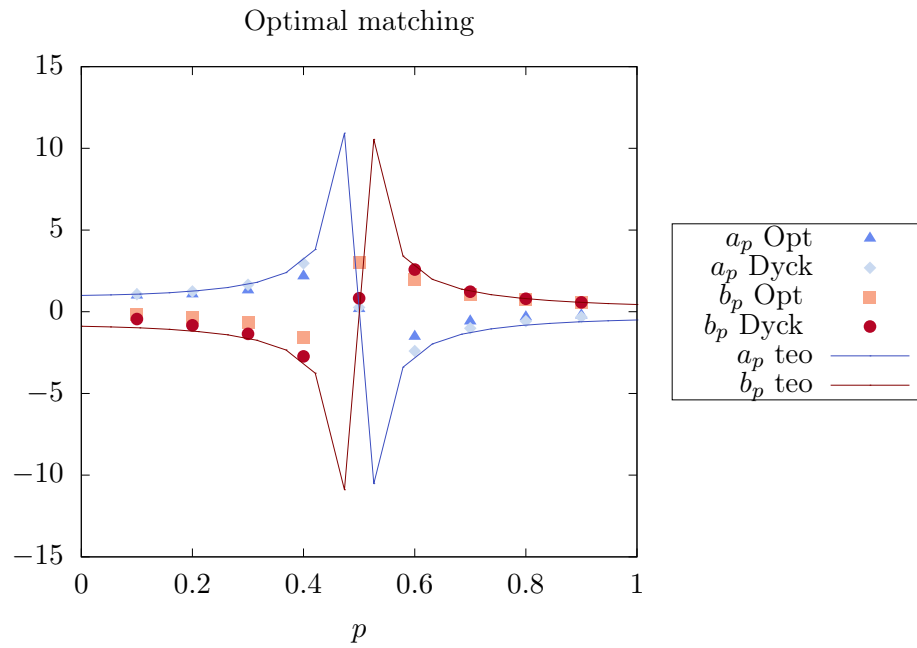


Figure 2.16. – *Fitted scaling coefficients as a function of p .*

confirm the hypothesis that the two average costs have the same scaling exponents with different coefficients.

To completely confirm such hypothesis, we suggest that lower bounds for the cost could be computed. We expect such lower bounds to share the same scaling as that found in this paper, but with different constants. We leave such matter open for future work.

2.8. Chapter provisional conclusions and research perspectives

IN this Chapter we have investigated the one dimensional Euclidean Random Assignment Problem. After reviewing the state of the art, we have presented some new results concerning both the convex and concave regime. For the sake of clarity, let us split our concluding remarks, provisional conclusions and perspectives in two paragraphs according to the involved regimes.

2.8.1. Convex regime

In the case $p = 2$ several variants of the problem can be studied in much detail essentially due to Fourier Duality. Here, we have focused on the statistical properties of the optimal transport field in both the Poisson-Poisson and Grid-Poisson problem, both in the continuum and in the discrete setting. In particular, in the case of the Poisson-Poisson problem on the unit circle, we have shown that, in the continuum, the full ground state energy distribution is given explicitly as an elliptic ϑ_4 function, a calculation comforted by the results of numerical experiments already for moderately small values of n .

Then, we have considered the case $p \geq 1$ for a general probability distribution (not necessarily finitely supported) of blue and red points. In such a case we have studied the occurrence of an anomalous scaling with respect to the bulk behavior (the one fixed by the well-known brownian bridge qualitative picture) for a number of exemplifying choices of the probability density function.

In particular in § 2.5 we have studied this problem via a continuum approach which reduces the calculation of asymptotic constants to quadratures (if the involved integrals converge). If the involved integrals do not converge, the method suggests a cutoff-based regularization procedure to deal with the singularity(ies). The energy scaling behavior can be obtained by fixing a single unknown scalar parameter to a numerically determined value, which is easily accessible since the solution is ordered. The predictions of the method have been extensively verified by numerical experiments. We have also shown, through Beta integrals at fixed n , an exact expression of the expected ground state energy for points distributed according to an exponential of mean 1, a result which appears to be new in the literature. We notice that the importance of the discussed regularization method is not restricted to the one-dimensional ERAP. Indeed, analogous formulas for the expected optimal costs appear also in other one-dimensional random optimization problems, such as the random Euclidean 2-matching and the Traveling Salesman Problem in the bipartite and the monopartite case. The understanding of the proper regularization to be adopted, when the simpler expression cannot be used

and an anomalous scaling appears, is therefore relevant for a larger class of optimization problems, to which the analysis presented here can be applied. Also, in Ref. (149), an integral expression for the $\langle \mathcal{H}_{\text{opt}} \rangle$ in the large n limit was given for $d > 1$. As the authors stress therein, the higher dimensional case might also require a regularization, depending on the properties of the domain and on the disorder distribution associated to \mathcal{B} and \mathcal{R} . The criteria for such a regularization remain an open problem for future investigations.

In § 2.6 we investigated the possible emergence of an anomalous scaling by combinatorial and analytic methods whose aim was to postpone the $n \rightarrow \infty$ limit. By these methods, we have considered several cases in which logarithmic scaling of the expected ground state energy emerges, and determined both the scaling exponent and limit constants explicitly in terms of special functions. Our analytic-combinatorial approach, which holds at even-integer values of p , is extended by analytic continuation of the results in the whole $p \geq 1$ region, and is able to address (even if, admittedly, with considerable more efforts) also the case in which the continuum method of § 2.5 cannot be used due to ill-posed involved integrals.

Concave regime. In § 2.7 we have started to address the ERAP in dimension 1, for points chosen in an interval, with a cost function which is an increasing and concave power law, that is $c(|x|) = |x|^p$ for $0 < p < 1$. We have introduced a new special matching configuration, uniquely associated to an instance of the problem, that we called the *Dyck matching*, as it is produced from the Dyck bridge that describes the interlacing of red and blue points on the domain \mathcal{M} .

As this is a deterministic configuration, described directly in terms of the instance, instead of involving a complex optimisation problem, this configuration is much more tractable than the optimal matching. On top of this fact, we can exploit a large number of nice facts, from combinatorial enumeration, which provides us also with several results which are exact at finite size, this being, to some extent, surprising. In particular, we have been able to compute the average cost of Dyck matchings under a particular choice of probability measure (the one in which the spacings among consecutive points are i.i.d. exponential variables). Finally, we have performed numerical simulations that suggest that the average cost of Dyck matchings has the same scaling behaviour of the average cost of optimal matchings (Fig. 2.15). We leave this claim as a conjecture. A promising way to prove this conjecture seems to be that of providing a lower bound on the average cost of optimal matchings with the same scaling as our upper bound, by producing “sufficiently many” or “sufficiently large” sets of edge-lengths which must be taken by the optimal solution. If we assume our conjecture, this result allows to fill in a missing portion in the phase diagram of the model in one dimension, for what concerns the scaling of the average optimal cost as a function of p (see Figure 2.17).

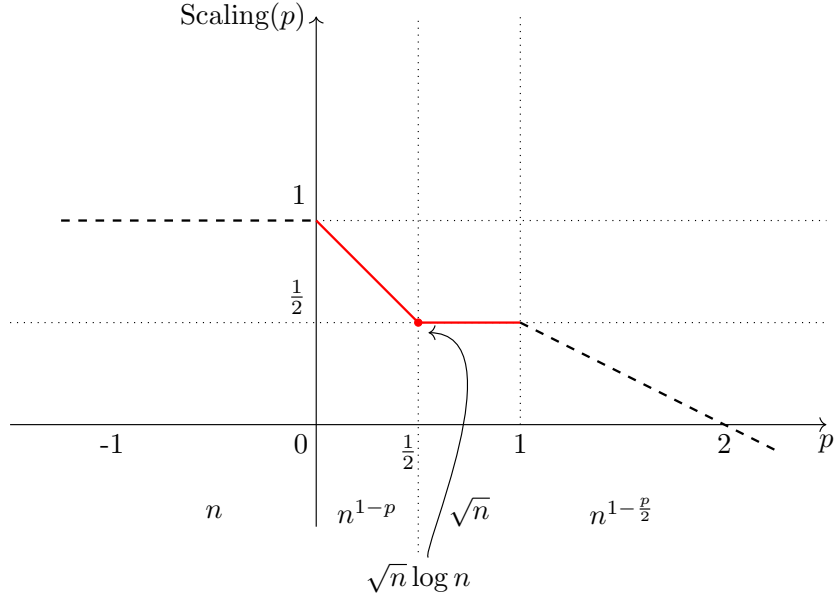


Figure 2.17. – *Scaling exponent of the average optimal cost as a function of p , in the case of cost function $\mathcal{C}(|x|) = +|x|^p$ (that is, attractive case for $p > 0$ and repulsive case for $p < 0$). In red (solid line), our conjectured result. In black (dashed line), existing results from (154) (notice that we have rescaled our results of Theorem 2.7.1 by a factor $(2n+1)^{-p}$ in order to make the comparison, i.e. we plotted the result for $\mathcal{M} = [0, 1]$).*

These new facts highlight a much richer structure than what could have been predicted in light of the previous results alone, with the concatenation of four distinct regions, and a new special point with logarithmic corrections at $p = 1/2$.

The case of uniformly spaced points needs further analysis in the region $p < 1/2$. One can define an interpolating family of independent spacing models, which encompasses both the ES and US cases, by taking as function $f(s)$ the Gamma distribution $\alpha g_\alpha(\alpha s)$, for $\alpha > 0$. For example, when α is an integer, each s_i is distributed as a sum of α i.i.d. exponential random variables, each with mean α^{-1} . The ES case is, of course, $\alpha = 1$, while, due to the central limit theorem, the US model is the limit as α tends to infinity. This generalised model appears to be treatable with the same technique that we employed for the pure ES case whenever α is a half-integer: the generating function of the average cost can be computed exactly in this case, and involves more and more complicated hypergeometric functions as α grows (namely, if $\alpha = k/2$, we have a ${}_kF_{k-1}$ hypergeometric function). Performing singularity analysis over such functions is a challenging task, which builds on classical results on generalised hypergeometric functions (due to Nørlund and Bühring), that we leave for future work.

Besides the above directions, for which an attacking strategy is at sight, other specific problems in the concave regime can be identified, for the understanding of which an alternative point of view may be useful. We sketch two of them in the following, in the form of Research Problems.

Research Problem 1 (Beyond the rule of three). We have recalled in several occasions (Lemmas 2.1.4 and 2.7.2) a characteristic property of the optimal permutation π_{opt} in the concave one dimensional regime, namely the non-crossing property. A further property is due to McCann (see (82), Theorem 2.5), who has shown that a π_{opt} in the concave regime must satisfy a geometric nesting inequality called “rule of three”. The name comes from the fact that, for two nested intervals $A = (b_i, r_{\pi(i)})$ and $B = (r_{\pi(j)}, b_j)$ corresponding to the situation $b_i < r_{\pi(j)} < b_j < r_{\pi(i)}$ (or the one with reverse inequality signs),

$$|B| \leq \frac{1}{3}|A|, \quad (2.8.1.1)$$

which is true *for all* strictly increasing, concave cost functions (as the non-crossing property). Unfortunately, the non-crossing property is not sufficient to fully characterize π_{opt} , and neither the rule of three is, so that the space of possible solutions remains fairly large (a partial reason for the introduction of Dyck matchings). Therefore, the discovery of additional properties could help to reduce the size of the space of the possible solutions. By the way, for the cost function $|x - y|^p$ with $p \in (0, 1)$, one can show that a bound tighter than the rule of three holds directly from the nesting requirement. For two nested sets B and A as above, consider the inequality

$$|B| \leq k(p)|A|$$

and call the lengths of three involved intervals in a nested configuration $x, 1$ and y (e.g. from left to right). In this parametrization, the nesting requirement becomes

$$1 + (x + y + 1)^p \leq x^p + y^p \quad (2.8.1.2)$$

(which is false for any concave strictly increasing cost function if $1 + x + y \leq 3$ according to McCann). However, the requirement is already false for a larger constant in our case. To see this, fix $z = x + y$ which gives the equivalent parametrization

$$1 + (1 + z)^p \leq (tz)^p + ((1 - t)z)^p \quad (2.8.1.3)$$

that has to be true for all $t \in [0, 1]$, and it is easy to show that the worst case is attained at $t = 1/2$. In this parametrization, we simply have that $k(p) = \frac{1}{1+z(p)}$, where $z(p)$ solves

$$1 + (1 + z)^p = 2 \left(\frac{z}{2} \right)^p \quad (2.8.1.4)$$

in the appropriate (z, p) region. $z(p)$ is a monotone increasing curve, starting from $2(1 + \sqrt{2})$ at $p = 0$, and diverging as $p \rightarrow 1^-$. $k(p)$ is in good agreement with the results of numerical experiments already at fairly small values of n (Fig. 2.18).

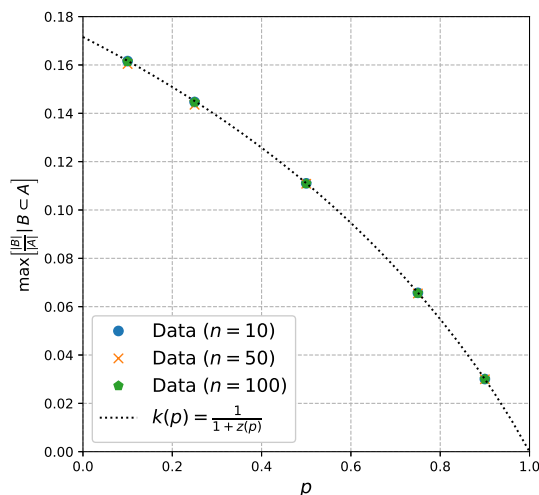


Figure 2.18. – Results of numerical experiments (colored dots) for the ratio of nested intervals corresponding to matching in opposite directions vs the theoretical prediction $k(p)$ from the nesting requirement (Eq. 2.8.1.4, dotted curve) as a function of p .

Research Problem 2 (Cycle structure of π_{opt} in the concave regime). A useful information about one dimensional ERAPs is the cycle structure of the optimal permutation π_{opt} (where the identical permutation is defined to be the ordered one). Indeed, a way of reformulating our discussion of § 2.1 is as follows. Take e.g. $\mathcal{M} = \mathbb{Q}^1$, and for a permutation $\pi \in \mathcal{S}_n$, introduce the observable $N_C(\pi)$ “number of permutation cycles in π with respect to the ordered one”. Assuming $\langle N_C(\pi_{\text{opt}})(p) \rangle \sim n^{\nu(p)}$ for large n , we know that, exactly,

$$\nu(p) = \begin{cases} 1 & p > 1 \\ 0 & p < 0 \end{cases} \quad (2.8.1.5)$$

without sub-leading corrections (we also consider 1-cycles or fixed points). Numerical experiments strongly suggest that $\nu(\pi_{\text{opt}}(p))$ is fairly constant in the concave regime (in particular for $p < 1/2$ where it hardly varies), and with high confidence satisfies $1/2 < \nu(\pi_{\text{opt}}(p)) < 2/3$ (Fig. 2.19). What is the value of the exponent ν for Dyck matchings, and how does it compare to the “true” exponent ν ? What

about the scaling exponent in n of other permutation related quantities, such as the number of inversions?

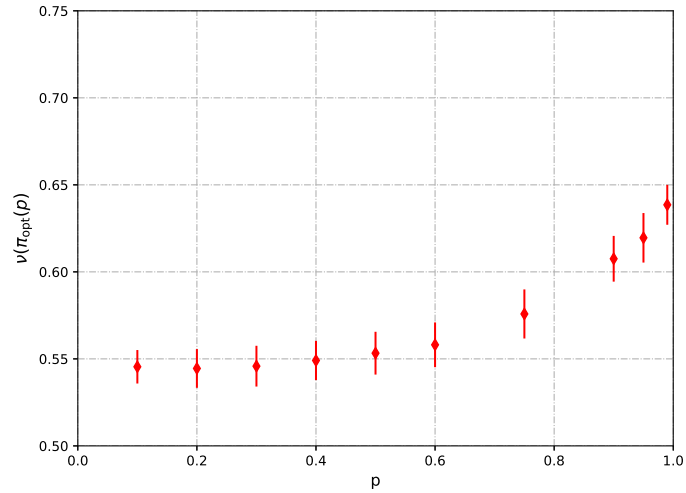


Figure 2.19. – Numerical estimates for the scaling exponent $\nu(\pi_{\text{opt}})(p)$ (red points and error-bars, see text for definitions) as a function of p in the concave regime (x -axis). Numerical protocol: $n \in \{10, 25, 50, 100, 250, 1000\}$, $p \in \{.1, .2, .3, .4, .5, .6, .75, .9, .95, .99\}$, 10^4 repetitions at each fixed (n, p) value. $\nu(\pi_{\text{opt}})(p)$ obtained as slope in a least square fit in log-log coordinates.

FIELD-THEORETIC APPROACH TO THE EUCLIDEAN RANDOM ASSIGNMENT PROBLEM

IT is a longstanding question to understand the asymptotic behaviour, for large n , of the expected ground state energy $E_\Omega(n)$ for a domain Ω in general dimension. When $d \geq 2$, the results are very partial for *any* choice of a domain Ω , including the conceptually simplest ones (like the unit hypercube, or the unit hypertorus), and *any* value of p , including the special cases $p = 1$ and $p = 2$. A first attempt was carried on by Mézard and Parisi (50) that showed how, for $d > 2$, the random-link result can be used as a zero-order approximation for the finite-dimensional solution, adding perturbatively a series of corrections. In the same years, a remarkable result was obtained by Ajtai and coworkers (37) for $d = 2$: they proved that, if the problem is considered on the unit square $\Omega = [0, 1]^2$, then $E_\Omega(n) \sim \ln n$.*

Recently, the forementioned result has been refined. In particular, by means of non-rigorous arguments, in Refs. (145, 148) it was claimed that, on the unit square $\mathbb{R} := [0, 1]^2$,

$$E_{\mathbb{R}}(n) = \frac{1}{2\pi} \ln n + 2c_{\mathbb{R}}(n) \tag{3.0.0.1}$$

where $c_{\mathbb{R}}(n) = o(\ln n)$ (the factor 2 is for later convenience). This result has been later rigorously proved by Ambrosio and coworkers (164) and extended to any 2-dimensional compact manifold Ω (163). The latter paper also proves rigorous bounds for c_Ω , namely that $c_\Omega(n) = \mathcal{O}(\sqrt{\ln n \ln \ln n})$. It has been recently conjectured that Eq. (3.0.0.1) holds also in the case of points generated from non-uniform densities (166). In the following Section we wish to argue, in the context of the field-theoretic approach to this problem, that all possibly divergent terms in $c_\Omega(n)$ are universal, in the sense that the first finite-size correction depending on the domain Ω is a constant, verify this statement for several (flat and curved) manifolds, and compare our predictions with numerical experiments for several choices of the surfaces Ω .

*More precisely Ajtai *et al.* studied the case $p = 1$, but they also sketch how their analysis can be extended to p a positive integer, and predicted the scaling $E_\Omega(n) \sim n^{1-\frac{p}{2}}(\ln n)^{\frac{p}{2}}$ in this generality. See also (167) for a recently proposed alternative proof of the AKT theorem.

3.1. Random Assignment Problems on $2d$ manifolds

THE content of this Section is part of a submitted paper ([172](#)).

Let $\mathcal{M} \equiv \Omega \subset \mathbb{R}^2$ be a compact domain, and let us assume that $\mathcal{B} = \{X_i\}_{i=1}^n$ and $\mathcal{R} = \{Y_i\}_{i=1}^n$ are generated via a homogeneous Poisson Point Process (PPP) on Ω . Let us introduce the two atomic measures

$$\begin{aligned}\nu_x &:= \frac{dx}{n} \sum_{i=1}^n \delta_{X_i}, \\ \nu_y &:= \frac{dy}{n} \sum_{i=1}^n \delta_{Y_i}.\end{aligned}\tag{3.1.0.1}$$

The energy of a permutation $\pi \in \mathcal{S}_n$ is

$$E_n(\pi|\mathcal{B}, \mathcal{R}) := \sum_{i=1}^n |X_i - Y_{\pi(i)}|^2,\tag{3.1.0.2}$$

where $|x - y|$ is two dimensional Euclidean distance between the points x and y . The average ground state energy is

$$E_{n,\Omega} := \mathbb{E}[\min_{\pi} E_n(\pi|\mathcal{B}, \mathcal{R})]\tag{3.1.0.3}$$

where \mathbb{E} denotes expectation w.r.t. the disorder distribution. We have recalled in the Introduction (Eq. [1.5.0.3](#)) that

$$\min_{\pi} E_n(\pi|\mathcal{X}, \mathcal{Y}) = nW_2^2(\nu_x, \nu_y)\tag{3.1.0.4}$$

holds, where W_2^2 is the squared Kantorovich distance between the measures [3.1.0.1](#), and promised to elaborate further on this connection in a subsequent Chapter. This is where we do it.

Under the hypothesis that the atomic measures in Eq. [\(3.1.0.1\)](#) have the same distribution limit, in ([144](#), [145](#), [148](#)) it has been suggested to solve the ERAP by means of a linearization of the Monge-Ampère equation which solves the variational problem in the continuum. The result requires a proper regularization that takes into account the finite- n effects to avoid divergences. In this approach, a close analogy naturally emerges between the evaluation of the ground state energy in the ERAP and the evaluation of the electrostatic energy of $n + n$ particles of opposite charge, respectively located at the blue and red points. In a sense, the proposed

linearization follows the opposite track of the suggestion by Born and Infeld (9) of a non-linear version of electrodynamics to solve the problem of divergencies. See also the more recent proposals by Brenier for fluid motion (83, 102).

In order to fix some notations, let us introduce, for each permutation π , a corresponding field μ_π , such that $\mu_\pi(X_i) = Y_{\pi(i)} - X_i$, corresponding to the map T , so that the energy of a configuration can be written as

$$E_n(\pi|\mathcal{X}, \mathcal{Y}) = \int_{\Omega} \mu_\pi^2(x) \nu_x(\mathrm{d}x). \quad (3.1.0.5)$$

On the other hand, the field μ_π has to satisfy a mass-conservation condition, i.e., for any function $\phi: \Omega \rightarrow \mathbb{R}$,

$$\int_{\Omega} \phi(x + \mu_\pi(x)) \nu_x(\mathrm{d}x) = \int_{\Omega} \phi(x) \nu_y(\mathrm{d}x), \quad x \in \Omega. \quad (3.1.0.6)$$

This condition is simply a rewriting of the fact that μ_π corresponds to a permutation that maps bijectively blue points onto red points. The idea is now to write down a Lagrangian that combines the cost expression in Eq. (3.1.0.2) with the mass-conservation condition in Eq. (3.1.0.6) as

$$L[\mu, \phi] := \int_{\Omega} \mu^2(x) \nu_x(\mathrm{d}x) + \int_{\Omega} [\phi(x + \mu(x)) \nu_x(x) - \phi(x) \nu_y(\mathrm{d}x)], \quad (3.1.0.7)$$

where ϕ plays the role of a Lagrange multiplier. Here we dropped the subscript π , whose meaning is incorporated in the condition (3.1.0.6). The optimal map $\mu(x)$ satisfies the nonlinear Lagrange equations obtained from the Lagrangian above. The next observation, at this point, is that for $n \rightarrow +\infty$ we expect $\mu(x) \rightarrow 0$ for any $x \in \Omega$, due to the fact that the matched pairs become infinitesimally close. Setting

$$\delta\nu(x) := \frac{1}{n} \sum_{i=1}^n [\delta(x - X_i) - \delta(x - Y_i)], \quad (3.1.0.8)$$

the Lagrangian is approximated, in this limit, by its linearized version,

$$\hat{L}[\mu, \phi] := \int_{\Omega} [\mu^2(x) + \mu(x) \cdot \nabla\phi(x)] \mathrm{d}x + \int_{\Omega} \delta\nu(x) \phi(x) \mathrm{d}x, \quad (3.1.0.9)$$

where we have used the fact that the flux of the field μ through the boundary is zero (points cannot be moved outside Ω) and $\nu_x(\mathrm{d}x) \xrightarrow{n \rightarrow +\infty} \mathrm{d}x$, uniform measure.

The new Lagrangian is extremized for μ and ϕ satisfying the equations

$$\mu(x) = -\nabla\phi(x), \quad (3.1.0.10a)$$

$$\nabla \cdot \mu(x) = \delta\nu(x), \quad (3.1.0.10b)$$

implying the Poisson equation

$$\Delta\phi(x) = \delta\nu(x) \quad (3.1.0.10c)$$

to be solved with Neumann boundary conditions. Here $\Delta := -\nabla^2 := \Delta_\Omega$ (note the minus sign) is the Laplacian operator on Ω . Starting from these equations and using the fact that

$$\mathbb{E}[\delta\nu(x)\delta\nu(y)] = \frac{2}{n}(\delta(x-y) - 1) \quad (3.1.0.11)$$

in Ref. (148) it is argued that, for $n \gg 1$, the formal result

$$E_{n,\Omega} = -2 \operatorname{Tr} \Delta_\Omega^{-1} \quad (3.1.0.12)$$

holds, where Δ_Ω^{-1} is the inverse Laplace operator on Ω . The expected ground state energy is therefore directly related to the spectrum of the Laplacian on the domain Ω , a result that is valid in the limit of the linearization approximation (148). Moreover, the arguments above can be repeated replacing Neumann boundary conditions with other boundary conditions, depending on the domain of interest. The simple intuition to regularize the Eq. (3.1.0.12) is observing that, at finite n , there is an intrinsic lengthscale in the problem, i.e., the typical distance between a point and its nearest neighbour. This lengthscale goes as $n^{-1/2}$ for large n and effectively induces a cutoff that allows us to neglect the largest eigenvalues of the Laplacian (148). At the leading order, the details of such a cut-off are not relevant and Eq. (3.1.0.12) becomes

$$E_n[\Omega] = \frac{1}{2\pi} \log n + 2c_\Omega + o(1), \quad (3.1.0.13)$$

for some constant c_Ω depending on the cut-off (the inessential factor 2 appears for matters of convention) and possibly on n . The leading term in Eq. (3.1.0.13) is indeed the correct result on the unit square $\Omega = [0, 1]^2$ (see Refs. (163–165) for proofs), the presence of a logarithm being known since the work of Ajtai, Komlós and Tusnády (37).

3.1.1. Regularisation through the integral of the zero-mean regular part of the Green function

Consider the Green function $G(x, y)$ of the Laplacian on the orthogonal complement of the locally constant functions, defined by

$$\int_{\Omega} G(x, y) \Delta f(y) \, dy = f(x) - \int_{\Omega} f(y) \, dy, \quad (3.1.1.1)$$

where f is a test function defined on Ω . The Green function is symmetric and satisfies the equations

$$\Delta_y G(x, y) = \delta(x - y) - 1, \quad (3.1.1.2a)$$

$$\partial_n G(x, y)|_{y \in \partial\Omega} = 0. \quad (3.1.1.2b)$$

where $\partial_n G(x, y)|_{y \in \partial\Omega}$ is the normal derivative with respect to the boundary $\partial\Omega$ of the domain. The equations above identify a unique Green function up to an additive constant: we will fix this constant adopting the convention

$$\int_{\Omega} G(x, y) \, dx = 0. \quad (3.1.1.2c)$$

The operator Δ^{-1} is thus defined then by

$$\Delta^{-1} f(x) := \int_{\Omega} G(x, y) f(y) \, dy. \quad (3.1.1.3)$$

It is well-known that the Green function of Δ_{Ω} can be written as

$$G_{\Omega}(x, y) = -\frac{1}{2\pi} \ln|x - y| + m(y) + \mathcal{O}(|x - y|) \quad (3.1.1.4)$$

and is thus logarithmically divergent in the ultraviolet limit $x \rightarrow y$ (which is the classical issue of self-interaction in two-dimensional electrostatics, as $G(x, y)$ can be interpreted as the potential generated at position y by a unit charge at position x).

Following Ref. (148), a regularization can be performed starting from the correlation function of the optimal transport field $\bar{\mu}$ which is the gradient of the Lagrange multiplier, $\mu = \nabla\phi$, where $\Delta\phi = \delta\nu$. It is

$$C(x, y) := n\mathbb{E}[\mu(x) \cdot \mu(y)] = 2 \int_{\Omega} \nabla_x G(z, x) \cdot \nabla_y G(z, y) \, dz. \quad (3.1.1.5)$$

The “diagonal” $C(x, x) \equiv n\mathbb{E}[\mu^2(x)]$ plays the role of a “cost density” and the

optimal cost is given by its “trace” $E_n[\Omega] = \int_{\Omega} C(x, x) \, dx$. The quantity $C(x, x)$ is itself divergent for any $x \in \Omega$ and must be regularized. Let us introduce therefore $\Omega_{\delta} = \Omega \setminus B_{\delta}(x)$, where $B_{\delta}(x)$ is the ball of radius $0 < \delta \ll 1$ centered in x . We can introduce a regularized version of $C(x, x)$,

$$C_{\delta}(x) := 2 \int_{\Omega_{\delta}} |\nabla_x G(z, x)|^2 \, dz, \quad (3.1.1.6)$$

and a corresponding “regularized cost”

$$\begin{aligned} E_{\delta}[\Omega] &:= \int_{\Omega} C_{\delta}(x) \, dx = 2 \iint_{\Omega \times \Omega} \nabla_x (G(z, x) \nabla_x G(z, x)) \theta(|z - x| > \delta) \, dx \, dz \\ &= 2 \int_{\Omega} dz \int_{S=\partial B_{\delta}(z)} G(z, u) \partial_n G(z, u)|_{u \in S} \, dS \end{aligned} \quad (3.1.1.7)$$

where the second integral runs over the border $\partial B_{\delta}(z) := \{x \in \Omega : |x - z| = \delta\}$ of $B_{\delta}(z)$, and ∂_n is the derivative in the direction of the versor orthogonal to the surface of the ball $B_{\delta}(z)$. For $0 < \delta \ll 1$, the inner integral can be estimated using the expression in Eq. 3.1.1.4, so that

$$E_{\delta}[\Omega] = -\frac{\ln \delta}{\pi} + 2 \int_{\Omega} m(x) \, dx + O(\delta). \quad (3.1.1.8)$$

The logarithmic divergence is recovered in the ultraviolet limit $\delta \rightarrow 0$, and the constant part depends only on the local function $m(y)$, sometimes called *Robin mass* (120, 125), which determines the corrections only through its integral

$$R_{\Omega} := \int_{\Omega} m(x) \, dx. \quad (3.1.1.9)$$

3.1.2. Zeta regularisation and the Kronecker mass

Eq. (3.1.0.12) can be rewritten as

$$E_n[\Omega] = 2 \sum_{i \geq 1} \frac{1}{\lambda_i} \quad (3.1.2.1)$$

where $0 = \lambda_0 < \lambda_1 \leq \lambda_2 \leq \dots$ is the spectrum of $-\Delta_{\Omega}$, and the sum is logarithmically divergent for any domain Ω (recall that Weyl’s law in two dimensions implies that the number $\mathcal{N}(\lambda)$ of eigenvalues less than λ grows as λ , and therefore $\sum_i \lambda_i^{-1} \sim \int \lambda^{-1} \, d\mathcal{N}(\lambda)$). A widely adopted way to regularize expressions such as

Eq. 3.1.2.1 is via analytic continuation in the so-called zeta regularization considered e.g. by Hawking (30). Consider the generating function

$$Z(s) := \sum_{i \geq 1} \frac{1}{\lambda_i^s}, \quad (3.1.2.2)$$

which is known to be absolutely convergent for $\Re(s) > 1$. Then, $-\text{Tr } \Delta^{-1}$ can be regularized by looking at $Z(s)$ near $s = 1$ (51)

$$Z(s) = \frac{1}{4\pi} \frac{1}{s-1} + K_\Omega + O(s-1) \quad (3.1.2.3)$$

and by removing the pole at $s = 1$. We will call the constant K_Ω the *Kronecker's mass*.

3.1.3. Connection between Robin and Kronecker masses

The constant R_Ω depends on Ω only, being related to the expansion in Eq. (3.1.1.4) for the Laplacian. Eq. (3.1.0.13) is recovered assuming that

$$\delta \sim n^{-1/2} \quad (3.1.3.1)$$

at the leading order, as one would expect: this is indeed the scaling of the typical distances between points uniformly generated on Ω , i.e., the scale at which the discrete nature of the problem becomes relevant. However, having no information about δ (or, in general, on the proper cure of the divergence of the Green function to get the correct cost), the result will be determined up to an unknown additive contribution (possibly scaling with n). From the arguments above it is clear that the regularization is related to the local behavior of the solution, and in particular to the local distribution of points.

On the other hand, in zeta regularization the scaling in Eq. (3.1.0.13) is formally recovered imposing

$$\frac{1}{s-1} = \ln n + O(1). \quad (3.1.3.2)$$

Obviously, $K_\Omega \neq R_\Omega$ in general. However, it can be proved that, given a domain Ω , $R_\Omega - K_\Omega$ is a universal constant that does not depend on Ω , being given by (94, 109, 120, 121)

$$R_\Omega - K_\Omega = -\frac{\gamma_E}{2\pi} + \frac{\ln 2}{2\pi} = 0.0184511\dots \quad (3.1.3.3)$$

We expect that, if different domains are considered with uniform distribution of points on them, the proper regularization to be adopted is the same and provides therefore the same, regularization-dependent additive contribution. In other

words, given two compact domains of equal measure Ω and Ω' , we expect for $n \rightarrow +\infty$

$$E_n[\Omega] - E_n[\Omega'] = c_\Omega - c_{\Omega'} = R_\Omega - R_{\Omega'}, \quad (3.1.3.4)$$

i.e., the differences are expected to be regularization-independent.

3.1.4. Applications

To test our conjecture we will first compute both Kronecker's and Robin's masses for different domains and different boundary conditions, and then compare our analytical results to numerical experiments in § 3.1.5.

The flat torus

Let us start considering the flat torus. Consider the lattice of points on \mathbb{R}^2 ,

$$\Lambda = \{\underline{\omega} \cdot n, \quad n \in \mathbb{Z}^2\} \quad (3.1.4.1)$$

generated by the matrix

$$\underline{\omega} := \begin{pmatrix} \ell & 0 \\ s & h \end{pmatrix} \quad \ell, h \in \mathbb{R}^+, \quad s \in \mathbb{R}, \quad (3.1.4.2)$$

corresponding to the base vectors

$$\omega_1 := \begin{pmatrix} \ell \\ 0 \end{pmatrix}, \quad \omega_2 := \begin{pmatrix} s \\ h \end{pmatrix}. \quad (3.1.4.3)$$

In such lattice it is possible to define fundamental parallelograms, containing no further lattice points in its interior or boundary. A fundamental parallelogram is given for example by

$$\mathcal{D} := \{r \in \mathbb{R}^2 : r = \underline{\omega} \cdot x, \quad x \in [0, 1]^2\} \quad (3.1.4.4)$$

of area $A := \ell h$. For each ω , we introduce the half-period ratio

$$\tau := \frac{s + ih}{\ell} \in \mathbb{C}. \quad (3.1.4.5)$$

It is a well known fact that, given a lattice Λ generated by $\underline{\omega}$, the same lattice is also generated by the pair

$$\underline{\omega}' = \underline{a} \cdot \underline{\omega} \quad (3.1.4.6)$$

where \underline{a} is an element of the modular group $\text{SL}(2, \mathbb{Z})$. Note that τ is not a modular invariant, and it is usually specified fixing a fundamental region, i.e., a subset of

\mathbb{R}^2 such that no two distinct points of it are equivalent under the action of the modular group (each fundamental parallelogram is an example of fundamental region) (27). Having fixed the fundamental region, a value τ can be uniquely associated to each lattice Λ .

Given a lattice Λ , it is possible to associate to it a dual lattice Λ^* defined as

$$\Lambda^* = \{\gamma^* \in \mathbb{R}^2: \gamma^* \cdot \gamma \in \mathbb{Z}, \quad \forall \gamma \in \Lambda\}. \quad (3.1.4.7)$$

Given the generator ω of the lattice Λ , a generator ω^* of the lattice Λ^* has to satisfy $\underline{\omega}^* \cdot \underline{\omega}^T = \mathbb{I}$, identity matrix, i.e.,

$$\omega^* := \frac{1}{A} \begin{pmatrix} h & -s \\ 0 & \ell \end{pmatrix} \quad (3.1.4.8)$$

so that for this lattice $\tau = 1/\bar{\tau}$.

The torus is defined as a quotient between the complex plane and a lattice Λ , $\mathbb{T} := \mathbb{R}^2/\Lambda$. In other words, each point $x \in \mathcal{D}$ is identified with the set of points $\{x + \underline{\omega} \cdot n, n \in \mathbb{Z}^2\}$, the distance between two points in \mathcal{D} being the minimum distance between the elements of their equivalence classes. Each torus can be associated to a dual torus given by $\mathbb{T}^* := \mathbb{R}^2/\Lambda^*$.

In the following, we will restrict, without loss of generality, to the case of fundamental parallelograms of unit area, choosing

$$\underline{\omega} = \frac{1}{\sqrt{\rho}} \begin{pmatrix} 1 & 0 \\ \sigma & \rho \end{pmatrix} \Rightarrow \tau = \sigma + i\rho, \quad (3.1.4.9)$$

such that $\rho \in \mathbb{R}^+$ and $\sigma \in \mathbb{R}$, and we will denote the corresponding torus by $\mathbb{T}(\tau)$.

The Kronecker mass Due to the periodicity conditions, the eigenfunctions of Δ on $\mathbb{T}(\tau)$ have the form

$$u_{\gamma^*}(x) = \exp(2\pi i \gamma^* \cdot x) \quad (3.1.4.10)$$

for all $\gamma^* = \bar{\Omega}^* \cdot k \in \Lambda^*$, $k = \begin{pmatrix} n \\ m \end{pmatrix} \in \mathbb{Z}^2$. The corresponding eigenvalue is

$$\lambda_{n,m} = |2\pi \gamma^*|^2 = (2\pi)^2 \frac{|n + \tau m|^2}{\rho}. \quad (3.1.4.11)$$

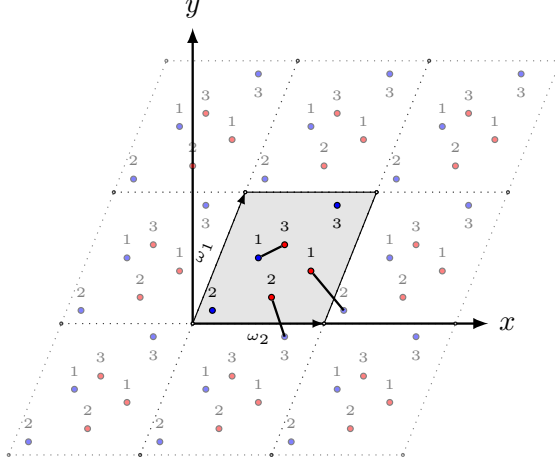


Figure 3.1. – Pictorial representation of an assignment at $n = 3$ on a torus generated by quotient of \mathbb{R}^2 with a periodic lattice, with fundamental parallelogram and the corresponding base vectors.

As in the case of the torus, we compute the Kronecker mass using the regularized function

$$Z(s) = \sum_{\gamma^*} \frac{1}{|2\pi\gamma^*|^{2s}} = \frac{1}{(2\pi)^{2s}} \sum_{\substack{(m,n) \in \mathbb{Z}^2 \\ n^2+m^2 \neq 0}} \frac{[\Im(\tau)]^s}{|n + \tau m|^{2s}} \quad (3.1.4.12)$$

and removing the pole in $s \rightarrow 1$ as discussed with reference to Eq. (3.1.2.2). Here we have introduced $\tau = i\rho$. This calculation is readily performed observing that

$$\zeta_\tau(s) := \sum_{\substack{(m,n) \in \mathbb{Z}^2 \\ n^2+m^2 \neq 0}} \frac{[\Im(\tau)]^s}{|n + \tau m|^{2s}} = \frac{\pi}{s-1} + 2\pi \left[\gamma_E - \ln(2\sqrt{\Im(\tau)}|\eta(\tau)|^2) \right] + o(s-1), \quad (3.1.4.13)$$

where γ_E is the Euler-Mascheroni constant, and $\eta(\tau)$ is the Dedekind η function. In Fig. 3.2 we show a contour plot of $\Im(\tau)|\eta(\tau)|^4$ in the complex plane τ . The expansion in the proximity of the pole is a result due to Kronecker (see Appendix B.1 for further details). Kronecker's formula allows us to immediately obtain

$$K_{\mathbb{T}}(\tau) = \frac{\gamma_E}{2\pi} - \frac{1}{4\pi} \ln(16\pi^2 \Im(\tau) |\eta(\tau)|^4). \quad (3.1.4.14)$$

We will see in the following that Eq. (3.1.4.13) will allow us to extract the Kronecker's mass for many types of flat domains.

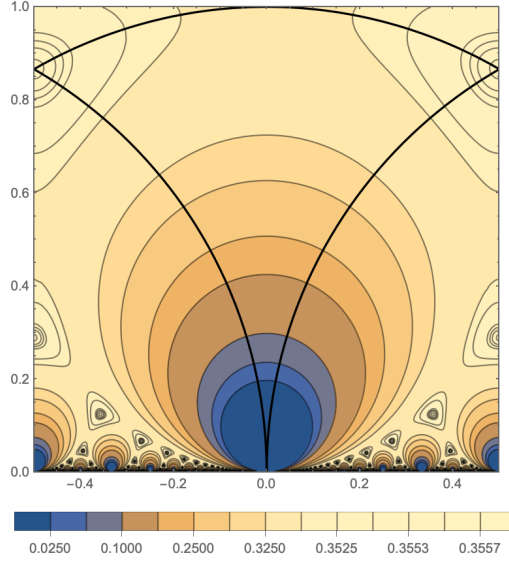


Figure 3.2. – Contour plot of $\Im(\tau)|\eta(\tau)|^4$ in the complex plane τ .

The Robin mass Let us now evaluate, for the generic flat torus $\mathbb{T}(\tau)$, the Robin mass $R_{\mathbb{T}(\tau)}$. The Green's function on the torus is given in this case by (131)

$$G(x, y) = -\frac{1}{2\pi} \ln \left| \frac{\vartheta_1 \left(\sqrt{\Im(\tau)} z; \tau \right)}{\eta(\tau)} \right|_{z=(x_1-y_1)+i(x_2-y_2)} + \frac{\Im(\tau)(x_2 - y_2)^2}{2} \quad (3.1.4.15)$$

where $\vartheta_1(z; \tau)$ is an elliptic ϑ function. The Robin mass is obtained from

$$\begin{aligned} R_{\mathbb{T}(\tau)} &:= -\lim_{z \rightarrow 0} \left[\frac{1}{2\pi} \ln \left| \frac{\vartheta_1 \left(\sqrt{\Im(\tau)} z; \tau \right)}{\eta(\tau)} \right| - \frac{\ln |z|}{2\pi} \right] \\ &= -\frac{1}{4\pi} \ln [4\pi^2 \Im(\tau) |\eta(\tau)|^4]. \end{aligned} \quad (3.1.4.16)$$

It is immediately seen that Eq. (3.1.3.3) is satisfied.

Example: the rectangular torus The rectangular torus is obtained assuming $\tau = i\rho$, with $\rho > 0$. In this case

$$K_{\mathbb{T}(i\rho)} = \frac{\gamma_E - \ln(4\pi\sqrt{\rho})}{2\pi} - \frac{1}{\pi} \ln |\eta(i\rho)|, \quad (3.1.4.17)$$

which is invariant, by modular invariance, under the map $\rho \mapsto \rho^{-1}$. In the region $\rho \in (0, 1]$ the lowest value is achieved at $\rho = 1$ (see also Fig. 3.2) where

$$K_{\mathbb{T}}(i) = \frac{\gamma_E}{2\pi} + \frac{\ln \pi}{4\pi} - \frac{1}{\pi} \ln \Gamma(1/4). \quad (3.1.4.18)$$

In particular

$$K_{\mathbb{T}}(i\rho) - K_{\mathbb{T}}(i) = -\frac{\ln \rho}{4\pi} - \frac{1}{\pi} \ln \frac{\eta(i\rho)}{\eta(i)} = -\frac{1}{2\pi} \ln \frac{\eta(i\rho)\eta(i\rho^{-1})}{\eta^2(i)}. \quad (3.1.4.19)$$

We also remark that

$$\lim_{\rho \rightarrow \infty} \frac{2K_{\mathbb{T}}(i\rho) - 2K_{\mathbb{T}}(i)}{\rho} = \lim_{\rho \rightarrow \infty} \rho[2K_{\mathbb{T}}(i\rho) - 2K_{\mathbb{T}}(i)] = \frac{1}{6}, \quad (3.1.4.20)$$

which is the asymptotic energy of the one-dimensional problem on the circle (see Eq. 2.3.1.10).

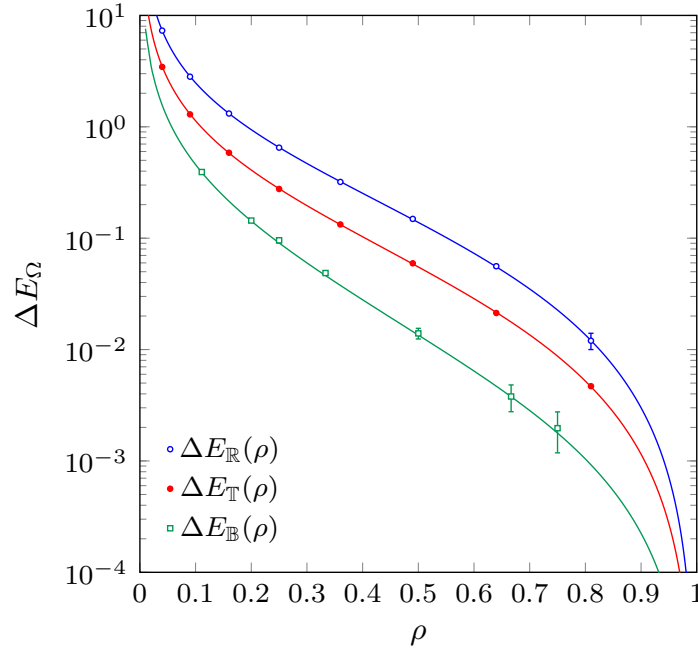


Figure 3.3. – Differences on expected ground state energies on the rectangle $\mathbb{R}(\rho)$, on the torus $\mathbb{T}(i\rho)$ and on the Boy surface $\mathbb{B}(\rho)$ with the corresponding costs for $\rho = 1$. The numerical results, represented by the dots, are compared with the analytical prediction obtained from Kronecker's masses.

Example: the hexagonal torus Let us consider $\tau = e^{i\theta}$, with $0 < \theta \leq \pi/2$, obtained for example using

$$\omega_1 = \frac{1}{\sqrt{\sin \theta}} \quad (3.1.4.21)$$

$$\omega_2 = (\cot \theta + i)\sqrt{\sin \theta} \quad (3.1.4.22)$$

in order to keep unit area. Then

$$K_{\mathbb{T}}(e^{i\theta}) = \frac{\gamma_E - \ln(4\pi)}{2\pi} - \frac{1}{4\pi} \ln \sin \theta - \frac{1}{\pi} \log |\eta(e^{i\theta})|. \quad (3.1.4.23)$$

By using the results in (51), in (120) it is recovered that the minimum is achieved at $\theta = \pi/3$, the hexagonal torus.

Unit rectangle

In the previous paragraphs we have considered the case of a periodic domain. Let us consider now the problem on the rectangle

$$\mathbb{R}(\rho) := [0, \sqrt{\rho}] \times \left[0, \frac{1}{\sqrt{\rho}}\right], \quad \rho > 0, \quad (3.1.4.24)$$

with Neumann boundary conditions. The eigenfunctions of Δ on $\mathbb{R}(\rho)$ are given by

$$u_{m,n}(x, y) = \cos(\sqrt{\rho}\pi mx) \cos\left(\frac{\pi}{\sqrt{\rho}}ny\right), \quad (3.1.4.25)$$

with $(x, y) \in \Omega$ and $(m, n) \in \mathbb{N}^2 \setminus (0, 0)$. The corresponding eigenvalues are

$$\lambda_{(m,n)} = \pi^2 \left(\rho m^2 + \frac{n^2}{\rho} \right) \quad (3.1.4.26)$$

We proceed computing the Kronecker mass using the regularized function

$$Z(s) = \left(\frac{\rho}{\pi^2}\right)^s \sum_{\substack{(m,n) \in \mathbb{N}^2 \\ n^2 + m^2 \neq 0}} \frac{1}{(\rho^2 m^2 + n^2)^s} \stackrel{\tau=i\rho}{=} \frac{\zeta_{\tau}(s)}{4\pi^{2s}} + \frac{\rho^s + \rho^{s-2}}{2\pi^{2s}} \sum_{n=1}^{\infty} \frac{1}{n^{2s}}. \quad (3.1.4.27)$$

Here we have introduced $\tau = i\rho$, in analogy with the flat torus parametrization. As in the torus case, Eq. (3.1.4.13) gives us an expression for the Kronecker's mass,

$$K_{\mathbb{R}}(\rho) = \frac{\gamma_E}{2\pi} - \frac{\ln(4\pi^2 \rho |\eta(i\rho)|^4)}{4\pi} + \frac{1}{2\pi^2} \left(\rho + \frac{1}{\rho} \right) \zeta(2) \quad (3.1.4.28)$$

that for $\rho = 1$ (unit square) simplifies as

$$K_{\mathbb{R}}(1) = \frac{\gamma_E}{2\pi} + \frac{\ln(4\pi)}{4\pi} - \frac{\ln \Gamma(1/4)}{\pi} + \frac{1}{6}. \quad (3.1.4.29)$$

Other boundary conditions on the unit rectangle

The unit rectangle and the rectangular torus are obtained starting from the fundamental domain

$$\mathcal{D} := [0, \sqrt{\rho}] \times \left[0, \frac{1}{\sqrt{\rho}}\right], \quad \rho > 0, \quad (3.1.4.30)$$

and assuming respectively open and periodic boundary conditions. Other choices of boundary conditions are possible. Each choice corresponds to a different spectrum of the Laplacian and, in particular, to a different finite-size correction to ground state energy of the ERAP.

Cylinder

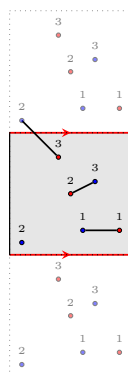


Figure 3.4. – *The Cylinder.*

Let us consider the domain \mathcal{D} and let us take periodic boundary conditions in the x direction at size $\sqrt{\rho}$ and Neumann boundary conditions in the y direction at size $1/\sqrt{\rho}$, see Fig. 3.4. This is the topology of a cylinder $\mathbb{C}(\rho)$. The eigenfunctions of Δ are the set of functions

$$u_{m,n}(x, y) = \exp\left(\frac{2i\pi mx}{\sqrt{\rho}}\right) \cos(\pi\sqrt{\rho}ny), \quad m \in \mathbb{Z}, \quad n \in \mathbb{N}. \quad (3.1.4.31)$$

The corresponding eigenvalues are therefore

$$\lambda_{(m,n)} = \pi^2 \left(4\frac{m^2}{\rho} + \rho n^2\right) \quad m \in \mathbb{Z}, \quad n \in \mathbb{N}. \quad (3.1.4.32)$$

Repeating the same type of calculations performed for the rectangle, we obtain

$$K_{\mathbb{C}}(\rho) = \frac{\gamma_E}{2\pi} - \frac{\ln(16\pi^2\rho)}{4\pi} - \frac{1}{\pi} \log \eta(2i\rho) + \frac{\zeta(2)}{4\pi^2\rho} \quad (3.1.4.33)$$

so that

$$K_{\mathbb{C}}(1) = \frac{\gamma_E}{2\pi} + \frac{3 \ln 2}{8\pi} + \frac{\ln \pi}{4\pi} - \frac{\log \Gamma(1/4)}{\pi} + \frac{1}{24}. \quad (3.1.4.34)$$

We also remark that

$$\lim_{\rho \rightarrow \infty} \frac{2K_{\mathbb{C}}(\rho) - 2K_{\mathbb{C}}(1)}{\rho} = \frac{1}{3}, \quad (3.1.4.35)$$

which is the cost density for the one-dimensional assignment problem with open boundary conditions, while

$$\lim_{\rho \rightarrow 0} \rho[2K_{\mathbb{C}}(\rho) - 2K_{\mathbb{C}}(1)] = \frac{1}{6} \quad (3.1.4.36)$$

which is the density of cost for the one-dimensional assignment problem with periodic boundary conditions. The nontrivial solution of the equation $K_{\mathbb{C}}(\rho) = K_{\mathbb{C}}(1)$ is $\rho = 0.625352\dots$. The minimum value of the mass occurs instead for $\rho = 0.793439\dots$.

Möebius strip

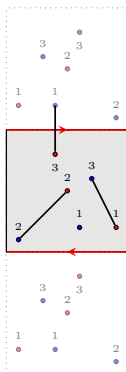


Figure 3.5. – *The Möebius strip.*

Starting again from the rectangle \mathcal{D} , we can identify each point $(x, y) \in \mathcal{D}$ with all its images obtained through the law $(x, y) \sim (x + \sqrt{\rho}, 1/\sqrt{\rho} - y)$. This is equivalent to assume antiperiodic boundary conditions in the x direction. The obtained domain $\mathbb{M}(\rho)$ has the topology of the Möebius strip, see Fig. 3.5. The

eigenfunctions of Δ are

$$u_{m,n}(x, y) = \exp\left(\frac{i\pi m x}{\sqrt{\rho}}\right) \cos(\pi\sqrt{\rho} n y), \quad m \in \mathbb{Z}, \quad n \in \mathbb{N}, \quad (3.1.4.37)$$

but such that n and m are constrained to have the same parity (to fulfill the antiperiodicity requirement). The corresponding eigenvalues are

$$\lambda_{(m,n)} = \pi^2 (\rho^{-1} m^2 + \rho n^2). \quad (3.1.4.38)$$

Repeating now the usual arguments we get

$$K_{\mathbb{M}}(\rho) = \frac{\gamma_{\mathbb{E}}}{2\pi} - \frac{\ln(4\pi^2 \rho)}{4\pi} - \frac{1}{\pi} \log \frac{\eta^3(i\rho)}{\eta(i2\rho)\eta(i\frac{\rho}{2})} + \frac{\zeta(2)}{4\pi^2 \rho}, \quad (3.1.4.39)$$

so that

$$K_{\mathbb{M}}(1) = \frac{\gamma_{\mathbb{E}}}{2\pi} + \frac{\ln(2\pi)}{4\pi} - \frac{\ln \Gamma(1/4)}{\pi} + \frac{1}{24}. \quad (3.1.4.40)$$

We also remark that

$$\lim_{\rho \rightarrow \infty} \frac{2K_{\mathbb{M}}(\rho) - 2K_{\mathbb{M}}(1)}{\rho} = \frac{1}{12} \quad (3.1.4.41)$$

while

$$\lim_{\rho \rightarrow 0} \rho [2K_{\mathbb{M}}(\rho) - 2K_{\mathbb{M}}(1)] = \frac{1}{6}, \quad (3.1.4.42)$$

which is the asymptotic value for the ground state energy of the Poisson-Poisson ERAP with periodic boundary conditions, Eq. 2.3.1.10.

A nontrivial solution of the equation $K_{\mathbb{M}}(\rho) = K_{\mathbb{M}}(1)$ is found for $\rho = 4.1861 \dots$, whereas the the minimum of the mass is achieved at $\rho = 2.30422 \dots$.

Klein bottle

If we add periodic boundary conditions in the y direction to the Möebius strip we obtain the topology of the Klein bottle $\mathbb{K}(\rho)$, see Fig. 3.6. The eigenfunctions of Δ are in this case

$$u_{m,n}(x, y) = e^{\frac{\pi i m}{\sqrt{\rho}} x} \cos(2\pi n \sqrt{\rho} y), \quad m \in \mathbb{Z}, \quad n \in \mathbb{N} \text{ with same parity} \quad (3.1.4.43)$$

and

$$v_{m,n}(x, y) = e^{\frac{2m+1}{\sqrt{\rho}} \pi i x} \sin(2\pi n \sqrt{\rho} y), \quad m \in \mathbb{Z}, \quad n \in \mathbb{N}^+. \quad (3.1.4.44)$$

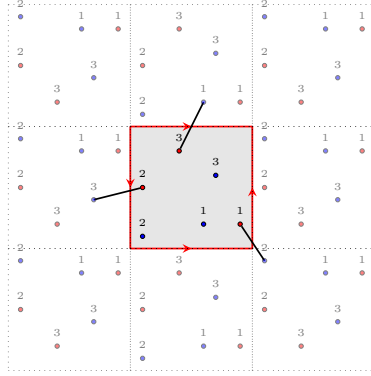


Figure 3.6. – *The Klein bottle.*

As before one can obtain

$$K_{\mathbb{K}}(\rho) = \frac{\gamma_E}{2\pi} - \frac{\ln(4\pi^2\rho)}{4\pi} - \frac{1}{\pi} \ln \eta \left(i \frac{\rho}{2} \right) - \frac{\zeta(2)}{2\pi^2\rho} \quad (3.1.4.45)$$

so that in particular

$$K_{\mathbb{K}}(1) = \frac{\gamma_E}{2\pi} + \frac{7}{8\pi} \log 2 + \frac{1}{4\pi} \log \pi - \frac{\ln \Gamma(1/4)}{\pi} - \frac{1}{12}. \quad (3.1.4.46)$$

We also remark that, in analogy with the Möbius strip

$$\lim_{\rho \rightarrow \infty} \frac{2K_{\mathbb{K}}(\rho) - 2K_{\mathbb{K}}(1)}{\rho} = \frac{1}{12}, \quad (3.1.4.47)$$

while

$$\lim_{\rho \rightarrow 0} \rho[2K_{\mathbb{K}}(\rho) - 2K_{\mathbb{K}}(1)] = \frac{1}{6}. \quad (3.1.4.48)$$

Here $K_{\mathbb{K}}(\rho) = K_{\mathbb{K}}(1)$ for $\rho = 1.09673\dots$, whereas the the minimum is obtained at $\rho = 1.04689\dots$

Boy surface

As final example, let us take antiperiodic boundary conditions in both directions on \mathcal{D} , obtaining the topology of the so-called Boy surface \mathbb{B} , see Fig. 3.7. The

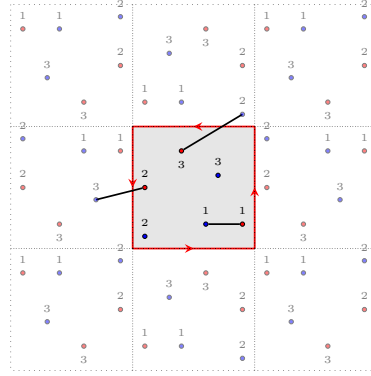


Figure 3.7. – *The Boy surface.*

eigenfunctions of Δ are

$$u_{m,n}(x, y) = \cos\left(\frac{\pi m}{\sqrt{\rho}}x\right) \cos(\pi n\sqrt{\rho}y),$$

$m, n \in \mathbb{N}$ with same parity (3.1.4.49a)

$$v_{m,n}(x, y) = \sin\left(\frac{\pi m}{\sqrt{\rho}}x\right) \cos(\pi n\sqrt{\rho}y),$$

$m, n \in \mathbb{N}$ with opposite parity. (3.1.4.49b)

The calculation proceeds as in the other cases, giving

$$K_{\mathbb{B}}(\rho) = \frac{\gamma_{\mathbb{E}}}{2\pi} - \frac{\ln(4\pi^2\rho)}{4\pi} - \frac{\ln \eta(i\rho)}{\pi} - \frac{1}{4\pi^2} \left(\rho + \frac{1}{\rho}\right) \zeta(2)$$

(3.1.4.50)

so that in particular

$$K_{\mathbb{B}}(\rho) = \frac{\gamma_{\mathbb{E}}}{2\pi} + \frac{3}{8\pi} \log 2 + \frac{1}{4\pi} \log \pi - \frac{\ln \Gamma(1/4)}{\pi} - \frac{1}{12}.$$

(3.1.4.51)

In analogy with the Möbius strip, once again,

$$\lim_{\rho \rightarrow \infty} \frac{K_{\mathbb{B}}(\rho) - K_{\mathbb{B}}(1)}{\rho} = \lim_{\rho \rightarrow 0} \rho[2K_{\mathbb{B}}(\rho) - 2K_{\mathbb{B}}(1)] = \frac{1}{12}.$$

(3.1.4.52)

Notice in particular that $K_{\mathbb{B}}(1/\rho) = K_{\mathbb{B}}(\rho)$ since $\sqrt{\rho}\eta(i\rho) = \eta(i/\rho)$.

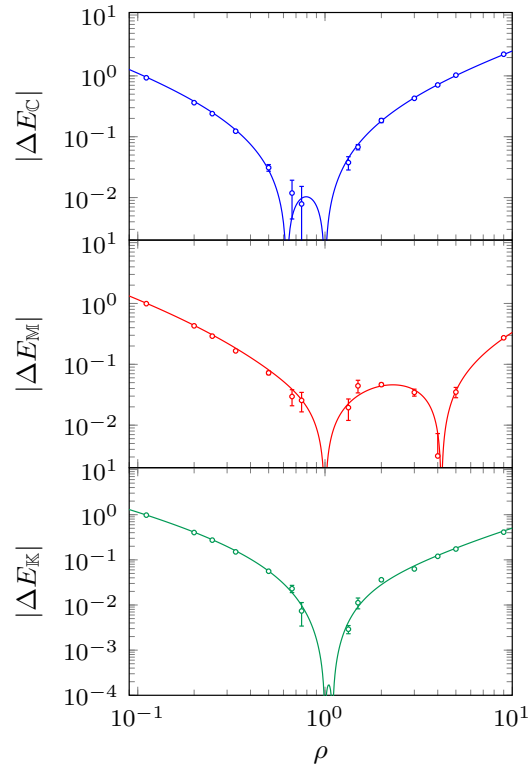


Figure 3.8. – Absolute shift of ground state energies for the cylinder $\mathbb{C}(\rho)$, the Möbius strip $\mathbb{M}(\rho)$ and the Klein bottle $\mathbb{K}(\rho)$ with respect to the case $\rho = 1$. Numerical results, represented by dots, are compared with the analytical prediction obtained from Kronecker’s masses as function of ρ .

Disc

Up to now, we have solved the problem using the zeta regularization of the Laplacian, and relying on Kronecker's first limit formula. To exemplify a calculation of a Robin mass, we consider here the disc of radius $r > 0$,

$$\mathbb{D}(\pi r^2) = \{x \in \mathbb{R}^2: |x| \leq r\} . \quad (3.1.4.53)$$

It can be verified by direct inspection that the function

$$g(x, y) = -\frac{1}{2\pi} \ln |x - y| - \frac{1}{2\pi} \log \left| y - \frac{xr^2}{|x|^2} \right| \quad (3.1.4.54)$$

satisfies

$$\begin{cases} \Delta_y g(x, y) = \delta(x - y) & \text{for } |y| < r, \\ \partial_{n(y)} g(x, y) = 0 & \text{for } |y| = r. \end{cases} \quad (3.1.4.55)$$

The function in Eq. (3.1.4.54) can be found with the method of image charges. Here, however, we look for the function $G(x, y)$ that satisfies Eq. (3.1.1.2), i.e.,

$$\begin{cases} \Delta_y G(x, y) = \delta(x - y) - \frac{1}{\pi r^2} & \text{for } |y| < r \\ \partial_{n(y)} G(x, y) = 0 & \text{for } |y| = r, \end{cases} \quad (3.1.4.56)$$

and such that its average for y in the disc is null. Therefore, noticing that $\Delta_y \frac{1}{4\pi r^2} |y|^2 = \frac{1}{\pi r^2}$, we can define G as

$$G(x, y) = g(x, y) + \frac{1}{4\pi r^2} |y|^2 - c(x) \quad (3.1.4.57)$$

where $c(x)$ is

$$c(x) := \frac{1}{\pi r^2} \int_{|y| < r} \left(g(x, y) + \frac{1}{4\pi r^2} |y|^2 \right) dy \quad (3.1.4.58)$$

Therefore the regular part of the Green function is

$$\gamma(x, y) = -\frac{1}{2\pi} \ln \left| y - \frac{xr^2}{|x|^2} \right| + \frac{1}{4\pi r^2} |y|^2 - c(x). \quad (3.1.4.59)$$

and, finally,

$$\int_{|x| < r} dx \gamma(x, x) = \frac{r^2 \log r}{2} + \frac{3}{8} r^2, \quad (3.1.4.60)$$

where we used the fact that c is a radial function, and we repeatedly applied the divergence Theorem. In particular, the Robin mass for the disc of area 1 is

$$R_{\mathbb{D}} = \frac{1}{\pi} \left(\frac{3}{8} - \frac{\ln \pi}{4} \right). \quad (3.1.4.61)$$

The Kronecker mass is readily obtained using Eq. (3.1.3.3). Observe that the Kronecker mass can be also directly estimated using the spectrum of the Laplacian on the disc.

Other surfaces

Unit sphere \mathbb{S}^2

The transportation problem on the surface of the sphere \mathbb{S}^2 has already been considered in Ref. (159), where the problem of transporting a uniform mass distribution into a set of random points on \mathbb{S}^2 is analyzed. Here we consider the problem in our usual setting, i.e., a transportation between two atomic measures of random points. As in the previous cases, the information on the finite-size corrections is partially contained in the spectrum of the Laplace-Beltrami operator on the manifold. It is well-known that the eigenfunctions of $-\Delta$ on the surface of a sphere of radius r are the spherical harmonics $Y_{l,m}(\theta, \phi)$ with $l \in \mathbb{N}$ and $m \in \mathbb{Z}$ with $-l \leq m \leq l$. The corresponding eigenvalues are

$$\lambda_{l,m} = \frac{l(l+1)}{r^2} \quad \text{with multiplicity } 2l+1. \quad (3.1.4.62)$$

By fixing unit area of the surface taking $r = (4\pi)^{-1/2}$, we proceed using the zeta regularization, i.e., computing

$$Z(s) = \frac{1}{(4\pi)^s} \sum_{l \geq 1} \frac{2l+1}{[l(l+1)]^s}. \quad (3.1.4.63)$$

In this case we just recall that for the Riemann zeta function

$$\zeta(s) := \sum_{k \geq 1} \frac{1}{k^s} = \frac{1}{s-1} + \gamma_{\mathbb{E}} + O(s-1) \quad (3.1.4.64)$$

so that

$$Z(s) = \frac{1}{4\pi(s-1)} - \frac{\ln(4\pi)}{4\pi} + \frac{\gamma_{\mathbb{E}}}{2\pi} - \frac{1}{4\pi} + O(s-1). \quad (3.1.4.65)$$

The Kronecker mass for the unit sphere is thus

$$K_{\mathbb{S}^2} = -\frac{\ln(4\pi)}{4\pi} + \frac{\gamma_E}{2\pi} - \frac{1}{4\pi}. \quad (3.1.4.66)$$

Projective sphere $\mathbb{P}\mathbb{S}$

The real projective sphere $\mathbb{P}\mathbb{S}^2$ is obtained from the sphere \mathbb{S}^2 by identification of antipodal points. The eigenfunctions of the Laplace-Beltrami operator are still the spherical harmonics $Y_{l,m}(\theta, \phi)$ with $l \in \mathbb{N}$ and $m \in \mathbb{Z}$, $-l \leq m \leq l$, but we have to restrict ourselves to eigenfunctions that invariant under the transformation $(\theta, \pi) \mapsto (\pi - \theta, \phi + \pi)$, i.e., to even values of l . Working on the unit-area sphere as before, we get the zeta function

$$\begin{aligned} Z(s) &= \frac{1}{(4\pi)^s} \sum_{l \geq 1} \frac{4l + 1}{[2l(2l + 1)]^s} \\ &= \frac{1}{4\pi(s-1)} - \frac{\ln(2\pi)}{4\pi} + \frac{\gamma_E}{2\pi} - \frac{1}{2\pi} + O(s-1) \end{aligned} \quad (3.1.4.67)$$

so that the Kronecker's mass is

$$K_{\mathbb{P}\mathbb{S}^2} = -\frac{\ln(2\pi)}{4\pi} + \frac{\gamma_E}{2\pi} - \frac{1}{2\pi}. \quad (3.1.4.68)$$

3.1.5. Numerical results

Assignment problems have been solved with the Jonker-Volgenant algorithm, which has complexity $O(n^3)$ (47) (i.e. the same of Gaussian elimination in linear algebra). For a domain Ω and \mathcal{N} independent instances, so that $E_n^{k,\Omega}(\pi^*|\mathcal{X},\mathcal{Y})$ is the k -th instance at size n , we fitted the data assuming

$$\frac{1}{2} \left(\frac{1}{\mathcal{N}} \sum_{k=1}^{\mathcal{N}} E_n^{k,\Omega}(\pi^*|\mathcal{X},\mathcal{Y}) - \frac{1}{2\pi} \log n \right) = c_\Omega + \frac{c_{1,\Omega}}{n} + \frac{c_{2,\Omega}}{n^2} \quad (3.1.5.1)$$

via least square linear regression (protocol: $n \in \{32, 64, \dots, 1024\}$ and $\mathcal{N} = 10^4$ instances for each n). Results for c_Ω have relative errors within 1%, and $c_\Omega - K_\Omega$ are compatible with each other within the errors for all considered domains. The smallest relative errors were observed for the cylinder and the Boy surface, for which (Tab. 3.1)

$$c^* = c_\Omega - K_\Omega = 0.2915(1). \quad (3.1.5.2)$$

	K_Ω	c_Ω	$c_\Omega - K_\Omega$
$\mathbb{T}(i)$	-0.2270289...	0.0653(9)	0.2923(9)
$\mathbb{T}(\exp(\frac{\pi i}{3}))$	-0.2287134...	0.064(2)	0.293(2)
$\mathbb{R}(1)$	0.0499556...	0.341(1)	0.291(1)
$\mathbb{C}(1)$	-0.1026239...	0.1889(1)	0.2915(1)
$\mathbb{M}(1)$	-0.1302033...	0.160(1)	0.290(1)
$\mathbb{K}(1)$	-0.2276239...	0.0646(8)	0.2922(8)
$\mathbb{B}(1)$	-0.2000444...	0.0915(1)	0.2915(1)
$\mathbb{D}(1)$	0.0098204...	0.302(1)	0.292(1)
\mathbb{S}	-0.1891233...	0.1016(9)	0.2908(9)
\mathbb{PS}	-0.2135418...	0.079(1)	0.292(1)

Table 3.1.: Kronecker mass and finite-size corrections c_Ω evaluated by numerical simulations of random assignments on different domains. In the last column, the difference between the finite-size correction and the Kronecker mass is given.

3.1.6. Uniform–Poisson transportation and grid effects

Up to now, we have considered the transportation between two sets of points uniformly generated on the given domain. A related and also interesting problem is the optimal transportation from the uniform measure on Ω to a set of n points (obtained by a Poisson process) on the same domain. We will refer to this problem as to the *Uniform–Poisson* (UP) problem. The functional approach described in Section 3.1 can be repeated to consider this case, substituting $\nu_y(x)$ with $\nu_u(x) = 1$ and observing then that in this case $\mathbb{E}[\delta\nu(x)\delta\nu(x)] = n^{-1}(\delta(x-y) - 1)$ [†]. The final expression for the cost is

$$E_n^u[\Omega] = \text{Tr } \Delta^{-1}, \quad (3.1.6.1)$$

that, upon regularization, reads

$$E_n^u[\Omega] = \frac{1}{4\pi} \ln n + c_\Omega^u + o(1). \quad (3.1.6.2)$$

The correctness of the leading term coefficient has been proven in Ref. (164). Eq. (3.1.6.1) differs from Eq. (3.1.0.12) by an overall factor 2: however, there is no guarantee that $c_\Omega = c_\Omega^u$ at fixed Ω as one might naively expect. One intuitive reason is that the nature of the transportation is, at small scale, different in the two problems. In Ref. (164) it is proved that

$$c_\Omega \leq c_\Omega^u. \quad (3.1.6.3)$$

As in the PP case, however, the value of the constant c_Ω^u is out of the reach of the linear approximation.

One way to numerically approximate the uniform distribution, and then estimate c_Ω^u , is to perform an assignment between two sets of points, supposing that one of them (e.g., the blue ones) is fixed on a grid and not random. We will call this version of the problem *Grid–Poisson* (GP) problem. The approach in Ref. (148) predicts indeed for this case the same Eq. (3.1.6.1), so that the average optimal cost is

$$E_n^g[\Omega] = \frac{1}{4\pi} \ln n + c_\Omega^g + o(1). \quad (3.1.6.4)$$

with a constant $c_\Omega^g \neq c_\Omega^u$. For example, let us consider the case of the unit square with $n = L^2$ and let us take a square grid, in positions $L^{-1}(1/2 + n, 1/2 + m)$, $n = 1, \dots, L$ and $m = 1, \dots, L$. In this case, we numerically estimate the constant

[†]That is, in this variant of the problem the density cross-correlation is halved with respect to the Poisson–Poisson case, in analogy with the discussion about Eq. 2.3.1.9.

to be

$$c_{\mathbb{R}}^g = 0.458(1), \quad (3.1.6.5)$$

The constant c_{Ω}^g however depends in general on the specific adopted grid and by

	K_{Ω}	c_{Ω}^g	$c_{\Omega}^g - K_{\Omega}$
$\mathbb{T}(i)$	-0.2270289...	0.1883(3)	0.4154(3)
$\mathbb{T}(\exp(\frac{\pi i}{3}))$	-0.2287134...	0.184(1)	0.413(1)
$\mathbb{R}(1)$	0.0499556...	0.458(1)	0.408(3)
$\mathbb{C}(1)$	-0.1026239...	0.3088(6)	0.4114(6)
$\mathbb{M}(1)$	-0.1302033...	0.281(1)	0.411(1)
$\mathbb{K}(1)$	-0.2276239...	0.1878(1)	0.4154(1)
$\mathbb{B}(1)$	-0.2000444...	0.2153(6)	0.4153(6)
\mathbb{D}	0.0098204...	0.423(3)	0.413(3)
\mathbb{S}	-0.1891233...	0.2255(8)	0.4146(8)
\mathbb{PS}	-0.2135418...	0.2022(8)	0.4157(8)

Table 3.2.: Kronecker mass and finite-size corrections c_{Ω}^g evaluated by numerical simulations of random assignments on different domains using a lattice. In the last column, the difference between the finite-size correction and the Kronecker mass is given. For all domains, except for the disc, the sphere and the projective sphere, a square lattice has been used: the corresponding difference $c_{\Omega}^g - K_{\Omega}$ is in this case domain-independent and equal to $c_{\Omega}^g - K_{\Omega} \simeq 0.413(2)$. In the case of the disc, we used a sunflower lattice (68).

the adopted boundary conditions. In Ref. (149) it has been observed numerically that, considering the constant $c_{\mathbb{T}}^g$ for the GP problem on the flat torus $\mathbb{T}(i)$, $c_{\mathbb{T}}^g \neq c_{\mathbb{R}}^g$, being

$$c_{\mathbb{T}}^g = 0.1879(3). \quad (3.1.6.6)$$

As in the case discussed in Section 3.1, we expect that the grid effects enter in the regularization in such a way that two domains covered with the same grid have the same grid-contribution to the finite-size corrections. We expect therefore that

$$c_{\Omega}^g = c_g^* + K_{\Omega}, \quad (3.1.6.7)$$

so that c_g^* depends on the adopted grid and K_{Ω} is the usual Kronecker's mass. This ansatz is numerically verified, when c_g^* is evaluated comparing different domains with the same grid (see Table 3.2). The results in Table 3.2 also suggest that the effects of the details of the grid are quite weak, although the presence of the grid makes $c_g^* \neq c^*$.

As aforementioned, the constants c_Ω^g are different from c_Ω^u . However, as intuitively expected, they provide some information on c_Ω^u . For example, by classical convexity properties of the squared Kantorovich distance, it can be proved that, given $n = L^2$ and considering a squared $L \times L$ grid on the unit flat 2-torus,

$$c_{\mathbb{T}}^g - \frac{1}{6} \leq c_{\mathbb{T}}^u \leq c_{\mathbb{T}}^g. \quad (3.1.6.8)$$

One can perform a transportation between a grid of cardinality M and a set of n random points. Proceeding in this way, it can be proved that the GP constant approaches the UP one for $M \gg n$ (see (172), Appendix A).

3.1.7. Section provisional conclusions

In this Section we have considered the random assignment problem of two sets of n points on a smooth, two-dimensional manifold Ω of unit area. Within the linearization framework of the field-theoretical formulation of the problem, we have studied the asymptotic series of the expected ground state energies beyond the known leading $\log n$ divergence. We have argued that, in the remainder, the first Ω -dependent finite size corrections contribute to the constant (in n) part of the expected ground state energy. These contributions can be computed exactly using zeta-regularization of the trace of the inverse Laplace-Beltrami operator on Ω in several variations. Our analysis, which has been applied to a number of different manifolds (from the unit square to the projective sphere) suggests the following picture: the remainder “splits” into an Ω independent part, depending on the choice of local randomness (among the ones considered in this section) and on the choice of grid; and a “geometric” correction depending only on the manifold Ω , and not on the local choice of randomness or grid. The latter quantity can be computed either directly as the Kronecker’s mass in zeta regularization, or as a Robin mass from the regular part of the appropriate Green function, the two constants differing by a universal constant, as established in a Theorem due to Morpurgo. Our numerical experiments strongly suggest that, indeed, (within our computational limitations) the remainder does not diverge with n (while it is currently only known that it diverges at most as $\sqrt{\log n \log \log n}$ (163)). A further investigation of such a remainder part (and possibly its limit value in the $n \rightarrow \infty$ limit) is an interesting open question.

3.2. On approximate linear relations among energies

3.2.1. General remarks

FOR a domain Ω , let $\{f_\lambda\}$ be an orthonormal basis of eigenfunctions of the Laplace-Beltrami operator $-\Delta$, λ the corresponding eigenvalues, and \mathcal{T} a unitary transformation of the basis, which commutes with $-\Delta$, and leaves invariant the uniform measure, that is

$$-\Delta f_\lambda = \lambda f_\lambda \implies -\Delta(\mathcal{T} \circ f_\lambda) = \lambda \mathcal{T} \circ f_\lambda. \quad (3.2.1.1)$$

and $d\nu(x) = d\nu(\mathcal{T}x)$ (where the action of \mathcal{T} on the coordinates is the action on the Dirac delta function, induced by the action on the basis).

Let ρ_1, ρ_2 be the empirical measures of two independent Poisson Point Processes of size n , and let $\rho_1^{\mathcal{T}}, \rho_2^{\mathcal{T}}$ be shortcuts for $\mathcal{T} \circ \rho_1, \mathcal{T} \circ \rho_2$. Let us also consider the shortcuts

$$(h, g) F_n = \sum_{\lambda} \frac{\hat{h}(\lambda) \hat{g}(\lambda)}{\lambda} F\left(\frac{\lambda}{n}\right) \quad (3.2.1.2)$$

and

$$(h, g) F_{an}^{bn} = (h, g) F_{bn} - (h, g) F_{an}, \quad (3.2.1.3)$$

where F is the unknown cutoff function of the field theoretical approach, and the Fourier coefficients

$$\hat{h}(\lambda) = \int_{\Omega} h f_\lambda \quad (3.2.1.4)$$

have been introduced.

Let us consider the following list of instances constructed from ρ_1 and ρ_2 :

instance	size	\mathcal{R}	\mathcal{B}
1	n	ρ_1	ρ_2
2	$2n$	$\rho_1 + \rho_1^{\mathcal{T}}$	$\rho_2 + \rho_2^{\mathcal{T}}$
3	$2n$	$\rho_1 + \rho_2$	$\rho_1^{\mathcal{T}} + \rho_2^{\mathcal{T}}$
4	n	ρ_1	$\rho_1^{\mathcal{T}}$
5	n	ρ_2	$\rho_2^{\mathcal{T}}$
6	n	ρ_1	$\rho_2^{\mathcal{T}}$
7	n	ρ_2	$\rho_1^{\mathcal{T}}$

Table 3.3.: The seven instances considered.

According to the linearized field theory, for a system at size αn , and distribution

of reds and blues $\rho_{\mathcal{R}}$ and $\rho_{\mathcal{B}}$, the energy of a single instance is given by

$$\begin{aligned} E[\rho_{\mathcal{B}}, \rho_{\mathcal{R}}] &= \frac{1}{\alpha n} \sum_{\lambda} \frac{1}{\lambda} |(\widehat{\rho_{\mathcal{R}} - \rho_{\mathcal{B}}})(\lambda)|^2 F\left(\frac{\lambda}{\alpha n}\right) \\ &= \frac{1}{\alpha n} (\rho_{\mathcal{B}} - \rho_{\mathcal{R}}, \rho_{\mathcal{B}} - \rho_{\mathcal{R}}) F_{\alpha n}, \end{aligned} \quad (3.2.1.5)$$

for some unknown cutoff function $F(x)$. Therefore

$$\begin{aligned} E_1 &= \frac{1}{n} (\rho_1 - \rho_2, \rho_1 - \rho_2) F_n \\ E_2 &= \frac{1}{2n} (\rho_1 + \rho_1^{\mathcal{T}} - \rho_2 - \rho_2^{\mathcal{T}}, \rho_1 + \rho_1^{\mathcal{T}} - \rho_2 - \rho_2^{\mathcal{T}}) F_{2n} \\ E_3 &= \frac{1}{2n} (\rho_1 + \rho_2 - \rho_1^{\mathcal{T}} - \rho_2^{\mathcal{T}}, \rho_1 + \rho_2 - \rho_1^{\mathcal{T}} - \rho_2^{\mathcal{T}}) F_{2n} \\ E_4 &= \frac{1}{n} (\rho_1 - \rho_1^{\mathcal{T}}, \rho_1 - \rho_1^{\mathcal{T}}) F_n \\ E_5 &= \frac{1}{n} (\rho_2 - \rho_2^{\mathcal{T}}, \rho_2 - \rho_2^{\mathcal{T}}) F_n \\ E_6 &= \frac{1}{n} (\rho_1 - \rho_2^{\mathcal{T}}, \rho_1 - \rho_2^{\mathcal{T}}) F_n \\ E_7 &= \frac{1}{n} (\rho_2 - \rho_1^{\mathcal{T}}, \rho_2 - \rho_1^{\mathcal{T}}) F_n. \end{aligned} \quad (3.2.1.6)$$

Since \mathcal{T} is unitary, we have

$$(\rho_i^{\mathcal{T}}, \rho_j^{\mathcal{T}}) F_n = (\rho_i, \rho_j) F_n, \quad (3.2.1.7)$$

for all $i, j \in \{1, 2\}$, and all $a > 0$, and hence we can identify the different contributions as follows (we consider only combinations which are symmetric under exchange of ρ_1 and ρ_2):

	E_1	E_2	E_3	$E_4 + E_5$	$E_6 + E_7$
$[(\rho_1, \rho_1) + (\rho_2, \rho_2)] F$	$\frac{1}{n} (\dots) F_n$	$\frac{2}{2n} (\dots) F_{2n}$	$\frac{2}{2n} (\dots) F_{2n}$	$\frac{2}{n} (\dots) F_n$	$\frac{2}{n} (\dots) F_n$
$[(\rho_1, \rho_2) + \text{c.c.}] F$	$-\frac{1}{n} (\dots) F_n$	$-\frac{2}{2n} (\dots) F_{2n}$	$\frac{2}{2n} (\dots) F_{2n}$	0	0
$(\rho_1, \rho_1^{\mathcal{T}}) + (\rho_2, \rho_2^{\mathcal{T}}) + \text{c.c.}] F$	0	$\frac{1}{2n} (\dots) F_{2n}$	$-\frac{1}{2n} (\dots) F_{2n}$	$-\frac{1}{n} (\dots) F_n$	0
$(\rho_1, \rho_2^{\mathcal{T}}) + (\rho_1^{\mathcal{T}}, \rho_2) + \text{c.c.}] F$	0	$-\frac{1}{2n} (\dots) F_{2n}$	$-\frac{1}{2n} (\dots) F_{2n}$	0	$-\frac{1}{n} (\dots) F_n$

Table 3.4.: (Part [1/2]). Contributions entering in our list of energies Tab. 3.3 (c.c. denotes complex conjugate of preceding expression).

Our goal is to devise linear combinations in which the terms combine into expressions of the form $(f, g)F_n^{2n}$. In this respect, we should analyse the (left) kernel of the matrix

	E_1	E_2	E_3	$E_4 + E_5$	$E_6 + E_7$
$[(\rho_1, \rho_1) + (\rho_2, \rho_2)] F$	1	1	1	2	2
$[(\rho_1, \rho_2) + \text{c.c.}] F$	-1	-1	1	0	0
$[(\rho_1, \rho_1^T) + (\rho_2, \rho_2^T) + \text{c.c.}] F$	0	1/2	-1/2	-1	0
$[(\rho_1, \rho_2^T) + (\rho_1^T, \rho_2) + \text{c.c.}] F$	0	-1/2	-1/2	0	-1

The kernel is generated by the vectors $v_1 = (0, 1, 1, 0, -1)$ and $v_2 = (2, -1, 1, -1, 0)$. Indeed, if we analyse the quantity associated to v_1 , we get

$$\begin{aligned}
\delta E^{(1)} &:= 2E_1 - E_2 + E_3 - E_4 - E_5 \\
&= \frac{1}{n} \left\{ -2 [(\rho_1, \rho_2) + \text{c.c.}] (F_n - F_{2n}) + [(\rho_1, \rho_1^T) + (\rho_2, \rho_2^T) + \text{c.c.}] (F_n - F_{2n}) \right\} \\
&= \frac{1}{n} [(\rho_1 - \rho_2^T, \rho_1 - \rho_2^T) + (\rho_2 - \rho_1^T, \rho_2 - \rho_1^T)] (F_{2n} - F_n) \\
&= \frac{1}{n} \sum_{\lambda} \frac{1}{\lambda} \left(|\widehat{(\rho_1 - \rho_2^T)}(\lambda)|^2 + |\widehat{(\rho_2 - \rho_1^T)}(\lambda)|^2 \right) \left(F \left(\frac{\lambda}{2n} \right) - F \left(\frac{\lambda}{n} \right) \right).
\end{aligned} \tag{3.2.1.8}$$

This expression has the form that we are demanding. The consequence of this fact is that, in the field-theoretical perspective, it takes contributions only from large momenta, $n \lesssim \lambda \lesssim 2n$, and hence is analogous to a shift in the free energy that one would get from implementing the flow of the renormalisation group on the two systems E_6 and E_7 (by a scaling factor $1/\sqrt{2}$).

More concretely, as we see in a moment, this stochastic quantity will turn out to be expressed as a deterministic shift of order 1, plus a zero-mean stochastic shift of variance $O(\frac{1}{n})$.

The deterministic shift can be easily computed taking averages. For example, at $d = 1$ we immediately get that such shift is zero since $F = 1$ independently on n (recall that the sum over the modes is convergent there). At $d = 2$ we get

$$\begin{aligned}
\left\langle \frac{1}{n} \sum_{\lambda} \frac{1}{\lambda} |\widehat{(\rho_1 - \rho_2^T)}(\lambda)|^2 F \left(\frac{\lambda}{n} \right) \right\rangle &\approx \frac{2}{2\pi} \int_{0^+}^{\sqrt{n}} \frac{d\lambda}{\lambda} = \frac{2}{2\pi} \left(\frac{1}{2} \log n + c \right) \\
\left\langle \frac{1}{n} \sum_{\lambda} \frac{1}{\lambda} |\widehat{(\rho_1 - \rho_2^T)}(\lambda)|^2 F \left(\frac{\lambda}{2n} \right) \right\rangle &\approx \frac{2}{2\pi} \int_{0^+}^{\sqrt{2n}} \frac{d\lambda}{\lambda} = \frac{2}{2\pi} \left(\frac{1}{2} \log 2n + c \right)
\end{aligned} \tag{3.2.1.9}$$

from which we get

$$\langle \delta E^{(1)} \rangle = \langle 2E_1 - E_2 + E_3 - E_4 - E_5 \rangle \approx \frac{\log 2}{2\pi} = 0.110317\dots \quad (3.2.1.10)$$

Numerical data corresponding to this combination is reported in Fig. 3.9.

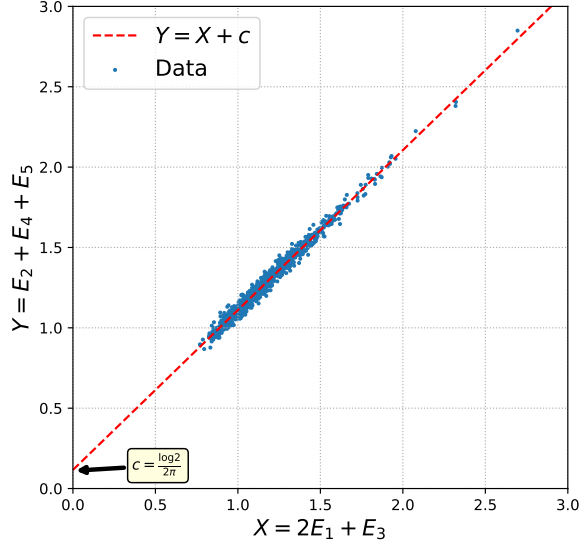


Figure 3.9. – Typical scatter plot of numerical data ($n = 10^3$, 10^3 points) corresponding to $\delta E^{(1)}$ (Eq. 3.2.1.8) for a domain with an involution (see § 3.2.3).

Another vector in the kernel is the combination $(-1, 1, 0, \frac{1}{2}, -\frac{1}{2})$, that is

$$\delta E^{(2)} := -E_1 + E_2 + \frac{1}{2}(E_4 + E_5) - \frac{1}{2}(E_6 + E_7) \quad (3.2.1.11)$$

which, by calculations analogous to the ones performed above, gives

$$\begin{aligned} \delta E^{(2)} &:= -E_1 + E_2 + \frac{1}{2}(E_4 + E_5) - \frac{1}{2}(E_6 + E_7) \\ &= \frac{1}{n} \sum_{\lambda} \frac{1}{\lambda} |(\hat{\rho}_1 + \hat{\rho}_1^{\mathcal{T}} - \hat{\rho}_2 - \hat{\rho}_2^{\mathcal{T}})(\lambda)|^2 \left(F\left(\frac{\lambda}{2n}\right) - F\left(\frac{\lambda}{n}\right) \right), \end{aligned} \quad (3.2.1.12)$$

which now is analogous to a shift in the free energy that one would get from implementing the flow of the renormalisation group on the systems E_2 . This combination has a small simplification in the case in which \mathcal{T} is an involution, which implies $(f^{\mathcal{T}}, g) = (f, g^{\mathcal{T}})$ and in particular $E_6 = E_7$.

In § 3.2.3, the average of $\delta E^{(2)}$ is considered in details in some examples of domains with an involution.

3.2.2. On linear relations in domains with no symmetries

In the previous section we have considered linear relations emerging from the combination of two point distributions, ρ_1 and ρ_2 , and one unitary transformation on the domain, \mathcal{T} . In this section we show that similar relations exist also in absence of the transformation \mathcal{T} , at the price of combining now four point distributions, ρ_1, \dots, ρ_4 .

Let ρ_1, ρ_2 be the empirical measures of two independent Poisson Point Processes of size n , and let ρ_3, ρ_4 be the empirical measures associated of two independent Poisson Point Processes of size m . Note that n and m may differ.

Let us consider the following list of instances constructed from ρ_1, \dots, ρ_4 :

instance	size	\mathcal{R}	\mathcal{B}
1 2	n	ρ_1	ρ_2
3 4	m	ρ_3	ρ_4
13 24	$n + m$	$\rho_1 + \rho_3$	$\rho_2 + \rho_4$
14 23	$n + m$	$\rho_1 + \rho_4$	$\rho_2 + \rho_3$

Table 3.5.: The four instances considered.

Repeating the reasonings of the previous section, we get

$$\begin{aligned}
 E_{1|2} &= \frac{1}{n} (\rho_1 - \rho_2, \rho_1 - \rho_2) F_n \\
 E_{3|4} &= \frac{1}{m} (\rho_3 - \rho_4, \rho_3 - \rho_4) F_m \\
 E_{13|24} &= \frac{1}{n + m} (\rho_1 + \rho_3 - \rho_2 - \rho_4, \rho_1 + \rho_3 - \rho_2 - \rho_4) F_{n+m} \\
 E_{14|23} &= \frac{1}{n + m} (\rho_1 + \rho_4 - \rho_2 - \rho_3, \rho_1 + \rho_4 - \rho_2 - \rho_3) F_{n+m}.
 \end{aligned} \tag{3.2.2.1}$$

Again, we identify the various contributions as follows:

	$[(\rho_1, \rho_1) + (\rho_2, \rho_2)] F$	$[(\rho_3, \rho_3) + (\rho_4, \rho_4)] F$	$[(\rho_i, \rho_j) + \text{c.c.}] F$
$E_{1 2}$	$\frac{1}{n} (\dots) F_n$	0	$-\frac{1}{n} (\cdot 1, 2) F_n$
$E_{3 4}$	0	$\frac{1}{m} (\dots) F_m$	$-\frac{1}{m} (\cdot 3, 4) F_m$
$E_{13 24}$	$\frac{1}{n+m} (\dots) F_{n+m}$	$\frac{1}{n+m} (\dots) F_{n+m}$	$\frac{1}{n+m} [- (\cdot 1, 2) + (\cdot 1, 3) - (\cdot 1, 4) - (\cdot 2, 3) + (\cdot 2, 4) - (\cdot 3, 4)] F_{n+m}$
$E_{14 23}$	$\frac{1}{n+m} (\dots) F_{n+m}$	$\frac{1}{n+m} (\dots) F_{n+m}$	$\frac{1}{n+m} [- (\cdot 1, 2) - (\cdot 1, 3) + (\cdot 1, 4) + (\cdot 2, 3) - (\cdot 2, 4) - (\cdot 3, 4)] F_{n+m}$

Table 3.6.: Contributions entering in our list of energies (c.c. denotes complex conjugate of preceding expression).

Again, our goal is to devise linear combinations in which the terms combine into expressions of the form $(f, g) F_m^{n+m}$ or $(f, g) F_n^{n+m}$. In this respect, calling $\tau = \frac{n}{n+m}$,

we should analyse the (left) kernel of the matrix

$E_{1 2}$	$\frac{1}{\tau}$	0	$-\frac{1}{\tau}$	0	0	0	0	0
$E_{3 4}$	0	$\frac{1}{1-\tau}$	0	0	0	0	0	$-\frac{1}{1-\tau}$
$E_{13 24}$	1	1	-1	1	-1	-1	1	-1
$E_{14 23}$	1	1	-1	-1	1	1	-1	-1

Now the kernel is generated by a unique vector, $(-2\tau, -2(1-\tau), 1, 1)$. Indeed, if we analyse the quantity associated to this vector, we get

$$\begin{aligned}
\delta E^{(3)} &:= -2\tau E_{1|2} - 2(1-\tau)E_{3|4} + E_{13|24} + E_{14|23} \\
&= \frac{1}{n+m} \{(\rho_1 - \rho_2, \rho_1 - \rho_2) F_n^{n+m} + (\rho_3 - \rho_4, \rho_3 - \rho_4) F_m^{n+m}\} \\
&= \frac{1}{n+m} \sum_{\lambda} \frac{1}{\lambda} \left[|(\widehat{\rho_1 - \rho_2})(\lambda)|^2 \left(F\left(\frac{\lambda}{n+m}\right) - F\left(\frac{\lambda}{n}\right) \right) + \right. \\
&\quad \left. + |(\widehat{\rho_3 - \rho_4})(\lambda)|^2 \left(F\left(\frac{\lambda}{n+m}\right) - F\left(\frac{\lambda}{m}\right) \right) \right]. \tag{3.2.2.2}
\end{aligned}$$

This expression has the form that we are demanding. The consequence of this fact is that, in the field-theoretical perspective, if both n and m are large, it takes contributions only from large momenta, $n, m \lesssim \lambda \lesssim n+m$, and hence is analogous to a shift in the free energy that one would get from implementing the flow of the renormalisation group on the two systems $E_{1|2}$ (by a scaling factor $\sqrt{\tau}$) and $E_{3|4}$ (by a scaling factor $\sqrt{1-\tau}$). And also, yet again, this stochastic quantity will turn out to be expressed as a deterministic shift of order 1 (which is a function of τ), plus a zero-mean stochastic shift of variance $O\left(\frac{1}{n} + \frac{1}{m}\right)$. As previously, the deterministic shift can be easily computed taking averages, and at $d = 1$ is zero since $F = 1$ as the sum over the modes is convergent there. At $d = 2$ we get

$$\left\langle \frac{1}{n} \sum_{\lambda} \frac{1}{\lambda} |(\widehat{\rho_i - \rho_j})(\lambda)|^2 F\left(\frac{\lambda}{n}\right) \right\rangle \approx \frac{2}{2\pi} \int_{0^+}^{\sqrt{n}} \frac{d\lambda}{\lambda} = \frac{2}{2\pi} \left(\frac{1}{2} \log n + c \right) \tag{3.2.2.3}$$

from which we have

$$\begin{aligned}
\langle \delta E^{(3)} \rangle &= \langle -2\tau E_{1|2} - 2(1-\tau)E_{3|4} + E_{13|24} + E_{14|23} \rangle \\
&\approx \frac{2}{2\pi} \left[\left(\frac{1}{2} \log(n+m) + c \right) (-2\tau - 2(1-\tau) + 1 + 1) + \tau \log \tau + (1-\tau) \log(1-\tau) \right] \\
&= \frac{2}{2\pi} [\tau \log \tau + (1-\tau) \log(1-\tau)] \tag{3.2.2.4}
\end{aligned}$$

In terms of the parameter $\alpha = \frac{1-\tau}{\tau} = \frac{m}{n}$, we get the expression

$$f_\alpha := \frac{1+\alpha}{2} \langle \delta E^{(3)} \rangle = \frac{1}{2\pi} (\alpha \log \alpha - (1+\alpha) \log(1+\alpha)) \quad (3.2.2.5)$$

which is easily confirmed by numerical experiments * (Fig. 3.10).

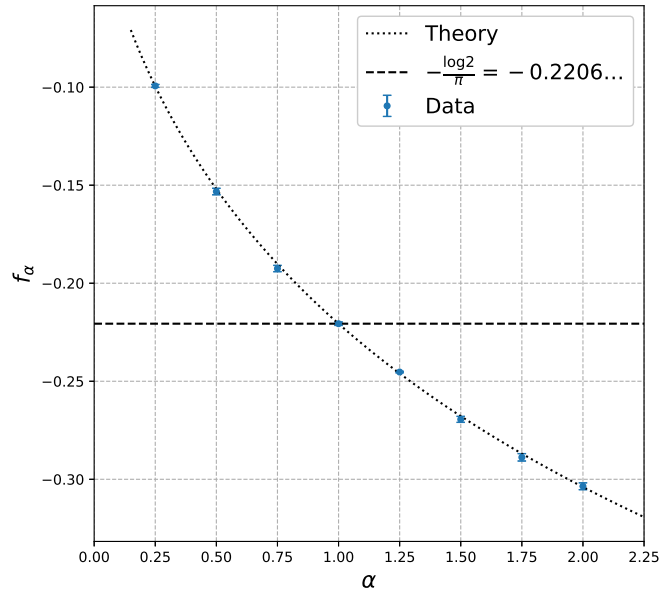


Figure 3.10. – Comparison of Eq. 3.2.2.5 (dotted black line) and results of numerical experiments, obtained by a linear fit as in Fig. 3.9 (blue dots with error bars). The horizontal black, dashed line denotes the value when the two involved sets have the same cardinality, $\alpha = 1$ ($\tau = 1/2$).

3.2.3. Kronecker masses in the case of involutions

Let us consider domains Ω for which a natural involution I exists, that is, a map $I : \Omega \rightarrow \Omega$ such that $I(I(z)) = z, \forall z \in \Omega$. Instead of the cutoff function regularization approach of § 3.2.1, in this section we will work in zeta regularization to compute the Kronecker masses (in analogy with § 3.1), and then exploit the relations between different models and the parity of the relevant contributions under I to obtain Eq. 3.2.1.11.

*Numerical protocol: $\alpha \in \{\frac{1}{4}, \frac{1}{2}, \dots, 2\}$, $n \in \{32, 64, \dots, 512\}$ and 10^3 realizations for each (n, α) point. At fixed α , f_α extracted by a quadratic fit (least square) of $\langle \frac{1+\alpha}{2} (E_{13|24} + E_{14|23}) - E_{1|2} - \alpha E_{3|4} \rangle$ in $1/n$.

We will assume that I admits a set of fixed points of zero d -dimensional Lebesgue measure, so that, for $\Omega' = I(\Omega)$, we can write $\Omega'' = \Omega \setminus \Omega'$. In order to fulfill the requirement of Eq. 3.2.1.1 we will assume that I preserves the appropriate boundary conditions for the Poisson equation. Let us consider the following examples.

Example 1 Let $\Omega = \mathbb{T}(1)$ be the 2-torus of aspect ratio 1 and let the involution I be

$$\begin{cases} r_{i,x} = b_{i,x} + \frac{1}{2} \pmod{1} \\ r_{i,y} = b_{i,y} \end{cases} \quad i = 1, \dots, n. \quad (3.2.3.1)$$

so that $\Omega' = [0, \frac{1}{2}] \times [0, 1]$. The eigenfunctions of Δ are factorized along the two coordinate directions, so that in our choice only the factor depending on x matters. In this case we have all the eigenfunctions, i.e. both ‘‘sines and cosines’’ $e^{2\pi il}$, and they are odd or even according to the parity of l as an integer.

Example 2 Let $\Omega = \mathbb{S}^2$ be the 2-sphere of unit area (i.e. the sphere of radius $\frac{1}{2\sqrt{\pi}}$). I is the antipodal map $z \mapsto -z$ acting in spherical coordinates as

$$\begin{cases} \theta_{r_i} = \pi - \theta_{b_i} \\ \phi_{r_i} = \pi + \phi_{b_i} \end{cases} \quad i = 1, \dots, n, \quad (3.2.3.2)$$

where $\theta_{r_i(b_i)} \in [0, \pi)$ is the colatitude of r_i (resp. b_i) and $\phi_{r_j(b_j)} \in [0, 2\pi)$ is the longitude of r_j (resp. b_j). In this case Ω' can be chosen to be the northern hemisphere $z \geq 0$ w.l.o.g., and the eigenfunctions are the spherical harmonics $Y_{lm}(\theta, \phi)$ with l an integer.

Example 3 Let $\Omega = \mathbb{S}^2$ and I the rotation of π along the z axis, that is

$$\begin{cases} \theta_{r_i} = \theta_{b_i} \\ \phi_{r_i} = \pi + \phi_{b_i} \end{cases} \quad i = 1, \dots, n \quad (3.2.3.3)$$

for $\theta_{r_i(b_i)}$ and $\phi_{r_j(b_j)}$ as in Example 2. Now the eigenfunctions are $Y_{lm} \pm Y_{l-m}$, where the \pm sign corresponds to the parity under I . Instances at small n for Examples 2 and 3 are given in Fig. 3.11.

In the case of involutions, recalling that $\{f_\lambda\}_\lambda$ is the basis of eigenvectors of $-\Delta$, we can just write

$$\delta\rho(z) = \sum_\lambda \delta\rho_\lambda f_\lambda(z) = \sum_\lambda \delta\rho_{\lambda,+} f_{\lambda,+}(z) + \sum_\lambda \delta\rho_{\lambda,-} f_{\lambda,-}(z), \quad (3.2.3.4)$$

where \pm denotes parity under I . For $\{\lambda_k\}_k$ the Laplacian spectrum, for large n

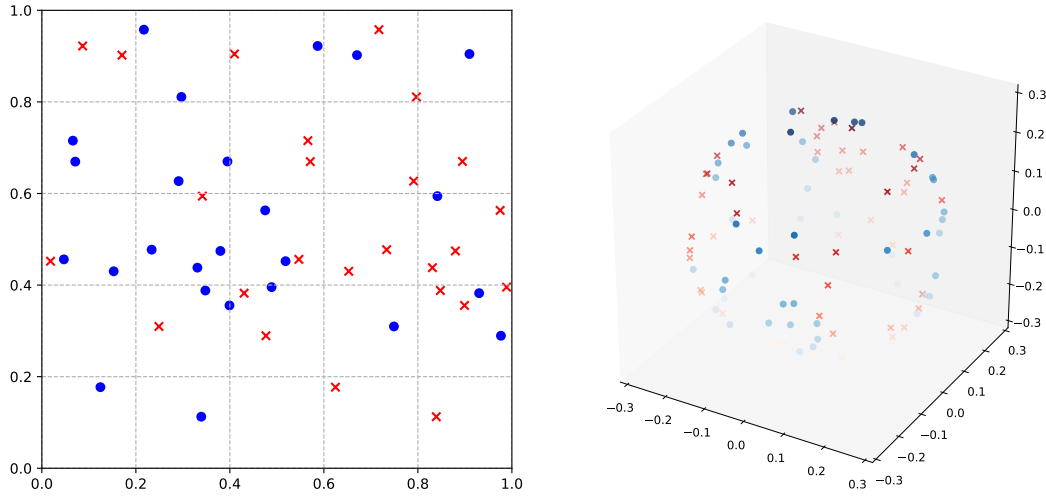


Figure 3.11. – (Left) An instance from Example 2 ($n = 25$). (Right) An instance from Example 3 ($n = 50$).

the (non-regularized) energy of a single instance can be written as

$$E = n \sum_{k \neq 0} \frac{|\delta \rho_k|^2}{\lambda_k} = n \left(\sum_{k \neq 0} \frac{|\delta \rho_{k,+}|^2}{\lambda_k} + \sum_k \frac{|\delta \rho_{k,-}|^2}{\lambda_k} \right) \quad (3.2.3.5)$$

where we are summing over the modes orthogonal to the zero mode(s).

For the problem with charge densities $\rho_{\mathcal{R}}(z)$ and $\rho_{\mathcal{B}}(z)$ and involution I we consider the 5 energies:

► E_1 : the “usual” Poisson-Poisson case where \mathcal{B} and \mathcal{R} are not related, that is

$$\delta \rho^{(1)}(z) = \rho_{\mathcal{R}}(z) - \rho_{\mathcal{B}}(z), \quad (3.2.3.6)$$

and hence

$$E_1 = n \left(\sum_{k \neq 0} \frac{|\rho_{\mathcal{R},k,+} - \rho_{\mathcal{B},k,+}|^2}{\lambda_k} + \sum_k \frac{|\rho_{\mathcal{R},k,-} - \rho_{\mathcal{B},k,-}|^2}{\lambda_k} \right). \quad (3.2.3.7)$$

► E_2 : This is the instance at size $2n$ in which the starting points \mathcal{B} and \mathcal{R} are complemented with their images under I , i.e. we consider the assignment of $\mathcal{B}' = \mathcal{B} \cup I(\mathcal{B})$ to $\mathcal{R}' = \mathcal{R} \cup I(\mathcal{R})$. In this case

$$\delta \rho^{(5)}(z) = \frac{\rho_{\mathcal{R}}(z) + \rho_{\mathcal{R}}(I(z)) - \rho_{\mathcal{B}}(z) - \rho_{\mathcal{B}}(I(z))}{2} \quad (3.2.3.8)$$

so that only the even parts under I survive, giving

$$E_2 = 2n \sum_{k \neq 0} \frac{|\rho_{\mathcal{B},k,+} - \rho_{\mathcal{R},k,+}|^2}{\lambda_k}. \quad (3.2.3.9)$$

► E_4 : now \mathcal{B} are distributed according to $\rho_{\mathcal{R}}(I(z))$, so that

$$\delta\rho^{(3)}(z) = \rho_{\mathcal{R}}(z) - \rho_{\mathcal{R}}(I(z)) = -\delta\rho^{(3)}(I(z)) \quad (3.2.3.10)$$

is odd under I , and hence

$$E_4 = 4n \sum_k \frac{|\rho_{\mathcal{R},k,-}|^2}{\lambda_k}. \quad (3.2.3.11)$$

► E_5 : same as above, but with $\mathcal{B} \leftrightarrow \mathcal{R}$, and hence

$$E_5 = 4n \sum_k \frac{|\rho_{\mathcal{B},k,-}|^2}{\lambda_k}. \quad (3.2.3.12)$$

► E_7 : now $\rho_{\mathcal{R}}(z) = \rho_{\mathcal{R}}(I(z))$, so that

$$\delta\rho^{(2)}(z) = \rho_{\mathcal{R}}(I(z)) - \rho_{\mathcal{B}}(z) \quad (3.2.3.13)$$

and

$$E_7 = n \left(\sum_{k \neq 0} \frac{|\rho_{\mathcal{R},k,+} - \rho_{\mathcal{B},k,+}|^2}{\lambda_k} + \sum_k \frac{|\rho_{\mathcal{R},k,-} + \rho_{\mathcal{B},k,-}|^2}{\lambda_k} \right). \quad (3.2.3.14)$$

We remark that $E_6 = E_7$ for an involution.

Example 1

Let us consider first the one dimensional torus, for which $f_l(z) = e^{2\pi ilz}$ with $l \in \mathbb{Z}$, so that the parity under I is just the parity of l as an integer. We have for the unrestricted sums

$$\langle E_1 \rangle = \langle E_7 \rangle = \frac{1}{\pi^2} \sum_{l=1}^{\infty} \frac{1}{l^2} = \frac{1}{\pi^2} \zeta(2) = \frac{1}{6}, \quad (3.2.3.15)$$

as is well-known. The sum over the odd modes gives

$$\langle E_4 \rangle = \langle E_5 \rangle = \frac{2}{\pi^2} \sum_{l=0}^{\infty} \frac{1}{(2l+1)^2} = \frac{1}{4} \quad (3.2.3.16)$$

while the sum over even modes gives

$$\langle E_2 \rangle = \frac{2}{\pi^2} \sum_{l=1}^{\infty} \frac{1}{(2l)^2} = \frac{1}{12} \quad (3.2.3.17)$$

so that in one dimension we get

$$\begin{aligned} \langle \delta E^{(2)} \rangle &= \left\langle -E_1 + E_2 + \frac{1}{2}(E_4 + E_5) - E_7 \right\rangle = -\frac{1}{6} + \frac{1}{12} + \frac{1}{2} \left(\frac{1}{4} + \frac{1}{4} \right) - \frac{1}{6} \\ &= \frac{-2 + 1 + 3 - 2}{12} = 0 \end{aligned} \quad (3.2.3.18)$$

as expected.

For the two-dimensional torus, recall that the spectral zeta function (Eq. 3.1.4.13) satisfies, at aspect ratio 1,

$$\begin{aligned} 2 \sum_{k \neq 0} \frac{1}{\lambda_k^s} &= \frac{2}{(2\pi)^{2s}} \sum_{(n,m) \neq (0,0)} \frac{1}{(n^2 + m^2)^s} \\ &= \frac{8}{(2\pi)^{2s}} \sum_{n,m=1}^{\infty} \frac{1}{(n^2 + m^2)^s} + \frac{8}{(2\pi)^{2s}} \sum_{l \geq 1} \frac{1}{l^{2s}} \\ &= \frac{2}{(2\pi)^{2s}} \left[\frac{\pi}{s-1} + 2\pi (\gamma_E - \log 2 |\eta(i)|^2) \right] + o(s-1) \end{aligned} \quad (3.2.3.19)$$

where η is Dedekind's function. Therefore, around $s = 1$, we get for the unrestricted sums

$$\langle E_1 \rangle = \langle E_7 \rangle = \frac{1}{2\pi(s-1)} + \frac{1}{\pi} [\gamma_E + \log \sqrt{\pi} - 2 \log \Gamma(1/4)] + o(s-1) \quad (3.2.3.20)$$

where we can directly read the Kronecker mass. The sum over the odd modes is

$$\frac{8}{(2\pi)^{2s}} \sum_{n=0}^{\infty} \sum_{m=1}^{\infty} \frac{1}{[(2n+1)^2 + m^2]^s} + \frac{4}{(2\pi)^{2s}} \sum_{l=0}^{\infty} \frac{1}{(2l+1)^{2s}} \quad (3.2.3.21)$$

so that, expanding around $s = 1$, we get

$$\langle E_4 \rangle = \langle E_5 \rangle = \frac{1}{2\pi(s-1)} + \frac{1}{\pi} \left[\gamma_E + \frac{1}{2} \log \sqrt{2} + \frac{1}{2} \log \pi - 2 \log \Gamma(1/2) \right] + o(s-1). \quad (3.2.3.22)$$

Lastly, the sum over the even modes is

$$\begin{aligned} &= \frac{2}{(2\pi)^{2s}} \sum_{(n,m) \neq (0,0)} \frac{1}{(4n^2 + m^2)^s} \\ &= \frac{8}{(2\pi)^{2s}} \sum_{n=1}^{\infty} \sum_{m=1}^{\infty} \frac{1}{[4n^2 + m^2]^s} + \frac{4}{(2\pi)^{2s}} \sum_{l=0}^{\infty} \frac{1}{(2l)^{2s}} + \frac{4}{(2\pi)^{2s}} \sum_{n=1}^{\infty} \frac{1}{n^{2s}} \quad (3.2.3.23) \\ &= \frac{2^{1-s}}{(2\pi)^{2s}} \left[\frac{\pi}{s-1} + 2\pi \left(\gamma_E - \log(2\sqrt{2}|\eta(2i)|^2) \right) \right] + o(s-1) \end{aligned}$$

so that near $s = 1$ we get

$$\langle E_2 \rangle = \frac{1}{2\pi(s-1)} + \frac{1}{\pi} \left[\gamma_E - \frac{1}{2} \log \sqrt{2} + \frac{1}{2} \log \pi - 2 \log \Gamma(1/4) \right] + o(s-1). \quad (3.2.3.24)$$

Reminding that at leading order $\langle E_2 \rangle \sim \frac{\log 2n}{2\pi}$ (since in instance 2 the size is $2n$), we just have

$$\langle E_2 \rangle = \langle E_4 \rangle = \langle E_5 \rangle \quad (3.2.3.25)$$

so that

$$\langle \delta E^{(2)} \rangle = \frac{\log 2}{2\pi} \quad (3.2.3.26)$$

as expected.

Example 2

The discussion of § 3.2.3 is extended almost verbatim to Example 2. Now the eigenfunctions of $-\Delta$ are the spherical harmonics Y_{lm} and their parity under I is just the parity of l as an integer. Now the unrestricted sum over all (i.e. both even and odd under I) modes gives

$$\begin{aligned} \langle E_1 \rangle &= \langle E_7 \rangle \\ &= \frac{2}{(4\pi)^s} \sum_{l=1}^{\infty} \frac{2l+1}{[l(l+1)]^2} = \frac{1}{2\pi(s-1)} + \frac{1}{\pi} \left[\gamma_E - \frac{1}{2} \log(4\pi) - \frac{1}{2} \right] + o(s-1), \end{aligned} \quad (3.2.3.27)$$

the sum over the odd modes gives

$$\begin{aligned} \langle E_4 \rangle &= \langle E_5 \rangle = \frac{4}{(4\pi)^s} \sum_{l=1}^{\infty} \frac{4l-1}{[2l(2l-1)]^s} \\ &= \frac{16}{(16\pi)^s} \sum_{l=1}^{\infty} \frac{1}{l^{2s-1}} + \frac{1}{\pi} \sum_{l=1}^{\infty} \left(\frac{4l-1}{2l(2l-1)} - \frac{1}{l} \right) + o(s-1) \quad (3.2.3.28) \\ &= \frac{1}{2\pi(s-1)} + \frac{1}{\pi} \left(\gamma_E - \frac{1}{2} \log(4\pi) \right) + o(s-1), \end{aligned}$$

and the sum over the even modes gives

$$\begin{aligned} \langle E_2 \rangle &= \frac{4}{(4\pi)^s} \sum_{l=1}^{\infty} \frac{4l+1}{[2l(2l+1)]^s} \\ &= \frac{16}{(16\pi)^s} \sum_{l=1}^{\infty} \frac{1}{l^{2s-1}} + \frac{1}{\pi} \sum_{l=1}^{\infty} \left(\frac{4l+1}{2l(2l+1)} - \frac{1}{l} \right) + o(s-1) \quad (3.2.3.29) \\ &= \frac{1}{2\pi(s-1)} + \frac{1}{\pi} \left(\gamma_E - \frac{1}{2} \log(4\pi) - 1 \right) + o(s-1). \end{aligned}$$

Recalling that at size $2n$

$$\langle E_2 \rangle = \frac{\log 2}{2\pi} + \frac{\log n}{2\pi} + \frac{1}{\pi} \left(\gamma_E - \frac{1}{2} \log(4\pi) - 1 \right) + o(1) \quad (3.2.3.30)$$

we find again

$$\langle \delta E^{(2)} \rangle = \frac{\log 2}{2\pi}. \quad (3.2.3.31)$$

An analogous calculation can be done for Example 3. The predictions of Eqs. 3.2.3.26 and 3.2.3.31 are in good agreement with results of extremely simple numerical ex-

periments, which are reported in Tab. 3.7.

Example	$\langle \delta E^{(2)} \rangle$ (Eq. 3.2.1.11)
1	0.111(1)
2	0.110(1)
3	0.108(1)
Eq. Tr., ρ_h	0.109(1)
$\log 2/2\pi$	0.110317...

Table 3.7.: Numerical results for Eq. 3.2.1.11 for different involutions in $d = 2$. “Eq. Tr.” denotes a (unit area) equilateral triangle and $\rho_h = I$ denotes a reflexion along a height. Numerical protocol: $n = 1000$, 1000 disorder realizations, direct average of Eq. 3.2.1.11.

3.2.4. Section provisional conclusions

In this Section we have shown that, within the context of the field-theoretic approach to the Euclidean Random Assignment Problem, unitary symmetries can be exploited to build certain (simple) linear combinations of energies with rational coefficients, which evaluate to a deterministic constant plus a (small) stochastic error. In the case of an involutive symmetry I , the linear relations hold due to cancellations among unrestricted, odd and even modes under I , in the common basis of the Laplace-Beltrami operator, as we have shown explicitly in zeta regularization. Our findings can be of interest since, while the linear relations are exact at a single instance in the continuum theory, they are only approximate at finite n , due to the non-linear contributions which are neglected by the linearization in the field theoretic approach, and can be thus useful to study such non-linearities in great generality. As a by-product, due to their simplicity and robustness, the linear relations can be used as an easy numerical protocol to unveil possible logarithmic scaling of the ground state energy in less studied regimes at $p = 2$ at $d \neq 2$ (an example will be discussed in § 4.6).

3.3. The Lattice Helmholtz decomposition of the transport field on \mathbb{T}_2 at $p = 2$

IN the previous Section we have considered the ERAP for several two dimensional compact geometries and discussed a persistence of universality beyond the leading asymptotics by considering a functional analytical and a zeta regularization of the logarithmically divergent ground state energy. Among other things, we have shown that the relative ground state energies for domains with rectangular fundamental polygons at varying aspect ratios are given exactly in terms of certain logarithmic ratios of the Dedekind η function (provided the domains have the same area). However, the overall constant, common to all these domains, cannot be determined with the methods of the previous sections, and remains elusive (we cannot even exclude that it is not a constant, but rather a slowly-increasing function of n).

In this Section we wish to investigate further the grid-regularization approach. Somehow in analogy with § 2.3, we will set aside continuum methods and discuss a lattice statistical field theory approach to this problem, with an emphasis on the statistical properties of the optimal transport field and its Fourier modes. After introducing the appropriate formalism (the one of lattice calculus, aspects useful for our discussion are reported in Appendix C.1), one can work out some consequences of the theory which appear to not be easily accessible by continuum methods. However one is left with the task of understanding the scaling limit of the theory, as it is non-obvious a priori if expectations of relevant observables (such as the ground state energy) depend on the particular lattice chosen, an aspect that we shall discuss elsewhere. More generally, the sub-leading, constant term is not accessible to the linearized field theoretical approach, whose Euler-Lagrange equations give the optimal transport field as $\mu = \nabla\phi$, or equivalently, only a divergence part is present. Therefore, here we start to study the correction to the linearized theory perturbatively, in which ϕ also admits a curl part, in the hope that this approach will help clarifying aspects inaccessible to the linearized theory.

For this reason, in this Section we shall start this endeavor by considering the simplest possible case, namely, the two dimensional Grid-Poisson ERAP with periodic conditions (or on \mathbb{T}_2), in which e.g. the blue points sit on a regular square grid. Here, Fourier Duality at $p = 2$ and the well-known self-duality of the square lattice at $d = 2$ imply considerable simplifications of the theory. A guiding principle in our discussion is the notion of a natural “change of variables” on the $2n$ degrees of freedom of the field. The change of variable, which is inspired by electrodynamics, consists in decomposing the optimal transport field (which is defined on the direct lattice) as a sum of appropriate longitudinal and transverse part,

namely, “derivatives” of potentials (which are defined on the dual lattice). The decomposition is the analogue of the Helmholtz decomposition in electrodynamics, where an electric field can be written as the sum of a conservative and a solenoidal part. In particular, we shall elucidate some statistical properties of the lattice laplacians of both potentials, both in coordinate and momentum representations, which turn out to be very different. Then we shall study their Fourier modes and report numerical evidence that their contributions to the (unknown) asymptotic series of the expected ground state energy are at different orders in n .

3.3.1. Setup and notations

Let us consider the Grid-Poisson ERAP on the flat two dimensional torus \mathbb{T}_2 , that is, for $n = L^2$ and L an integer, blues $\mathcal{B} = \{b_i\}_{i=1}^n$ sit on a $L \times L$ square grid which can be chosen by translation invariance to be

$$\Lambda_n = \left\{0, \frac{1}{L}, \dots, 1 - \frac{1}{L}\right\} \times \left\{0, \frac{1}{L}, \dots, 1 - \frac{1}{L}\right\}, \quad (3.3.1.1)$$

where \times denotes Cartesian product. Reds are Poisson, that is $\mathcal{R} = \{r_i\}_{i=1}^n$ is a family of i.i. random variables uniformly distributed on the unit square \mathbb{Q}_2 . The dual lattice is obtained by translating rigidly Λ_n by $(1/2L, 1/2L)$, that is

$$\hat{\Lambda}_n := \left\{\frac{1}{2L}, \frac{3}{2L}, \dots, 1 - \frac{1}{2L}\right\} \times \left\{\frac{1}{2L}, \frac{3}{2L}, \dots, 1 - \frac{1}{2L}\right\}. \quad (3.3.1.2)$$

We impose periodic boundary conditions so that the squared distance between two points $z_1 = (z_{1,x}, z_{1,y})$ and $z_2 = (z_{2,x}, z_{2,y})$ is

$$\mathcal{D}_{\mathbb{T}_2}^2(z_1, z_2) = [\min(|z_{1,x} - z_{2,x}|, 1 - |z_{1,x} - z_{2,x}|)]^2 + [\min(|z_{1,y} - z_{2,y}|, 1 - |z_{1,y} - z_{2,y}|)]^2. \quad (3.3.1.3)$$

At fixed disorder \mathcal{R} , the $n \times n$ assignment cost matrix is thus

$$c_{kl}^{(2)} := \mathcal{D}_{\mathbb{T}_2}^2(b_k, r_l), \quad k, l = 1, \dots, n, \quad (3.3.1.4)$$

so that the energy of a microscopic configuration is just

$$\mathcal{H}(\pi) := \sum_{k=1}^n c_{k\pi(k)}^{(2)} \quad (3.3.1.5)$$

for a permutation π . As usual, a π_{opt} satisfies

$$\mathcal{H}_{\text{opt}} := \mathcal{H}(\pi_{\text{opt}}) = \min_{\pi \in \mathcal{S}_n} \mathcal{H}(\pi). \quad (3.3.1.6)$$

The usual optimal transport field $\vec{\mu} : \Lambda_n \rightarrow \mathbb{T}_2$ is

$$\vec{\mu}(b_k) := r_{\pi_{\text{opt}}(k)} - b_k \pmod{1} = \begin{pmatrix} \mu_x(b_k) \\ \mu_y(b_k) \end{pmatrix}, \quad k = 1, \dots, n, \quad (3.3.1.7)$$

so that the components μ_x and μ_y of $\vec{\mu}$ are scalar fields valued onto \mathbb{S}_1 (the circumference of radius $\frac{1}{2\pi}$). When treated as real numbers, the components of $\vec{\mu}$ are chosen as to be valued in $] -1/2, 1/2]$ (a choice with small loss of generality, as we expect that $|\mu| \sim \sqrt{\log n/n}$).

Let us use for any function $f : \Lambda_n \rightarrow \mathbb{C}$ the notation $f(i, j)$ to denote the value of f at site (i, j) in the lattice (and the analogous notation for a function on $\hat{\Lambda}_n$), as induced by the lexicographic order of our definition (3.3.1.1) (so that $i, j = 0, \dots, L-1$)*. For

$$R(\theta) = \begin{pmatrix} \cos \theta & -\sin \theta \\ \sin \theta & \cos \theta \end{pmatrix} \quad (3.3.1.8)$$

the standard rotation matrix of angle θ , we can consider the “rotated” optimal transport field

$$\vec{\mu}_{-\pi/4} = \begin{pmatrix} \mu_1(i, j) \\ \mu_2(i, j) \end{pmatrix} := R\left(-\frac{\pi}{4}\right) \vec{\mu} = \frac{1}{\sqrt{2}} \begin{pmatrix} \mu_x(i, j) + \mu_y(i, j) \\ \mu_y(i, j) - \mu_x(i, j) \end{pmatrix}. \quad (3.3.1.9)$$

The crucial point is to write $\vec{\mu}_{-\pi/4}$ in terms of appropriate functions on the dual lattice through diagonal derivatives (a pictorial representation of the action of diagonal derivatives is given in Fig. 3.12a, see Def. (C.1.0.8) for details).

By simple manipulations (which are detailed in Appendix C.1), we can show that $\vec{\mu}_{-\pi/4}$ (like any vector field) admits a *Helmholtz decomposition*

$$\vec{\mu}_{-\pi/4} = \nabla \phi - \nabla \wedge \psi, \quad (3.3.1.10)$$

for two scalar fields $\phi, \psi : \hat{\Lambda}_n \rightarrow \mathbb{R}$. More explicitly, Eq. 3.3.1.10 can be written component-wise as

$$\mu_\alpha = \nabla_\alpha \phi - \epsilon_{\alpha\beta} \nabla_\beta \psi, \quad \alpha, \beta = 1, 2, \quad (3.3.1.11)$$

where ϵ is the two-dimensional Levi-Civita symbol and the convention on repeated indices has been used. Borrowing from standard terminology in classical electrodynamics, we shall call ϕ the *scalar potential* and ψ the *vector potential* of $\vec{\mu}_{-\pi/4}$.

*That is, $k = 1 + iL + j$ with $i, j = 0, \dots, L-1$.

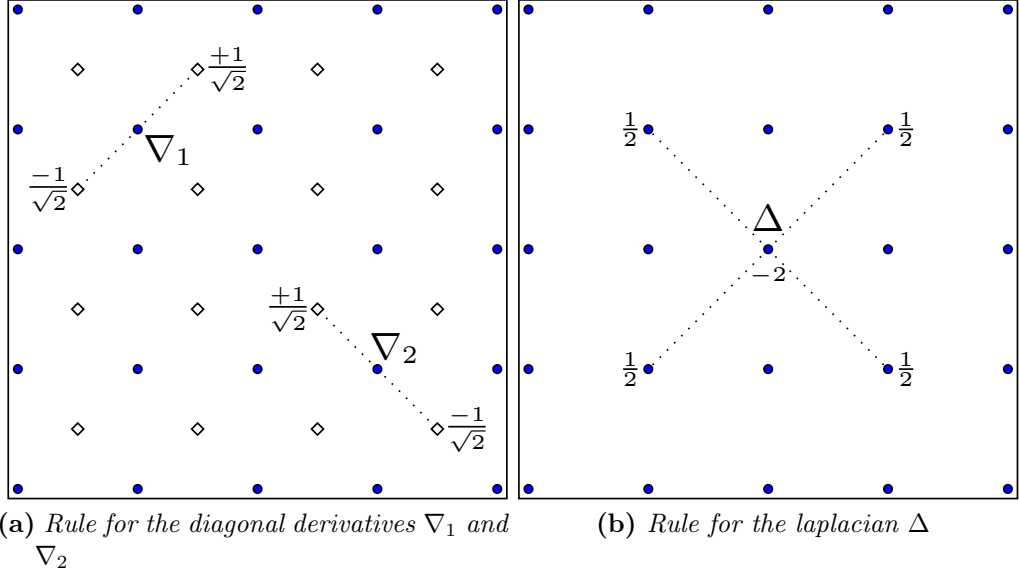


Figure 3.12. – Pictorial rules of lattice calculus for diagonal derivatives (Fig. 3.12a) and the laplacian (Fig. 3.12b). Sites of the direct lattice are depicted as full blue circles and sites of the dual lattice as empty diamonds.

In local form, the Helmholtz decomposition Eqs. (3.3.1.11) are

$$\begin{aligned}
 \mu_1(i, j) &= \frac{1}{\sqrt{2}} \left[\phi \left(i + \frac{1}{2}, j + \frac{1}{2} \right) - \phi \left(i - \frac{1}{2}, j - \frac{1}{2} \right) \right. \\
 &\quad \left. - \psi \left(i - \frac{1}{2}, j + \frac{1}{2} \right) + \psi \left(i + \frac{1}{2}, j - \frac{1}{2} \right) \right], \\
 \mu_2(i, j) &= \frac{1}{\sqrt{2}} \left[\phi \left(i - \frac{1}{2}, j + \frac{1}{2} \right) - \phi \left(i + \frac{1}{2}, j - \frac{1}{2} \right) \right. \\
 &\quad \left. + \psi \left(i + \frac{1}{2}, j + \frac{1}{2} \right) - \psi \left(i - \frac{1}{2}, j - \frac{1}{2} \right) \right].
 \end{aligned} \tag{3.3.1.12}$$

where, e.g. for a site (i, j) in the direct lattice, $(i + \frac{1}{2}, j + \frac{1}{2})$ denotes the site sitting northeast to it in the dual lattice (see Fig. 3.12), for $i, j = 0, \dots, L - 1$.

3.3.2. Longitudinal and transverse contributions to the ground state energy \mathcal{H}_{opt}

In continuing to pursue the analogy with the local formulation of electrodynamics in terms of potentials, one is tempted to take derivatives of the Helmholtz decomposition for $\vec{\mu}_{-\pi/4}$, Eq. (3.3.1.11). This task, which is standard in the continuum, is not straightforwardly accomplished on the lattice if one uses the standard discrete directional derivatives, as fields and potentials cannot be defined on the same space in the discrete setting. This fact was among our motivations for introducing diagonal derivatives (Eq. (C.1.0.9)).

Let us recall the divergence and curl of a vector field $\vec{E} : \Lambda_n(\hat{\Lambda}_n) \rightarrow \mathbb{T}_2$

$$\begin{aligned}\nabla \cdot \vec{E} &= \nabla_\alpha E_\alpha, \\ \nabla \wedge \vec{E} &= \epsilon_{\alpha\beta} \nabla_\alpha E_\beta, \quad (\alpha, \beta = 1, 2).\end{aligned}\tag{3.3.2.1}$$

Taking the divergence (resp., the curl) of both sides in the Helmholtz decomposition 3.3.1.10 for $\vec{\mu}_{-\pi/4}$, by simple manipulation (e.g. specialize Eq. (C.1.0.12) to ϕ and ψ) we just get

$$\begin{aligned}\nabla \cdot \vec{\mu}_{-\pi/4} &= \nabla_\alpha \mu_\alpha = \Delta\phi, \\ \nabla \wedge \vec{\mu}_{-\pi/4} &= \epsilon_{\alpha\beta} \nabla_\alpha \mu_\beta = \Delta\psi,\end{aligned}\tag{3.3.2.2}$$

where also the laplacian is a lattice laplacian, more precisely it is the diagonal lattice laplacian described in Appendix C.1, and here depicted in Fig. 3.12b. At this point, using (3.3.2.2) and straightforward lattice calculus computations (which are recalled for convenience in Appendix C.1), we can separate the ground state energy \mathcal{H}_{opt} (Eq. (3.3.1.6)) into a sum of two contributions, as

$$\begin{aligned}\mathcal{H}_{\text{opt}} = (\vec{\mu}, \vec{\mu}) &= (\vec{\mu}_{-\pi/4}, \vec{\mu}_{-\pi/4}) = (\nabla_\alpha \phi - \epsilon_{\alpha\beta} \nabla_\beta \psi, \mu_\alpha) \\ &= -(\phi, \nabla_\alpha \mu_\alpha) - (\psi, \epsilon_{\alpha\beta} \nabla_\alpha \mu_\beta) \\ &= -(\phi, \Delta\phi) - (\psi, \Delta\psi) \\ &= \mathcal{H}^{(\phi)} + \mathcal{H}^{(\psi)}.\end{aligned}\tag{3.3.2.3}$$

Borrowing terminology from classical electrodynamics, we shall call $\mathcal{H}^{(\phi)} := -(\phi, \Delta\phi)$ and $\mathcal{H}^{(\psi)} := -(\psi, \Delta\psi)$, respectively, the *longitudinal* and *transverse* contributions to the ground state energy \mathcal{H}_{opt} . We remark that such a decomposition, as the analogue decomposition in continuum electrodynamics, is independent on the disorder distribution, in the same manner as Maxwell's equations are valid for any distribution of charges. Everything we have discussed up to now is indeed valid beyond our current choice of red points uniformly distributed on the domain, and

in fact can be performed for any lattice vector field μ , even if it does not correspond to the optimal transport field of an ERAP.

3.3.3. Synthesis of results

In the following we shall introduce “the charges”, and namely, we will study some statistical properties of the scalar fields $\Delta\phi$ and $\Delta\psi$ (and hence ϕ and ψ upon inversion of the lattice laplacian), both in coordinate and momentum representations, in the special case of \mathcal{R} uniformly distributed on the torus. We will show that upon simple rescaling and translation $\Delta\phi$ is log-normally distributed, while $\Delta\psi$ is gaussian, and give numerical estimates for their two point-correlation functions. Afterwards, we will go to Fourier space and estimate the large n limit of expected longitudinal and transverse contributions

$$\begin{aligned} E_n(\phi) &:= \langle \mathcal{H}^{(\phi)} \rangle, \\ E_n(\psi) &:= \langle \mathcal{H}^{(\psi)} \rangle \end{aligned} \tag{3.3.3.1}$$

which will turn out to be of qualitatively different nature (and quantitatively different order of magnitudes) inside the asymptotic expansion for the expected total ground state energy $E_n := \langle \mathcal{H}_{\text{opt}} \rangle$. In particular, we shall discuss their relative contribution to Eq. 3.1.6.4 for $\Omega = \mathbb{T}(1)$, namely

$$E_n = \frac{1}{4\pi} \log n + c_0 + \mathcal{O}\left(\frac{1}{n}\right) = E_n(\phi) + E_n(\psi) \tag{3.3.3.2}$$

where the constant c_0 is estimated* “directly” (Fig. 3.13) to $c_0 = 0.1875(4)$, in agreement with 0.1879(3) of previous numerical studies (see (149), Eq. 60).

3.3.4. Statistical properties of $\Delta\phi$ and $\Delta\psi$ in coordinate representation

Independently on $n = L^2$, the empirical histograms of $L\Delta\phi + 2$ can be reasonably described by a lognormal distribution (Fig. 3.14, top); the histograms for $L\Delta\psi$ are well described by a single, centered gaussian (Fig. 3.14, bottom) of standard deviation $\sigma = 0.6349(1)$ (obtained by bootstrapping).

Observation 3.3.1. $\Delta\phi$ and $\Delta\psi$ appear to satisfy the inequality (Fig. 3.15)

$$L (|\Delta\psi| - \Delta\phi) \leq 2 \tag{3.3.4.1}$$

*Numerical protocol: $n \in \{64, 144, 256, 400, 576, 784, 1444, 2116\}$, 10^4 realisations for each n .

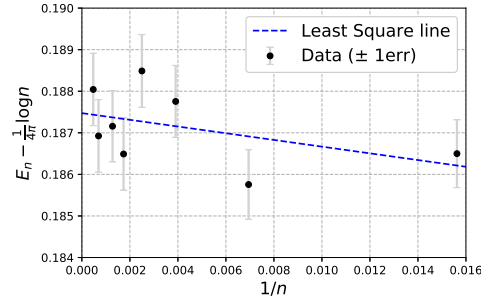


Figure 3.13. – Numerical estimation for the sub-leading constant appearing in the asymptotics for E_n (Eq. (3.3.3.2), black dots \pm one error). Data analysis: least square linear regression in $\frac{1}{n}$ (blue dashed line).

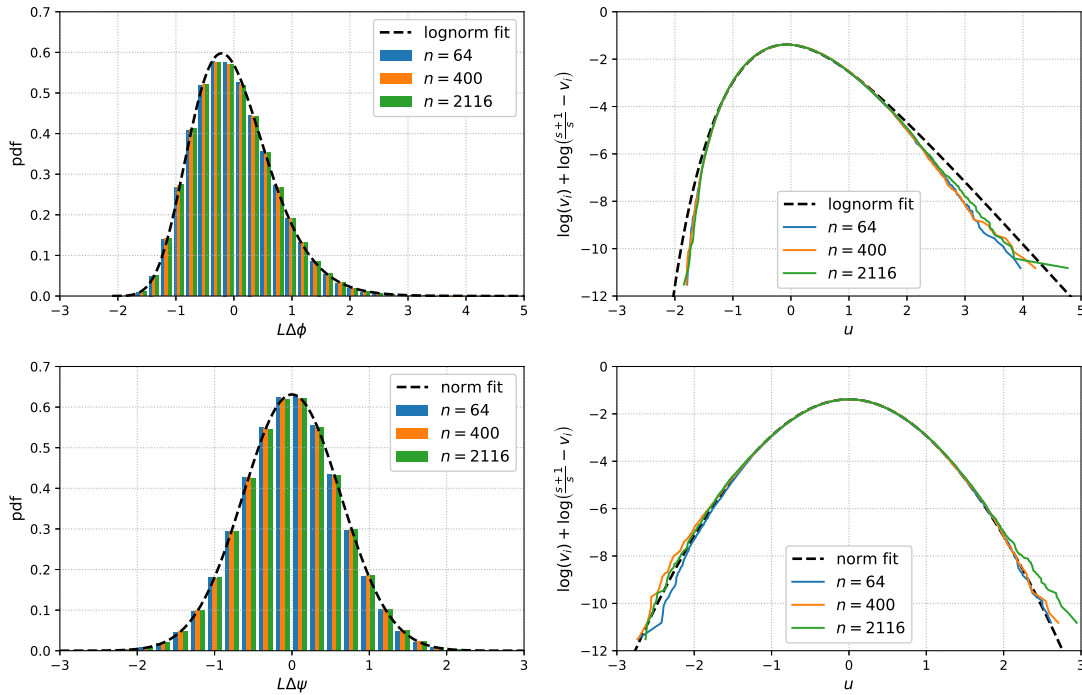


Figure 3.14. – Experimental histograms for the fields $L\Delta\phi$ (top-left, with corresponding symmetrized log probability functions at top-right, where $v_i = \frac{i}{\text{sample size}}$) and $L\Delta\psi$ (bottom-left, symmetrized log probability functions on the right). Colors encode different sizes $n = L^2$ (see legend) and the dashed black lines denote either the corresponding continuum fits (left), or the symmetrized log probability of an empirical sample of 10^6 from the fits (right).

which would imply in particular that, independently on $z \in \hat{\Lambda}_n$ and n , $L\Delta\phi$ is lower bounded as

$$L\Delta\phi \geq -2. \quad (3.3.4.2)$$

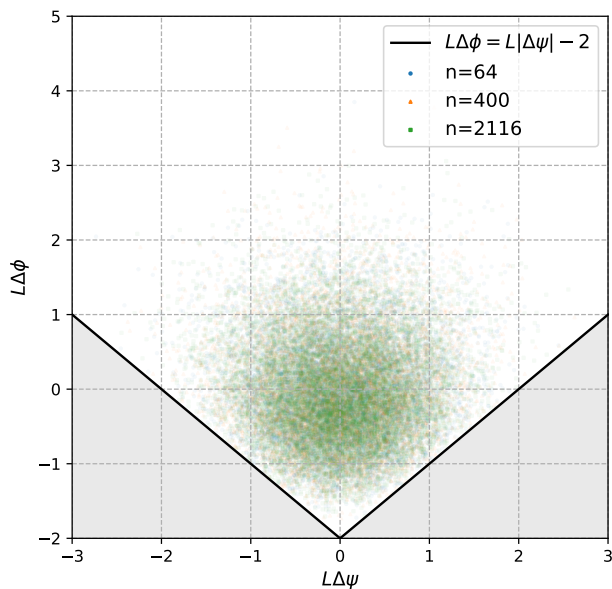


Figure 3.15. – Scatter plot of $(L\Delta\phi, L\Delta\psi)$ at different values of n (colors). Each colored cloud contains $10n$ uniformly sampled values $\{L(\Delta\phi(z_i), L\Delta\psi(z_i))\}_{i=1}^{10n}$ and it is centered at $(0, 0)$ within statistical errors. The grey area appears to be forbidden.

3.3.5. Two-point correlation functions

Let us go beyond single-site analysis and consider the extent of spatial correlations for the fields $\Delta\phi$ and $\Delta\psi$. By discrete translation invariance, for $e_1 = (1, 0)$ $e_2 = (0, 1)$ we can restrict our analysis to the two point correlation functions

$$\begin{aligned} C_{\Delta\phi, \Delta\phi}^{(n)}(i, j) &:= n \langle \Delta\phi(0) \Delta\phi(i e_1 + j e_2) \rangle, \\ C_{\Delta\psi, \Delta\psi}^{(n)}(i, j) &:= n \langle \Delta\psi(0) \Delta\psi(i e_1 + j e_2) \rangle, \\ C_{\Delta\phi, \Delta\psi}^{(n)}(i, j) &:= n \langle \Delta\phi(0) \Delta\psi(i e_1 + j e_2) \rangle, \end{aligned} \quad (3.3.5.1)$$

i/j	0	1	2	3
0	$0.4936(2) - 0.93(3)/n$	$0.1115(1) - 0.95(2)/n$	$0.0093(1) - 0.99(2)/n$	$0.0025(1) - 0.92(2)/n$
1	-	$-0.0086(1) - 0.98(1)/n$	$0.0050(2) - 1.00(3)/n$	$0.00114(7) - 1.06(1)/n$
2	-	-	$-0.00251(6) - 1.08(1)/n$	$-0.00040(8) - 1.06(1)/n$
3	-	-	-	$-0.0002(1) - 1.03(2)/n$

Table 3.8.: Numerical results for $C_{\Delta\phi,\Delta\phi}^{(n)}(i, j)$.

i/j	0	1	2	3
0	$0.40287(9) - 0.67(1)/n$	$0.0125(2) - 0.06(2)/n$	$0.0039(1) + 0.01(1)/n$	$-0.0007(2) - 0.01(3)/n$
1	-	$-0.10067(9) + 0.04(1)/n$	$-0.0050(1) + 0.07(2)/n$	$0.00007(5) - 0.070(8)/n$
2	-	-	$-0.00233(6) + 0.074(9)/n$	$-0.00037(8) - 0.04(1)/n$
3	-	-	-	$-0.00043(7) + 0.02(1)/n$

Table 3.9.: Numerical results for $C_{\Delta\psi,\Delta\psi}^{(n)}(i, j)$.

i/j	0	1	2	3
0	$0.0075(1) + 0.31(1)/n$	$0.2204(1) + 0.09(1)/n$	$-0.0364(1) + 0.0(2)/n$	$-0.0086(1) + 0.03(6)/n$
1	$-0.1688(1) + 0.20(2)/n$	$0.02987(1) + 0.02(1)/n$	$-0.0189(2) - 0.12(3)/n$	$-0.01091(3) + 0.087(9)/n$
2	$0.03900(6) + 0.13(1)/n$	$0.0210(1) - 0.04(2)/n$	$-0.0066(2) - 0.23(4)/n$	$-0.0098(1) + 0.11(6)/n$
3	$0.0255(1) + 0.03(5)/n$	$0.01555(9) + 0.06(3)/n$	$0.00014(3) + 0.15(1)/n$	$-0.0058(1) + 0.20(5)/n$

Table 3.10.: Numerical results for $C_{\Delta\phi,\Delta\psi}^{(n)}(i, j)$.

for integers i, j . The value at (i, j) was obtained by an extrapolation to $n \rightarrow \infty$, and first-finite size corrections could be estimated [†]. Intra-field numerical results for $C_{\Delta\phi,\Delta\phi}^{(n)}(i, j)$ (resp., $C_{\Delta\psi,\Delta\psi}^{(n)}(i, j)$), which are invariant under the exchange of $i \rightarrow j$, are reported in Tab. 3.8 (resp., Tab. 3.9). Inter-field numerical results for $C_{\Delta\phi,\Delta\psi}^{(n)}(i, j)$ (which is not invariant under the exchange of $i \rightarrow j$) are reported in Tab. 3.10.

[†]Notice that we are aided in this task by the large statistical power guaranteed by translation invariance.

3.3.6. On $L^2 \langle |\widehat{\Delta\phi}|^2 \rangle$ and $L^2 \langle |\widehat{\Delta\psi}|^2 \rangle$

In this Section we shall provide the numerical estimation of the typical transverse and longitudinal contributions through Fourier analysis. The Fourier components of $\Delta\phi$ and $\Delta\psi$ are (see C.1.0.4)

$$\begin{aligned}\widehat{\Delta\phi}(p) &= \frac{1}{L} \sum_{z \in \widehat{\Lambda}_n} e^{-iz \cdot p} \Delta\phi(z) \\ \widehat{\Delta\psi}(p) &= \frac{1}{L} \sum_{z \in \widehat{\Lambda}_n} e^{-iz \cdot p} \Delta\psi(z).\end{aligned}\tag{3.3.6.1}$$

Recalling the modified laplacian in momentum space

$$\hat{p}_{\text{mod}}^2 := \hat{p}^2 - \frac{1}{2} \hat{p}_1^2 \hat{p}_2^2,\tag{3.3.6.2}$$

we are thus concerned with the expectation of the random variables (see Eq. C.1.0.19)

$$\mathcal{H}^{(\phi)} = \sum_{p \neq 0} \frac{n |\widehat{\Delta\phi}|^2}{\hat{p}_{\text{mod}}^2} \quad \text{and} \quad \mathcal{H}^{(\psi)} = \sum_{p \neq 0} \frac{n |\widehat{\Delta\psi}|^2}{\hat{p}_{\text{mod}}^2},\tag{3.3.6.3}$$

which are two-dimensional analogues of Eq. 2.3.3.9. Heatmaps of $n |\widehat{\Delta\phi}(p)|^2$ and $n |\widehat{\Delta\psi}(p)|^2$ at large n are reported in Fig. 3.16a. The longitudinal part (left) displays the characteristic area near $\mathbf{n} = (0, 0)$ (upper left-corner and periodic images) responsible for the logarithmic divergence, and also remarkable rotational symmetry around $\mathbf{n} = (\frac{L}{2}, \frac{L}{2})$. The transverse part (right) shares the same symmetries of \hat{p}_{mod}^2 , with the small $\mathbf{n} = (0, 0)$ and large $\mathbf{n} = (\frac{L}{2}, \frac{L}{2})$ wavelengths both depleted, and connected through a saddle-point at $\mathbf{n} = (\frac{L}{4}, \frac{L}{4})^\ddagger$. On the basis of these observations, the numerical data were fitted as follows. Let us consider the six-dimensional linear subspace spanned by $f_{r,s}(x, y) = \cos(\frac{2\pi}{L}rx) \cos(\frac{2\pi}{L}sy)$ with

[‡]Notice that the zero mode at $\mathbf{n} = (0, 0)$ corresponds to the conservation law

$$\sum_z \Delta\phi(z) = 0,\tag{3.3.6.4}$$

and the one at $\mathbf{n} = (\frac{L}{2}, \frac{L}{2})$ corresponding to the vanishing of the ‘‘checkerboard’’ sum

$$\sum_{i,j=0}^{L-1} (-1)^{i+j} \Delta\psi(i, j) = 0.\tag{3.3.6.5}$$

$r, s = 0, 1, 2$. Setting

$$n|\widehat{\Delta\phi}(p)|^2 = \left(1 - \frac{1}{8}\hat{p}^2\right) + X_n^{(\phi)}(p), \quad (3.3.6.6)$$

in this subspace we have

$$X_n^{(\phi)} = a_{0,0} + a_{1,0}(f_{1,0} + f_{0,1}) + a_{2,0}(f_{2,0} + f_{0,2}) + a_{1,1}f_{1,1} + a_{2,1}(f_{2,1} + f_{1,2}) + a_{2,2}f_{2,2}. \quad (3.3.6.7)$$

However, the Fourier coefficients $a_{i,j}$ are not all independent, as two of them may be expressed in terms of the others via the conservation laws at $\mathbf{n} = (0, 0)$ and $\mathbf{n} = (\frac{L}{2}, \frac{L}{2})$, giving e.g. $a_{2,1} = -a_{1,0}$ and $a_{2,2} = -(a_{0,0} + 2a_{2,0} + 2a_{1,1})$. We are thus left with a 4 parameter fit which can be solved in the least square sense to give

$$\begin{aligned} a_{0,0} &= -0.00432 & a_{1,0} &= -0.02454 \\ a_{2,0} &= 0.02223 & a_{1,1} &= -0.01875. \end{aligned} \quad (3.3.6.8)$$

We can proceed analogously for the transverse part: setting (see also Eq. C.1.0.18)

$$n|\widehat{\Delta\psi}(p)|^2 = \frac{1}{4}\hat{p}_{\text{mod}}^2 + Y_n^{(\psi)}(p) = \frac{1}{4}\left(\hat{p}^2 - \frac{1}{2}\hat{p}_1^2\hat{p}_2^2\right) + Y_n^{(\psi)}(p), \quad (3.3.6.9)$$

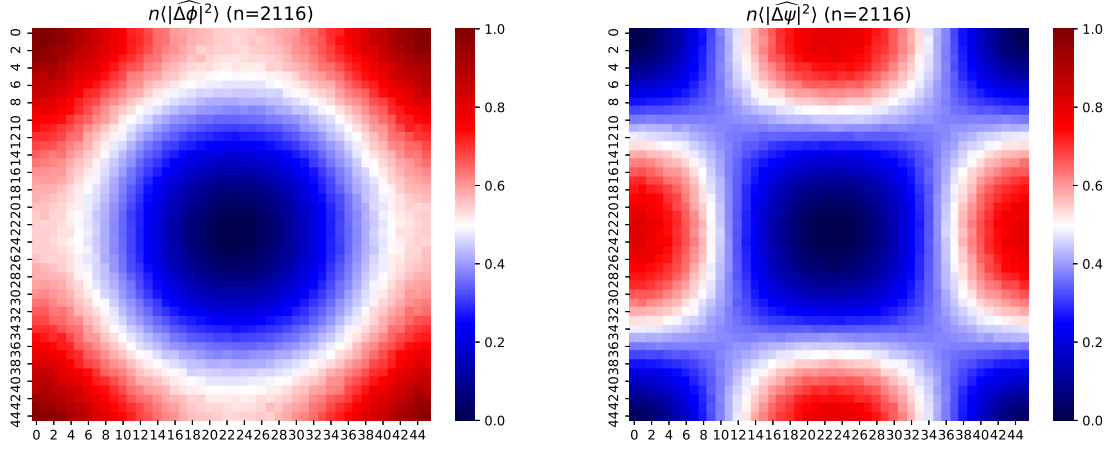
for the expansion

$$Y_n^{(\psi)} = b_{0,0} + b_{1,0}(f_{1,0} + f_{0,1}) + b_{2,0}(f_{2,0} + f_{0,2}) + b_{1,1}f_{1,1} + b_{2,1}(f_{2,1} + f_{1,2}) + b_{2,2}f_{2,2}, \quad (3.3.6.10)$$

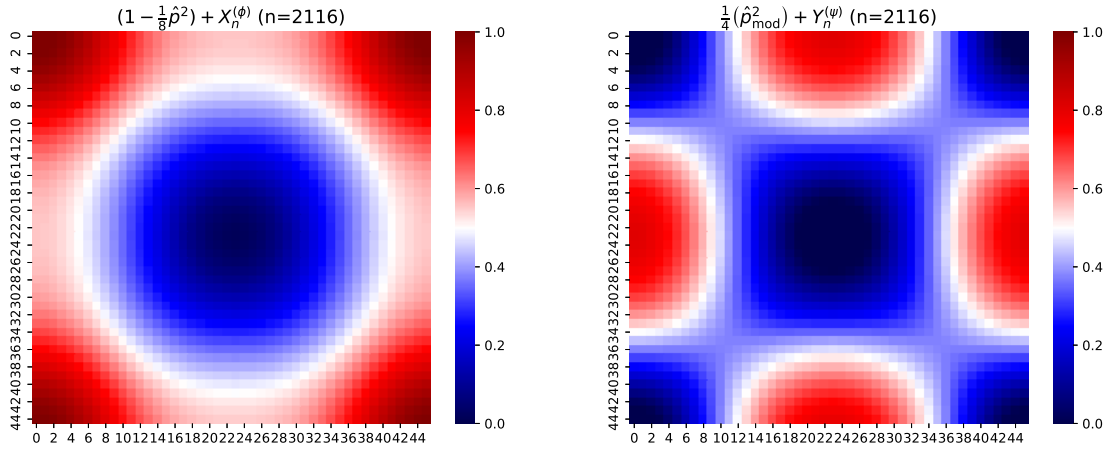
which is also to be complemented by $b_{2,1} = -b_{1,0}$ and $b_{2,2} = -(b_{0,0} + 2b_{2,0} + 2b_{1,1})$, we get

$$\begin{aligned} b_{0,0} &= 0.10156 & b_{1,0} &= 0.02353 \\ b_{2,0} &= -0.00030 & b_{1,1} &= 0.06375. \end{aligned} \quad (3.3.6.11)$$

The results of fits to Eq. 3.3.6.7 and Eq. 3.3.6.9 are reported in Fig. 3.16b and are in excellent agreement with numerical data. The remainder is localized in small regions related by the lattice symmetries.



(a) Numerical data for energy contributions in momentum space as a function of momentum indices (axes) for the longitudinal (left) and transverse (right) part (notice the normalization).



(b) Fits.

Figure 3.16. – Heatmaps of longitudinal (Fig. 3.16a, left) and transverse (Fig. 3.16a, right) contributions in momentum space (indices \mathbf{n} on axes). Notice the (approximate) complete invariance under the action of any element of the symmetry group of the square (so that one could symmetrize and consider the region $\mathbf{n} \in [0, \frac{L}{4}) \times [0, \frac{L}{4})$ only). Below (Fig. 3.16b) we report the least square fits discussed in the main text.

One may now perform the division by \hat{p}_{mod}^2 and sum over the momenta. Assuming the functional form

$$E_n(\phi) - \frac{1}{2\pi} \log L = c_{\phi,0} + \frac{c_{\phi,1}}{n} + \frac{c_{\phi,2}}{n^2} \quad (3.3.6.12)$$

we have obtained by least squares $c_{\phi,0} = -0.0163(4)$, $c_{\phi,1} = 0.63(6)$ and $c_{\phi,2} = -9(1)$ (errors on last digits in parentheses, see Fig. 3.17a). Analogously, the typical longitudinal contribution can be fitted assuming

$$E_n(\psi) = c_{\psi,0} + \frac{c_{\psi,1}}{n} + \frac{c_{\psi,2}}{n^2} \quad (3.3.6.13)$$

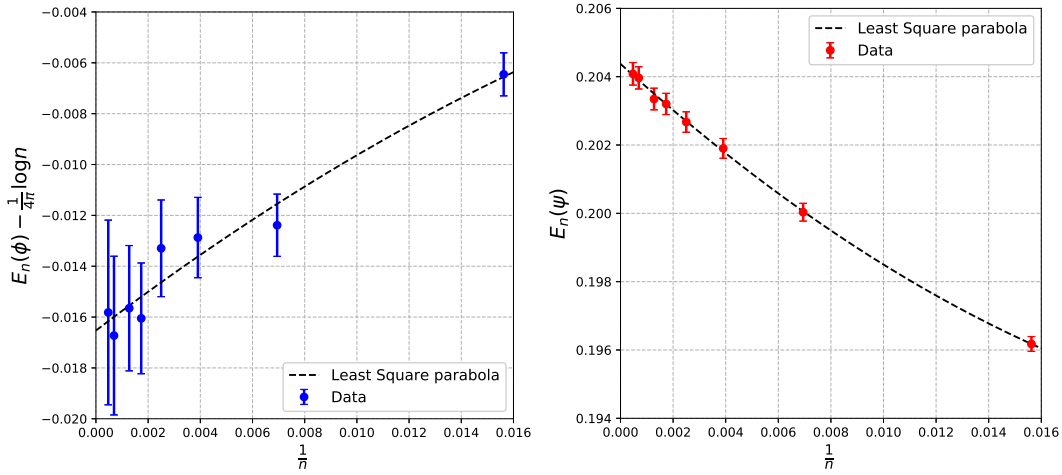
giving $c_{\psi,0} = 0.20437(6)$, $c_{\psi,1} = -0.70(3)$ and $c_{\psi,2} = 11(1)$ (errors on last digits in parentheses, see Fig. 3.17b). Recalling the Kronecker mass for the 2-torus (Eq. 3.1.4.18)

$$K_{\mathbb{T}(i)} = \frac{\gamma_E}{2\pi} + \frac{\ln \pi}{4\pi} - \frac{1}{\pi} \ln \Gamma(1/4) = -0.2270289 \dots \quad (3.3.6.14)$$

we get

$$c_{\psi,0} - K_{\Omega} + c_{\phi,0} = 0.4151(4), \quad (3.3.6.15)$$

in agreement with the universal constant for the Grid-Poisson problem, Tab. 3.2.



(a) Fit of the regular part of longitudinal contribution $E_n(\phi) - \frac{1}{4\pi} \log n$ (y -axis) vs $1/n$ (x -axis). Notice the small value of $c_{\phi,0}$. (b) Transverse contribution $E_n(\psi)$ (y -axis) vs $1/n$ (x -axis). The dashed black curve is the least square parabola, Eq. 3.3.6.13.

Figure 3.17. –

3.3.7. Section provisional conclusions and perspectives

In this Section we have introduced a statistical field theory approach to the GP-ERAP, in which blue points sit on a deterministic square grid and red points are uniformly distributed on the domain. In particular, we have considered some consequences of the theory for the special case $(d, p) = (2, 2)$. Inspired by classical electrodynamics, we have examined a “change of variables” for the optimal transport field and shown that the new variables have a different statistical nature: their average values contribute at different orders in the asymptotic expansion of the ground state energy. More precisely, the longitudinal (or conservative) part, which is associated to an approximately lognormal field, and through Fourier analysis, fully responsible for the well-known logarithmic divergence of the expected ground state energy; and a transverse (or solenoidal) part, associated to a gaussian field appearing to enjoy the self-averaging property in the large n limit, and contributing to the ground state energy through a constant plus corrections in $1/n$ that have been numerically estimated with good precision. Not only the sum of (the regular part of) transverse and longitudinal contributions recovers within errors the known numerically estimated constant (149)

$$c_0 = 0.1879(3) \quad 0.1880(4) = c_\phi + c_\psi \quad (3.3.7.1)$$

but, once the Kronecker mass of the torus is taken into account, the longitudinal part carries most of the sub-leading constant (Eq. 3.3.6.15). In doing so, we have also devised the stable numerical method of § 3.3.6, which indicates the way to the theoretical understanding of the origin of such strange sub-leading constants. As a by-product, our findings imply that the cutoff function F for the GP-ERAP is different from the one of the PP-ERAP, and also different from 1, as one could have possibly guessed. Lastly, we remark that the Helmholtz decomposition can be readily applied for studying the GP-ERAP in which random points are distributed with a measure different from the uniform measure and, without conceptual modifications, to other choices for the grid, and thus may serve as useful tool for investigating anomalous behaviors in two dimensions.

EUCLIDEAN RANDOM ASSIGNMENT PROBLEMS AT NON INTEGER HAUSDORFF DIMENSIONS $d_H \in (1, 2)$

4.1. Introduction

DESPITE recent efforts, even at integer values of p and d and for the simplest choices of disorder, the phase diagram of an ERAP (that is, the leading exponent of the expected ground state energy E_n for large n as a function of (p, d)) remains in part mysterious. It has already been established that, already in the “simplest” case $d = 1$, it is rather rich (154, 169) especially in the concave region $p \in (0, 1)$. In this case we have conjectured the existence of a critical point with logarithmic scaling

$$E_n \sim \sqrt{n} \log n = n^{1-\frac{p}{d}} (\log^{2p} n)|_{(p,d)=(1/2,1)} \quad (4.1.0.1)$$

separating a trivial region ($p \in [0, 1/2)$) where a nearest neighbor argument applies, $E_n \sim n^{1-\frac{p}{d}}|_{d=1}$ from the Dyck scaling region at $p \in (1/2, 1]$ where $E_n \sim \sqrt{n}$ (see Fig. 2.17). On the other hand, at $d > 2$ with uniform disorder, it is known (60) that points are optimally assigned with high probability in their Euclidean neighborhoods, so that

$$E_n \sim c_{p,d} n \left(n^{-\frac{1}{d}} \right)^p \quad (4.1.0.2)$$

for asymptotic constants $c_{p,d}$ which are not known in closed form but can be addressed by the mean-field theory (namely, the random assignment problem) with Mézard-Parisi exponent $1/(r+1) = 1 - p/d$ (154). It is not known how the critical points at $(p, d) = (1/2, 1)$ and $(p, d) = (1, 1)$ “enter” as critical lines in the phase diagram at generic (p, d) , and vanish at $d > 2$.

As we have recalled in Chapter 3, many efforts have been devoted during the years to the special case $d = 2$, where the ground state energy is logarithmically divergent at large n (see § 3.1) and logarithmic corrections may already appear at

$d = 1$, if the disorder distribution vanishes (§ 2.6).

In this Chapter we shall take a first step into the unknown (as far as we know) region of the phase diagram with the introduction of a notion of ERAP at non-integer Hausdorff dimensions $d_H \in (1, 2)$. In this problem, the disorder distribution is identical for $\mathcal{B} = \{b_i^{d_H}\}_{i=1}^n \subset \mathcal{M}$ and $\mathcal{R} = \{r_i^{d_H}\}_{i=1}^n \subset \mathcal{M}$, and it is the uniform measure supported on a fractal set \mathcal{M} . The fractal sets depend on a simple geometrical parameter in a way that the corresponding Hausdorff dimensions give different interpolations of the interval $d_H \in (1, 2)$, providing us a simple proxy for universality of the energy leading scaling exponent.

It is interesting to notice that statistical properties of sets of points sampled from measures supported on fractal sets using the two dimensional distance have been considered during the years for vastly different reasons, ranging from grow rates of the number of points defining the convex hull of a random sample of size n (81) to the crossover transition in the distribution of nearest-neighbors distances, in connection with random matrix theory (108, 112). Our main motivations stem from the question of whether universal behavior extends “beyond” $d = 2$, in particular in the perspective of one dimensional anomalous behavior, § 2.6. The latter suggested that, beyond the bulk behavior, the scaling is determined by “holes” in the support of the disorder distribution (i.e. endpoints of the measure μ at $d = 1$). As a consequence, one is naturally led to wonder about the geometry of the optimal assignment also at higher dimensions, in a situation in which neighborhoods of blue and red points are not anymore homogeneous but, from the point of view of the embedding space, are full of inhomogeneities.

4.2. Setup

For a real number $p > 0$, consider the random variable

$$\mathcal{H}_{\text{opt}} = \min_{\pi \in \mathcal{S}_n} \sum_{i=1}^n \mathcal{D}^p(b_{\pi(i)}^{d_H}, r_i^{d_H}), \quad (4.2.0.1)$$

where \mathcal{S}_n is the symmetric group on n objects and $\mathcal{D}^2(x, y) = \sum_{i=1}^2 (x_i - y_i)^2$ is the (squared) two dimensional Euclidean distance. Denoting with $\langle O \rangle_{\mathcal{M}}$ expectation of observable O with respect to the uniform measure on \mathcal{M} , we wish to investigate the large n asymptotics of the expected ground state energy

$$E_{n,(p,d_H)}^{\mathcal{M}} := \langle \mathcal{H}_{\text{opt}} \rangle_{\mathcal{M}} \quad (4.2.0.2)$$

depending on (p, d_H) and on the fractal set \mathcal{M} considered.

4.3. Choice of randomness

4.3.1. Peano fractal

The construction of our first fractal is inspired by properties of space-filling curves, such as the Peano curve (1) (see also e.g. (117), Chapter 2). Consider the aspect ratio parameter $\alpha_{(\text{Peano})} \in [0, 1]$ depending on the Hausdorff dimension d_H as

$$\alpha_{(\text{Peano})} = (2^{d_H-1} - 1)^{1/d_H} \quad (4.3.1.1)$$

and introduce the deterministic quantities

$$\begin{aligned} \mathbf{P} &= \frac{1}{2(1 + \alpha_{(\text{Peano})}^{d_H})} \left(1, \alpha_{(\text{Peano})}^{d_H}, \alpha_{(\text{Peano})}^{d_H}, 1 \right), \\ \mathbf{\Lambda} &= \frac{1}{2} \left(1, \alpha_{(\text{Peano})}^{d_H}, \alpha_{(\text{Peano})}^{d_H}, 1 \right), \\ \mathbf{\Phi} &= (1, i, -i, 1), \\ \mathbf{V} &= \frac{1}{2} (0, 1, 1 + i\alpha_{(\text{Peano})}^{d_H}, 1). \end{aligned} \quad (4.3.1.2)$$

Calling R the cumulative distribution function of \mathbf{P} , and R^{-1} its inverse function, draw a random integer $i = \lfloor R^{-1}(u) \rfloor$, $i \in \{1, 2, 3, 4\}$, for u chosen uniformly in $[0, 1]$, where $\lfloor x \rfloor$ is the largest integer smaller than x . For $P = (\xi, z) \in \mathbb{C}^2$, Eq. (4.3.1.2) and i uniquely define the random map $f_{\mathbf{P}} : \mathbb{C}^2 \rightarrow \mathbb{C}^2$

$$f_{\mathbf{P}}(P) := (\Lambda_i \Phi_i \xi, z + V_i \xi). \quad (4.3.1.3)$$

Starting from an initial datum $P_0 = (1, 0)$, we apply $f_{\mathbf{P}}$ recursively as

$$P_g = f_{\mathbf{P}}^g(P_0) = \underbrace{f_{\mathbf{P}} \circ f_{\mathbf{P}} \cdots \circ f_{\mathbf{P}}}_{g \text{ times}}(P_0) \quad (4.3.1.4)$$

for a suitably large g^* , and then consider the second component of P_g , $z_g := (P_g)_2$. We will say that z_g (which can be either a red or blue point) is uniformly distributed on the *Peano fractal* of Hausdorff dimension d_H . In order to enforce the $y \leftrightarrow -y$ symmetry, as an additional step we consider either z_g or \bar{z}_g with probability 1/2 (\bar{z} being the complex conjugate of z). Example instances of the disorder from the Peano fractal at increasing Hausdorff dimensions are displayed in Fig. 4.1.

*In our settings $g = 10$ appeared to be large enough to prevent issues due to floating point precision.

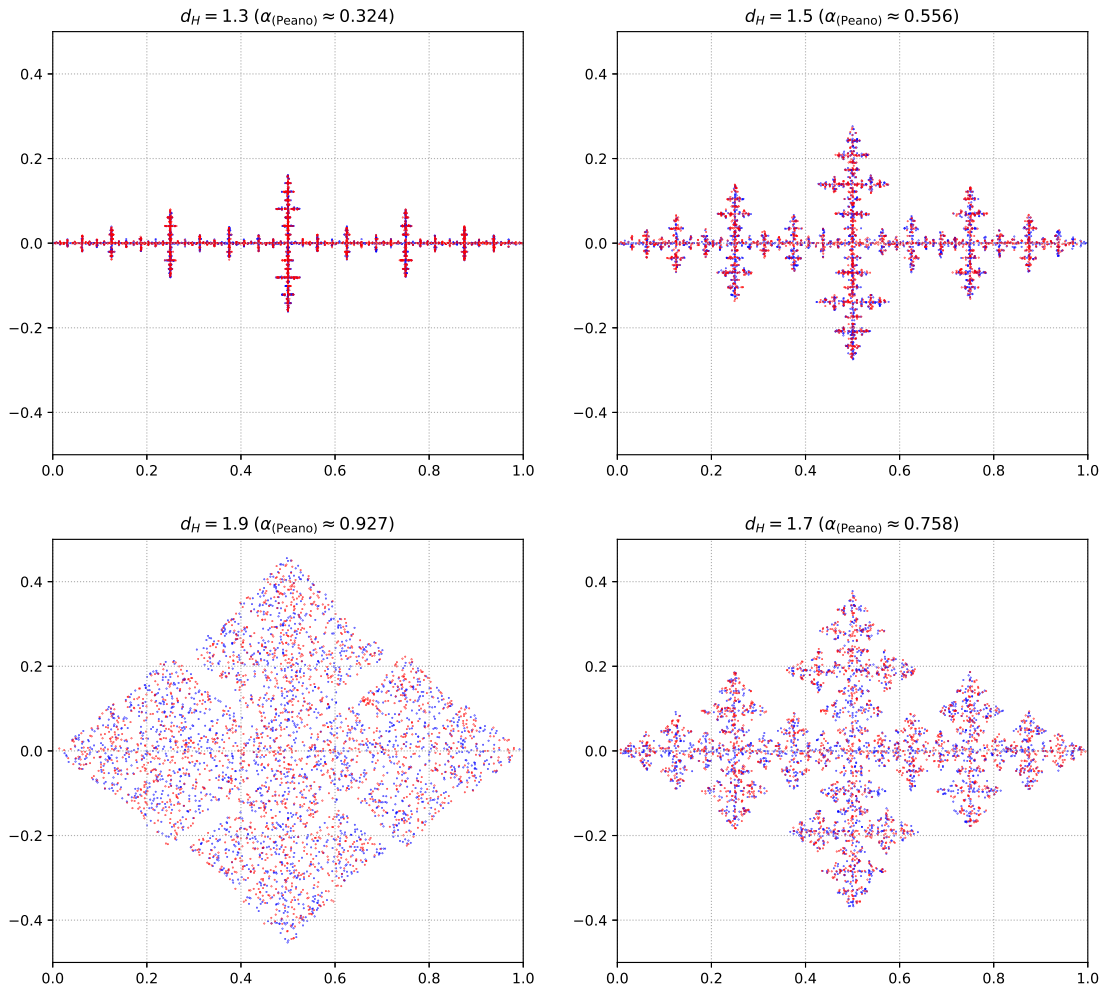


Figure 4.1. – Instances with $n = 2^{12}$ blue and red points drawn uniformly from the Peano fractal at increasing Hausdorff dimensions d_H , in clock-wise increasing order from $d_H = 1.3$ (top-left) to $d_H = 1.9$ (bottom-left).

4.3.2. Cesàro fractal

The construction of our second fractal takes inspiration from the Koch curve (2), which has Hausdorff dimension $d_H = \ln 4 / \ln 3 \approx 1.26186^\dagger$. The Koch curve has also been considered by Cesàro who, among other things, described a geometrical construction for inscribing the Koch curve between two lines drawable in the plane, and gave a binary representation of its points (3). The construction proceeds in analogy with § 4.3.1. Given a bending angle $\alpha_{(\text{Cesàro})} \in [0, \pi/2]$ related to the Hausdorff dimension d_H by

$$\alpha_{(\text{Cesàro})} = \arccos(2^{\frac{2}{d_H}-1} - 1), \quad (4.3.2.1)$$

as in 4.3.1.2 we first build the quantities

$$\begin{aligned} \mathbf{\Pi} &= \frac{1}{2(1 + \cos(\alpha_{(\text{Cesàro})}))} (1, 1, 1, 1) \\ \lambda &= \frac{1}{2} \left(1, \alpha_{(\text{Cesàro})}^{d_H}, \alpha_{(\text{Cesàro})}^{d_H}, 1 \right) \\ \phi &= (1, e^{i\alpha_{(\text{Cesàro})}}, e^{-i\alpha_{(\text{Cesàro})}}, 1) \\ \mathbf{v} &= \frac{1}{2} (0, 1, 1 + e^{i\alpha_{(\text{Cesàro})}}, 1 + e^{i\alpha_{(\text{Cesàro})}} + e^{-i\alpha_{(\text{Cesàro})}}). \end{aligned} \quad (4.3.2.2)$$

and get a random index $i \in \{1, 2, 3, 4\}$ with the inverse cumulative distribution function associated with $\mathbf{\Pi}$. For $P = (\xi, z) \in \mathbb{C}^2$, i and Eq. 4.3.2.2 we consider the action of the random map

$$f_{\text{Cesàro}}(P) := (\lambda_i \phi_i \xi, z + v_i \xi), \quad (4.3.2.3)$$

and apply it a large number of times g to the initial datum $P_0 = (1, 0)$

$$P_g := f_{\text{Cesàro}}^g(P_0) = \underbrace{f_{\text{Cesàro}} \circ f_{\text{Cesàro}} \cdots \circ f_{\text{Cesàro}}}_{g \text{ times}}(P_0). \quad (4.3.2.4)$$

We will correspondingly say that z_g is uniformly distributed on the *Cesàro fractal* of Hausdorff dimension d_H , and again to preserve the $y \rightarrow -y$ symmetry we take either z_g or $\overline{z_g}$ with probability 1/2. Example instances of disorder on the Cesàro fractal at several Hausdorff dimensions are displayed in Fig. 4.2.

[†]The Koch curve is often used at school as an example of continuous curve which is not differentiable at any point (see (116) for an elementary proof), but has also been considered in applications. For example, due to the space filling property, small antennas with the design of the first few iterations of the Koch curve display practical advantages over linear designs, such as larger radiation resistance and smaller reactance (78).

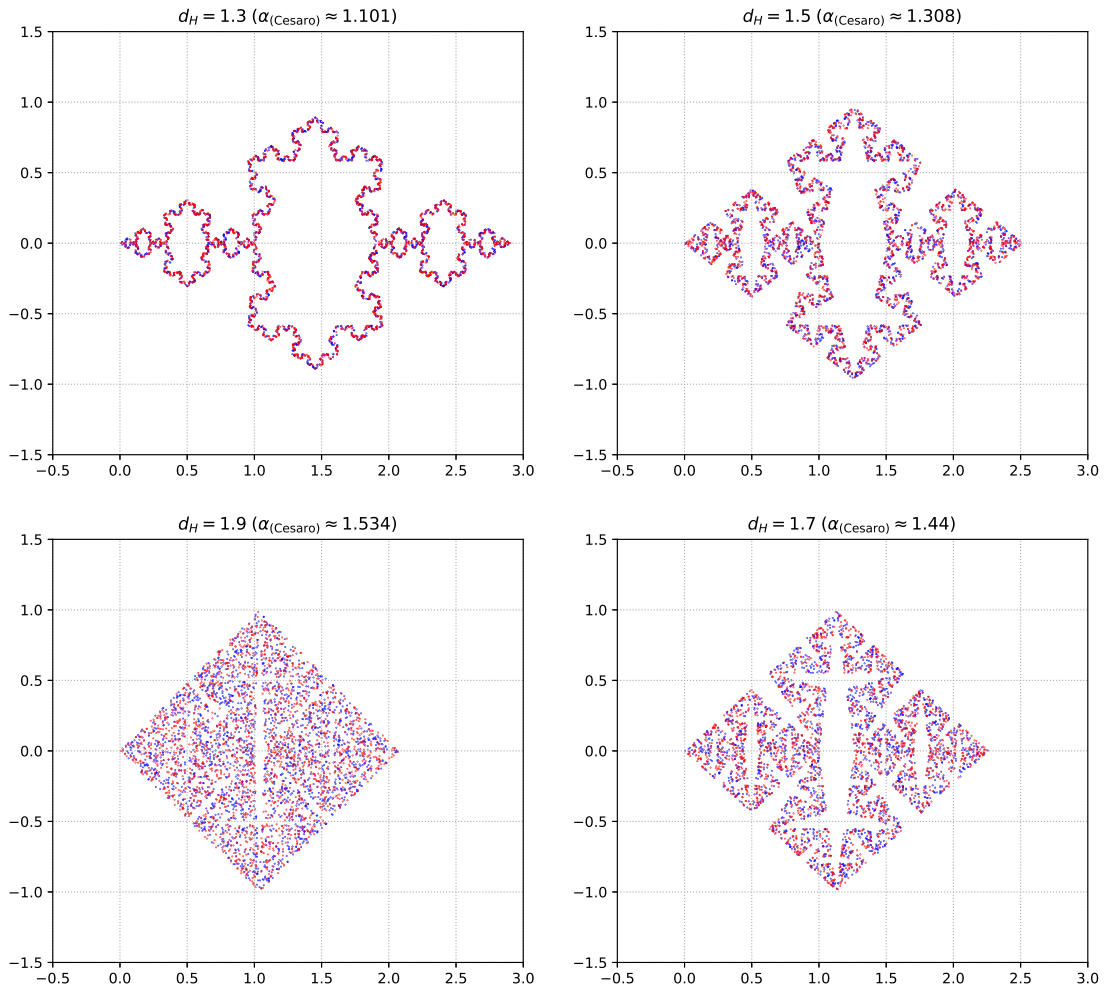


Figure 4.2. – $n = 2^{12}$ blue and red points generated on Cesàro fractals at increasing Hausdorff dimensions d_H , in clock-wise increasing order from $d_H = 1.3$ (top-left) to $d_H = 1.9$ (bottom-left).

4.4. Numerical protocol, data analysis, and results

Values of p, d_H, n considered in our numerical experiments are reported in Table 4.1. At fixed (n, p, d_H) we have simulated 10^4 instances for both Peano and Cesàro disorder, resulting in about two weeks of simulation time on a single machine of commodity hardware.

p	.33, .66, 1.0, 1.33, 1.66, 2.0, 2.33, 2.66, 3.0, 3.33
d_H	1.1, 1.3, 1.5, 1.7, 1.9
n	32, 64, 128, 256, 512, 1024

Table 4.1.: Numerical protocol (10^4 instances).

At fixed (p, d_H) and choice of fractal (Peano (P) or Cesàro (C)), we have assumed that the expected ground state energy $E_{(p,d_H)}^{\text{P(C)}} = \langle \mathcal{H}_{\text{opt}} \rangle_{\text{P(C)}}$ grows at leading order as[‡]

$$E_{n,(p,d_H)}^{\text{P(C)}} \sim c_{(p,d_H)}^{\text{P(C)}} n^{\gamma_{(p,d_H)}^{\text{P(C)}}} \quad (4.4.0.1)$$

for a scaling exponent $\gamma_{(p,d_H)}^{\text{P(C)}}$ and for some function $c_{(p,d_H)}^{\text{P(C)}}$ independent on n . It follows that

$$E_{2n,(p,d_H)}^{\text{P(C)}} \sim c_{(p,d_H)}^{\text{P(C)}} (2n)^{\gamma_{(p,d_H)}^{\text{P(C)}}} \sim 2^{\gamma_{(p,d_H)}^{\text{P(C)}}} E_{n,(p,d_H)}^{\text{P(C)}}. \quad (4.4.0.2)$$

The functions $c_{(p,d_H)}^{\text{P(C)}}$ depend in a complicated way on the ensemble used and will be discussed elsewhere. The scaling exponents $\gamma_{(p,d_H)}^{\text{P(C)}}$ have been estimated by two methods:

- Method 1. We have first computed $E_{(p,d_H)}^{\text{P(C)}}$, and then estimated the two free parameters in

$$\left[\log_2 E_{n,(p,d_H)}^{\text{P(C)}} - (\gamma_{(p,d_H)}^{\text{P(C)}} \log_2 n + \log_2 c_{(p,d_H)}^{\text{P(C)}}) \right]^2 \quad (4.4.0.3)$$

in the least square sense.

- Method 2. Called $h_{n,(p,d_H)}^{\text{P(C)}}$ the sorted vector of numerical data (so that $h_{n,(p,d_H)}^{\text{P(C)}} \in \mathbb{R}^{10^4}$), we have first minimized $\|h_{2n,(p,d_H)}^{\text{P(C)}} - h_{n,(p,d_H)}^{\text{P(C)}}\|^2$ in the least square sense (so to obtain 5 estimates for $\gamma_{r,(p,d_H)}^{\text{P(C)}}$ with our choice of numerical protocol, see Table 4.1), and afterwards we have averaged among such estimates.

[‡]Our current numerical protocol does not allow us to draw reliable conclusions about possible logarithmic corrections.

For each fractal set, numerical estimates for $\gamma_{(p,d_H)}^{P(C)}$ obtained by the two methods agree with each other within two statistical errors at most. They are reported, respectively, in Table 4.2 (Peano fractal) and 4.3 (Cesàro fractal).

Method 1						Method 2					
$p \backslash d_H$	1.1	1.3	1.5	1.7	1.9	$p \backslash d_H$	1.1	1.3	1.5	1.7	1.9
0.33	.718(7)	.773(3)	.802(2)	.822(1)	.836(1)	0.33	.71(1)	.772(5)	.802(3)	.822(2)	.836(2)
0.66	.574(5)	.614(4)	.647(3)	.673(3)	.691(2)	0.66	.571(8)	.612(7)	.645(5)	.671(5)	.689(4)
1.00	.504(2)	.522(2)	.538(3)	.549(3)	.558(3)	1.00	.502(4)	.520(5)	.534(4)	.547(5)	.556(4)
1.33	.358(3)	.394(2)	.419(2)	.418(3)	.415(4)	1.33	.360(9)	.390(4)	.415(2)	.414(4)	.411(6)
1.66	.205(3)	.265(3)	.299(3)	.291(2)	.272(5)	1.66	.200(5)	.261(8)	.294(6)	.286(4)	.265(8)
2.00	.047(3)	.135(3)	.175(2)	.168(2)	.128(5)	2.00	.040(9)	.133(9)	.169(4)	.159(5)	.119(9)
2.33	-.103(3)	.003(3)	.054(2)	.047(1)	-.018(5)	2.33	-.109(5)	-.001(6)	.05(1)	.036(6)	-.033(7)
2.66	-.254(2)	-.126(3)	-.064(3)	-.070(4)	-.156(7)	2.66	-.26(1)	-.130(5)	-.070(6)	-.08(1)	-.17(1)
3.00	-.417(6)	-.248(5)	-.175(3)	-.188(5)	-.298(7)	3.00	-.42(2)	-.25(1)	-.18(1)	-.20(1)	-.31(1)
3.33	-.550(9)	-.380(5)	-.287(4)	-.302(7)	-.445(6)	3.33	-.56(3)	-.376(9)	-.29(1)	-.31(2)	-.469(9)

Table 4.2.: Estimated scaling exponents $\gamma_{(p,d_H)}^P$ (see Eq. 4.4.0.1). Errors on the last digit in parentheses.

Method 1						Method 2					
$p \backslash d_H$	1.1	1.3	1.5	1.7	1.9	$p \backslash d_H$	1.1	1.3	1.5	1.7	1.9
0.33	.757(4)	.787(3)	.808(3)	.824(2)	.832(2)	0.33	.756(6)	.786(5)	.808(4)	.823(4)	.831(4)
0.66	.600(4)	.632(4)	.659(3)	.678(3)	.690(2)	0.66	.598(7)	.630(7)	.657(6)	.677(5)	.688(4)
1.00	.516(2)	.531(2)	.543(4)	.552(3)	.557(3)	1.00	.513(3)	.529(4)	.541(6)	.550(4)	.555(5)
1.33	.397(2)	.423(1)	.420(2)	.416(3)	.415(4)	1.33	.397(4)	.423(3)	.418(4)	.412(4)	.411(7)
1.66	.253(4)	.310(1)	.304(1)	.284(2)	.271(4)	1.66	.255(9)	.312(3)	.300(4)	.278(2)	.264(6)
2.00	.111(5)	.188(1)	.189(4)	.152(3)	.127(5)	2.00	.11(1)	.187(5)	.184(8)	.144(2)	.118(7)
2.33	-.036(6)	.073(2)	.075(5)	.023(3)	-.019(5)	2.33	-.03(1)	.071(7)	.07(1)	.014(9)	-.032(7)
2.66	-.180(6)	-.046(3)	-.036(8)	-.104(5)	-.162(7)	2.66	-.18(1)	-.039(5)	-.04(2)	-.12(1)	-.18(1)
3.00	-.319(8)	-.166(3)	-.147(7)	-.228(8)	-.311(7)	3.00	-.30(2)	-.163(8)	-.15(2)	-.24(2)	-.33(1)
3.33	-.473(7)	-.297(4)	-.25(1)	-.35(1)	-.45(1)	3.33	-.47(2)	-.30(1)	-.26(3)	-.37(3)	-.47(1)

Table 4.3.: Estimated scaling exponents $\gamma_{(p,d_H)}^C$ (see Eq. 4.4.0.1). Errors on the last digit in parentheses.

4.5. On the qualitative behavior of $\gamma_{(p,d_H)}^{C(P)}$ and evidence of universality

From Tables 4.2 and 4.3 it can be evinced that $\gamma_{(p,d_H)}^{C(P)} > 1 - \frac{p}{d_H}$. Moreover $\frac{\partial}{\partial p}\gamma_{(p,d_H)}^{C(P)}|_{d_H} < 0$, while $\frac{\partial}{\partial d_H}\gamma_{(p,d_H)}^{C(P)}|_p$ appears to change sign at some (non-trivial) critical value $d_H^{*,C(P)}(p)$ inside the explored parameter space. More generally, the absolute difference $|\gamma_{(p,d_H)}^P - \gamma_{(p,d_H)}^C|$ is small throughout the whole investigated area, being at most ≈ 0.1 (at $(p,d_H) = (3,1.1)$). In a whole sub-region of the considered domain, which appears to “engulf” the line $d_H = 2$, it is on the order of 10^{-3} and hence indistinguishable from statistical errors. This fact is consistent with the existence of a whole universal region in the (p, d_H) plane, corresponding roughly to $d_H \gtrsim \max\left(2 - p, 2 - \frac{1}{p^2}\right)$ (Fig. 4.3, qualitative separation line in dash-dotted black). The area appears to extend down to $d_H = 1$ in a narrow region around $p = 1$.

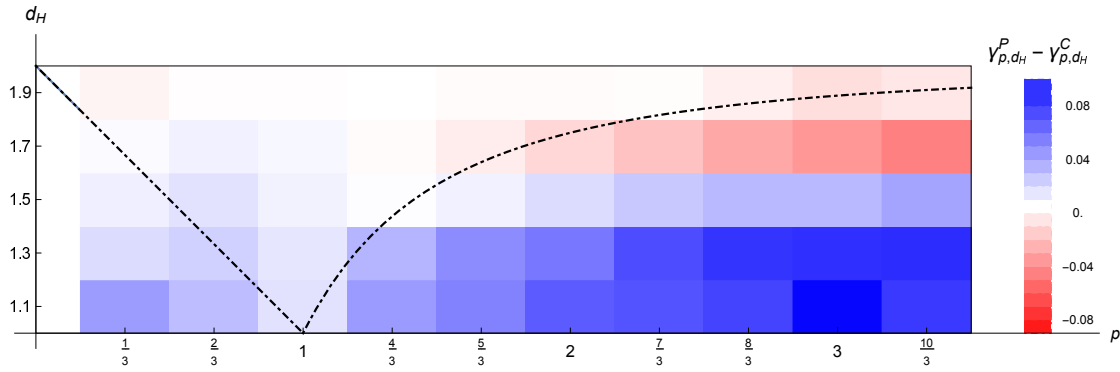


Figure 4.3. – Shift in the numerically obtained ground state energy leading scaling exponents $\gamma_{(p,d_H)}^P - \gamma_{(p,d_H)}^C$ (colorbar) as a function of (p, d_H) (axes). Raw values (resp. Tables 4.2 and 4.3). The white area denotes the region where scaling appears to be universal.

4.6. Energy approximate linear relations

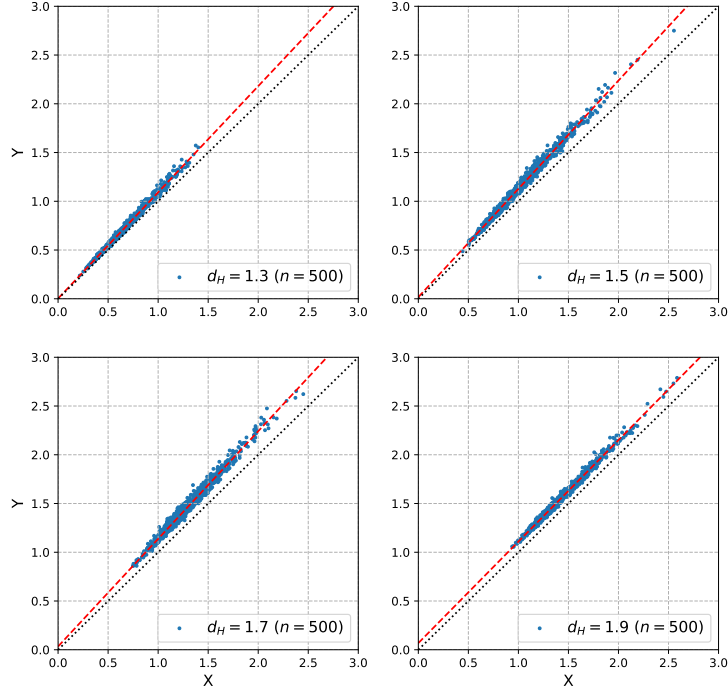


Figure 4.4. – X and Y variables for the Peano fractal at $p = 2$ and $n = 500$ (scatter plots) and their linear fits (dashed, red lines). The bisector $Y = X$ is represented by a dotted black line. Notice that the linear fits appear to acquire an intercept as d_H grows, a signature of logarithmic scaling.

The setting discussed in § 3.2.2 is motivated by a prediction, from the linearised field theory, that two suitable linear combinations of ground-state energies for certain instances differ only by a quantity of order $1/n$. Although in the present setting, of fractal domains, we do not have a satisfactory field-theoretical description, we can experiment with the same numerical setting, and possibly use the numerical results to get a hint towards such a theory. So, consider four sets of n points P_1, P_2, P_3, P_4 , uniformly distributed on a fractal set of choice, and let $E_{i,j}$ be the ground state energy for the assignment problem of P_i to P_j (we omit the dependence on p, d_H, n and the fractal set for notational convenience). At a fixed instance, we have considered the quantities

$$\begin{cases} X &= E_{1,2} + E_{3,4} \\ Y &= E_{1\cup 3, 2\cup 4} + E_{1\cup 4, 2\cup 3} \end{cases} \quad (4.6.0.1)$$

where e.g. $E_{1\cup 3,2\cup 4}$ denotes the optimal cost of assigning the set $P_1 \cup P_3$ to $P_2 \cup P_4$ (i.e. an assignment problem between two sets of $2n$ points each). Independently on the considered fractal set and robustly in the range of considered (p, d_H) values, Y and X appear to satisfy in good approximation a linear relation (that is, the scatter plots X vs Y describe a cloud of variance of order 1 along a direction and of order $1/n$ in the orthogonal direction). An example is provided in Fig. 4.4 for the Peano case. These findings may be useful for acquiring information on scaling exponents $\gamma_{(p,d_H)}^P$ (e.g. via the slope of least square linear regression) and sub-leading constants, in presence of pure logarithmic scaling (i.e. via the intercepts).

4.7. Energy profile at fixed disorder along the $(2, d_H)$ line in the Cesàro fractal

In the Cesàro fractal construction (Eq. 4.3.2.2) the transition probabilities do not depend on d_H . This fact allows, for example, to fix the pseudo-random sequence for generating blue and red points and study the average energy profile $E_{n,(p,d_H)}^C$ “along” the d_H direction. For example, at $p = 2$, we have found numerical evidence that $E_{n,(2,d_H)}^C$ is a rather smooth function of d_H , admitting a global maximum around $d_H \approx 1.07$. When subtracted the bi-dimensional, universal $\frac{\log n}{2\pi}$ asymptotics, $E_{n,(2,d_H)}^C$ appears to converge rapidly to a constant as $d_H \rightarrow 2$.

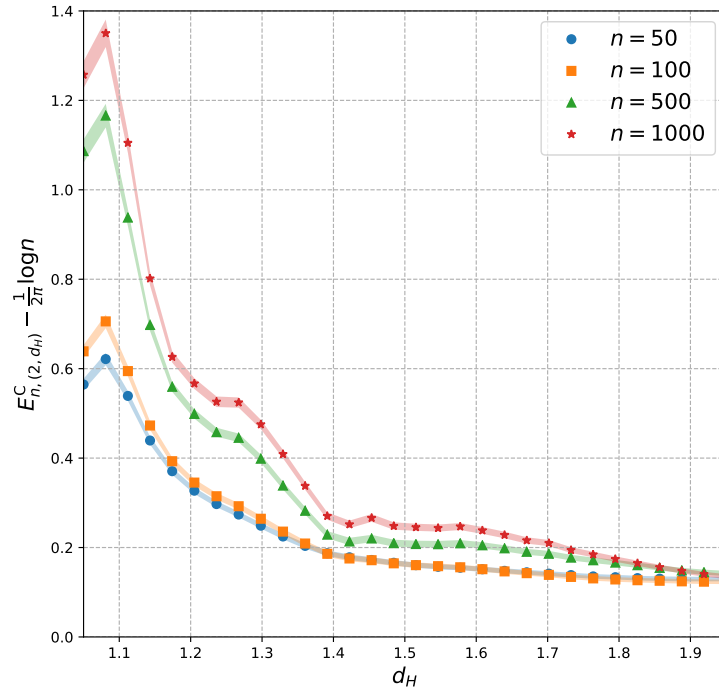
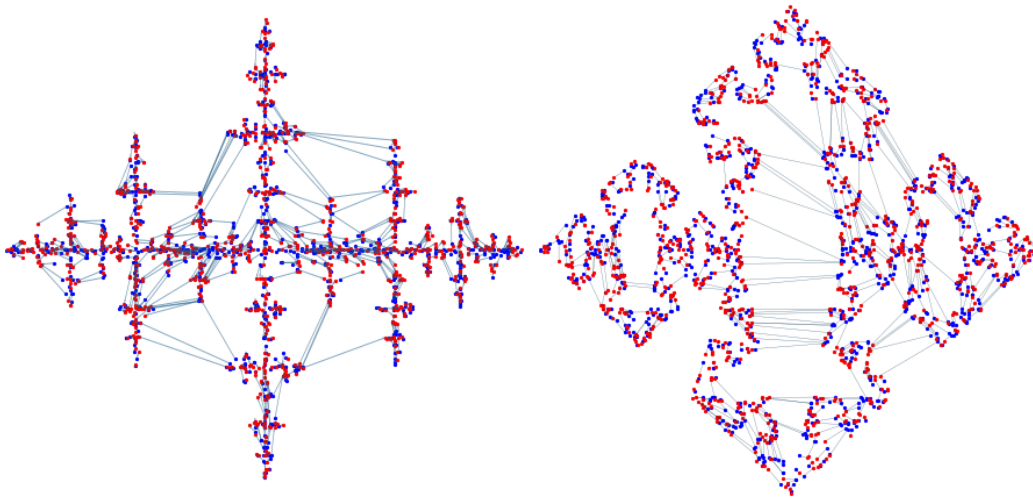


Figure 4.5. – Average energy profiles $E_{n,(2,d_H)}^C$ (y -axis, after subtraction of $\frac{\log n}{2\pi}$) for increasing values of the size n (legend) vs Hausdorff dimension d_H (x -axis). Shaded areas denote \pm one error on the average. Numerical protocol: d_H in steps of $1/29$ from 1.05 to 1.95, 1000 disorder realizations for each value of d_H . The non-monotone behavior of the curves may be related to accidental properties of the Cesàro fractal, as the peaks at $d_H \simeq 1.08, 1.26$ correspond to $\alpha_{\text{Cesàro}} \simeq \pi/5, \pi/3$.

4.8. Conclusions and research perspectives

In this Chapter we have introduced a notion of ERAP at non-integer Hausdorff dimensions. By considering two fractal ensembles, the Peano and Cesàro fractals, providing different interpolations of the interval $(1, 2)$ in Hausdorff dimension, we have provided numerical evidences that the scaling exponents $\gamma_{(p, d_H)}$ are larger than the nearest-neighbors exponents $1 - p/d_H$, and generically display non-monotone behavior in the d_H direction. Our numerical findings suggest the existence of a universality region in the plane (p, d_H) where $\gamma_{(p, d_H)}$ appears to be independent on the fractal set considered (two cases having the same scaling exponent are reported in Fig. 4.6). Providing a first application of the general method discussed in § 3.2.2, we have also shown that energies associated to certain combinations of two independent systems appear to be roughly linearly related. Also, for the Cesàro fractal, we have obtained the energy profile along the d_H direction at “fixed disorder”, showing surprising features (such as a maximum at $d_H \in (1, 1.1)$) that may be worth investigating further. We leave the elucidation of these novel findings (especially the possible critical line which separates a universal region from a non-universal one) to future work.



(a) Instance on the Peano fractal.

(b) Instance on the Cesàro fractal.

Figure 4.6. – Example instances for the Peano (4.6a) and Cesàro (4.6b) ensemble at $d_H = 1.5$, together with the solutions at $p = 1.33$ (arrows, only the longest are visible), giving the same energy scaling exponent $\gamma_{(1.33, 1.5)} = .417(2)$.

GENERAL PROVISIONAL CONCLUSIONS AND RESEARCH PERSPECTIVES

IN this PhD Thesis we have studied a random combinatorial optimization problem, the Euclidean Random Assignment Problem. Our focus has been on the statistical properties of the optimal configuration, depending on the energy-distance exponent p and on the dimension and geometry of the ambient space. In particular, we have presented some new contributions on the asymptotic behavior of the cost at low dimensions, where the Parisi–Mézarid mean-field description is less satisfactory.

In one dimension (Chapter 2) we have reviewed the state of the art and discussed some properties of Fourier modes of the optimal solution at $p = 2$, both in the discrete and continuum case. As an application, we have shown that the probability distribution of the ground state energy can be written in terms of an elliptic function in the latter case on the circle. The determination of such a probability distribution for general finite $p > 1$ remains an open problem.

In the one dimensional ordered regime, motivated by the problem with non-uniform disorder, we have introduced the notion of an *anomalous scaling*. In this case, the leading asymptotic behavior of the ground state energy is determined by a sub-extensive number of edges, the ones nearer to a depleted region. In order to study possible anomalous behaviors we have first considered a simple continuum method, inspired by cutoff regularisation methods in quantum field theory, which reduces the problem to the study of convergence (and possible regularization) of an integral (169). If the integral diverges, the anomalous behavior can be determined fixing a constant by trivial numerical experiments. If the integral is not divergent, the problem is “reduced to quadratures”. It is truly remarkable that our physical motivations led us to consider questions that, in the continuum, appear to be related to topics of current interest in probability (see e.g. the extensive memory (168)).

Still in the ordered regime, we have also shown that, at the price of setting aside simpler continuum methods, in the problem at finite n a qualitatively simple picture appears, where anomalous and bulk scaling are separated by critical

lines. The critical lines are hyperbolic relations involving only two parameters, the energy distance exponent p and the leading exponent characterizing the local behavior of the pdf of \mathcal{B} and \mathcal{R} near endpoints at a finite or infinite value. Generically, logarithmic corrections appear at the critical line (marginally-anomalous scaling), and for a generic stretched-exponential tail. Our combinatorial approach has allowed us to address also the case in which the continuum method does not exist (due to non-convergence of Riemann’s sums), and to point out several connections with topics in Number Theory (such as, in particular, with multiple zeta values). Anomalous behaviors at $p \in (0, 1)$ is not expected, except for a “gapped” distribution, and at $p \in (1/2, 1]$ where the the system is marginal. We shall elucidate this matter elsewhere.

In the concave or non-crossing regime, we have introduced the notion of Dyck matching, a sub-optimal configuration independent on both p and the disorder distribution and completely determined by the ordered list of colors. We have given analytical expressions for the energy scaling of Dyck matchings through analytic-combinatorial methods. On the basis of numerical experiments, we have conjectured that the scaling behavior of the expected energy of Dyck matchings and ground state energy coincide. Our conjecture implies a logarithmic correction to scaling at $p = 1/2$, the origin of which should be investigated further. A proof of our conjecture is still incomplete (it goes through the determination of lower bounds which have the same scaling of the Dyck upper bound), but it is under development, and we are optimistic on its completion in a near future. On the contrary, the analytical determination of the constant in front of the true asymptotics for the ground-state energy (or, in other words, the asymptotics of the ratio between the cost of the Dyck matching and the optimal cost), besides the bounds that would be implied by the forementioned analysis, seems out of reach with our techniques.

In two dimensions (Chapter 3), we have focused on the case $p = 2$ using both continuum and lattice methods, investigating (among other aspects) the logarithmically divergent series for the expected ground state energy, predicted by the Caracciolo–Lucibello–Parisi–Sicuro formalism, beyond the leading divergence. For a generic Riemannian manifold, we have argued, within the linearization framework of the field theoretical approach to this problem, that universality persists at sub-leading level with respect to the leading $\log n$ behavior. Among other aspects, we have related several regularisations methods for the divergent traces of the inverse Laplace-Beltrami operators on the manifold: the integral of the Robin mass and the Kronecker mass via zeta regularization. We have considered the problem for several domains and shown that Robin and Kronecker masses are the only relevant quantities in determining relative energies for different manifolds. Moreover, for domains with a rectangular fundamental polygon, we have given

explicit expression for shifts at varying aspect ratios, in terms of linear combinations of rational functions and logarithmic ratios of the Dedekind η function, admitting non trivial extrema. Our findings point at the existence of a universal constant for the Poisson-Poisson problem, independent on the considered domain and regularisation method used. On the basis of extensive numerical experiments, in the accompanying paper (172) we have given a four-digit estimate of this constant, with the hope of comparing this result with a future theoretical prediction. In § 3.2 we have studied some conditions under which, in the linearised theory, the energies of a collection of related instances are not linearly independent. In particular we have considered 1) instances built acting on the domain Ω with a spectrum preserving, unitary transformation: among them, some explicit examples of involutive symmetries have been studied in details, also in zeta regularization; and 2) instances built via the union of independent point processes. As a by-product, the study of the latter case has indicated a simple numerical procedure for providing evidence of logarithmic scaling of the ground state energy. As in the field-theoretical approach our predicted linear relations are exact (and with simple coefficients), our findings constitute a promising tool to study non-linear contributions in a rather general setting, and will be the content of a future paper.

In order to elucidate the grid-regularised problem (or Grid-Poisson problem), where ultraviolet divergence of the theory are automatically removed, we have introduced a lattice statistical field theory approach and studied some of its properties in the case of the square grid on the two dimensional torus. By means of appropriate lattice calculus operators, we have been naturally led to an exact decomposition of the optimal transport field $\mu = \nabla\phi + \nabla \wedge \psi$, where the conservative part $\nabla\phi$ and solenoidal part $\nabla \wedge \psi$ are in complete analogy with the Helmholtz decomposition of classical electrodynamics. For the choice of uniform distribution of one set of points, the statistical properties of the potentials ϕ and ψ appear to be very different, contributing at different orders to the asymptotic series of the expected ground state energy. In particular, the conservative part appears to be responsible of the $\log n$ divergence (plus possible sub-leading divergencies, which cannot be addressed by our current methods), while the transverse part appears to converge to a finite (and grid-dependent) constant in the large n limit. Our findings appear to be very promising and certainly require further investigation. In particular, with only technical modifications, our proposed statistical field theory approach may be applied to other choices for the grid (such as the hexagonal lattice), giving different UV regularizations. It would be interesting to compare the results for the same disorder to understand if and in what sense they give the same continuum limit. Also, the approach can be readily extended to other choices of the “charges” (that is, disorder distribution associated to red points other than uniform). The latter extension appears to be particularly promising towards devel-

oping an understanding of two-dimensional anomalous behaviors. For example, it is known that stretched edges may contribute additional logarithmic terms to the leading behavior of $\mathbb{E}[\mathcal{H}_{\text{opt}}]$, such as in the case of a gaussian disorder on $\mathcal{M} = \mathbb{R}^2$, where $\mathbb{E}[\mathcal{H}_{\text{opt}}] \sim c(\log n)^2$ for some unknown constant c , as was recently shown by Talagrand (162) and Ledoux (171).

Finally, in order to understand a possible phase diagram of the model in the plane (p, d) , interpolating between the known results for integer values of d , we have introduced a notion of ERAP at non integer Hausdorff dimensions. By considering two fractal ensembles, the Peano and Cesàro fractals, which give different interpolations of the interval $(1, 2)$ in Hausdorff dimension, we have addressed the simplest possible question, namely if there is an indication of universal scaling of the ground state energy at Hausdorff dimensions different from 2. On the basis of extensive numerical experiences, we have strong evidence of the persistence of such a universal scaling well below $d_H = 2$, and exhibited very different geometries resulting in the same scaling exponent (see Fig. 4.6), suggesting that the scaling exponent should be a function of p and the Hausdorff dimension only. The analytical determination of such exponents giving the extent of such universal region as a function of p will be a matter of future work.

A major unsatisfactory point of our work concerns the problem at $p \neq 2$. The special role of the problem at $p = 2$ is interesting on its own, and possibly still to be explored on the basis of our introductory remarks (Fig. 1.4) which seem to indicate that the solution at $p = 2$ could capture most features of the solutions at $(p - \epsilon, p + \epsilon)$ for some $\epsilon > 0$. However, as at $p \neq 2$ tools such as Fourier transforms or lattice duality do not appear to be easily exploitable (of course, Fourier transform always exists, but the fact that the energy is the ℓ^2 norm of the transport field, instead of the ℓ^p norm as is generally the case, is an important simplification, as only the ℓ_2 norm is preserved by Fourier transform), so that the problem is much less understood (even more so at the rigorous level). Our opinion is that substantial mathematical work may profit from the many numerical evidences accumulated during the years (144, 151). Besides the need of a better mathematical understanding of these problems which –as we stressed in several occasions– have been already capable of stimulating mathematical work, several physical questions remains untouched by our present work, especially in the light of the physics of spin-glasses. To mention but one, the existence, determination and characterization of glassy phases for the ERAP is not established. Neither replica nor cavity calculation to address this problem is known (to the best of the author knowledge). Some work in this direction has been started only recently, addressing mono-partite Euclidean matching problem (156) (which however, contrarily to the mean-field case, in low dimension has a completely different thermodynamics w.r.t. the bipartite case).

Another major unsatisfactory point pertains the little studied case $p = 1$, which appears to be special at $d = 1$ as it separates the Dyck from the ordered regime. In particular, in two dimensions, one easily shows that edges connecting optimally assigned points cannot cross. Heuristically, this two dimensional non-crossing property appears to promote the formation of “long combs” in the optimal transport field, regions where the typical edge is much longer than $\sqrt{\frac{\log n}{n}}$ in finite volume. Consequences of the non-crossing property in two dimension have not been worked out even in the simplest cases, and it is expected that the field-theoretical approach should not hold in this case. Extensions in two dimensions for $p < 0$ also appear also to be interesting, as this problem may share analogies with the two-components log-gas (155) (except that one does not consider intra-color contributions).

Lastly, it appears fair to state that the phase diagram of the Euclidean Random Assignment Problem at low dimensions displays interesting but still poorly understood features. For example, we have given strong experimental evidence of persistence of universality below $d = 2$ (in a certain sense), and have evidence of a phase transition, accompanied by a logarithmic correction factor at the critical point, at $(d, p) = (1, 1/2)$.

Specific research problems, the resolution of which may in our opinion help to find an angle of attack to some of the previous questions, have been detailed at the end of each Chapter in the hope of providing “soft” entry points to the topic. In the following, we would like to mention five, broader research themes sharing tight relations with the present work in the hope of promoting new approaches to possibly interesting problems on a longer time-scale research perspective.

Permanent of random matrices and ERAP at non-zero temperature.

We have mentioned in the introduction that the canonical partition function of an ERAP at finite temperature $\mathcal{Z}(\beta)$ satisfies $\mathcal{Z}(\beta) = \text{perm}[W(\beta)]$, where perm is matrix permanent and the positive matrix $W(\beta)$ is the Hadamard (entry-wise) exponential of the assignment cost matrix (see Eq. 1.5.0.4). The statistical properties of the “elementary excitations” in an ERAP, that is, closed cycles of even length (in units of edges of the underlining bipartite graph) which are alternating on the optimal solution, are well-exposed if the cost matrix is brought in the so-called *Hungarian gauge* (that is, with the zeros of assigned positions along the diagonal, as in the standard output of the Hungarian algorithm). Let $W^{(h)}(\beta)$ be the Hadamard exponential of the assignment cost matrix in the Hungarian gauge. As the bound $|\det[W(\beta)]| \leq \mathcal{Z}(\beta)$ is gauge-invariant, a promising research direction appears to be the study of the distribution of $|\det(FW^{(h)}(\beta))|$, where F_{ij} is an uniformly random complex number of modulus 1 and FW is element-wise multiplication of the matrices. A study of the statistical properties of the complex zeros of $\text{perm}[W(\beta)]$, depending on $\beta > 0$ and the choice of μ , in the $n \rightarrow \infty$ limit appears also to be a promising research perspective in this direction. Lastly, for $\alpha \in \mathbb{C}$, a possible generalization of the partition function is

$$\phi(\alpha, \beta) = \sum_{\pi \in \mathcal{S}_n} \alpha^{n-\nu(\pi)} \prod_{i=1}^n W(\beta)_{i\pi(i)}, \quad (5.0.0.1)$$

where $\nu(\pi)$ is the number of cycles in the permutation π . Eq. (5.0.0.1) is related to the α -permanent considered by Vere-Jones and others (70, 138), and provides an interpolation between the determinant ($\alpha = -1$) and permanent ($\alpha = 1$), and at high temperatures $\beta \rightarrow 0$ reduces to $\phi(\alpha, 0) = \prod_{j=1}^{n-1} (1 + j\alpha)$ (that is, the ordinary generating function of the Stirling numbers of the first kind).

ERAP and the d -dimensional Brownian loop. Very little is known for an ERAP in which \mathcal{M} has non-integer Hausdorff dimension d_H , even considering a cost function which can be canonically related to the dimension of an ambient space. For example, on the basis of numerical evidences, we have argued that the scaling exponent of $\mathbb{E}[\mathcal{H}_{\text{opt}}]$ appears to be universal in a region $p_{\min}(d_H) < p < p_{\max}(d_H)$ comprising the line $p = 1$, and expanding at large d_H (see Chapter 4, Fig. 4.3). Within this context, one is naturally led to consider blue and red points distributed with the (e.g.) uniform measure on a d -dimensional Brownian loop (an instance at $d = 2$ being shown in Fig. 5.1). We propose that the latter may be a conceivable natural model for a charged polymer in solution. One finds that local violations of the “charge neutrality” condition are associated with “bottlenecks” of a certain physical flow. Especially at $d = 2$, a possible connection between

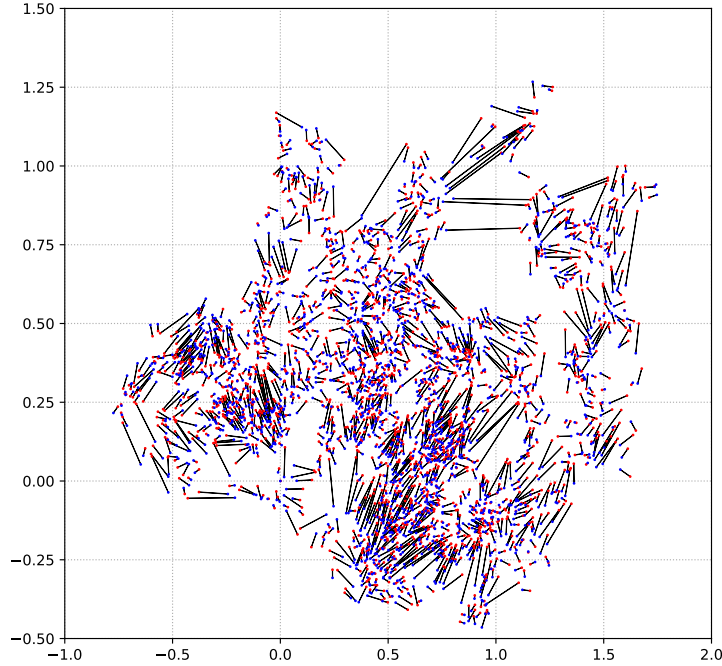


Figure 5.1. – *Optimal assignment of $n_b = 2^{12}$ blue points onto $n_r = 2^{12}$ red points unif. distr. on a two dimensional Brownian loop rooted at the origin (the solution at $p = 1$ is depicted by black arrows, which do not cross due to the parallelogram inequality). Notice the presence of long arrows assigning regions where, locally, the “conservation law” $n_b - n_r = 0$ is violated.*

the statistical properties of such bottlenecks and cut times of the simple random walk appears possible, in particular in connection with the well-studied intersection exponents ζ_d (65), which may be related to the large n scaling exponent of $\mathbb{E}[\mathcal{H}_{\text{opt}}]$.

Field theoretic approach to the ERAP beyond linearization. In (144), Caracciolo-Lucibello-Parisi-Sicuro (CLPS) first proposed a field theoretic approach to the ERAP which allowed to recover certain aspects of the asymptotic expansion of $\mathbb{E}[\mathcal{H}_{\text{opt}}]$ depending on the dimensionality d of \mathcal{M} . In that approach, the authors considered the action of a free field complemented by a constraint enforcing the transport condition. The variational principle for the linearized action gives rise to a Poisson equation which can be interpreted as a linearization of the Monge-Ampère equation arising in optimal transport. As customary in Quantum Field Theory, the authors assumed the existence of a cutoff function $F(x)$ in momentum space with prescribed small argument behavior $\lim_{x \rightarrow 0} F(x) = 1$ and such that $\lim_{x \rightarrow \infty} F(x) = 0$. At $d = 2$, the CLPS approach allowed to access

the leading (Ajtai-Komlós-Tusnàdy) behavior, which, in retrospective, is typical of the renormalization group acting on the critical dimension, where the defining term appearing in the action is a marginal operator. However, sub-leading terms of the asymptotic series are not directly accessible with this approach. Moreover, the alternative PDE approach introduced by Ambrosio-Stra-Trevisan (164), which allowed to establish rigorously the value of limit constants, also cannot go beyond the leading behavior and does not appear to be easily generalizable, due to essential technical aspects in their proof. However, in the field theoretical approach, one can go beyond linearization and consider the full perturbative series arising from the exact action. This approach allows to describe the full distribution of \mathcal{H}_{opt} by means of a diagrammatic (possibly asymptotic) series with intriguing combinatorial properties (some results having been presented by Sportiello at the IHP). We wish to develop further these aspects, in particular in connection with the extension of the ERAP at arbitrary densities on possibly non-compact underlying spaces \mathcal{M} , and explore the connections of this problem with the recently introduced classification of the scaling of $\mathbb{E}[\mathcal{H}_{\text{opt}}]$ into anomalous and bulk regimes for the ERAP at $d = 1$.

On logarithmic derivatives of the Dedekind η function appearing in regularisations of the ERAP at $d = 2$ and $p = 2$. In § 3.1 we have considered two regularization schemes for the ERAP at $(p, d) = (2, 2)$ on several highly symmetrical domains \mathcal{M} , also in connection to certain classical invariants expressed in terms of the spectrum of the Laplace-Beltrami operator associated to the surface \mathcal{M} (51, 120). We have also considered a regularisation of the (logarithmically) divergent spectral sum by performing the analytic continuation of the associated zeta function in the Kronecker limit. The method allowed for example to compute differences in sub-leading constants among different domains \mathcal{M} and \mathcal{M}' . The theoretical predictions were in excellent agreement with numerical experiments performed on several geometries.

A motivation behind this work was that very little is known about the asymptotic series of $\mathbb{E}[\mathcal{H}_{\text{opt}}]$ beyond the now-established universal $\sim \frac{1}{2\pi} \log n$ behavior, and indeed no method appears to be currently able to address this problem directly.

In our studies we have considered domains with a rectangular, $l_1 \times l_2$ fundamental polygon (such as the cylinder or the torus), and shifts at fixed geometry but variable aspect ratio $\rho = \frac{l_1}{l_2}$. Quite surprisingly, we have observed a number of instances in which such relative energies between different geometries admit (unique) global extrema at non-trivial values of the aspect ratio ρ . In these “extremal geometries” a fundamental building block appeared to be logarithmic derivatives of the Dedekind η function. More precisely, optimal ρ are determined by solutions

to equations of the type

$$\frac{a}{\rho^2} + \frac{b}{\rho} = ic \frac{\eta'(i\rho)}{\eta(i\rho)} \quad (5.0.0.2)$$

where η is the Dedekind function, and $a, b, c \in \mathbb{R}$, and we have been able to solve these kind of equations only numerically. On the other hand, it is well-known that the rhs of Eq. 5.0.0.2, at certain special values of ρ (which are not extremal for our considered problems), reduces to the evaluation of series of reciprocal hyperbolic functions (see e.g. Prop. 2.25 in (29), and (157)), and some of these series have already been considered in the context of the Neumann problem on the rectangle (28). The possibility that different extremal geometries (that is, optimal aspect ratios for different domains \mathcal{M}) may be related through non-trivial relationship appears to be an interesting research perspective.

Cycle structure of the optimal permutation for the ERAP on a general graph. We have argued that an understanding of the combinatorial structure of the optimal configuration π_{opt} for an ERAP in cases where \mathcal{B} and \mathcal{R} can be naturally ordered (as in $d = 1$ and $\mathcal{M} = \mathbb{R}$) can be very useful, but has been possible for a handful choices of the cost function only. Indeed, combinatorial results either allowed to study the exact solution with analytical methods (e.g. when $c(x) = |x|^p$ and $p > 1$, in which case π_{opt} is the identity, or $p < 0$, in which case π_{opt} is cyclical (154)), either served as a guiding principle for the introduction of approximate solutions, such as the ‘‘Dyck matchings’’ (173), which conjecturally have the same asymptotic behavior of the optimal one. In this direction, even weaker notions of order for points could be further exploited. A typical example would be to consider points distributed along the edges of some graphs (such as star graphs). In such a problem, starting from the simplest choices of cost function, is it possible to relate the combinatorial properties of π_{opt} (or the π_{opt} s?) to the topology of the graph?

Dynamics of indistinguishable agents. Tracking the motion of many identical agents can be seen as an assignment problem in which the positions of agents at time t_i (\mathcal{B}) have to be assigned to positions of agents at time t_{i+1} (\mathcal{R}) by preserving their individual identities. An analogous construction arises in the Feynman-Kac representation of the Bose gas, upon interpreting time as inverse temperature (122). If $t_{i+1} - t_i$ is sufficiently small, and the cost function is the maximum likelihood function for ‘‘recognising’’ the dynamics (e.g., $c(x) = |x|^2$ is the maximum likelihood function for diffusive motion, or ballistic motion with minor modifications), one expects the transport field to correspond to the actual displacement field in the limit $t_{i+1} - t_i \rightarrow 0$. An approximate algorithm to address similar questions, based on belief propagation, has been already applied to turbu-

lent flow (129). However, in many real-life situations of interest, the motion of many individual agents displays long-range correlations. For example, evidences have been reported that the motion of a flock of birds displays an intriguing collective response to external perturbations (128). How to extend the assignment approach to such dynamical situations in order to understand deviations from uncorrelated dynamics appears to be an interesting research perspective, especially in light of the availability of extensive empirical data.

We hope to address some of these research directions in future work.

Appendices

A.1. The number of edges of length $2k + 1$ in a Dyck matching at size n (§ 2.7.7)

The goal of this Appendix is to compute the coefficients $v_{n,k}$, crucially used in the calculation of the average cost of the Dyck matching, starting with Eq. 2.7.7.9. These coefficients count, among the n edges of all the possible $\binom{2n}{n}$ Dyck matchings on $2n$ points, the number of edges e of length $\|e\| = 2k + 1$. That is, $v_{n,k} \frac{(n-1)!^2}{2(2n-1)!}$ is the probability that, taking a random Dyck matching π_{Dyck} uniformly, and an edge $e \in \pi_{\text{Dyck}}$ uniformly, we have $\|e\| = 2k + 1$.

Dyck matchings correspond to Dyck “bridges”, w.r.t. the notation introduced in § 2.7.5. We proceed with the calculation by first computing the analogous quantity on a restricted ensemble, associated to Dyck “excursions” (that is, the ordinary Dyck paths), which are Dyck bridges satisfying the extra condition $\sum_{i=1}^j \sigma_i \geq 0$ for all $1 \leq j \leq 2n$.

In the whole class of Dyck paths of length $2n$ there are

$$r_{n,k} := \frac{n - k + 1}{2} C_k C_{n-k} = \frac{1}{2} C_k B_{n-k} \quad (\text{A.1.0.1})$$

edges of length $\|e\| = 2k + 1$ (see <http://oeis.org/A141811>), with $0 \leq k \leq n - 1$. These numbers obey the recursion relation, which determines them univocally (together with the initial conditions)

$$r_{n,k} = C_k C_{n-k-1} + \sum_{m=0}^{n-1} [r_{m,k} C_{n-m-1} + r_{n-m-1,k} C_m] . \quad (\text{A.1.0.2})$$

The recursion can be understood in terms of a first-return decomposition. If we decompose the path into its *first return*, i.e. the portion between its left endpoint and its first zero (say at position $2m + 2$, $0 < m < n - 1$), and into its *tail*, i.e. the remaining portion of the path on the right, then:

- the first term counts all the paths in which the link between the first step and the first zero is of the required length. The multiplicity of paths in

which this situation arise is given by all the possible paths composing the first excursion times all the possible paths composing the tail;

- the sum counts, for all the possible positions of the first zero, the possible links of the required length hidden in the first excursion or in the tail of the path. To count links of the required length hidden in the first excursion, one can use $r_{m,l}$ itself, times all the possible tails C_{n-m-1} . The tail case is symmetric.

It is easy to prove by induction that

$$r_{n,k} = C_k R_{n-k-1} \quad (\text{A.1.0.3})$$

and the recursion reduces to

$$R_s = C_s + 2 \sum_{m=1}^{s-1} C_{s-m} R_{m-1}. \quad (\text{A.1.0.4})$$

By introducing the generating function

$$R(z) := \sum_{n \geq 0} R_n z^n \quad (\text{A.1.0.5})$$

we get the equation

$$R(z) = C(z) + 2z C(z) R(z) \quad (\text{A.1.0.6})$$

and therefore

$$\begin{aligned} R(z) &= \frac{C(z)}{1 - 2z C(z)} = C(z) B(z) = \frac{1}{2z} \left[\frac{1}{\sqrt{1-4z}} - 1 \right] \\ &= -\frac{1}{2z} + \frac{1}{2z} + \sum_{n \geq 0} \frac{B_{n+1}}{2} z^n = \sum_{n \geq 0} \frac{B_{n+1}}{2} z^n \end{aligned} \quad (\text{A.1.0.7})$$

indeed

$$\sum_{k=1}^n C_k B_{n-k} = \frac{B_{n+1}}{2}. \quad (\text{A.1.0.8})$$

It follows that

$$R_{n-k-1} = \frac{B_{n-k}}{2} \quad (\text{A.1.0.9})$$

as announced.

The preliminary computation of the $r_{n,k}$ coefficients suggests to use the same

technique for the $v_{n,k}$, and provides an ingredient to write a recursion for the $v_{n,k}$:

$$\begin{aligned}
v_{n,k} &= 2 C_k B_{n-k-1} + 2 \sum_{m=0}^{n-1} (r_{m,k} B_{n-m-1} + v_{n-m-1,k} C_m) \\
&= 2 C_k B_{n-k-1} + \sum_{m=k+1}^{n-1} C_k B_{m-k} B_{n-m-1} + 2 \sum_{m=k+1}^{n-1} v_{m,k} C_{n-m-1} \\
&= 2 C_k B_{n-k-1} + \sum_{m=1}^{n-k-1} C_k B_m B_{n-k-m-1} + 2 \sum_{m=1}^{n-k-1} v_{m+k,k} C_{n-k-m-1}
\end{aligned} \tag{A.1.0.10}$$

and if we again set

$$v_{n,k} := C_k V_{n-k-1} \tag{A.1.0.11}$$

we get

$$\begin{aligned}
V_s &= 2 B_s + \sum_{m=1}^s B_m B_{s-m} + 2 \sum_{m=1}^s V_{m-1} C_{s-m} \\
&= B_s + \sum_{m=0}^s B_m B_{s-m} + 2 \sum_{m=1}^s V_{m-1} C_{s-m} \\
&= B_s + 4^s + 2 \sum_{m=1}^s V_{m-1} C_{s-m}.
\end{aligned} \tag{A.1.0.12}$$

We introduce now the generating function

$$V(z) := \sum_{k \geq 0} V_k z^k \tag{A.1.0.13}$$

to get the relation

$$V(z) = \frac{1}{\sqrt{1-4z}} + \frac{1}{1-4z} + 2z \frac{1-\sqrt{1-4z}}{2z} V(z) \tag{A.1.0.14}$$

so that

$$V(z) = \frac{1}{1-4z} + \frac{1}{(1-4z)^{\frac{3}{2}}} = \sum_{k \geq 0} \left[4^k + \frac{(2k+1)!}{(k!)^2} \right] z^k, \tag{A.1.0.15}$$

which is our seeked result. We can finally check that the recursion above is indeed

satisfied, as

$$\begin{aligned} v_{n,k} &= C_k \left[4^{n-k-1} + \frac{(2n-2k-1)!}{[(n-k-1)!]^2} \right] \\ &= C_k \left[4^{n-k-1} + \frac{(n-k)^2}{2(n-k)} B_{n-k} \right] \\ &= 4^{n-k-1} C_k + (n-k) r_{n,k}. \end{aligned} \tag{A.1.0.16}$$

A.2. Expansion of the generating function $S(z; p)$ via singularity analysis (§ 2.7.7)

Singularity analysis is a technique that allows to extract information on the coefficients of a generating function $f(z)$ when an explicit series expansion around $z = 0$ is not available. Roughly speaking, two main principles hold (see e.g. (123, pg. 227)):

1. the moduli of the singularities of f dictate the asymptotic exponential growth of its coefficients. If $z = a$ is a singularity of $f(z) = \sum_{n \geq 0} f_n z^n$, then $f_n \sim |a|^{-n}$;
2. the nature of the singularities of f dictate the asymptotic sub-exponential growth of its coefficients, i.e. they determine the (typically polynomial or logarithmic) function $\theta(n)$ such that $f_n \sim |a|^{-n} \theta(n)$.

We will specialise this analysis to the case of a single singularity, along the real positive axis, which is pertinent to series with positive coefficients, and no oscillatory behaviour. Generalizations of these principles (and of the related theorem below) for the case of multiple singularities at the same radius hold as well, but in our case are not relevant and will not be discussed.

The main result that we are going to need is a theorem (see (123, Theorem VI.4)) that states that if $f(z)$ is a “well-behaved” complex function analytic in \mathbb{D} , with a singularity at $z = \zeta + i0$ such that

$$f(z) = \sigma(z/\zeta) + o(\tau(z/\zeta)) \tag{A.2.0.1}$$

for some functions $\sigma = \sum_{n \geq 0} \sigma_n z^n$ and $\tau = \sum_{n \geq 0} \tau_n z^n$ in the span of the reference set

$$\mathcal{S} = \left\{ (1-z)^\alpha \left(\frac{1}{z} \log \frac{1}{1-z} \right)^\beta \mid \alpha, \beta \in \mathbb{C} \right\}, \tag{A.2.0.2}$$

then

$$f_n = \zeta^{-n} \sigma_n + o(\zeta^{-n} \tau_n). \tag{A.2.0.3}$$

Here, “well behaved” means that there exists an indented disk of radius bigger than ζ , with the indentation that specifically excludes $z = \zeta + i0$, where $f(z)$ can be analytically continued. This means that the theorem is applicable to functions with very general singularities (isolated poles, branch cuts, ...), and in particular to hypergeometric functions.

The reference set \mathcal{S} is composed of functions whose expansion can be computed exactly thanks to generalizations of the binomial theorem. These functions are

ubiquitous in series expansions around poles of complex functions, so that the theorem is extremely versatile.

In our specific case of the ES model, the generating function to study is of the form

$$f(z) = s(4z) F \left(\begin{matrix} a, b \\ c \end{matrix} \middle| 4z \right) \quad (\text{A.2.0.4})$$

where $s(z) \in \text{span } \mathcal{S}$ is singular at $z = 1$, and $F = {}_2F_1$ is the $(2, 1)$ -hypergeometric function defined by

$$F \left(\begin{matrix} a, b \\ c \end{matrix} \middle| z \right) = \sum_{n \geq 0} \frac{\Gamma(n+a) \Gamma(n+b)}{\Gamma(a) \Gamma(b)} \frac{\Gamma(c)}{\Gamma(n+c)} \frac{z^n}{n!}, \quad (\text{A.2.0.5})$$

or, equivalently, by

$$F \left(\begin{matrix} a, b \\ c \end{matrix} \middle| z \right) = \sum_{n \geq 0} s_n \frac{z^n}{n!}; \quad (\text{A.2.0.6})$$

$$\frac{s_{n+1}}{s_n} = \frac{(a+n)(b+n)}{c+n}; \quad s_1 = 1. \quad (\text{A.2.0.7})$$

To expand and study the hypergeometric function around $z = 1$, a celebrated “inversion formula” due to Gauss is available

$$F \left(\begin{matrix} a, b \\ c \end{matrix} \middle| z \right) = \frac{\Gamma(c)\Gamma(c-a-b)}{\Gamma(c-a)\Gamma(c-b)} F \left(\begin{matrix} a, b \\ a+b+1-c \end{matrix} \middle| 1-z \right) + \frac{\Gamma(c)\Gamma(a+b-c)}{\Gamma(a)\Gamma(b)} (1-z)^{c-a-b} F \left(\begin{matrix} c-a, c-b \\ c+1-a-b \end{matrix} \middle| 1-z \right). \quad (\text{A.2.0.8})$$

This formula restates the sought expansion around $z = 0$ in terms of an expansion near the singularity at $z = 1$. As the hypergeometric function is analytic in $z = 0$, the singular behaviour at $z = 1$ of the right-hand side combination is described by the power-law prefactors in the inversion formula.

In our specific case, $a = \frac{p+1}{2}$, $b = \frac{p+2}{2}$ and $c = 2$ with $p \in [0, 1]$, giving $c - a - b = \frac{1-2p}{2} \in [-\frac{1}{2}, \frac{1}{2}]$. Thus, the leading terms of the expansion of $f(z)$ are:

$$f(z) = s(4z) \left[\frac{\Gamma(c)\Gamma(c-a-b)}{\Gamma(c-a)\Gamma(c-b)} + \frac{\Gamma(c)\Gamma(a+b-c)}{\Gamma(a)\Gamma(b)} (1-4z)^{c-a-b} + \Theta((1-4z), (1-4z)^{c-a-b+1}) \right]. \quad (\text{A.2.0.9})$$

The above expression is valid only for $p \neq \frac{1}{2}$. A limit procedure combines the

diverging Γ 's and the $(1 - 4z)$ term to give

$$f(z) = s(4z) \left[-\frac{1}{\Gamma(\frac{3}{4})\Gamma(\frac{5}{4})} (\ln(1 - 4z) + 2\gamma_E + \psi_0(\frac{3}{4}) + \psi_0(\frac{5}{4})) + \Theta((1 - 4z) \ln(1 - 4z)) \right]. \quad (\text{A.2.0.10})$$

where γ_E is the Euler-Mascheroni constant and ψ_0 is the digamma function. The limit is to be performed with care: each term must be written as a function of $\epsilon = p - \frac{1}{2}$ and expanded in powers series. The expansion of the hypergeometric functions must be performed using their definition. When everything is expanded, $o(\epsilon)$ are discarded taking the limit $\epsilon \rightarrow 0$, and the leading terms in the $(1 - 4z)$ are found by taking $n = 0$ in the sum of the hypergeometric function definition.

≈ APPENDIX B ≈

B.1. The first Kronecker limit formula (§ 3.1.2)

In this Appendix we will summarize some results obtained in the realm of analytic number theory that have been useful to obtain our results. General references for our discussion are Siegel (20) (Chapter 1) and Lang (48).

Let $z \in \mathbb{C}$. The Riemann ζ -function $\zeta(z)$ is defined in the half-plane $\Re(z) > 0$ by

$$\zeta(z) := \sum_{k \geq 1} \frac{1}{k^z}. \quad (\text{B.1.0.1})$$

The series converges absolutely for $\Re(z) \geq 1 + \epsilon$ for every $\epsilon > 0$. Riemann proved that $\zeta(z)$ has an analytic continuation in the whole z -plane which is regular except a simple pole at $z = 1$ with residue 1. At $z = 1$, $\zeta(z)$ has an expansion

$$\zeta(z) - \frac{1}{z-1} = \sum_{k=1}^{\infty} \int_k^{k+1} du (k^{-z} - u^{-z}) = \gamma_E + o(z-1). \quad (\text{B.1.0.2})$$

As generalization of the Riemann ζ -function, we consider a positive-definite binary quadratic form, in the real variables $u, v \in \mathbb{R}$

$$Q(u, v) := au^2 + 2buv + cv^2 \quad (\text{B.1.0.3})$$

where, $a, b, c \in \mathbb{R}$ and $a > 0$ and $d := ac - b^2 > 0$. Let us define

$$\zeta_Q(z) := \sum_{\substack{(m,n) \in \mathbb{Z}^2 \\ n^2 + m^2 \neq 0}} \frac{1}{[Q(m, n)]^z}. \quad (\text{B.1.0.4})$$

Now

$$\begin{aligned}
Q(u, v) &= a \left(u + \frac{b}{a} \right)^2 + \frac{v^2 d}{a} \\
&= a \left(u + \frac{b + i\sqrt{d}}{a} v \right) \left(u + \frac{b - i\sqrt{d}}{a} v \right) \\
&= a |u + \tau v|^2
\end{aligned} \tag{B.1.0.5}$$

where

$$\tau = \frac{b + i\sqrt{d}}{a} \tag{B.1.0.6}$$

with $\Im(\tau) = a^{-1}\sqrt{d} > 0$.

If $d = 1$, $\zeta_Q(z) \equiv \zeta_\tau(z)$, associated to Q , is defined for $\Re(z) > 1$ can be analytically continued into a regular function for $\Re(z) > 1/2$ except for a simple pole at $z = 1$ with residue π , and the function $\zeta_Q(z)$, has an expansion (first limit formula of Kronecker)

$$\zeta_\tau(s) - \frac{\pi}{z-1} = 2\pi \left[\gamma_E - \ln(2\sqrt{\Im(\tau)}|\eta(\tau)|^2) \right] + o(z-1), \tag{B.1.0.7}$$

where

$$\eta(z) := e^{\frac{\pi iz}{12}} \prod_{n=1}^{\infty} (1 - e^{2\pi inz}) \tag{B.1.0.8}$$

is the Dedekind η -function (27), which satisfies the functional equations

$$\eta(z+1) = e^{\frac{\pi i}{12}} \eta(z) \tag{B.1.0.9a}$$

$$\eta\left(-\frac{1}{z}\right) = \sqrt{-iz} \eta(z). \tag{B.1.0.9b}$$

Known particular values are

$$\eta(i) = \frac{\Gamma(1/4)}{2\pi^{3/4}} \approx 0.76823 \tag{B.1.0.10a}$$

$$\eta(2i) = \frac{\Gamma(1/4)}{2^{11/8}\pi^{3/4}} \approx 0.59238 \tag{B.1.0.10b}$$

$$\eta(4i) = \left(-1 + \sqrt{2}\right)^{1/4} \frac{\Gamma(1/4)}{2^{29/16}\pi^{3/4}} \approx 0.35092. \tag{B.1.0.10c}$$

≈ APPENDIX C ≈

C.1. Calculus on the square lattice (§ 3.3)

In this Appendix we shall recall some basic definitions of calculus on the lattice. Our review could have been independent on the two-dimensional Grid-Poisson ERAP, but for the sake of definiteness we shall restrict to the square lattice used in § 3.3.

For a complex valued function f defined on the d -dimensional regular lattice, for $\nu = 1, \dots, d$ recall the positive and negative directional derivatives

$$\begin{aligned}\nabla_{\nu}^{+} f(z) &:= f(z + e_{\nu}) - f(z) \\ \nabla_{\nu}^{-} f(z) &:= f(z) - f(z - e_{\nu}) = \nabla_{\nu}^{+} f(z - e_{\nu})\end{aligned}\tag{C.1.0.1}$$

in terms of which the *lattice laplacian* is

$$\begin{aligned}\Delta f(z) &:= \sum_{\nu} \nabla_{\nu}^{-} \nabla_{\nu}^{+} f(z) = \sum_{\nu} \nabla_{\nu}^{+} \nabla_{\nu}^{-} f(z) \\ &= \sum_{\nu} [f(z + e_{\nu}) + f(z - e_{\nu}) - 2f(z)] \\ &= \sum_{\nu} [\nabla_{\nu}^{+} - \nabla_{\nu}^{-}] f(z).\end{aligned}\tag{C.1.0.2}$$

Δ is a self-adjoint operator with respect to the lattice inner product defined, for any two complex valued functions $f, g : \Lambda_n \rightarrow \mathbb{C}$, by

$$(f, g) = \sum_{z \in \Lambda_n} \bar{f}(z) g(z),\tag{C.1.0.3}$$

where \bar{z} is complex conjugate of z (an analogous definition holds for the dual lattice). In our setting at $d = 2$, where $n = L^2$, the discrete Fourier representation of a function f is

$$f(z) = \frac{1}{L} \sum_p e^{ip \cdot z} \hat{f}(p)\tag{C.1.0.4}$$

where the discrete lattice momenta $p = \frac{2\pi}{L} \begin{pmatrix} n_1 \\ n_2 \end{pmatrix}$ depend on $(n_1, n_2) \in \mathbb{Z}^2$. It follows that

$$\Delta \hat{f}(p) = -\hat{p}^2 \hat{f}(p) \quad (\text{C.1.0.5})$$

where

$$\hat{p}_i := 2 \sin \frac{p_i}{2}, \quad i = 1, 2 \quad (\text{C.1.0.6})$$

is a generalization of Eq. 2.3.1.18. If vector fields are considered, Definition C.1.0.4 holds component-wise, and when obvious we shall always understand sum over components, so that e.g.

$$\mathcal{H}_{\text{opt}} = (\vec{\mu}, \vec{\mu}) = \sum_{i=1}^2 (\mu_i, \mu_i). \quad (\text{C.1.0.7})$$

A main tool of our discussion are *diagonal derivatives*, which informally are finite differences operators acting “between” the direct and the dual lattice. More precisely, for a function $h : \Lambda_n \cup \hat{\Lambda}_n \rightarrow \mathbb{C}$, defined both on the direct lattice Λ_n and on the dual lattice $\hat{\Lambda}_n$, they are defined as

$$\begin{aligned} \nabla_1 h(i, j) &= \frac{1}{\sqrt{2}} \left[h \left(i + \frac{1}{2}, j + \frac{1}{2} \right) - h \left(i - \frac{1}{2}, j - \frac{1}{2} \right) \right], \\ \nabla_2 h(i, j) &= \frac{1}{\sqrt{2}} \left[h \left(i - \frac{1}{2}, j + \frac{1}{2} \right) - h \left(i + \frac{1}{2}, j - \frac{1}{2} \right) \right] \end{aligned} \quad (\text{C.1.0.8})$$

for $i, j = 0, \dots, L-1$ (see Fig. 3.12a for a graphical rule). In terms of diagonal derivatives, it is possible to introduce the *divergence* and *curl* of any vector field $\vec{E} : \Lambda_n(\hat{\Lambda}_n) \rightarrow \mathbb{T}_2$. They are the scalar fields

$$\begin{aligned} \nabla \cdot \vec{E} &= \nabla_\alpha E_\alpha, \\ \nabla \wedge \vec{E} &= \epsilon_{\alpha\beta} \nabla_\alpha E_\beta, \quad (\alpha, \beta = 1, 2), \end{aligned} \quad (\text{C.1.0.9})$$

where $\epsilon_{\alpha\beta}$ is the 2-dimensional Levi-Civita symbol (and the convention on repeated indices has been used). Remark that for a complex valued vector field defined on $\Lambda_n(\hat{\Lambda}_n)$, its divergence and curl are defined on $\hat{\Lambda}_n(\Lambda_n)$. Moreover, they satisfy the zero-sum conservation laws

$$\sum_{z \in \Lambda_n(\hat{\Lambda}_n)} (\nabla \cdot \vec{E})(z) = \sum_{z \in \Lambda_n(\hat{\Lambda}_n)} (\nabla \wedge \vec{E})(z) = 0 \quad (\text{C.1.0.10})$$

by two-dimensional telescoping*. On the other hand, recall that the lattice laplacian Δ acts either “on” the direct or “on” the dual lattice, but not “between” them: for any function $f : \Lambda_n(\hat{\Lambda}_n) \rightarrow \mathbb{C}$, we can write locally

$$(\Delta f)(i, j) = \frac{1}{2} [f(i+1, j+1) + f(i-1, j-1) + f(i-1, j+1) + f(i+1, j-1) - 4f(i, j)] . \quad (\text{C.1.0.12})$$

for $i, j = 0, \dots, L-1$ (see Fig. 3.12b for a graphical rule). Of course, the laplacian of any function also satisfies the zero-sum condition

$$\sum_{z \in \Lambda_n(\hat{\Lambda}_n)} (\Delta f)(z) = 0 . \quad (\text{C.1.0.13})$$

To elucidate the combined effect of our “rotation” (Eq. 3.3.1.9) and expression of the rotated field in terms of diagonal derivatives (Defs. C.1.0.8), it may be useful to observe that the divergence of $\vec{\mu}_{-\pi/4}$ can be written locally as

$$\begin{aligned} (\nabla \cdot \vec{\mu}_{-\pi/4}) \left(i + \frac{1}{2}, j + \frac{1}{2} \right) &= \frac{\mu_1(i+1, j+1) - \mu_1(i, j) + \mu_2(i, j+1) - \mu_2(i+1, j)}{\sqrt{2}} \\ &= \frac{\mu_x(i+1, j+1) - \mu_x(i, j) - \mu_x(i, j+1) + \mu_x(i+1, j)}{2} + \\ &\quad \frac{\mu_y(i+1, j+1) - \mu_y(i, j) + \mu_y(i, j+1) - \mu_y(i+1, j)}{2} , \end{aligned} \quad (\text{C.1.0.14})$$

or, in terms of the standard directional lattice derivatives and ordinary $\vec{\mu}$ components as

$$\begin{aligned} (\nabla \cdot \vec{\mu}_{-\pi/4}) \left(i + \frac{1}{2}, j + \frac{1}{2} \right) &= \nabla_x^+ \left[\frac{\mu_x(i, j+1) + \mu_x(i, j)}{2} \right] + \nabla_y^+ \left[\frac{\mu_y(i+1, j) + \mu_y(i, j)}{2} \right] \\ &= \nabla_x^+ \mu_x(i, j) + \nabla_y^+ \mu_y(i, j) + \nabla_x^+ \nabla_y^+ \left[\frac{\mu_x(i, j) + \mu_y(i, j)}{2} \right] . \end{aligned} \quad (\text{C.1.0.15})$$

*Indeed, the stronger conservation laws

$$\sum_{z \in \Lambda_n(\hat{\Lambda}_n)} (\nabla_i \vec{E})(z) = 0, \quad i = 1, 2 \quad (\text{C.1.0.11})$$

hold separately.

Correspondingly, the curl can be written as

$$\begin{aligned}
(\nabla \wedge \vec{\mu}_{-\pi/4}) \left(i + \frac{1}{2}, j + \frac{1}{2} \right) &= \frac{\mu_2(i+1, j+1) - \mu_2(i, j) - \mu_1(i, j+1) + \mu_1(i+1, j)}{\sqrt{2}} \\
&= \frac{-\mu_x(i+1, j+1) + \mu_x(i, j) - \mu_x(i, j+1) + \mu_x(i+1, j)}{2} + \\
&\quad \frac{\mu_y(i+1, j+1) - \mu_y(i, j) - \mu_y(i, j+1) + \mu_y(i+1, j)}{2} \\
&= \nabla_x^+ \left[\frac{\mu_y(i, j+1) + \mu_y(i, j)}{2} \right] - \nabla_y^+ \left[\frac{\mu_x(i+1, j) + \mu_x(i, j)}{2} \right] \\
&= \nabla_x^+ \mu_y(i, j) - \nabla_y^+ \mu_x(i, j) + \nabla_x^+ \nabla_y^+ \left[\frac{\mu_y(i, j) - \mu_x(i, j)}{2} \right].
\end{aligned} \tag{C.1.0.16}$$

As of the role of the modified lattice laplacian, observe that it follows from our definition 3.3.1.10 that the components of $\vec{\mu}_{-\pi/4}$ have the Fourier representation

$$\begin{aligned}
\mu_1(z) &= i \frac{\sqrt{2}}{L} \sum_p e^{ip \cdot z} \left[\sin \frac{p_x + p_y}{2} \hat{\phi}(p) - \sin \frac{p_y - p_x}{2} \hat{\psi}(p) \right] \\
\mu_2(z) &= i \frac{\sqrt{2}}{L} \sum_p e^{ip \cdot z} \left[\sin \frac{p_y - p_x}{2} \hat{\phi}(p) + \sin \frac{p_x + p_y}{2} \hat{\psi}(p) \right]
\end{aligned} \tag{C.1.0.17}$$

and hence [†]

$$\begin{aligned}
(\nabla \cdot \vec{\mu}_{-\pi/4})(z) &= -\frac{2}{L} \sum_p e^{ip \cdot z} \left[\sin^2 \frac{p_x + p_y}{2} + \sin^2 \frac{p_x - p_y}{2} \right] \hat{\phi}(p) \\
&= -\frac{1}{L} \sum_p e^{ip \cdot z} \left[\hat{p}^2 - \frac{\hat{p}_1^2 \hat{p}_1^2}{2} \right] \hat{\phi}(p), \\
(\nabla \wedge \vec{\mu}_{-\pi/4})(z) &= -\frac{1}{L} \sum_p e^{ip \cdot z} \left[\hat{p}^2 - \frac{\hat{p}_1^2 \hat{p}_2^2}{2} \right] \hat{\psi}(p).
\end{aligned} \tag{C.1.0.19}$$

[†]As can be readily verified using the trigonometric identity

$$\begin{aligned}
2 \sin^2 \frac{p_1 + p_2}{2} + 2 \sin^2 \frac{p_1 - p_2}{2} &= 2 - \cos(p_1 + p_2) - \cos(p_1 - p_2) \\
&= 2 - 2 \cos p_1 \cos p_2 = 2 - 2 \left(1 - \frac{\hat{p}_1^2}{2} \right) \left(1 - \frac{\hat{p}_2^2}{2} \right) \\
&= \hat{p}_1^2 + \hat{p}_2^2 - \frac{\hat{p}_1^2 \hat{p}_2^2}{2}.
\end{aligned} \tag{C.1.0.18}$$

BIBLIOGRAPHY

1. G. Peano, Sur une courbe, qui remplit toute une aire plane. *Mathematische Annalen* **36**, 157–160, DOI [10.1007/BF01199438](https://doi.org/10.1007/BF01199438) (1890) (cit. on p. [187](#)).
2. H von Koch, Sur une courbe continue sans tangente, obtenue par une construction géométrique élémentaire. *Ark. Mat. Astron. Fys.* **1**, 681–702 (1904) (cit. on p. [189](#)).
3. E. Cesàro, Remarques sur la courbe de von Koch. *Atti della Reale Accademia di Scienze Fisiche e Matematiche* (1905) (cit. on pp. [i](#), [189](#)).
4. D. König, Über Graphen und ihre Anwendung auf Determinantentheorie und Mengenlehre. *Mathematische Annalen* **77**, 453–465, DOI [10.1007/BF01456961](https://doi.org/10.1007/BF01456961) (1916) (cit. on p. [3](#)).
5. G. D. Birkhoff, Proof of the Ergodic Theorem. *Proceedings of the National Academy of Sciences* **17**, 656–660, DOI [10.1073/pnas.17.2.656](https://doi.org/10.1073/pnas.17.2.656) (1931) (cit. on p. [2](#)).
6. J. Egerváry, Matrixok kombinatorius tulajdonságairól (in Hungarian), 38: 16–28. *Matematikai és Fizikai Lapok* **38**, 16–28 (1931) (cit. on p. [3](#)).
7. J. V. Neumann, Proof of the Quasi-Ergodic Hypothesis. *Proceedings of the National Academy of Sciences* **18**, 70–82, DOI [10.1073/pnas.18.1.70](https://doi.org/10.1073/pnas.18.1.70) (1932) (cit. on p. [2](#)).
8. A. N. Kolmogorov, Sulla Determinazione Empirica di Una Legge di Distribuzione. *Giornale dell'Istituto Italiano degli Attuari* **4**, 83–91 (1933) (cit. on p. [27](#)).
9. M. Born, L. Infeld, Foundations of the new field theory. *Proceedings of the Royal Society of London. Series A, Containing Papers of a Mathematical and Physical Character* **144**, 425–451, DOI [10.1098/rspa.1934.0059](https://doi.org/10.1098/rspa.1934.0059) (1934) (cit. on p. [133](#)).
10. F. J. Massey, The Kolmogorov-Smirnov Test for Goodness of Fit. *Journal of the American Statistical Association* **46**, 68, DOI [10.2307/2280095](https://doi.org/10.2307/2280095) (1951) (cit. on p. [27](#)).
11. J. Nash, Non-Cooperative Games. *The Annals of Mathematics* **54**, 286, DOI [10.2307/1969529](https://doi.org/10.2307/1969529) (1951) (cit. on p. [1](#)).

12. G. B. Dantzig, “Comments on J. Von Neumann’s ‘The problem of optimal assignment in a two-person game’”, tech. rep. (RAND CORP SANTA MONICA CA, 1952., 1952) (cit. on p. 2).
13. M. D. Donsker, Justification and Extension of Doob’s Heuristic Approach to the Kolmogorov- Smirnov Theorems. *The Annals of Mathematical Statistics* **23**, 277–281, DOI [10.1214/aoms/1177729445](https://doi.org/10.1214/aoms/1177729445) (1952) (cit. on p. 25).
14. J. von Neumann, in *Contributions to the Theory of Games (AM-28), Volume II*, ed. by H. W. Kuhn, A. W. Tucker (Princeton University Press, Princeton, 1953), pp. 5–12, DOI [10.1515/9781400881970-002](https://doi.org/10.1515/9781400881970-002) (cit. on pp. 1–3).
15. H. W. Kuhn, The Hungarian method for the assignment problem. *Naval Research Logistics Quarterly* **2**, 83–97, DOI [10.1002/nav.3800020109](https://doi.org/10.1002/nav.3800020109) (1955) (cit. on p. 3).
16. T. C. Koopmans, M. Beckmann, Assignment Problems and the Location of Economic Activities. *Econometrica* **25**, 53, DOI [10.2307/1907742](https://doi.org/10.2307/1907742) (1957) (cit. on p. 2).
17. J. Munkres, Algorithms for the Assignment and Transportation Problems. *Journal of the Society for Industrial and Applied Mathematics* **5**, 32–38, DOI [10.1137/0105003](https://doi.org/10.1137/0105003) (1957) (cit. on p. 3).
18. J. Beardwood, J. H. Halton, J. M. Hammersley, The shortest path through many points. *Mathematical Proceedings of the Cambridge Philosophical Society* **55**, 299–327, DOI [10.1017/S0305004100034095](https://doi.org/10.1017/S0305004100034095) (1959) (cit. on p. 18).
19. L. V. Kantorovich, Mathematical Methods of Organizing and Planning Production. *Management Science* **6**, 366–422, DOI [10.1287/mnsc.6.4.366](https://doi.org/10.1287/mnsc.6.4.366) (1960) (cit. on p. 3).
20. C. L. Siegel, *On advanced analytic number theory* (Tata Institute of Fundamental Research, 1961) (cit. on p. 216).
21. G. S. Watson, Goodness-of-fit tests on a circle. *Biometrika* **48**, 109–114, DOI [10.1093/biomet/48.1-2.109](https://doi.org/10.1093/biomet/48.1-2.109) (1961) (cit. on p. 37).
22. G. B. Dantzig, *Linear Programming and Extensions*, ed. by Intergovernmental Panel on Climate Change (RAND Corporation, Cambridge, 1963), vol. 53, pp. 1–30, DOI [10.7249/R366](https://doi.org/10.7249/R366), arXiv: [arXiv:1011.1669v3](https://arxiv.org/abs/1011.1669v3) (cit. on p. 3).
23. W. E. Donath, Algorithm and Average-value Bounds for Assignment Problems. *IBM Journal of Research and Development* **13**, 380–386, DOI [10.1147/rd.134.0380](https://doi.org/10.1147/rd.134.0380) (1969) (cit. on p. 6).

24. J. Edmonds, R. M. Karp, Theoretical Improvements in Algorithmic Efficiency for Network Flow Problems. *Journal of the ACM (JACM)* **19**, 248–264, DOI [10.1145/321694.321699](https://doi.org/10.1145/321694.321699) (1972) (cit. on p. 3).
25. S. F. Edwards, P. W. Anderson, Theory of spin glasses. *J. Phys. F: Metal Phys.* **5**, 965–974, DOI [10.1002/pssb.2220700123](https://doi.org/10.1002/pssb.2220700123) (1975) (cit. on p. 6).
26. D. Sherrington, S. Kirkpatrick, Solvable model of a spin-glass. *Physical Review Letters* **35**, 1792–1796, DOI [10.1103/PhysRevLett.35.1792](https://doi.org/10.1103/PhysRevLett.35.1792), arXiv: [arXiv:1011.1669v3](https://arxiv.org/abs/1011.1669v3) (1975) (cit. on p. 6).
27. T. M. Apostol, in, vol. 24, pp. 47–73, DOI [10.1007/978-1-4684-9910-0_3](https://doi.org/10.1007/978-1-4684-9910-0_3) (cit. on pp. 139, 217).
28. F. P. Sayer, The sums of certain series containing hyperbolic functions. *Fibonacci Quart* **14**, 215–223 (1976) (cit. on p. 206).
29. B. C. Berndt, Modular transformations and generalizations of several formulae of Ramanujan. *Rocky Mountain Journal of Mathematics* **7**, 147–190, DOI [10.1216/RMJ-1977-7-1-147](https://doi.org/10.1216/RMJ-1977-7-1-147) (1977) (cit. on p. 206).
30. S. W. Hawking, Zeta function regularization of path integrals in curved spacetime. *Communications in Mathematical Physics* **55**, 133–148, DOI [10.1007/BF01626516](https://doi.org/10.1007/BF01626516) (1977) (cit. on p. 137).
31. J Vannimenus, G Toulouse, Theory of the frustration effect. II. Ising spins on a square lattice. *Journal of Physics C: Solid State Physics* **10**, L537–L542, DOI [10.1088/0022-3719/10/18/008](https://doi.org/10.1088/0022-3719/10/18/008) (1977) (cit. on p. 5).
32. S. Kirkpatrick, D. Sherrington, Infinite-ranged models of spin-glasses. *Physical Review B* **17**, 4384–4403, DOI [10.1103/PhysRevB.17.4384](https://doi.org/10.1103/PhysRevB.17.4384), arXiv: [arXiv:1011.1669v3](https://arxiv.org/abs/1011.1669v3) (1978) (cit. on p. 6).
33. G. Parisi, Toward a mean field theory for spin glasses. *Physics Letters A* **73**, 203–205, DOI [10.1016/0375-9601\(79\)90708-4](https://doi.org/10.1016/0375-9601(79)90708-4) (1979) (cit. on p. 6).
34. G. Parisi, A sequence of approximated solutions to the S–K model for spin glasses. *Journal of Physics A: Mathematical and General* **13**, L115–L121, DOI [10.1088/0305-4470/13/4/009](https://doi.org/10.1088/0305-4470/13/4/009) (1980) (cit. on p. 6).
35. G. Parisi, The order parameter for spin glasses: A function on the interval 0–1. *Journal of Physics A: Mathematical and General* **13**, 1101–1112, DOI [10.1088/0305-4470/13/3/042](https://doi.org/10.1088/0305-4470/13/3/042) (1980) (cit. on p. 6).
36. S Kirkpatrick, C. D. Gelatt Jr, M. P. Vecchi, Optimization by Simulated Annealing. *Science* **220**, 671–680, DOI [10.1126/science.220.4598.671](https://doi.org/10.1126/science.220.4598.671), arXiv: [arXiv:1011.1669v3](https://arxiv.org/abs/1011.1669v3) (1983) (cit. on p. 5).
37. M. Ajtai, J. Komlós, G. Tusnády, On optimal matchings. *Combinatorica* **4**, 259–264, DOI [10.1007/BF02579135](https://doi.org/10.1007/BF02579135) (1984) (cit. on pp. 131, 134).

38. L. R. Foulds, *Combinatorial Optimization for Undergraduates* (Springer US, New York, NY, 1984), DOI [10.1007/978-1-4613-9511-9](https://doi.org/10.1007/978-1-4613-9511-9) (cit. on p. 4).
39. E. L. Lawler, The traveling salesman problem: a guided tour of combinatorial optimization. *Wiley-Interscience Series in Discrete Mathematics* (1985) (cit. on p. 18).
40. M. Mézard, G. Parisi, Replicas and optimization. *Journal de Physique Lettres* **46**, 771–778, DOI [10.1051/jphyslet:019850046017077100](https://doi.org/10.1051/jphyslet:019850046017077100) (1985) (cit. on pp. iii, 5, 6, 8).
41. H. Orland, Mean-field theory for optimization problems. *Journal de Physique Lettres* **46**, 763–770, DOI [10.1051/jphyslet:019850046017076300](https://doi.org/10.1051/jphyslet:019850046017076300) (1985) (cit. on pp. 5, 6).
42. K. Binder, A. P. Young, Spin glasses: Experimental facts, theoretical concepts, and open questions. *Reviews of Modern Physics* **58**, 801–976, DOI [10.1103/RevModPhys.58.801](https://doi.org/10.1103/RevModPhys.58.801) (1986) (cit. on p. 6).
43. L. Devroye, *Non-Uniform Random Variate Generation* (Springer New York, New York, NY, 1986), DOI [10.1007/978-1-4613-8643-8](https://doi.org/10.1007/978-1-4613-8643-8) (cit. on p. 58).
44. M. Mézard, G. Parisi, M. Virasoro, *Spin Glass Theory and Beyond* (WORLD SCIENTIFIC, World Scie, 1986), vol. 9, DOI [10.1142/0271](https://doi.org/10.1142/0271) (cit. on p. 5).
45. G. Carpaneto, P. Toth, Primal-dual algorithms for the assignment problem. *Discrete Applied Mathematics* **18**, 137–153, DOI [10.1016/0166-218X\(87\)90016-3](https://doi.org/10.1016/0166-218X(87)90016-3) (1987) (cit. on p. 3).
46. R. Jonker, A. Volgenant, A shortest augmenting path algorithm for dense and sparse linear assignment problems. *Computing* **38**, 325–340, DOI [10.1007/BF02278710](https://doi.org/10.1007/BF02278710) (1987) (cit. on pp. 3, 4).
47. R. Jonker, A. Volgenant, A shortest augmenting path algorithm for dense and sparse linear assignment problems. *Computing* **38**, 325–340, DOI [10.1007/BF02278710](https://doi.org/10.1007/BF02278710) (1987) (cit. on p. 153).
48. S. Lang, in *Elliptic Functions* (Springer New York, New York, NY, 1987), pp. 267–278, DOI [10.1007/978-1-4612-4752-4_20](https://doi.org/10.1007/978-1-4612-4752-4_20) (cit. on p. 216).
49. K. Mulmuley, U. V. Vazirani, V. V. Vazirani, Matching is as easy as matrix inversion. *Combinatorica* **7**, 105–113, DOI [10.1007/BF02579206](https://doi.org/10.1007/BF02579206) (1987) (cit. on p. 18).
50. M. Mézard, G. Parisi, The Euclidean matching problem. *Journal de Physique* **49**, 2019–2025, DOI [10.1051/jphys:0198800490120201900](https://doi.org/10.1051/jphys:0198800490120201900) (1988) (cit. on pp. iii, 9, 131).

51. B. Osgood, R. Phillips, P. Sarnak, Extremals of determinants of Laplacians. *Journal of Functional Analysis*, DOI [10.1016/0022-1236\(88\)90070-5](https://doi.org/10.1016/0022-1236(88)90070-5) (1988) (cit. on pp. [137](#), [143](#), [205](#)).
52. G. B. Dantzig, in *A history of scientific computing* (ACM, New York, NY, USA, 1990), vol. 28, pp. 141–151, DOI [10.1145/87252.88081](https://doi.org/10.1145/87252.88081) (cit. on p. [3](#)).
53. V. L. Girko, *Theory of Random Determinants* (Springer Netherlands, Dordrecht, 1990), vol. 13, pp. 231–232, DOI [10.1007/978-94-009-1858-0](https://doi.org/10.1007/978-94-009-1858-0) (cit. on p. [19](#)).
54. S. P. Lalley, Travelling salesman with a self-similar itinerary. *Probability in the Engineering and Informational Sciences* **4**, 1–18, DOI [10.1017/S026996480000142X](https://doi.org/10.1017/S026996480000142X) (1990) (cit. on p. [18](#)).
55. G. P. Jelliss, R. L. Graham, D. E. Knuth, O. Patashnik, Concrete Mathematics, a Foundation for Computer Science. *The Mathematical Gazette*, DOI [10.2307/3619021](https://doi.org/10.2307/3619021) (1991) (cit. on p. [113](#)).
56. M. Hoffman, Multiple harmonic series. *Pacific Journal of Mathematics* **152**, 275–290, DOI [10.2140/pjm.1992.152.275](https://doi.org/10.2140/pjm.1992.152.275) (1992) (cit. on p. [78](#)).
57. A. N. Shiriyayev, in *Selected Works of A. N. Kolmogorov*, ed. by A. N. Shiriyayev (Springer Netherlands, Dordrecht, 1992), pp. 139–146, DOI [10.1007/978-94-011-2260-3_15](https://doi.org/10.1007/978-94-011-2260-3_15) (cit. on p. [27](#)).
58. J. M. Steele, Probability and problems in euclidean combinatorial optimization. *Statistical Science* **8**, 48–56, DOI [10.1214/ss/1177011083](https://doi.org/10.1214/ss/1177011083) (1993) (cit. on pp. [7](#), [18](#)).
59. Y. Lee, J. B. Orlin, in *Large Scale Optimization*, ed. by W. Hager, D. Hearn, P. Pardalos (Springer US, Boston, MA, 1994), pp. 206–244, DOI [10.1007/978-1-4613-3632-7_12](https://doi.org/10.1007/978-1-4613-3632-7_12) (cit. on p. [4](#)).
60. M. Talagrand, The Transportation Cost from the Uniform Measure to the Empirical Measure in Dimension ≥ 3 . *The Annals of Probability* **22**, 919–959, DOI [10.1214/aop/1176988735](https://doi.org/10.1214/aop/1176988735) (1994) (cit. on p. [185](#)).
61. D. Zagier, Values of Zeta Functions and Their Applications. *First European Congress of Mathematics Paris, July 6–10, 1992*, 497–512, DOI [10.1007/978-3-0348-9112-7_23](https://doi.org/10.1007/978-3-0348-9112-7_23) (1994) (cit. on p. [79](#)).
62. A. S. Kechris, *Classical Descriptive Set Theory* (Springer New York, New York, NY, 1995), vol. 156, DOI [10.1007/978-1-4612-4190-4](https://doi.org/10.1007/978-1-4612-4190-4) (cit. on p. [17](#)).
63. I. P. Gent, T. Walsh, The TSP phase transition. *Artificial Intelligence* **88**, 349–358, DOI [10.1016/S0004-3702\(96\)00030-6](https://doi.org/10.1016/S0004-3702(96)00030-6) (1996) (cit. on p. [8](#)).

64. P. G. Higgs, Overlaps between RNA Secondary Structures. *Physical Review Letters* **76**, 704–707, DOI [10.1103/PhysRevLett.76.704](https://doi.org/10.1103/PhysRevLett.76.704) (1996) (cit. on p. 107).
65. G. Lawler, Cut Times for Simple Random Walk. *Electronic Journal of Probability* **1**, 1–24, DOI [10.1214/EJP.v1-13](https://doi.org/10.1214/EJP.v1-13) (1996) (cit. on p. 204).
66. G. Rempala, Asymptotic behavior of random permanents. *Random Operators and Stochastic Equations* **4**, 33–42, DOI [10.1515/rose.1996.4.1.33](https://doi.org/10.1515/rose.1996.4.1.33) (1996) (cit. on p. 19).
67. D. J. Broadhurst, D. Kreimer, Association of multiple zeta values with positive knots via Feynman diagrams up to 9 loops. *Physics Letters, Section B: Nuclear, Elementary Particle and High-Energy Physics* **393**, 403–412, DOI [10.1016/S0370-2693\(96\)01623-1](https://doi.org/10.1016/S0370-2693(96)01623-1) (1997) (cit. on p. 79).
68. E. B. Saff, A. B. Kuijlaars, Distributing many points on a sphere. *Mathematical Intelligencer*, DOI [10.1007/BF03024331](https://doi.org/10.1007/BF03024331) (1997) (cit. on p. 155).
69. J. M. Steele, *Probability Theory and Combinatorial Optimization* (SIAM, 1997), p. 159 (cit. on p. 18).
70. D. Vere-Jones, Alpha-permanents and their applications to multivariate gamma, negative binomial and ordinary binomial distributions. *New Zealand Journal of Mathematics* **26**, 125–149 (1997) (cit. on pp. 19, 203).
71. D. P. Bertsekas, *Network Optimization: Continuous and Discrete Methods*, xiii, 593 p. (Cit. on p. 3).
72. S. Caracciolo, A. Pelissetto, Corrections to finite-size scaling in the lattice N-vector model for N = infy. *Physical Review D* **58**, 105007, DOI [10.1103/PhysRevD.58.105007](https://doi.org/10.1103/PhysRevD.58.105007) (1998) (cit. on p. 31).
73. D. Coppersmith, G. B. Sorkin, in *Lecture Notes in Computer Science (including subseries Lecture Notes in Artificial Intelligence and Lecture Notes in Bioinformatics)*, vol. 1518, pp. 319–330, DOI [10.1007/3-540-49543-6_25](https://doi.org/10.1007/3-540-49543-6_25) (cit. on p. 7).
74. P. Flajolet, B. Salvy, Euler sums and contour integral representations. *Experimental Mathematics*, DOI [10.1080/10586458.1998.10504356](https://doi.org/10.1080/10586458.1998.10504356) (1998) (cit. on p. 79).
75. I. Karatzas, S. E. Shreve, *Brownian Motion and Stochastic Calculus* (Springer New York, New York, NY, 1998), vol. 113, DOI [10.1007/978-1-4612-0949-2](https://doi.org/10.1007/978-1-4612-0949-2) (cit. on p. 26).
76. I. G. I. MacDonald, *Symmetric functions and Hall polynomials* (Oxford university press, 1998), vol. 13, pp. 180–183 (cit. on p. 72).

77. G. Parisi, A Conjecture on random bipartite matching. *arXiv* **2**, 2, arXiv: [9801176](https://arxiv.org/abs/9801176) ([cond-mat](https://arxiv.org/abs/9801176)) (1998) (cit. on p. 6).
78. C. Puente, J. Romeu, R. Pous, J Ramis, A Hijazo, Small but long Koch fractal monopole. *Electronics Letters* **34**, 9–10, DOI [10.1049/e1:19980114](https://doi.org/10.1049/e1:19980114) (1998) (cit. on p. 189).
79. J. E. Yukich, *Probability Theory of Classical Euclidean Optimization Problems* (Springer Berlin Heidelberg, Berlin, Heidelberg, 1998), vol. 1675, DOI [10.1007/BFb0093472](https://doi.org/10.1007/BFb0093472) (cit. on p. 18).
80. R. E. Burkard, E. Çela, in *Handbook of Combinatorial Optimization* (Springer US, Boston, MA, 1999), pp. 75–149, DOI [10.1007/978-1-4757-3023-4_2](https://doi.org/10.1007/978-1-4757-3023-4_2) (cit. on p. 3).
81. I. Hueter, The convex hull of samples from self-similar distributions. *Advances in Applied Probability* **31**, 34–47, DOI [10.1239/aap/1029954264](https://doi.org/10.1239/aap/1029954264) (1999) (cit. on p. 186).
82. R. J. McCann, Exact solutions to the transportation problem on the line. *Proceedings of the Royal Society of London. Series A: Mathematical, Physical and Engineering Sciences* **455**, 1341–1380, DOI [10.1098/rspa.1999.0364](https://doi.org/10.1098/rspa.1999.0364) (1999) (cit. on pp. 23, 128).
83. Y. Brenier, Derivation of the Euler equations from a caricature of Coulomb interaction. *Communications in Mathematical Physics*, DOI [10.1007/s002200000204](https://doi.org/10.1007/s002200000204) (2000) (cit. on p. 133).
84. M. Dell’Amico, P. Toth, Algorithms and codes for dense assignment problems: the state of the art. *Discrete Applied Mathematics* **100**, 17–48, DOI [10.1016/S0166-218X\(99\)00172-9](https://doi.org/10.1016/S0166-218X(99)00172-9) (2000) (cit. on p. 3).
85. P. G. Higgs, RNA secondary structure: physical and computational aspects. *Quarterly Reviews of Biophysics* **33**, 199–253, DOI [10.1017/S0033583500003620](https://doi.org/10.1017/S0033583500003620) (2000) (cit. on p. 107).
86. S. Mertens, Computational Complexity for Physicists. *Computing in Science and Engineering* **4**, 31, DOI [10.1109/5992.998639](https://doi.org/10.1109/5992.998639), arXiv: [0012185](https://arxiv.org/abs/0012185) ([cond-mat](https://arxiv.org/abs/0012185)) (2000) (cit. on p. 7).
87. A. Pagnani, G. Parisi, F. Ricci-Tersenghi, Glassy Transition in a Disordered Model for the RNA Secondary Structure. *Physical Review Letters* **84**, 2026–2029, DOI [10.1103/PhysRevLett.84.2026](https://doi.org/10.1103/PhysRevLett.84.2026) (2000) (cit. on p. 107).
88. D. J. Aldous, The $\zeta(2)$ limit in the random assignment problem. *Random Structures and Algorithms* **18**, 381–418, DOI [10.1002/rsa.1015](https://doi.org/10.1002/rsa.1015), arXiv: [0010063v1](https://arxiv.org/abs/0010063v1) (2001) (cit. on pp. iii, 6).

89. O. C. Martin, R. Monasson, R. Zecchina, Statistical mechanics methods and phase transitions in optimization problems. *Theoretical Computer Science* **265**, 3–67, DOI [10.1016/S0304-3975\(01\)00149-9](https://doi.org/10.1016/S0304-3975(01)00149-9), arXiv: [0104428 \(cond-mat\)](https://arxiv.org/abs/0104428) (2001) (cit. on p. 8).
90. H. Nishimori, *Statistical Physics of Spin Glasses and Information Processing* (Oxford University Press, Internatio, 2001), p. 252, DOI [10.1093/acprof:oso/9780198509417.001.0001](https://doi.org/10.1093/acprof:oso/9780198509417.001.0001) (cit. on p. 5).
91. R. Bundschuh, T. Hwa, Statistical mechanics of secondary structures formed by random RNA sequences. *Physical Review E* **65**, 031903, DOI [10.1103/PhysRevE.65.031903](https://doi.org/10.1103/PhysRevE.65.031903) (2002) (cit. on p. 107).
92. E. Marinari, A. Pagnani, F. Ricci-Tersenghi, Zero-temperature properties of RNA secondary structures. *Physical Review E - Statistical Physics, Plasmas, Fluids, and Related Interdisciplinary Topics* **65**, 7, DOI [10.1103/PhysRevE.65.041919](https://doi.org/10.1103/PhysRevE.65.041919) (2002) (cit. on p. 107).
93. M. Mezard, Analytic and Algorithmic Solution of Random Satisfiability Problems. *Science* **297**, 812–815, DOI [10.1126/science.1073287](https://doi.org/10.1126/science.1073287) (2002) (cit. on p. 8).
94. C. Morpurgo, Sharp inequalities for functional integrals and traces of conformally invariant operators. *Duke Mathematical Journal* **114**, 477–553, DOI [10.1215/S0012-7094-02-11433-1](https://doi.org/10.1215/S0012-7094-02-11433-1) (2002) (cit. on p. 137).
95. H. Orland, A. Zee, RNA folding and large N matrix theory. *Nuclear Physics B* **620**, 456–476, DOI [10.1016/S0550-3213\(01\)00522-3](https://doi.org/10.1016/S0550-3213(01)00522-3), arXiv: [0106359 \(cond-mat\)](https://arxiv.org/abs/0106359) (2002) (cit. on p. 107).
96. J. Riordan, *Introduction to Combinatorial Analysis* (John Wiley and Sons, New York, Dover, 2002) (cit. on p. 84).
97. F. Guerra, Broken replica symmetry bounds in the mean field spin glass model. *Communications in Mathematical Physics* **233**, 1–12, DOI [10.1007/s00220-002-0773-5](https://doi.org/10.1007/s00220-002-0773-5), arXiv: [0205123 \(cond-mat\)](https://arxiv.org/abs/0205123) (2003) (cit. on p. 6).
98. S. Linusson, J. Wästlund, A proof of Parisi’s conjecture on the random assignment problem. *Probab. Theory Relat. Fields* **62**, 1–7, DOI [10.1007/s00440-003-0308-9](https://doi.org/10.1007/s00440-003-0308-9) *Svante* (2003) (cit. on p. 7).
99. M. Müller, Statistical physics of RNA folding. *Physical Review E* **67**, 021914, DOI [10.1103/PhysRevE.67.021914](https://doi.org/10.1103/PhysRevE.67.021914) (2003) (cit. on p. 107).
100. A. Pagnani, G. Parisi, M. Ratiéville, Near-optimal configurations in mean-field disordered systems. *Physical Review E* **68**, 046706, DOI [10.1103/PhysRevE.68.046706](https://doi.org/10.1103/PhysRevE.68.046706), arXiv: [0307250 \(cond-mat\)](https://arxiv.org/abs/0307250) (2003) (cit. on p. 19).

101. M. Agrawal, N. Kayal, N. Saxena, PRIMES is in P. *Annals of Mathematics* **160**, 781–793, DOI [10.4007/annals.2004.160.781](https://doi.org/10.4007/annals.2004.160.781) (2004) (cit. on p. 7).
102. Y. Brenier, A Note on Deformations of 2D Fluid Motions Using 3D Born-Infeld Equations. *Monatshefte fur Mathematik* **142**, 113–122, DOI [10.1007/s00605-004-0240-9](https://doi.org/10.1007/s00605-004-0240-9) (2004) (cit. on p. 133).
103. P. Glasserman, in, pp. 79–184, DOI [10.1007/978-0-387-21617-1_3](https://doi.org/10.1007/978-0-387-21617-1_3) (cit. on p. 26).
104. O. C. Martin, M. Mézard, O. Rivoire, Frozen glass phase in the multi-index matching problem. *Physical Review Letters* **93**, 19–22, DOI [10.1103/PhysRevLett.93.217205](https://doi.org/10.1103/PhysRevLett.93.217205) (2004) (cit. on p. 8).
105. D. J. Aldous, A. Bandyopadhyay, A survey of max-type recursive distributional equations. *The Annals of Applied Probability* **15**, 1047–1110, DOI [10.1214/105051605000000142](https://doi.org/10.1214/105051605000000142), arXiv: [0401388v3](https://arxiv.org/abs/0401388v3) (arXiv:math) (2005) (cit. on p. 7).
106. O. C. Martin, M. Mézard, O. Rivoire, Random multi-index matching problems. *Journal of Statistical Mechanics: Theory and Experiment*, 159–193, DOI [10.1088/1742-5468/2005/09/P09006](https://doi.org/10.1088/1742-5468/2005/09/P09006) (2005) (cit. on p. 8).
107. C. Nair, B. Prabhakar, M. Sharma, Proofs of the Parisi and Coppersmith-Sorkin Random assignment conjectures. *Random Structures and Algorithms* **27**, 413–444, DOI [10.1002/rsa.20084](https://doi.org/10.1002/rsa.20084) (2005) (cit. on p. 7).
108. J. Sakhr, J. M. Nieminen, Poisson-to-Wigner crossover transition in the nearest-neighbor statistics of random points on fractals. *Physical Review E - Statistical, Nonlinear, and Soft Matter Physics* **72**, 1–4, DOI [10.1103/PhysRevE.72.045204](https://doi.org/10.1103/PhysRevE.72.045204), arXiv: [0511042](https://arxiv.org/abs/0511042) (nlin) (2005) (cit. on p. 186).
109. J. Steiner, A geometrical mass and its extremal properties for metrics on S^2 . *Duke Mathematical Journal* **129**, 63–86, DOI [10.1215/S0012-7094-04-12913-6](https://doi.org/10.1215/S0012-7094-04-12913-6) (2005) (cit. on p. 137).
110. G. Vernizzi, H. Orland, A. Zee, Enumeration of RNA Structures by Matrix Models. *Physical Review Letters* **94**, 168103, DOI [10.1103/PhysRevLett.94.168103](https://doi.org/10.1103/PhysRevLett.94.168103), arXiv: [0411004](https://arxiv.org/abs/0411004) (q-bio) (2005) (cit. on p. 107).
111. Y. Ohno, N. Wakabayashi, Cyclic sum of multiple zeta values. *Acta Arithmetica* **123**, 289–295, DOI [10.4064/aa123-3-5](https://doi.org/10.4064/aa123-3-5) (2006) (cit. on p. 79).
112. J. Sakhr, J. M. Nieminen, Spacing distributions for point processes on a regular fractal. *Physical Review E - Statistical, Nonlinear, and Soft Matter Physics* **73**, 1–12, DOI [10.1103/PhysRevE.73.036201](https://doi.org/10.1103/PhysRevE.73.036201) (2006) (cit. on p. 186).

113. M. Talagrand, The Parisi formula. *Annals of Mathematics* **163**, 221–263, DOI [10.4007/annals.2006.163.221](https://doi.org/10.4007/annals.2006.163.221) (2006) (cit. on p. 6).
114. A. M. Vershik, Kantorovich metric: Initial history and little-known applications. *Journal of Mathematical Sciences* **133**, 1410–1417, DOI [10.1007/s10958-006-0056-3](https://doi.org/10.1007/s10958-006-0056-3) (2006) (cit. on p. 17).
115. J. Raymond, A. Sportiello, L. Zdeborová, Phase diagram of the 1-in-3 satisfiability problem. *Physical Review E - Statistical, Nonlinear, and Soft Matter Physics* **76**, 1–30, DOI [10.1103/PhysRevE.76.011101](https://doi.org/10.1103/PhysRevE.76.011101), arXiv: [0702610 \(cond-mat\)](https://arxiv.org/abs/0702610) (2007) (cit. on p. 18).
116. Š. Ungar, The Koch Curve: A Geometric Proof. *The American Mathematical Monthly* **114**, 61–66, DOI [10.1080/00029890.2007.11920392](https://doi.org/10.1080/00029890.2007.11920392) (2007) (cit. on p. 189).
117. G. Edgar, *Measure, Topology, and Fractal Geometry*, ed. by G. Edgar (Springer New York, New York, NY, 2008), DOI [10.1007/978-0-387-74749-1](https://doi.org/10.1007/978-0-387-74749-1) (cit. on p. 187).
118. J.-F. Marckert, One more approach to the convergence of the empirical process to the Brownian bridge. *Electronic Journal of Statistics* **2**, 118–126, DOI [10.1214/07-EJS131](https://doi.org/10.1214/07-EJS131) (2008) (cit. on p. 25).
119. Y. Ohno, W. Zudilin, Zeta stars. *Communications in Number Theory and Physics* **2**, 325–347, DOI [10.4310/CNTP.2008.v2.n2.a2](https://doi.org/10.4310/CNTP.2008.v2.n2.a2) (2008) (cit. on p. 79).
120. K. Okikiolu, A negative mass theorem for the 2-torus. *Communications in Mathematical Physics*, DOI [10.1007/s00220-008-0644-9](https://doi.org/10.1007/s00220-008-0644-9) (2008) (cit. on pp. 136, 137, 143, 205).
121. K. Okikiolu, Extremals for logarithmic hardy-littlewood-sobolev inequalities on compact manifolds. *Geometric and Functional Analysis* **17**, 1655–1684, DOI [10.1007/s00039-007-0636-5](https://doi.org/10.1007/s00039-007-0636-5) (2008) (cit. on p. 137).
122. V. Betz, D. Ueltschi, Spatial Random Permutations and Infinite Cycles. *Communications in Mathematical Physics* **285**, 469–501, DOI [10.1007/s00220-008-0584-4](https://doi.org/10.1007/s00220-008-0584-4) (2009) (cit. on p. 206).
123. P. Flajolet, R. Sedgewick, *Analytic Combinatorics* (Cambridge University Press, Cambridge, 2009), pp. 1–810, DOI [10.1017/CB09780511801655](https://doi.org/10.1017/CB09780511801655) (cit. on pp. 119, 121, 213).
124. M. Mézard, A. Montanari, *Information, Physics, and Computation*, DOI [10.1093/acprof:oso/9780198570837.001.0001](https://doi.org/10.1093/acprof:oso/9780198570837.001.0001) (cit. on p. 5).

125. K. Okikiolu, A Negative Mass Theorem for Surfaces of Positive Genus. *Communications in Mathematical Physics* **290**, 1025–1031, DOI [10.1007/s00220-008-0722-z](https://doi.org/10.1007/s00220-008-0722-z) (2009) (cit. on p. 136).
126. F. Ollivier, Looking for the order of a system of arbitrary ordinary differential equations. *Applicable Algebra in Engineering, Communication and Computing* **20**, 7–32, DOI [10.1007/s00200-009-0087-3](https://doi.org/10.1007/s00200-009-0087-3) (2009) (cit. on p. 3).
127. C. Villani, *Optimal Transport, old and new* (Springer Berlin Heidelberg, Berlin, Heidelberg, Springer, 2009), vol. 338, p. 998, DOI [10.1007/978-3-540-71050-9](https://doi.org/10.1007/978-3-540-71050-9) (cit. on pp. 3, 17, 18).
128. A. Cavagna *et al.*, Scale-free correlations in starling flocks. *Proceedings of the National Academy of Sciences* **107**, 11865–11870, DOI [10.1073/pnas.1005766107](https://doi.org/10.1073/pnas.1005766107), arXiv: [0911.4393](https://arxiv.org/abs/0911.4393) (2010) (cit. on p. 207).
129. M. Chertkov, L. Kroc, F. Krzakala, M. Vergassola, L. Zdeborová, Inference in particle tracking experiments by passing messages between images. *Proceedings of the National Academy of Sciences of the United States of America* **107**, 7663–7668, DOI [10.1073/pnas.0910994107](https://doi.org/10.1073/pnas.0910994107) (2010) (cit. on p. 207).
130. R. M. Karp, in *50 Years of Integer Programming 1958-2008* (Springer Berlin Heidelberg, Berlin, Heidelberg, 2010), pp. 219–241, DOI [10.1007/978-3-540-68279-0_8](https://doi.org/10.1007/978-3-540-68279-0_8) (cit. on p. 18).
131. C.-S. Lin, C.-L. Wang, Elliptic functions, Green functions and the mean field equations on tori. *Annals of Mathematics* **172**, 911–954, DOI [10.4007/annals.2010.172.911](https://doi.org/10.4007/annals.2010.172.911) (2010) (cit. on p. 141).
132. J. M. Borwein, W. Zudilin, Math honours: multiple zeta values. *Computing* **353**, 752–798 (2011) (cit. on p. 79).
133. G. Chartrand, P. Zhang, *A first course in graph theory* (Dover Publications, Inc., 2012), p. 450 (cit. on pp. 3, 7).
134. J. Delon, J. Salomon, A. Sobolevski, Local matching indicators for transport problems with concave costs. *SIAM J. Discr.Math* **26**, 801–827, DOI [10.1137/110823304](https://doi.org/10.1137/110823304) (2012) (cit. on p. 113).
135. J. J. Sylvester, *The Collected Mathematical Papers of James Joseph Sylvester: Volume 1, 1837-1853* (Cambridge University Press, 2012), p. 664 (cit. on p. 3).
136. F. Barthe, C. Bordenave, Combinatorial Optimization Over Two Random Point Sets. 483–535, DOI [10.1007/978-3-319-00321-4_19](https://doi.org/10.1007/978-3-319-00321-4_19) (2013) (cit. on p. 18).

137. A. A. Borovkov, *Probability Theory* (Springer London, London, 2013), DOI [10.1007/978-1-4471-5201-9](https://doi.org/10.1007/978-1-4471-5201-9) (cit. on p. 26).
138. H. Crane, Some algebraic identities for the α -permanent. *Linear Algebra and Its Applications* **439**, 3445–3459, DOI [10.1016/j.laa.2013.09.028](https://doi.org/10.1016/j.laa.2013.09.028), arXiv: [1304.1772](https://arxiv.org/abs/1304.1772) (2013) (cit. on p. 203).
139. G. J. O. Jameson, Inequalities for Gamma Function Ratios. *The American Mathematical Monthly* **120**, 936, DOI [10.4169/amer.math.monthly.120.10.936](https://doi.org/10.4169/amer.math.monthly.120.10.936) (2013) (cit. on p. 114).
140. C. G. J. Jacobi, in *C. G. J. Jacobi's Gesammelte Werke*, ed. by K. Weierstrass (Cambridge University Press, Cambridge, 2013), vol. 5, pp. 191–216, DOI [10.1017/CB09781139567992.003](https://doi.org/10.1017/CB09781139567992.003) (cit. on p. 3).
141. S. K. Nechaev, A. N. Sobolevski, O. V. Valba, Planar diagrams from optimization for concave potentials. *Physical Review E, Statistical, nonlinear, and soft matter physics* **87**, 012102, DOI [10.1103/PhysRevE.87.012102](https://doi.org/10.1103/PhysRevE.87.012102) (2013) (cit. on p. 107).
142. D. Panchenko, *The Sherrington-Kirkpatrick Model* (Springer New York, New York, NY, 2013), DOI [10.1007/978-1-4614-6289-7](https://doi.org/10.1007/978-1-4614-6289-7) (cit. on p. 6).
143. E. Boniolo, S. Caracciolo, A. Sportiello, Correlation function for the Grid-Poisson Euclidean matching on a line and on a circle. *Journal of Statistical Mechanics: Theory and Experiment* **2014**, P11023, DOI [10.1088/1742-5468/2014/11/P11023](https://doi.org/10.1088/1742-5468/2014/11/P11023), arXiv: [arXiv:1403.1836v3](https://arxiv.org/abs/1403.1836v3) (2014) (cit. on pp. 21, 24, 25, 27, 36).
144. S. Caracciolo, G. Sicuro, One-dimensional Euclidean matching problem: exact solutions, correlation functions, and universality. *Physical Review. E, Statistical, nonlinear, and soft matter physics* **90**, 042112, DOI [10.1103/PhysRevE.90.042112](https://doi.org/10.1103/PhysRevE.90.042112) (2014) (cit. on pp. 13, 25, 27, 41, 46, 132, 201, 204).
145. S. Caracciolo, C. Lucibello, G. Parisi, G. Sicuro, Scaling hypothesis for the Euclidean bipartite matching problem. *Physical Review E* **90**, 012118, DOI [10.1103/PhysRevE.90.012118](https://doi.org/10.1103/PhysRevE.90.012118) (2014) (cit. on pp. vi, 20, 131, 132).
146. J. Larsson, The Minimum Perfect Matching in Pseudo-dimension $0 < q < 1$. *arXiv*, 1–14, arXiv: [1403.3635](https://arxiv.org/abs/1403.3635) (2014) (cit. on p. 7).
147. E. Artin, *The Gamma function* (Courier Dover Publications, 2015) (cit. on p. 114).
148. S. Caracciolo, G. Sicuro, Quadratic Stochastic Euclidean Bipartite Matching Problem. *Physical Review Letters* **115**, 230601, DOI [10.1103/PhysRevLett.115.230601](https://doi.org/10.1103/PhysRevLett.115.230601) (2015) (cit. on pp. 20, 131, 132, 134, 135, 154).

149. S. Caracciolo, G. Sicuro, Scaling hypothesis for the Euclidean bipartite matching problem. II. Correlation functions. *Physical Review E* **91**, 062125, DOI [10.1103/PhysRevE.91.062125](https://doi.org/10.1103/PhysRevE.91.062125) (2015) (cit. on pp. [126](#), [155](#), [176](#), [184](#)).
150. J. Salez, The Mézard-Parisi equation for matchings in pseudo-dimension $d > 1$. *Electronic Communications in Probability* **20**, 1–7, DOI [10.1214/ECP.v20-3791](https://doi.org/10.1214/ECP.v20-3791), arXiv: [arXiv:1409.2813v1](https://arxiv.org/abs/1409.2813v1) (2015) (cit. on p. [7](#)).
151. M. D’Achille, On Two Linear Assignment Problems: Random Assignment and Euclidean Bipartite Matching. *MSc Thesis, University of Milan* (2016) (cit. on pp. [3](#), [23](#), [201](#)).
152. D. Maclagan, B. Sturmfels, *Introduction to Tropical Geometry*, vol. 118, pp. 233–237, DOI [10.1365/s13291-016-0133-6](https://doi.org/10.1365/s13291-016-0133-6), arXiv: [0709.1049](https://arxiv.org/abs/0709.1049) (cit. on p. [18](#)).
153. S. Caracciolo, M. P. D’Achille, E. M. Malatesta, G. Sicuro, Finite-size corrections in the random assignment problem. *Physical Review E* **95**, 052129, DOI [10.1103/PhysRevE.95.052129](https://doi.org/10.1103/PhysRevE.95.052129), arXiv: [arXiv:0711.3445v1](https://arxiv.org/abs/0711.3445v1) (2017) (cit. on p. [8](#)).
154. S. Caracciolo, M. D’Achille, G. Sicuro, Random Euclidean matching problems in one dimension. *Physical Review E* **96**, 042102, DOI [10.1103/PhysRevE.96.042102](https://doi.org/10.1103/PhysRevE.96.042102), arXiv: [1707.05541](https://arxiv.org/abs/1707.05541) (2017) (cit. on pp. [21](#), [22](#), [25–27](#), [29](#), [41](#), [59](#), [68](#), [127](#), [185](#), [206](#)).
155. T. Leblé, S. Serfaty, O. Zeitouni, Large Deviations for the Two-Dimensional Two-Component Plasma. *Communications in Mathematical Physics* **350**, 301–360, DOI [10.1007/s00220-016-2735-3](https://doi.org/10.1007/s00220-016-2735-3), arXiv: [1510.01955](https://arxiv.org/abs/1510.01955) (2017) (cit. on p. [202](#)).
156. C. Lucibello, G. Parisi, G. Sicuro, One-loop diagrams in the random Euclidean matching problem. *Physical Review E* **95**, DOI [10.1103/PhysRevE.95.012302](https://doi.org/10.1103/PhysRevE.95.012302), arXiv: [1609.09310](https://arxiv.org/abs/1609.09310) (2017) (cit. on p. [201](#)).
157. C. Xu, Some infinite series involving hyperbolic functions. arXiv: [1707.06673](https://arxiv.org/abs/1707.06673) (2017) (cit. on p. [206](#)).
158. H. Brezis, Remarks on the Monge–Kantorovich problem in the discrete setting. *Comptes Rendus Mathématique* **356**, 207–213, DOI [10.1016/j.crma.2017.12.008](https://doi.org/10.1016/j.crma.2017.12.008) (2018) (cit. on p. [18](#)).
159. N. Holden, Y. Peres, A. Zhai, Gravitational allocation on the sphere. *Proceedings of the National Academy of Sciences* **115**, 9666–9671, DOI [10.1073/pnas.1720804115](https://doi.org/10.1073/pnas.1720804115), arXiv: [1704.08238](https://arxiv.org/abs/1704.08238) (2018) (cit. on p. [151](#)).
160. J. Pitman, M. Yor, A guide to Brownian motion and related stochastic processes. **0**, arXiv: [1802.09679](https://arxiv.org/abs/1802.09679) (2018) (cit. on pp. [26](#), [111](#)).

161. F. Santambrogio, A short story on optimal transport and its many applications. 1–16, DOI [10.14760/SNAP-2018-013-EN](https://doi.org/10.14760/SNAP-2018-013-EN) (2018) (cit. on p. 17).
162. M. Talagrand, Scaling and non-standard matching theorems. *Comptes Rendus Mathématique*, DOI [10.1016/j.crma.2018.04.018](https://doi.org/10.1016/j.crma.2018.04.018) (2018) (cit. on p. 201).
163. L. Ambrosio, F. Glaudo, Finer estimates on the 2-dimensional matching problem. *Journal de l'École polytechnique — Mathématiques* **6**, 737–765, DOI [10.5802/jep.105](https://doi.org/10.5802/jep.105) (2019) (cit. on pp. 131, 134, 156).
164. L. Ambrosio, F. Stra, D. Trevisan, A PDE approach to a 2-dimensional matching problem. *Probability Theory and Related Fields*, DOI [10.1007/s00440-018-0837-x](https://doi.org/10.1007/s00440-018-0837-x), arXiv: [1611.04960](https://arxiv.org/abs/1611.04960) (2019) (cit. on pp. 131, 134, 154, 205).
165. L. Ambrosio, F. Glaudo, D. Trevisan, On the optimal map in the 2-dimensional random matching problem. *Discrete and Continuous Dynamical Systems - A* **39**, 7291–7308, DOI [10.3934/dcds.2019304](https://doi.org/10.3934/dcds.2019304), arXiv: [1903.12153](https://arxiv.org/abs/1903.12153) (2019) (cit. on p. 134).
166. D. Benedetto, E. Caglioti, Euclidean random matching in 2D for non-constant densities. **2**, 1–14, arXiv: [1911.10523](https://arxiv.org/abs/1911.10523) (2019) (cit. on p. 131).
167. S. Bobkov, M. Ledoux, A simple Fourier analytic proof of the AKT optimal matching theorem. **1**, 1–20, arXiv: [1909.06193](https://arxiv.org/abs/1909.06193) (2019) (cit. on p. 131).
168. S. Bobkov, M. Ledoux, One-dimensional empirical measures, order statistics, and Kantorovich transport distances. *Memoirs of the American Mathematical Society* **261**, 0–0, DOI [10.1090/memo/1259](https://doi.org/10.1090/memo/1259) (2019) (cit. on pp. 60, 84, 198).
169. S. Caracciolo, M. D’Achille, G. Sicuro, M. D’Achille, G. Sicuro, Anomalous Scaling of the Optimal Cost in the One-Dimensional Random Assignment Problem. *Journal of Statistical Physics* **174**, 846–864, DOI [10.1007/s10955-018-2212-9](https://doi.org/10.1007/s10955-018-2212-9), arXiv: [1803.04723](https://arxiv.org/abs/1803.04723) (2019) (cit. on pp. vi, 20, 60, 68, 79, 81, 95, 185, 198).
170. S. Caracciolo, A. Di Gioacchino, E. M. Malatesta, L. G. Molinari, Selberg integrals in 1D random Euclidean optimization problems. *Journal of Statistical Mechanics: Theory and Experiment* **2019**, 063401, DOI [10.1088/1742-5468/ab11d7](https://doi.org/10.1088/1742-5468/ab11d7) (2019) (cit. on p. 59).
171. M. Ledoux, On Optimal Matching of Gaussian Samples. *Journal of Mathematical Sciences* **238**, 495–522, DOI [10.1007/s10958-019-04253-6](https://doi.org/10.1007/s10958-019-04253-6) (2019) (cit. on p. 201).

172. D. Benedetto *et al.*, Random assignment problems on $2d$ manifolds. 1–33, arXiv: [2008.01462](https://arxiv.org/abs/2008.01462) (2020) (cit. on pp. [i](#), [vi](#), [20](#), [132](#), [156](#), [200](#)).
173. S. Caracciolo, M. P. D’Achille, V. Erba, A. Sportiello, The Dyck bound in the concave 1-dimensional random assignment model. *Journal of Physics A: Mathematical and Theoretical* **53**, 064001, DOI [10.1088/1751-8121/ab4a34](https://doi.org/10.1088/1751-8121/ab4a34), arXiv: [1904.10867](https://arxiv.org/abs/1904.10867) (2020) (cit. on pp. [vi](#), [20](#), [40](#), [59](#), [66](#), [107](#), [206](#)).
174. M. D’Achille, A. Sportiello, Anomalous scaling of the optimal cost in the one-dimensional Euclidean Random Assignment Problem: some rigorous results. *In preparation* (cit. on pp. [20](#), [58](#)).
175. M. D’Achille, A. Sportiello, The Euclidean Random Assignment Problem at non-integer Hausdorff dimension $d_H \in (1, 2)$. *In preparation* (cit. on p. [20](#)).

Titre: Propriétés statistiques du problème de l'assignation aléatoire euclidienne

Mots clés: Problème de l'assignation aléatoire, Problème du transport de Monge-Kantorovitch, Théorie statistique des champs, Systèmes désordonnés en dimension finie

Résumé: Etant donné $2n$ points, n "rouge" et n "bleu", dans un espace euclidien, la résolution du problème d'assignation euclidienne associé consiste à trouver la bijection entre les points rouges et bleus qui minimise une fonctionnelle des positions de points. Dans la version stochastique de cette problème, les points sont un processus de point de Poisson, et un certain intérêt a développé au fil des ans sur les propriétés typiques et moyennes de la solution dans la limite $n \rightarrow \infty$. Cette thèse de doctorat porte sur ce problème dans un certain nombre de cas (plusieurs résultats exacts en $d = 1$, la dérivation de certaines propriétés fines en $d = 2$, en partie encore conjecturales, un étude des fractales auto-similaires avec $1 < d_H < 2, \dots$). En particulier, nous présentons de nouvelles contributions sur le comportement asymptotique du coût de la solution, motivé, parmi autres, par la physique des systèmes désordonnés, et par des résultats en analyse fonctionnelle sur le problème de Monge-Kantorovich dans le continuum.

Title: Statistical Properties of the Euclidean Random Assignment Problem

Keywords: Random Assignment Problem, Monge-Kantorovich transportation problem, Statistical field theory, Disordered systems in finite dimension

Abstract: Given $2n$ points, n "red" and n "blue", in a Euclidean space, solving the associated Euclidean Assignment Problem consists in finding the bijection between red and blue points that minimizes a functional of the point positions. In the stochastic version of this problem, the points are a Poisson Point Process, and some interest has developed over the years on the typical and average properties of the solution in the limit $n \rightarrow \infty$. This PhD thesis investigates this problem in a number of cases (many exact results in $d = 1$, the derivation of some fine properties in $d = 2$, in part still conjectural, an investigation on self-similar fractals with $1 < d_H < 2, \dots$). In particular, we present new contributions on the asymptotic behavior of the cost of the solution, motivated (among others) by the physics of Disordered Systems, and by results in Functional Analysis on the Monge-Kantorovich problem in the continuum.

